Experimental and Numerical Study of Fatigue Life in Aluminum 6061-T6 under Stochastic Loading

Bryan K. Ross

A thesis
submitted in partial fulfillment of the
requirements for the degree of

Master of Science in Mechanical Engineering

University of Washington
2012

Committee:
Mamidala Ramulu
Per Reinhall
Larry Parfitt

Program Authorized to Offer Degree:
Mechanical Engineering

University of Washington

Abstract

Experimental and Numerical Study of Fatigue Life in Aluminum 6061-T6 under Stochastic Loading

Bryan K. Ross

Chair of Supervisory Committee:
Professor Mamidala Ramulu
Mechanical Engineering

Numerically determining fatigue under stochastic vibrations are typically performed use computational intensive transient response models. This research will delve into an alternate less computation intensive method of applying linear modal analysis combined with Power Spectral Density (PSD) excitation functions to develop resultant stress PSD Functions. Statistical methods can be applied to evaluate the stress range occurrences. This research will compare the methods possible for such fatigue estimations by experimentally testing 6061-T6 under stochastic excitation induced by a hydraulic shake table. The experimental evaluation will also delve into the methods of measuring damping for numerical model application. This will be proven to be critical for accurate calculations of the stress frequency response functions. Resonance of the structure is also included in this experimentation to ensure the damping value is critical in developing correct stress response functions. The findings from the various approaches will provide guidance for application of spectral methods of fatigue life estimation for aluminum under high cycle low stress amplitudes.

Table of Contents

List of Figures

List of Tables

Acknowledgments

I would like to acknowledge the committee members that made this research possible. Prof. Ramulu provided wonderful mentoring on every step of this life altering research project. Not only did he provide technical guidance in engineering, but also assisted in developing my technical abilities. Great appreciation is expressed for his commitment to provide leadership and direction. His investment in time and energy will be remembered for my lifetime. Larry Parfitt provided invaluable experience for shake table testing. His past projects guided the development of the test apparatus and the methods that are commonly successful. Per Reinhall provided guidance for research in the application of spectral methods of vibration testing.

I would like to also thank all of the amazing support provided by Paccar Technical Center. The resources and equipment that was provided to conduct this experiment was graciously appreciated. There are too many names to mention, however, I would like to thank all the staff support from structures lab, metrology lab, fabrication shop, and materials lab. A special thank you to Marc van Sickle for his appreciated efforts in gaining budget approval for this testing, as well as providing numerical simulation software. This experimentation was made possible by the generosity of Kenworth Truck Company for financially backing the experimental testing, as well as providing training days to conduct this research. A special thank you must be given to Ben Spiers and John Anderson for guidance in numerical and experimental methods of specimen evaluation.

Finally, I must thank the friends and family who supported and fed me (Inoue Family) through this research and documentation process. Thanks must be given to the generous proof readers: Katherine, Evan, Keiko, Angus, Adrian, and Professor Ramulu.

Chapter 1 - Introduction

Fatigue validation is crucial in today's automotive and aeronautical industries. Both industries are pushing the boundaries of innovation and are focusing on weight reduction along with robust design. Aluminum alloy provides a high strength to weight ratio at a relatively low cost. However, aluminum also presents new challenges in fatigue life estimation since non-ferrous materials do not have well-defined fatigue limits. This presents challenges on life estimation under random amplitude variable loading excitations. These vibrations are referred to as "stochastic", derived from the Greek word meaning "*pertaining to chance*". Stochastic excitation can be expressed through statics by forming a probability density of the stress range occurrences. Hence, the vibrations will include large and small stress amplitudes. Traditionally stress ranges below the fatigue limit can be filtered out of the damage calculations, however since aluminum has no well-defined limit this develops a need to delve into the high cycle low stress amplitudes fatigue estimations.

Prior to computer technology advancements, random loading fatigue testing has required components to be validated in the field under product service loads. This method necessitates extremely long validation schedules and requires components to be instrumented with strain gages to measure the time series of strain response from service loads. These experimental methods provide designers with feedback from prototype testing; however, it is quite costly and requires a long lead time to fabricate the test specimens. Technology development has recently allowed for computer controlled shake rigs to replicate the service loads. These new systems enable validation engineers to record service loads and remove events from time series data that

cause little or no damage to the material being tested. Using shake tables greatly reduces the time required to run the equivalent service loads.

In addition, Finite Element Analysis (FEA), enable products to be pre-validated using numerical simulation for fatigue damage. Leveraging these computational tools helps improve reducing the design cost and time to production. Up-front design iterations prior to physical testing, significantly reduces the time to market for new products. To develop fatigue estimation, the models require accurate system parameters namely: boundary conditions, natural frequencies, damping, and material properties. Furthermore, fatigue life estimation requires the summated error across the entire lifecycle of the part. Because fatigue damage is calculated by summation over thousands of stress cycles, the analysis and testing requires precise damage estimation for each and every analysis cycle. If individual stress cycles are not precise, the summations of errors will likely result in significant fatigue life error estimation.

Service loads typical in automotive, aeronautical, and nautical require random vibration spectrums be evaluated for determining fatigue life estimation. Numerical methods have been applied using transient frequency response models; however, thousands of data points are required for the stress history. For large models this method is not efficient or feasible with the available computing power. This research details a comprehensive numerical and experimental evaluation using stochastic spectral vibration damage analysis. To compare the results, experimental testing applies vertical vibrations on a cantilevered specimens fabricated out of 6061-T6 aluminum. Aluminum being a non-ferrous material has no well-defined fatigue limit, therefore it is challenging to evaluate fatigue under low stress high cycle vibrations. This evaluation also includes system resonance to ensure the damping coefficients are crucial in developing a physical representative numerical model. As such, it is not the focus of this

research to delve into system coefficients and properties specifically, but rather to highlight the effects of combining various mathematical models and system parameters. This research provides guidance as to the areas of analysis that are critical in building confidence of numerical simulation models and fatigue estimation methods. The aggregation of this guidance will be justified through the use of aluminum 6061-T6 specimens subjected to stochastic excitation. Specimens will be symmetrical and are simply supported beams with concentrated end masses. The natural frequencies have a large enough second mode frequency that the modes can be isolated from each other. Hence the system can be treated as a SDOF (Single degree of Freedom). It should be noted the outlined methods of spectral damage calculation also apply to MDOF (Multiple Degree of Freedom) systems. However, this research will limit the complexity to testing only a SDOF system. Excitation will be a vertical motion to develop fully reversible bending stress on the top and bottom surfaces of the cantilevered specimen. The main cross sections of the specimens taper to the minor cross section in order to minimize stress concentrations at the transition zone. Three distinct masses are applied to determine accuracy effects based on the number of cycles possible from increased stress cycles under the same random excitation load file.

Chapter 2 - Literature Review

2.1 Overview

To develop numerical damage models for stochastic vibrations it is important to have a base knowledge in vibrations and finite element modeling. Developing numerical models that respond to excitation events in the same manner as the physical specimens requires several system behavior representations. The major system characteristics are, namely: natural frequencies, energy damping, and frequency response to excitation forcing frequencies. To develop the basic understanding of these system behaviors a simplistic spatial model consisting of a mass, spring, and damper are used. The secondary area of development is the formation of stochastic vibration profiles for representing random excitation from service load applications. These stochastic vibrations occur as airplanes fly through turbulent air, automobiles driving over cobblestone roads, or boats sailing in rough seas. The stress response from these excitation loads will be used to determine the stress history for material damage calculations. Traditionally deterministic methods are applied to evaluate damage from the time series stress data, an alternate less computational extensive method will be evaluated for analysis in the frequency domain by developing spectral vibration and spectral response models. The numerical models will be validated using experimental shake table testing to tune and validate the models response. The tools to develop these analyses of stochastic vibrations will be discussed in this chapter.

2.2 Time and Frequency Domain

Stochastic vibrations consist of random frequencies and random acceleration. This time domain vibration profile can be represented by a series of sine and cosine waves at each frequency in the series. This process is named the Fourier series, of which integrates each of these waves to develop the total time series as shown in Figure 2-1, Figure 2-2, and equation

(2.1). Alternate forms of the Fourier series allows for conversion of a time domain function to frequency domain by applying equation (2.5), as well converting frequency domain to time domain is possible by use of equation (2.4). The magnitudes $|C_n|$ and phase of each wave is determined by viewing the vibration data in the so called S-plane (i.e. –jω)

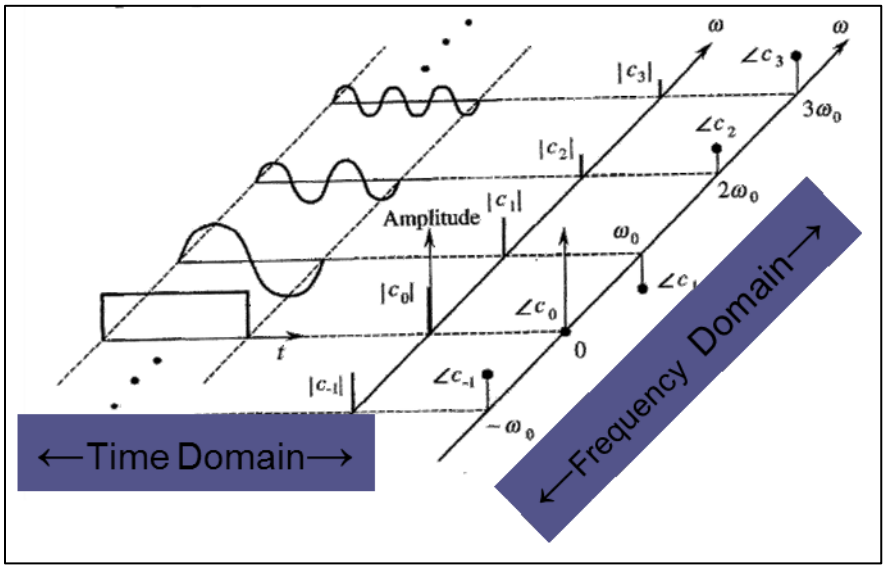

Figure 2-1 Time Domain verse Frequency Domain

Fourier
$$F(t) = \frac{a_0}{2} + \sum_{n=1}^{\infty}(a_n \, Cos \, n\omega t + b_n Sin \, n\omega t) \tag{2.1}$$

$$a_n = \frac{2}{T}\int_0^T F(t)Cos(n\omega t)\, dt \quad n = 0,1,2 \ldots \tag{2.2}$$

$$b_n = \frac{2}{T}\int_0^T F(t)Sin(n\omega t)\, dt \quad n = 1,2,3 \ldots \tag{2.3}$$

Inverse Fourier
$$X(t) = \int_{-\infty}^{\infty} X(\omega)e^{i\omega t}d\omega \tag{2.4}$$

Forward Fourier
$$X(\omega) = -\frac{1}{2\pi}\int_{-\infty}^{\infty} X(t)e^{-i\omega t}dt \tag{2.5}$$

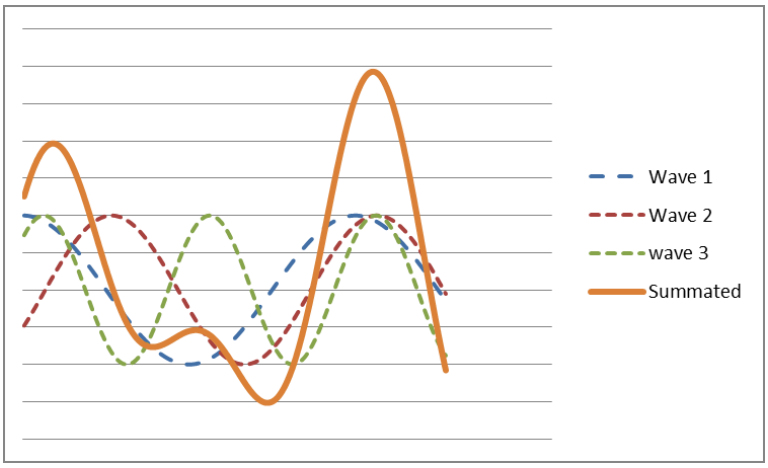

Figure 2-2 Superposition of Periodic Forcing Functions

An alternate method of calculating frequency domain form time series is by applying the Laplace transform by applying equation (2.6). Laplace function is similar to the Fourier series however instead of converting to a series of sine waves instead it applies statistics to determine the moments of the system. These moments represent the mean, variance, kurtosis of the probability distribution.

$$\mathrm{X}(\omega) = \mathcal{L}\{\mathrm{x}(\mathrm{t})\} = \int_0^\infty e^{-st} x(t) dt \qquad (2.6)$$

$$where\ s = \ \sigma + i\omega$$

2.3 Spatial Models

To understand the basic system components discussion will begin with a single degree of freedom spring, mass, and damper system. Spatial models provide a mathematical representation of the physical specimens mass, inertia, stiffness, and damping properties. These parameters are used to define an equation of motion of the system.

SDOF Free Response Methods

Figure 2-3 SDOF Vibrating System

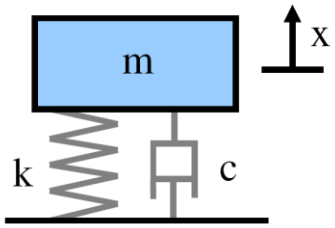

m = mass
c = damping coefficient
k = Spring stiffness
x(t) = specimen location from ordinate

Fundamental equation of motion

$$\sum \text{Forces} = \text{m}\ddot{x}$$

$$F_k + F_c = \text{m}\ddot{x}$$

$$F_k = kx$$
$$F_{kb} = c\dot{x}$$

Where: (m) is the mass, (k) is the spring stiffness, (c) is damping coefficient.

$$\text{m}\ddot{x} + c\dot{x} + kx = 0 \tag{2.7}$$

Divide by m to develop the standard form homogenous linear ODE.

$$\ddot{x} + \frac{c}{m}\dot{x} + \frac{\text{k}}{m}x = 0 \tag{2.8}$$

The characteristic equation to solve the homogenous ODE is:

$$\lambda^2 + \frac{c}{m}\lambda + \frac{\text{k}}{m} = 0 \tag{2.9}$$

Variables for viscous damping ratio (ζ), undamped natural frequency (ωn), and damped natural frequency (ωd) are defined as:

$$\omega_\text{n} = \sqrt{\text{k}/\text{m}} \tag{2.10}$$

$$\zeta = \frac{c}{2\sqrt{m\,k}} \tag{2.11}$$

$$\omega_\text{d} = \sqrt{1 - \zeta^2}\omega_\text{n} \tag{2.12}$$

The characteristic equation is now written as:

$$\lambda^2 + 2\zeta\omega_\text{n}\lambda + \omega_n^2 = 0 \tag{2.13}$$

The linear ODE will have two solutions or roots of $\lambda_{1,2}$

$$\lambda_{1,2} = -\zeta\omega_n \mp \omega_n\sqrt{\zeta^2 - 1} \tag{2.14}$$

Three cases of solutions exist (overdamped, critically damped, and underdamped).
Variables A and B below are constants that are derived by solving the boundary conditions.

Case I: Underdamped $\zeta < 1$
The roots ($\lambda_{1,2}$) of the characteristic equation are complex conjugates, corresponding to oscillatory motion with an exponential decay in amplitude

$$x(t) = e^{-\zeta\omega_n t}(A\cos\omega_d t + B\sin\omega_d t) \tag{2.15}$$

Case II: Critically damped $\zeta = 0$
The roots ($\lambda_{1,2}$) of the characteristic equation are repeated, corresponding to simple decaying motion with at most one overshoot of the system's resting position. This case yields the roots of $\lambda_1 = \lambda_2 = -\omega_n$

$$x(t) = (A + Bt)e^{-\omega_n t} \tag{2.16}$$

Case I: Overdamped $\zeta > 1$
The roots ($\lambda_{1,2}$) of the characteristic equation are purely real and distinct, corresponding to simple exponentially decaying motion.

$$x(t) = e^{-\zeta\omega_n t}\left(Ae^{-\beta t} + Be^{\beta t}\right) \tag{2.17}$$

$$\beta = \omega_n\sqrt{\zeta^2 - 1}$$

Case I: Underdamped $\zeta < 1$ **Case II: Critically damped $\zeta = 0$** **Case I: Overdamped $\zeta > 1$**

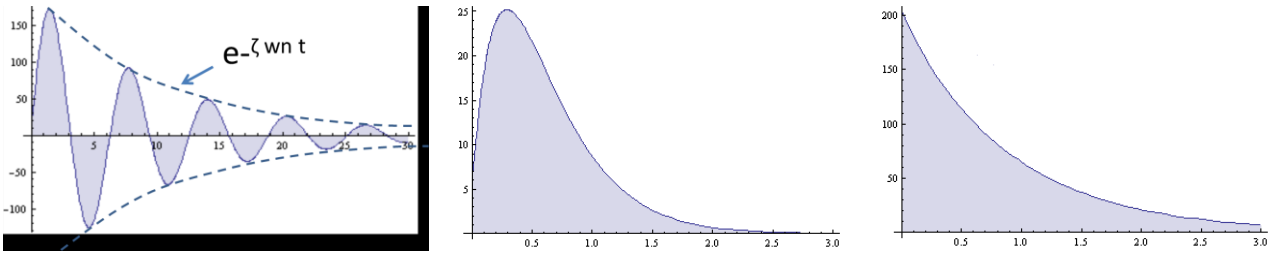

Figure 2-4 Solutions to Equation of Motion

These solutions demonstrate the effect to the response of the system from various magnitudes of the viscous damping ratio (ζ). Therefore, attention was placed upon correctly modeling damping in the numerical model. This examination will only focus on the underdamped models, since this represents the response of the test specimen

2.4 Vibration Profiles

Service loads on components may be deterministic as well as stochastic. Deterministic vibrations are specific events such as a vehicle striking a pot hole on a road, or an impulse event from an aircraft landing. To be deterministic excitation requires that at an event be determined at any given point in the data. Stochastic events are defined as steady state and random events such as: rough road surfaces, wind turbulence, engine vibrations, and ocean waves. This random loading can be represented with statistical values to represent the energy applied to the system in segmented frequency bands; this system is therefore expressed in the frequency domain instead of time domain. The functions developed using this method is called Power Spectral Density (PSD) functions. In this evaluation PSD methods are applied to evaluate fatigue estimations under these loading conditions.

2.4.1 Gaussian Probability Distribution

Random vibration must first be summarized into statistical distributions. One method is called Gaussian Probability Distribution. The probability of the occurrence of particular amplitudes are determined and expressed in a density function. The random vibration can be characterized using a mean and standard deviation to develop a probability distribution. Individual vibration amplitudes cannot be determined from this statistical distribution. Rather, the amplitudes are averaged over a large number of cycles and the cumulative effect is determined. This process enables thousands of data points to be expressed into much smaller

representative data sets which is advantageous for conveying test requirements. This function distribution is expressed as shown below.

Probability Density Function

$$f(x) = \frac{1}{\sqrt{2\pi\sigma}} e^{\frac{-(x-\mu)^2}{2\sigma^2}} \quad (2.18)$$

$$\mu = mean$$

$$\sigma = standard\ deviation$$

$$x = event\ desired\ for\ frequency\ counting\ (strain, accelration, \dots)$$

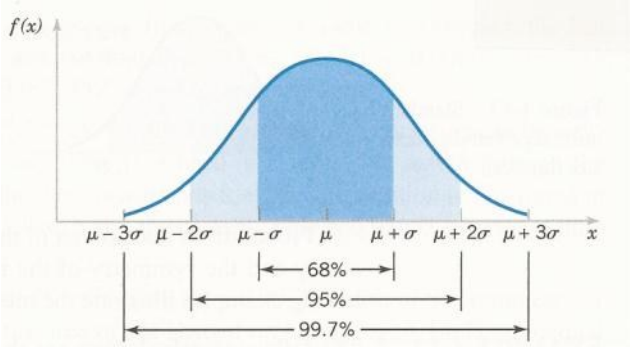

Figure 2-5 Probability Associated with a normal distribution [1]

The data is represented using a Gaussian distribution which unfortunately assumes the data is normally distributed, which can cause errors in the representation. This distribution forms a histogram of an occurrence of particular acceleration level. These bins represent the summation of frequency (occurrence) at which acceleration or strain levels are reached. This distribution is many times referred to as a zero-mean Gaussian distribution. This term was coined from the fact that the mean is centered at the zero of the histogram. Figure 2-6 demonstrates the 2D and 3D representation of the time history data.

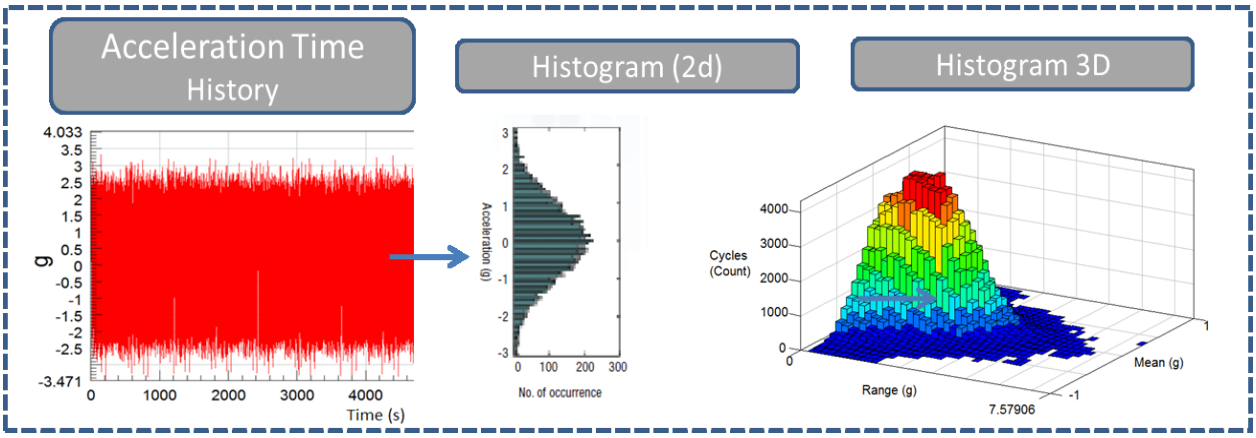

Figure 2-6 Random Vibration Statistical Distribution [2]

2.4.2 Autocorrelation Function of Random Process

A secondary commonly used approach is called autocorrelation. This time series vibration must be random stationary events in which the probability distribution for the combined events remains the same (stationary) for each time instant. Therefore, the combined mean, standard deviation, variance, and mean square are time invariant. This function is based on developing the mean value of the product of X (t_1) and X (t_2) which is expressed as $R(\tau)$ shown in Figure 2-7 and calculated by applying equation (2.19).

$$R(\tau) = E[X(t_1)X(t_2)] \tag{2.19}$$

$$\tau = |t_2 - t_2|$$

$$X(t_x)\ is\ a\ data\ point\ of\ X(t)$$

X (t) must be stationary therefore its mean and standard deviation are independent of t, therefore:

$$E[X(t_1)] = E[X(t_2)] = \mu_x \tag{2.20}$$

$$\sigma_x(t_1) = \sigma_x(t_2) = \sigma_x \tag{2.21}$$

The correlation between the two functions is express by ρ which is ±1 for a perfect correlation. If ρ=0 then no correlation exits.

$$\mu_x^2 - \sigma_x^2 \leq R_x(\tau) \leq \mu_x^2 + \sigma_x^2 \tag{2.22}$$

Figure 2-7 shows $R(\tau)$ as a function of time $\tau = |t_2 - t_2|$

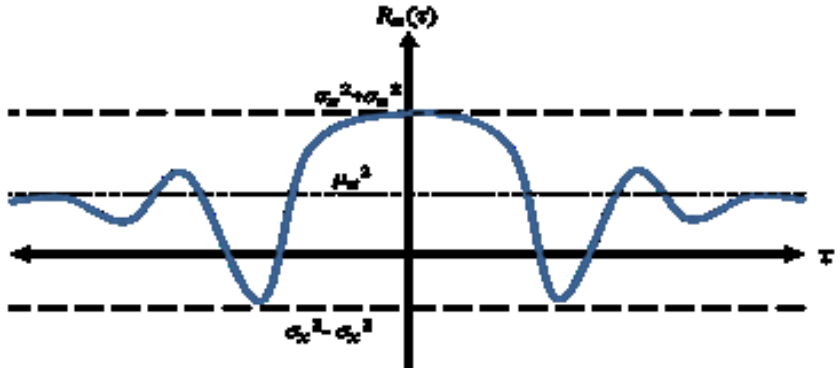

Figure 2-7 Autocorrelation function Rx (τ) of a Stationary Random Process

2.4.3 Power Spectrum Density (PSD)

Stochastic vibration can be expressed as a PSD (Power Spectral Density) function as long as the data is ergodic and a stationary Gaussian random process, the PSD function is shown in Figure 2-8. This function is a normalized density plot of the mean square amplitude of each sine wave in the frequency domain. Typical units are expressed as(g^2/Hz , σ^2/Hz). The forces on the system cannot be determined from this load profile at any one point in time. This is because the excitation is an averaged value of the magnitude of acceleration/stress measured during the initial testing used to create the PSD load file.

PSD testing does not evaluate certain magnitudes at various frequencies, but rather, looks at the total response of the system through all frequencies and amplitudes. The PSD function can be solved by applying equation (2.24) and is shown in Figure 2-8. Taking the integral of the area under the curve the Root Mean Square (RMS) of acceleration is determined as shown in equation (2.25).

The PSD function is expressed as $W_x(\omega)$

$$W_x(\omega) = 4\pi S_x(\omega) \tag{2.23}$$

The RMS of the function is expressed as $S_x(\omega)$

$$S_x(\omega) = \frac{1}{2\pi}\int_{-\infty}^{\infty} R_x(\tau)e^{-i\omega\tau}d\tau \tag{2.24}$$

Where $R_x(\tau)$ was defined in equation (2.19) as the mean value of the product of functions X (t_1) and X (t_2)

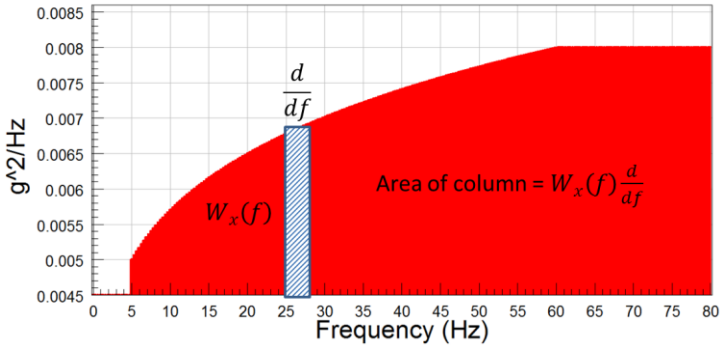

Figure 2-8 Power Spectral Density Plot – RMS stress

$$G_{RMS} = \sqrt{\int_{f1}^{f2} W_x(f)\,df} \tag{2.25}$$

2.5 Frequency Response Functions

Under excitation all structures will have a response that can be related to the excitation input. This relationship is called FRF (Frequency Response Function), an example of this is shown in Figure 2-9. Several forms of this function are used, however, only the receptance form will be highlighted for use in this research. The receptance FRF is a ratio of the displacement $X(s)$ (in frequency domain) over the force input $F(s)$ used to excite the structure. The Laplace transform equation (2.6) is used to convert the time series data to frequency domain. The spectral forms of displacement and force are then applied to Equation (2.26) to form the FRF. This ratio

is the normalized displacement that will occur under a unit load input at a chosen forcing frequency (s or ω).

$$[H(s)] = \frac{\{X(s)\}}{\{F(s)\}} \tag{2.26}$$

$$\text{s} = complex\ Laplace\ transform\ parameter (ie. -j\omega)$$

Where H(s) X(s), and F(s) are defined as:

$$\{X(s)\} = \{L(\vec{x}(t)\}\ (nx1)$$

$$\{F(s)\} = \{L(\vec{f}(t)\}\ (nx1)$$

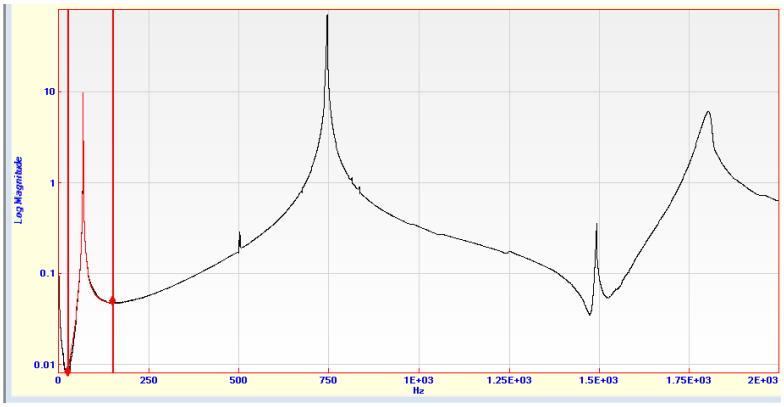

Figure 2-9 Frequency Response Function Plot

Free Response SDOF (Single Degree of Freedom) system

An FRF can be calculated by applying a forcing function to equation (2.7). Solving for the forced boundary conditions of the system allows for a forced response evaluation of $\vec{x}(t)$. Applying forcing function ($\vec{f}(t)$) and displacement response ($\vec{x}(t)$) into equation (2.26) the frequency response function can be determined. The forcing function applied is a unit load of acceleration, displacement, or force.

$$[M]\frac{d^2\vec{x}(t)}{dt^2} + [C]\frac{d\vec{x}(t)}{dt} + [K]\ \vec{x}(t) = \vec{f}(t) \tag{2.27}$$

$$[M] = Mass\ matrix\ (nxn)$$
$$[C] = Damping\ matrix\ (nxn)$$
$$[K] = Siffness\ matrix\ (nxn)$$
$$\vec{x}(t) = Displacements\ of\ the\ nth\ DOF\ (nx1)$$
$$\vec{f}(t) = Applied\ forces\ of\ the\ nth\ DOF\ (nx1)$$

$$[H(s)] = (s^2[M] + s[C] + K)^{-1}\ (nxn) \tag{2.28}$$

Free Response MDOF (Multiple Degree of Freedom) system

This SDOF system equation (2.7) can be rewritten into Multiple Degree of Freedom System (MDOF) by developing the mass matrix [M], damping matrix [C], and the stiffness matrix [K]. All of these matrix are n x n matrix were n is the number of modes in the system. This is highlighted for a basic understanding of MDOF however will not be required in this SDOF system analysis.

$$\mathrm{M}\ddot{x} + C\dot{x} + Kx = 0 \tag{2.29}$$

$$\begin{bmatrix} \mathrm{m}_1 & \cdots & 0 \\ \vdots & \ddots & \vdots \\ 0 & 0 & m_n \end{bmatrix} \begin{pmatrix} \ddot{x}_1(t) \\ \vdots \\ \ddot{x}_n(t) \end{pmatrix} + \begin{bmatrix} \mathrm{c}_1 & \cdots & 0 \\ \vdots & \ddots & \vdots \\ 0 & 0 & c_n \end{bmatrix} \begin{pmatrix} \dot{x}_1(t) \\ \vdots \\ \dot{x}_n(t) \end{pmatrix} + \begin{bmatrix} \mathrm{k}_1 & \cdots & 0 \\ \vdots & \ddots & \vdots \\ 0 & 0 & k_n \end{bmatrix} \begin{pmatrix} x_1(t) \\ \vdots \\ x_n(t) \end{pmatrix} = \begin{pmatrix} 0 \\ 0 \\ 0 \end{pmatrix} \tag{2.30}$$

SDOF Harmonic Forced Response Methods

Applying a harmonic forcing function to equation (2.7) a similar analysis can be completed. F_0 is the force applied and Ω is the excitation frequency.

$$\mathrm{m}\ddot{x} + c\dot{x} + Kx = \mathrm{F}_0 Sin(\Omega t) \tag{2.31}$$

The steady-state response $x_{ss}(t)$ of the system is assumed to be sinusoidal with the same frequency

$$x_{ss}(t) = X_0\ Sin(\omega t + \phi) \tag{2.32}$$

Substituting (2.32) into (2.31) the amplitude X_0 and phase angle ϕ can be solved

$$X_0 = \frac{F_0}{k} \frac{1}{\sqrt{(1 - r^2)^2 + 4\zeta^2 r^2}} \tag{2.33}$$

$$\phi = tan^{-1}\left(\frac{2\,\zeta\, r}{1-r^2}\right)$$

Where r is the frequency ratio ($r = \omega/\omega_n$) and the natural frequency (ω_n) and damping ratio (ζ) are from (2.10) and (2.11). From equation (2.33) the response maximum occurs when the drive frequency (Ω) equals the damped natural frequency (ωd) of the system (I.E. resonance). Equation (2.33) is reduced to equation (2.34) with the frequency ratio (r) equal to one. The effects of the damping ratio (ζ) is shown in Figure 2-10 A and B.

$$X_0(@r=1) = \frac{F_0}{k}\frac{1}{\sqrt{4\zeta^2}} \qquad (2.34)$$

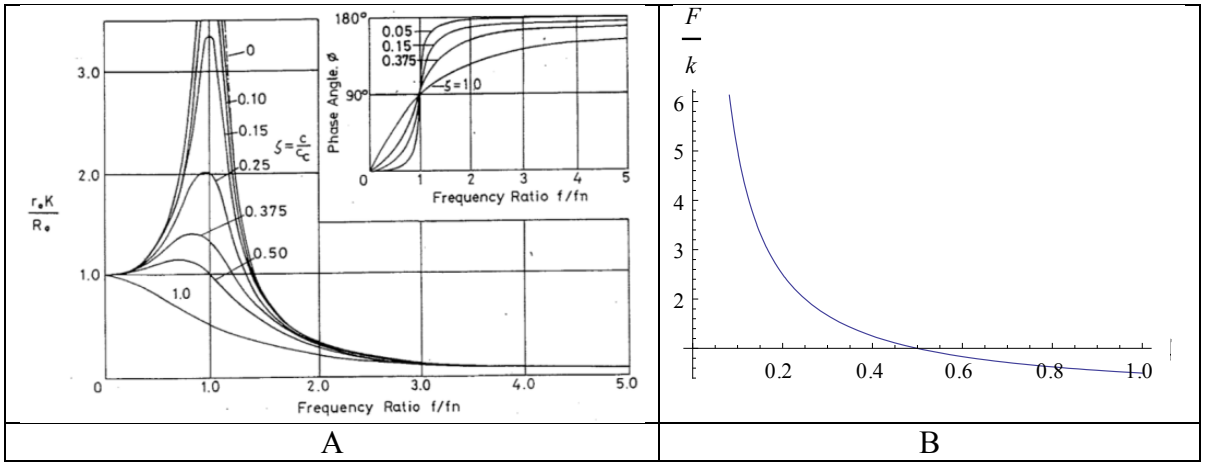

A B

Figure 2-10 Effects of Damping Ratio to Response Magnitude

The full response function can be formed by using the steady state response$x_{ss}(t)$, which is a particular solution to the homogenous equation formed from (2.31). The sum of equations (2.32) and (2.15) develops the response of the under damped case ($0 < \zeta < 1$).

$$x(t) = e^{-\zeta\omega_n t}(A cos\omega_d t + B sin\omega_d t) + X_0 Sin(\omega t + \phi) \qquad (2.35)$$

SDOF Periodic Forced Response Methods

Extending the approach used to develop equation (2.32), an equation can be established for periodic system response. The forcing function is a repeated function as used in harmonic analysis. The function repeats itself in a fixed period of time, $F(t+T) = F(t)$ and can be expanded into an infinite series of sinusoidal functions as described by the Fourier series from equation (2.6). Where, T is the length of the periodic excitation.

Formation of the underdamped system ($0 < \zeta < 1$) can be developed by summing all waves to develop equation (2.36).

$$x_p(t) = X_0 + \sum_{n=1}^{\infty} X_n \, Sin(n\omega t + \phi_n) \tag{2.36}$$

Where:

$$X_0 = {}^{a_0}/_{2k}$$

$$X_n \, Sin(n\omega t + \phi) \; is \; the \; solution \; to \; the \; homogenous \; eqn:$$

$$\mathrm{m}\ddot{x}(t) + c\dot{x}(\mathrm{t}) + Kx(t) = a_n \, Cos \, n\omega t + b_n Sin \, n\omega t$$

MDOF Arbitrary Forces Response Methods

To develop response models for arbitrary force inputs frequency response functions are used. Many different mathematical models have been developed for calculating frequency response, among which are convolution integral, Laplace and Fourier transforms. For the purpose of this examination Laplace transform from equation (2.6) will be applied to calculate frequency domain from the time domain. An arbitrary force f(t) is applied to fundamental equation of motion from equation (2.7) and expressed in (2.37).

$$\mathrm{m}\ddot{x} + c\dot{x} + kx = \mathrm{f(t)} \tag{2.37}$$

The initial boundary conditions must be set that:

$$x(0) = x_0, \dot{x}(0) = v_0$$

The Laplace transform is applied to equation (2.37) with respect to t (time)

$$\hat{\mathrm{x}}(s) = H(s)\{Mv_0 + Cx_0 + sMx_0 + \hat{f}(s)\} \qquad (2.38)$$

$$\hat{\mathrm{x}}(s) = Laplace\ transform\ of\ x(t)$$

$$\hat{\mathrm{f}}(s) = Laplace\ transform\ of\ f(t)$$

$$H(s) = (s^2 + sC + K)^{-1}$$

$$\mathrm{s} = complex\ Laplace\ transform\ parameter$$

Applying the inverse Laplace transform to equation (2.47) generates the response:

$$\mathrm{x}(t) = G(t)(Mv_0 + Cx_0) + \frac{d}{dt}G(t)Mv_0 + \int_0^t G(t-\tau)f(\tau)d\tau \qquad (2.39)$$

$$\mathrm{G(t)} = inverse\ Laplace\ Transform\ of\ H(s)(green\ impulse\ function)$$

The first two terms of equation (2.50) represent the vibration from the initial forcing function; the last term represents vibration due to external applied forces.

Modal Models

The system response to can be expressed as a modal models are a set of eigenvalues (natural frequencies) and eigenvectors (mode shapes) that describe the response of a system under no loading upon an initial impulse or displacement event. The mode shapes matrix Φ can be calculated by the below mass matrix and Stiffness matrix equations:

$$\Phi^T M \Phi = I$$

$$\Phi^T K \Phi = \bar{\omega}_r^2 \qquad (2.40)$$

$$\bar{\omega}_r = the\ natural\ frequency\ of\ mode\ nth\ of\ the\ sytem$$

$$\Phi = matrix\ of\ eigen\ vectors\ (mode\ shapes)$$

$$\mathrm{I} = Identity\ matrix$$

2.6 Experimental Damping Determination

Frequency response function can be used as well as vibration decay curve fitting to measure the system damping coefficient. To properly develop representative numerical models the correct system damping must be applied. Both free and forced response methods of measuring single degree of freedom systems damping ratio (ζ) will be reviewed in this research.

Free Response Impulse Testing

The first method applies only to single degree of freedom systems, this is performed by exciting the system by either an impulse event (IE modal hammer) or the specimen is displaced and then released to vibrate freely. A curve fit method is used to determine the decaying envelope of the response. The decay of the vibration function is defined by the $e^{-\zeta\omega_n t}$ portion of equation (2.15). The derived damping value can be calculated by using equations (2.41) and (2.42). This method is only possible for the first mode of the system.

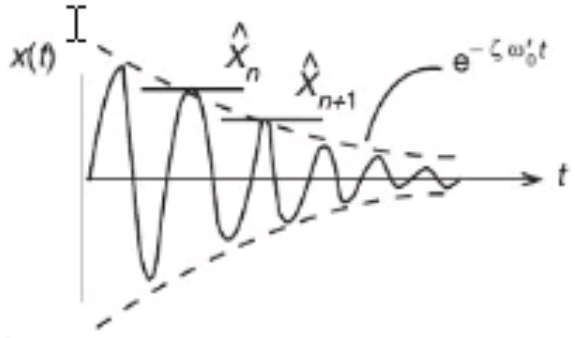

$$\zeta = \frac{\delta}{\sqrt{4\pi^2 + \delta^2}} \qquad (2.41)$$

$m = System\ mass$
$\omega_n = natural\ frequency$
$\beta_v = \ Viscous\ damping\ ccoefficient$
$k = \ System\ generalized\ stiffness\ coefficient$
$x_n = \ \ displacement\ at\ time\ n$

$$\delta = \log_e \frac{x_n}{x_{n+1}} = \frac{\pi \beta_v}{m \omega_d} = \frac{\pi \beta_v \omega_n}{k} = 2\pi\zeta \qquad (2.42)$$

Forced Response Characteristic for SDOF systems

Using forced harmonic vibration response methods, the FRF $[H(j\omega)]$ can be solved by applying equation (2.26). Applying the spectral of response displacement over the measured spectral force input the frequency response function is formed from equation (2.26). Various methods are available for damping evaluation using FRF's, for the scope of this research only one method will be discussed. Measuring the magnitude of the response peak $\widehat{H}$ and determining the width of the FRF at the root mean square values ($0.707\widehat{H}$) of the function determines the damping ratio (ζ) as shown in Figure 2-11. This process of evaluating the system damping is referred to as the half power method. The damping ratio is evaluated by solving equation (2.43) with the points $\omega_1 \; and \; \omega_2$ and the damped natural frequency (ω_d) from equation (2.12). This method can only be applied to SDOF (Single Degree of Systems), or if large frequency separation in the modes of vibration exist.

$$\hat{x}(s) = Laplace\ transform\ of\ x(t)$$

$$\hat{f}(s) = Laplace\ transform\ of\ f(t)$$

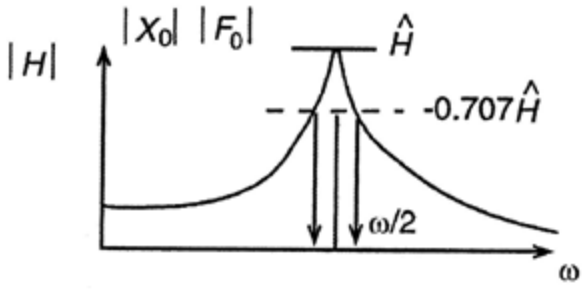

Figure 2-11 Forced Response Damping determination (modulus plot) [3]

$$\zeta = (\omega_1 - \omega_2)/2\omega_0 \tag{2.43}$$

$$\omega_1 = .707\hat{H}\ (left\ side)$$

$$\omega_2 = .707\hat{H}\ (right\ side)$$

$$\omega_0 = damped\ modal\ frequency\ @\ peak\ of\ \hat{H}$$

2.7 Numerical Methods of Damping

Various models have been developed to attempt to represent physical damping by numerical methods. The energy loss mechanisms causing damping can be difficult to determine as more than one mechanism contributes to the total damping. This value of system damping is described by a ratio of damping coefficient (C) over the critical damping value (C_c) and is called damping ratio (ζ). This ratio is also expressed as a % by multiplying the damping ratio by 100 as shown in equation (2.46). Damping coefficients may be affected by excitation amplitude, temperatures, or frequencies, meaning damping may become both frequency and mode dependent [4]. Three commonly used methods of damping will be discussed namely: viscous damping, proportional viscous damping (Raleigh), and hysteretic damping (structural).

$$\zeta = \frac{C}{C_c} \tag{2.44}$$

$$C_c = 2\sqrt{m\,k} \tag{2.45}$$

$$\text{percent damping ratio} = \zeta * 100 \tag{2.46}$$

2.7.1 Elemental viscous damping

As applied in equation (2.15), viscous damping provides for simplistic mathematical model of system behavior. The basis of this damping method must satisfy the material constitutive equation of the material. Applying the linear elastic constitutive equitation (2.47) shows that the instantaneous stress σ is proportional to the strain rate $\dot{\varepsilon}$.

$$\sigma = E\varepsilon + F\dot{\varepsilon} \tag{2.47}$$

$$E = material\ elastic\ coefficient$$
$$F = material\ strain\ rate\ coefficient$$

The solution of displacement for a SDOF system from a periodic excitation force input is given by equation (2.15)

$$x(t) = e^{-\zeta\omega_n t}(Acos\omega_d t + Bsin\omega_d t)$$

The force response of this method is investigated to determine the energy absorption per cycle

$$\mathrm{F_{vd}} = -\mathrm{C_v}\dot{\mathrm{x}} \tag{2.48}$$

$$Where:$$
$$F_{vd} = damping\ force$$
$$C_v = Viscous\ damping\ coefficient$$
$$C_c = critical\ damping\ coefficient$$

$$\dot{x} = velocity$$

Solving equation (2.9) the damping ratio (ζ) can be derived as below where it is a fractional form of the damping value or the:

$$\zeta = \frac{C_v}{2\sqrt{m\,k}} = \frac{C_v}{C_c} \tag{2.49}$$

The energy dissipated per cycle when the system is excited by a forcing function of frequency ω such that:

$$\Delta U = \pi C_v \Omega x_0^2 \tag{2.50}$$

$\Delta U =$ Change in energy in the system per cycle
$\Omega =$ forcing function frequency
$x_0 =$ amplitude of cycle n

Therefore the energy loss increases with the square of the amplitude and is directionally proportional to the frequency and damping constant. This form of damping provides for a convenient form of the equation of motion, however it is often found to correlate well with tested systems. Testing has shown that energy loss is only very weakly dependent on the excitation frequency [4]. Viscous damping frequently does not match observed behaviors of structures especially when excited to a large frequency range. As a result experimentally determining strain rate coefficients F if difficult for most materials. Alternate methods of damping are developed to attempt to improve the system modeling behavior.

2.7.2 Proportional Viscous (Raleigh) Damping

Proportional viscous damping is a subset of viscous damping that is a linear combination of the mass and stiffness matrices [equation (2.51)] and increases monotonically with frequency as displayed in Figure 2-12

$$C = \beta M + \gamma K \tag{2.51}$$

$$F_{vd} = (\beta M + \gamma K)\dot{x} \tag{2.52}$$

$Where$:
$F_{vd} = damping\ force$
$\beta =$ mass coefficient
$\gamma =$ stiffness coefficient
$\dot{x} = velocity$

Solving equation (2.9) the damping ratio (ζ) can be derived as:

$$\zeta = \frac{\beta}{2\omega_n} + \frac{\gamma}{2}\omega_n \tag{2.53}$$

It should be noted that this method causes the damping to decrease with frequency and then causes an increase in damping with increasing frequency. Figure 2-12 shows this effect when β was set to 100 and λ was set to 0.01 to demonstrate the effects of damping with frequency increasing.

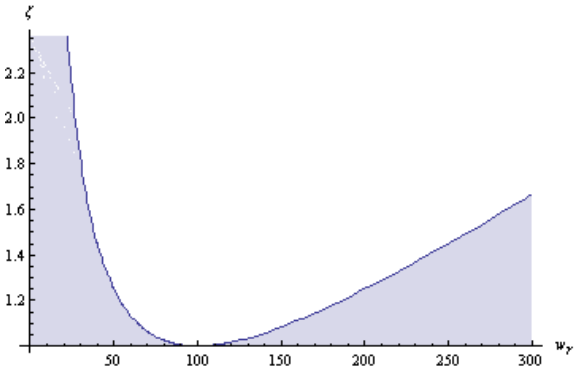

Figure 2-12 Proportional Viscous Damping (Modal Damping)

2.7.3 Structural (Hysteretic) Damping

Hysteretic damping was developed to generate a form of damping that is frequency independent. The general assumption was that the viscous damping value could be divided by the imposed forcing frequency (Ω). This method is defined by the combination of energy loss within the material and energy loss at joint and interfaces. The friction which exists in joints between components of the structure affects the damping of the parts. This can be from macro slip between adjacent parts or, more commonly, micro slip in the areas of connection between them [5]. The relationship between hysteretic damping and viscous is shown in equation (2.54). The damping ratio (ζ) for hysteretic damping is shown in equation (2.64).

$$C_{hystertic} = \frac{1}{\Omega} C_{viscous} = \frac{\gamma}{\Omega} K \tag{2.54}$$

$$\mathrm{M}\ddot{x} + \frac{\gamma}{\Omega} K\dot{x} + Kx = \mathrm{f}e^{i\Omega \mathrm{t}} \tag{2.55}$$

f = force
Ω = forcing function frequency

Considering the forced harmonic response of the system:

$$\mathrm{x(t)} = \mathrm{X}e^{i\Omega \mathrm{t}} \tag{2.56}$$

$$\dot{\mathrm{x}}(\mathrm{t}) = \mathrm{i}\Omega \mathrm{x}(\mathrm{t}) \tag{2.57}$$

These forced responses form the function:

$$\mathrm{M}\ddot{x} + (1 + i\gamma)Kx(t) = \mathrm{f}e^{i\Omega \mathrm{t}} \tag{2.58}$$

$$\gamma = \text{stiffness coefficient see (2.51)} \tag{2.59}$$

Applying the result that x(t) is harmonic at the forcing function frequency (2.43) can be written in the form:

MDOF $$[-\Omega^2 \mathrm{M} + (1 + i\gamma)K]x(\Omega) = \mathrm{f}e^{i\Omega \mathrm{t}} \tag{2.60}$$

SDOF $$[-\omega^2 \mathrm{m} + (1 + i\gamma)K]x(\omega) = \mathrm{f}e^{i\omega \mathrm{t}} \tag{2.61}$$

This method allows for the response function to have phase difference from the forcing function. A single damping value is now applied across the entire frequency range of evaluation. The force response of this method is investigated to determine the energy absorption per cycle.

Hysteretic Damping $$\mathrm{F_{sd}} = \frac{-\mathrm{C_h}\,|\mathrm{x}|\dot{\mathrm{x}}}{|\dot{\mathrm{x}}|} \tag{2.62}$$

Where:

$F_{sd} = Histeretic\ damping\ force$
$C_h = \ Histeretic\ damping\ constant$
$x = \ displacement$
$\dot{x} = \ velocity$

Equation (2.62) is only applicable under steady state excitation. The nature of this damping medium prevents it from use in transient analysis [4]. The energy dissipated per cycle then becomes:

$$\Delta U = \pi\, C_h\, {x_0}^2 \tag{2.63}$$

$\Delta U = Change\ in\ energy\ in\ the\ system\ per\ cycle$
$C_h = \ hystertic\ damping\ ccoefficient$
$\Omega = \ forcing\ function\ frequency$
$x_0 = amplitude\ of\ cycle\ n$

Hence the energy loss increases with the square of the amplitude, is independent of frequency and is directly proportional to the damping constant. When the system is excited by a harmonic motion the hysteretic damping value can be directly related to the viscous damping factor by:

$$\zeta = \frac{C}{2\omega_n \Omega} \tag{2.64}$$

2.8 Numerical Stress Response from Excitation

Frequency response of numerical models is performed by applying forcing functions to equation motion of the system. Applying the methods described in section 2.5 the systems frequency response function can be formed. From this function the stresses caused by the system displacements allow for the stress transfer function $H(\omega)$ equation (2.65) to be solved

$$[H(\omega)] = \frac{\{\sigma(\omega)\}}{\{g(\omega)\}} \tag{2.65}$$

Where $\{\sigma(\omega)\}$ is the spectral response stress from the excitation acceleration input $\{g(\omega)\}$. This function is the normalized stress response from typically 1g of acceleration, however force, or displacement may be used.

Finite Element Stress FRF

To develop this stress response function $\{\sigma(\omega)\}$ the principal stress or the eigenvalues from the stress tensor matrix must be solved as shown in equation (2.66). Stress transfer functions require a single stress value $\sigma(\omega)$, therefore the principal stress matrix is reduced to a 1x1 by applying either von-Mises (2.68) , Tresca (2.69), or absolute maximum principal (2.70) yield criterion. An example of the stress transfer function can be seen in Figure 2-13.

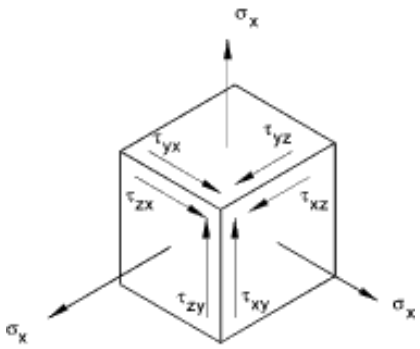

$$\begin{bmatrix} \sigma_x(\omega) & \tau_{xy}(\omega) & \tau_{xz}(\omega) \\ \tau_{xy}(\omega) & \sigma_y(\omega) & \tau_{yz}(\omega) \\ \tau_{xz}(\omega) & \tau_{yz}(\omega) & \sigma_z(\omega) \end{bmatrix} \tag{2.66}$$

Principal Stress Matrix $$\begin{bmatrix} \sigma_1(\omega) \\ \sigma_2(\omega) \\ \sigma_3(\omega) \end{bmatrix} \tag{2.67}$$

$$\sigma_{von-mises}(\omega) = \sqrt{\frac{1}{2}(|\sigma_1(\omega) - \sigma_2(\omega)|^2 + |\sigma_2(\omega) - \sigma_3(\omega)|^2 + |\sigma_3(\omega) - \sigma_1(\omega)|^2)} \tag{2.68}$$

$$\sigma_{Tresca}(\omega) = max(|\sigma_1(\omega) - \sigma_2(\omega)|, |\sigma_2(\omega) - \sigma_3(\omega)|, |\sigma_3(\omega) - \sigma_1(\omega)|) \tag{2.69}$$

$$\sigma_{max}(\omega) = max(|\sigma_1(\omega)|, |\sigma_2(\omega)|, |\sigma_3(\omega)|) \tag{2.70}$$

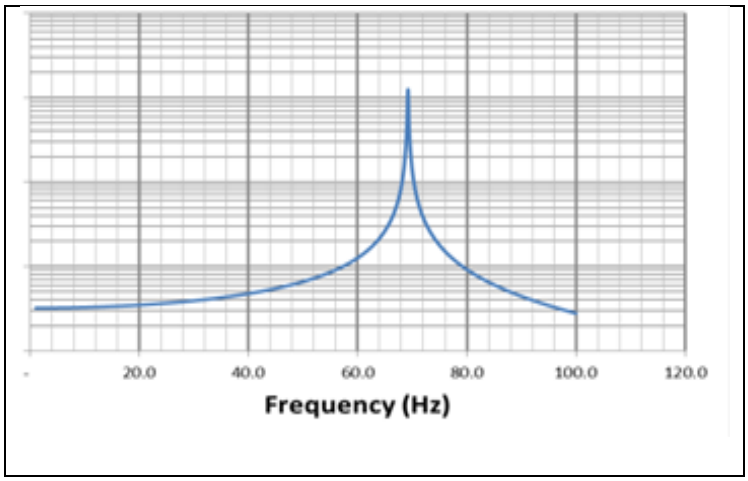

Figure 2-13 Stress Transfer Function

Doyle [6] and Gopalakrishnan [7] have applied this approach to determine finite element spectral functions with good results. Sondipon [8] has stated, " This method does not employ eigenfunction expansions and , consequently , a major step of the traditional finite-element analysis, namely, the determination of the natural frequencies and mode shape, is eliminated, which automatically avoids the errors attributable to series truncation: this makes the method attractive for situations in which a large number of modes participated in vibrations".

Excitation Stress Response Formulation

Frequency domain evaluation of the system response under frequency domain excitation is possible by applying the stress transfer function $H(\omega)$ to generate a response stress PSD. This is formed by the relationship of the nodal stress invariant $H(\omega)$ and applied load$W(\omega)$. Developing this stress PSD $G(\omega)$ for a single input load PSD $W(\omega)$ can be accomplished by multiplying the input PSD by the transfer function by applying equation (2.71), this process can be seen in Figure 2-14 as well.

$$G(\omega) = |H(\omega)|^2 \cdot W(\omega) \tag{2.71}$$

$$G(\omega) = Stress\ PSD\ \ ((MPa)^2/Hz)$$

$$H(\omega) = Stress\ transfer\ function -\ equations\ \ (2.68) or\ (2.69) or (2.70)$$

$$W(\omega) = PSD\ load\ profile$$

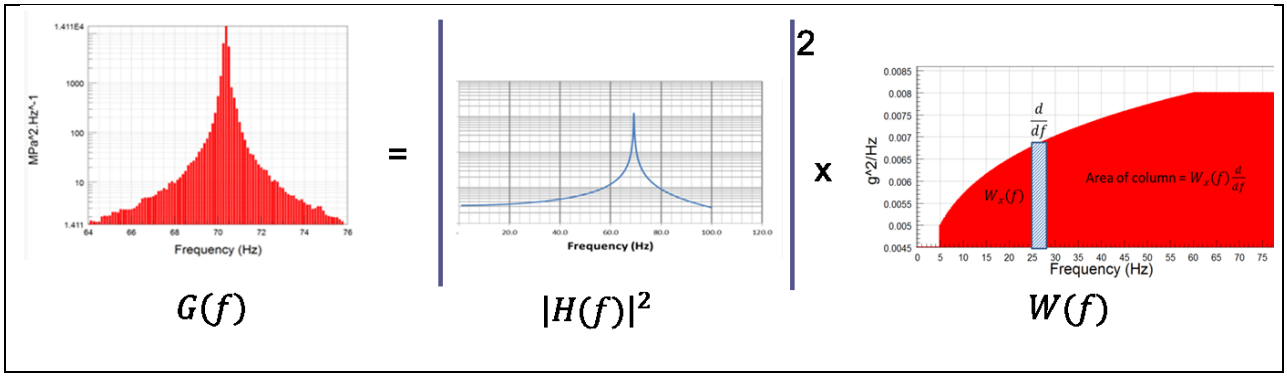

Figure 2-14 Stress PSD Generation Process Map
$\omega=2\pi f$

2.9 Cyclic Stress Counting and Damage Estimation Methods

Fatigue damage has typically been evaluated in the time domain using the stress cycles directly. The outlined method instead uses frequency domain to statistically evaluate occurrences of stress ranges from a stochastic excitation. Spectral methods of stress cycle counting will be based on using PSD (Power Spectral Density) functions for the vibration input. This research will examine the use of statistical methods to determine the occurrences of stress range cycles from a probability density function (equation (2.18) . First the deterministic rainflow stress counting method will be discussed to provide clarity on the intended spectral methods.

2.9.1 Determinant Stress loading Rainflow

The first step in stress counting of determinant time series data is to remove stress events which do not significantly add to the damage. This process is called rainflow counting .This process can be seen in the below Figure 2-15. Point D-E and G-H are filtered out as the range of stress does not add significant damage. Additionally filters can be applied to remove stress ranges that are below the fatigue limit of the material. From this filtered set of data stress-strain

hysteresis loops can be formed to calculate damage to the material. The details of this method can be found in references [9], [10], and [11] amongst many other published papers on this topic. For this research we will not delve into the details as this method is not applied for PSD methods of fatigue damage.

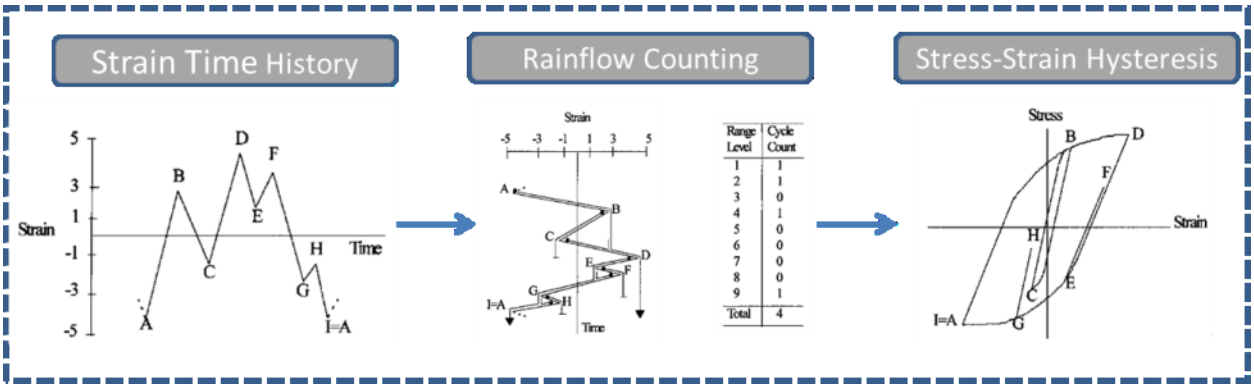

Figure 2-15Time Series - Rainflow Counting

2.9.2 Stochastic Stress loading Rainflow

Stress can be represented in PSD functions for stochastic load cycles as discussed in section 2.4.3 (steady-state and random in nature). Standard rainflow cycle counting is not applicable directly from the PSD stress results. If direct stress-strain damage is desired from the stress PSD stress $G(f)$ applying the Inverse Fourier Transformation could be applied to convert back into time series data. This requires that the loading is assumed to be ergodic stationary Gaussian and random. This method is computational intensive therefore methods of damage calculation directly from PSD stress functions are developed by Bendat [12] , Dirlik [13], Lalanne [14], and Rice [15]. The methods developed are dependent upon the signals bandwidth. An irregularity factor (λ) was later developed by Lalanne compensate for the data bandwidth measured. If the bandwidth is a narrow band the irregularity factor is near 1 at which time

equation (2.76) can be used. If the bandwidth is a wide band signal then the result is near zero therefore equation (2.77) or (2.78) shall be applied.

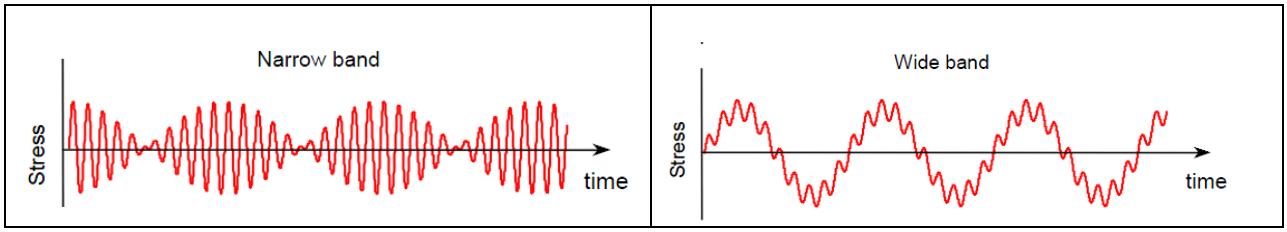

Figure 2-16 Signal Types: Narrow Band - Wide Band

To develop the damage models statistics are applied to determine the moments of the probability density function $G(\omega)$by applying equation (2.72).

$$M_j = moment\ of\ the\ area\ of\ the\ PSD$$

$$moment\ of\ the\ area\ of\ the\ PSD \quad M_j = \int_0^{\infty} f^j G(\omega) df \tag{2.72}$$

$$M_0 = Raw\ moment$$
$$M_1 = Mean$$
$$M_2 = Variance$$
$$M_4 = Kurtosis$$

Where $f^j$is the frequency of block segment being calculated and j being the moment parameter. $G_x(\omega)df$ is the area of each block, each of the block values are summed to calculate the total moment (M_j) of the function. An example of the calculation is in Appendix B. Probability density functions moments are used statistically evaluate the expected level crossings $E[0^+]$ from equation (2.73) as well as the number of peaks $E[P]$ in the function as derived by equation (2.74).

$$E[0^+] = \sqrt{\frac{M_2}{M_0}} \tag{2.73}$$

$$E[P] = \sqrt{\frac{M_4}{M_2}} \tag{2.74}$$

Additionally the function irregularity factor (γ) is developed to account for signal bandwidth.

$$\gamma = \sqrt{\frac{M_2^2}{M_0 M_4}} \tag{2.75}$$

These developed parameters are applied to various methods of spectral damage modeling developed by Dirlik [13] , Lalanne, and Rice [14]. The three analysis methods are shown below

$$N_i = \#\ of\ cycles\ in\ stress\ range\ (stress\ \text{min}\ to\ stress\ \text{max})$$

$$E[P] = expected\ number\ of\ stress\ or\ strain\ peaks$$
$$T = time\ period\ of\ evaluation\ (s)$$
$$S = Stress\ Range\ {}^{N}/_{mm^2}$$

Bendat Narrow Band (1964) [12]

$$N_i = E[P] * T * \int_{stress\ min}^{stress\ max} \frac{S}{4\,m_0} e^{\frac{s^2}{8\,m_0}}\, ds \tag{2.76}$$

Dirlik Method (1985) [13]

$$N_i = E[P] * T * \int_{stress\ min}^{stress\ max} S * P(S)\, ds \tag{2.77}$$

$$P(S) = \frac{\frac{D_1}{Q} e^{\frac{-Z}{Q} * S} + \frac{D_2 Z}{R^2} e^{\frac{-Z^2}{2R^2} * S^2} + D_3 Z e^{\frac{-Z^2}{2} * S^2}}{2\sqrt{M_0}}$$

$$Z = \frac{1}{2\sqrt{M_0}} \qquad \gamma = \frac{M_2}{\sqrt{M_0 M_4}} \qquad X_m = \frac{M_1}{M_2}\sqrt{\frac{M_2}{M_4}} \qquad R = \frac{\gamma - X_m - D_1^2}{1 - \gamma - D_1 - D_1^2} \qquad E[P] = \sqrt{\frac{M_4}{M_2}}$$

$$D_1 = \frac{2(X_m - \gamma^2)}{1 + \gamma^2} \qquad D_2 = \frac{1 - \gamma - D_1 + D_1^2}{1 - R} \qquad D_3 = 1 - D_1 - D_2 \qquad Q = \frac{1.25(\gamma - D_3 - D_2 R)}{D_1}$$

Lalanne Method (2002) [14]

$$N_i = \frac{1}{rms}\frac{\sqrt{1-\gamma^2}}{\sqrt{2\pi}} * \int_{stress\ min}^{Stress\ max} e^{\frac{-S^2}{2rms^2(1-\gamma^2)}} + \frac{S*\gamma}{2rms}\left[1 + erf\left(\frac{S*\gamma}{rms\sqrt{2(1-\gamma^2)}}\right)\right] ds \tag{2.78}$$

$$\text{erf}(x) = \frac{2}{\sqrt{2\pi}}\int_0^x e^{-t^2} dt$$

$$\gamma = irregularity\ factor = \frac{M_2}{\sqrt{M_0 M_4}} \quad \text{(adjusts for bandwidth of measurement)}$$

$$S = Stress\ Range\ {}^{N}/_{mm^2}$$

$$rms = .707$$

Work by Halfpenny [16] has shown in Figure 2-17 that these methods of applying probability density functions correlate well with the time series methods of stress counting with a high slope value on the SN material curve. The various methods converge as the irregularity factor (λ) from equation (2.79) nears one for both a small and large SN slope values.

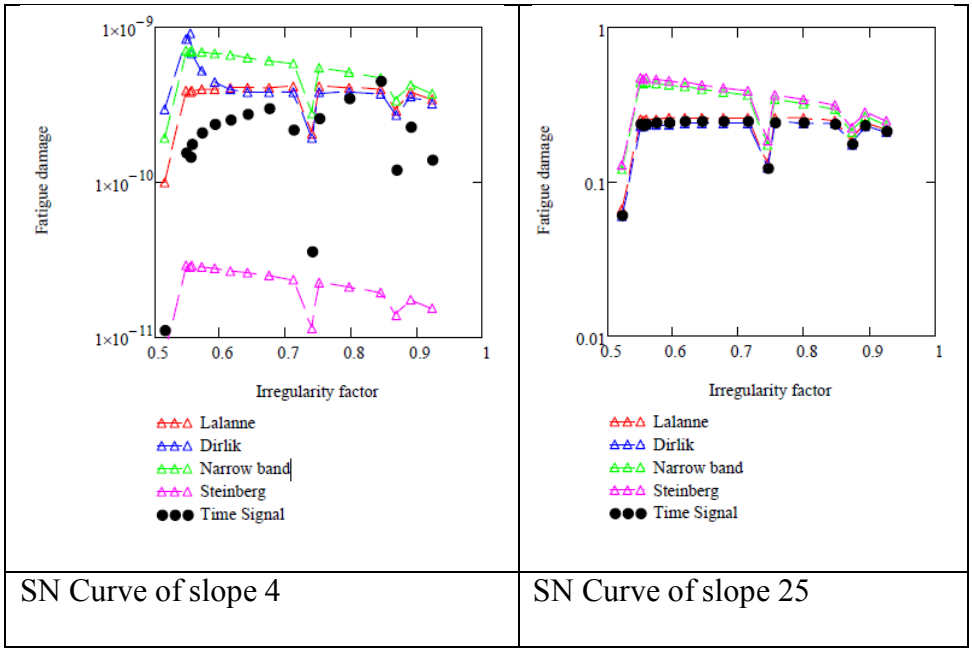

SN Curve of slope 4	SN Curve of slope 25

Figure 2-17 Damage Model Accuracy vs. Irregularity vs. SN slope [16]

2.9.3 Palmgren-Miner's Rule: Stress/Strain damage

The damage calculation for the determinate loading can be evaluated by applying the Palmgren-Miner's rule. The method uses defined functions of material fatigue life based on the number of cyclic loadings the material can survive under constant amplitude of either stress/strain. These material property curves are called Stress Life (S-N). The Palmgren-miner's rule leverages this principle to evaluate the total life under various stress/strain loadings. Where n_i is the number of cycles that occurred at the stress range value and N_{fi} is the total number of allowed cycles at that stress range. When each of these fractional damages is summated it equals the total damage the loading event caused. Ultimate failure occurs when the damage summation equals 1. Also this analysis can be converted to the reciprocal of the damage which is the number of cycles that can be completed before the specimen will fail. This process is demonstrated in Figure 2-18.

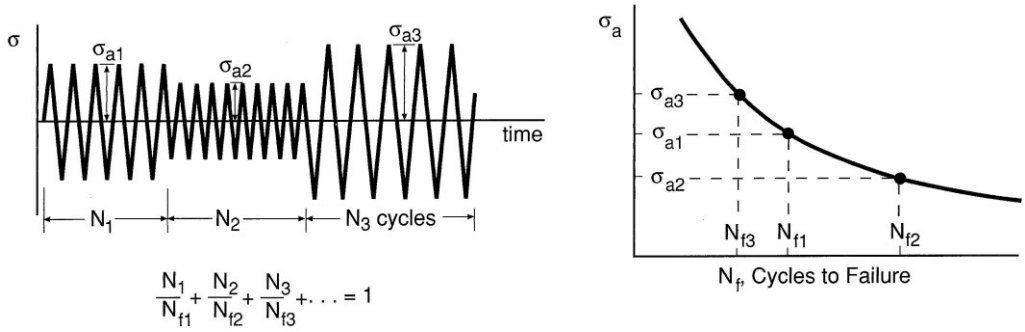

Figure 2-18 Palmgren-Minor Stress Damage Counting [17]

$$Failure = \sum_{i=1}^{m} \frac{n_i}{N_{fi}} \geq 1 \tag{2.79}$$

$$Individual\ stress\ cycles\ damage = \frac{n_i}{N_{fi}}$$

2.10 Fatigue Properties of 6061-T6

Fatigue damage occurs from cyclic loading below the yield strength of a material causing progressive and localized structural damage. The factors that significantly influence fatigue resistance are surface finish, material flaws, and specimen geometry. This change in fatigue resistance in turn affects S-N curves. In order to numerically determine fatigue damage the correct S-N fatigue curve is required. Reviewing various published S-N data for 6061-T6 it was determined that the differences in S-N curves are significant as shown in Table 2-1 and Figure 2-19. The method of experimental testing has significant effect on the formation of the S-N curve. Rotating bending tests induce cyclic stress around the circumference of the specimen. Whereas, axial loading induces cyclic stress on the entire cross sectional area of the specimen. Each of methods applied for the S-N curves evaluated are listed in Table 2-1.

Table 2-1 6061-T6 Published Material Properties

6061-T6 Material Properties	MIL-HDBK-5J	Steinberg 2nd Edition, 1988, John Wiley & Sons	6061-T6 Yahr Published Values Reversed bending
Yield Strength (MPa)	276	265	262
Ultimate Strength (MPa)	310	305	290
Elastic Modulus (MPa)	6.89E+04	7.17E+04	6.89E+04
Stress Intercept - SRI1	564.5	652	490.5
First Fatigue Strength Exponent - b1	-0.102	-0.0921	-0.135
Stress value @ 1E8 cycles (MPa)	119	86.6	21.9
Sample Cross Section	5mm	Not documented	Not documented
Method	Axial Loading	Reversed Bending	Reversed Bending
R value	R=-1	R=-1	R=-1

R is the stress ratio of the specimen loading defined by

$$R = \frac{\sigma_{min}}{\sigma_{max}} \tag{2.80}$$

R= -1 is fully reversed stress (mean stress = zero)

R=0 is zero to tension stressing

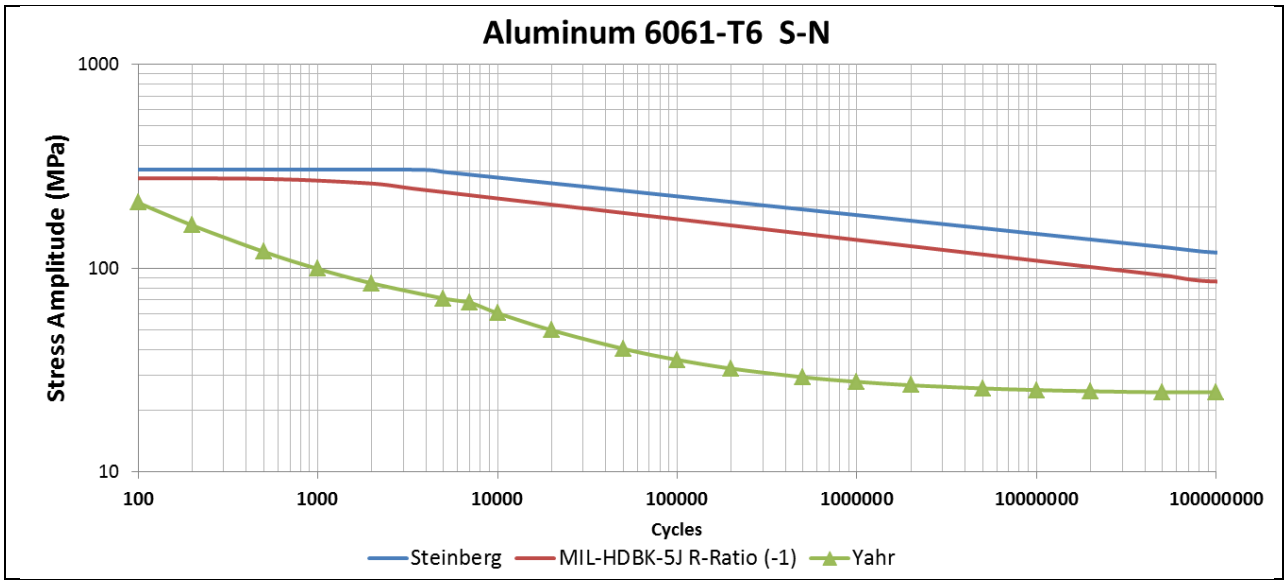

Figure 2-19 Aluminum 6061-T6 S-N curves [18], [19], [20]

Fatigue testing by Yhar [20] on Aluminum 6061-T6 determined aluminum exhibited no well-defined endurance limit. This imposed a challenge when applying the best fit equation method that was introduce by code section III criteria document [21]. Yhar was able to apply equation (2.81) to develop a best fit curve. The challenge was determining the value for B as this is the endurance limit (S_e) which does not exist for aluminum. Yhar the applied 96.5MPa for the value of B as this was the experimental best fit value. The A value was the percentage reduction in area of a tensile specimen.

$$S = \frac{E}{4\sqrt{N}} \ln\left(\frac{100}{100 - A}\right) + B \tag{2.81}$$

$$E = modulus\ of\ elasticity$$
$$N = number\ of\ cycles\ to\ failure$$
$$S = strain\ amplitude\ times\ elastic\ modulus$$
$$A\ \&\ B = Curve\ fit\ Correction\ factors$$

Yahr determined calculated the zero mean stress best fit equation for 6061-T6 Aluminum to be:

$$S = \frac{14{,}479}{\sqrt{N}} + 96.5\ \text{Mpa} \tag{2.82}$$

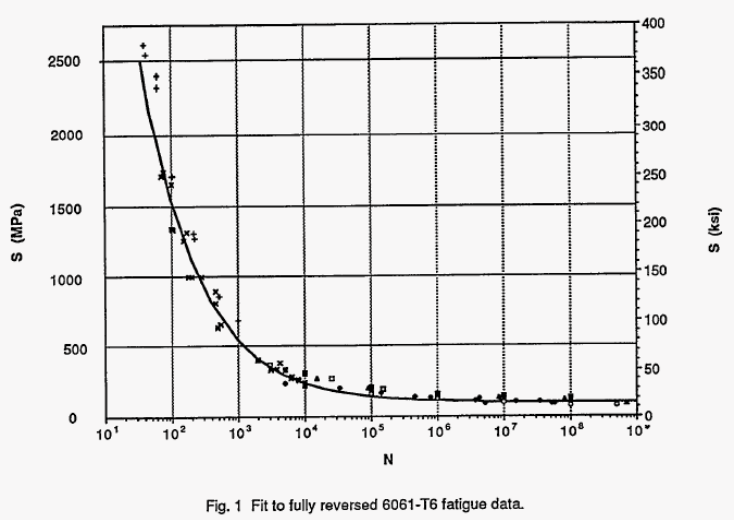

Figure 2-20 6061-T6 SN Curve [20]
**For tabulated data see Appendix D, Table 7-11*

Yahr constructed a design curve that reduced the stress factor by 2 or the number of cycles to failure by 20. This curve fit therefore will not be used in the numerical calculations. The design curve was truncated at twice the yield strength to prevent significant strain accumulation. Figure 2-21 below shows the resulting design life curve formulated. The Raw data for his Yahr's finding are in Appendix D, Table 7-11.

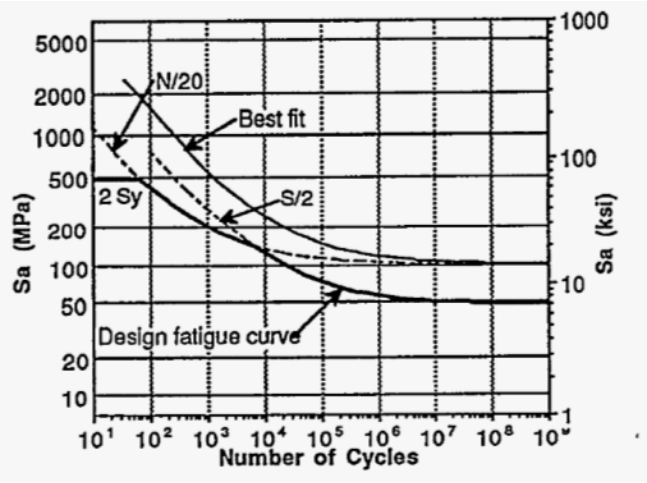

Figure 2-21 6061-T6 SN Design Curve [20]

Other methods of such as the Goodman equation or Gerber equation are developed for functions that have non-zero mean stress functions.

Fatigue life is affected by variations in surface finish, surface treatment, temperature, manufacturing process, heat treatment, etc. The required S-N curves that would be needed to encompass all of these factors are not practical. Therefore a modified S-N line can be developed to compensate for these associated parameters($m_{surface}, m_{size}, m_{load}, etc.$). Figure 2-22 demonstrates the modified S-N curve as calculated by equation (2.83).

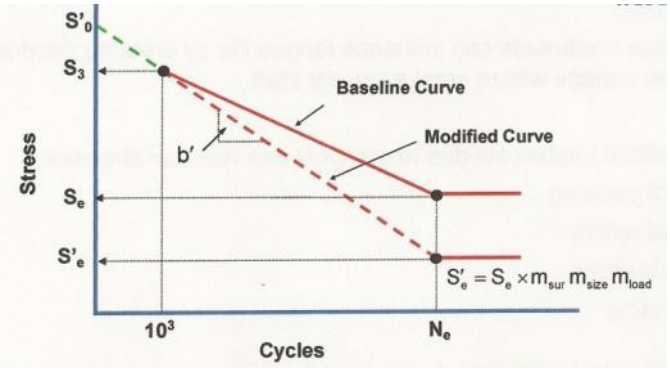

Figure 2-22 S-N offset Curves [22]

Modified Line $$S = S'_0 * N^b \quad (2.83)$$

$$S'_0 = S_3(1000)^{b'} \qquad Modified\ Intercept$$

$$b' = \frac{logS'_e - logS_3}{logN_e - 3} \quad Modified\ slope$$

$$S_3 = stress\ value\ at\ 10^3\ cycles\ of\ SN\ curve$$

$$S'_0 = Stress\ \ intercept$$

$$S'_e = Endurance\ stress$$

$$N_e = Cycles\ at\ fatigue\ endurance\ stress\ S'_e$$

$$N = Cycles$$

Experiments by Kauffman [23] were conducted on the effects of surface finish. Kauffman applied a rotating beam test using 6061-T6 rolled and drawn rod to develop the S-N curve of sharply notched specimens. From this testing the effects of residual stress and stress risers on the surface from notches or machining marks have great influence on the available stress levels per cycles (N) to failure. A range of about 20-35% reduction in stress allowed at N cycles can be noted in Figure 2-23.

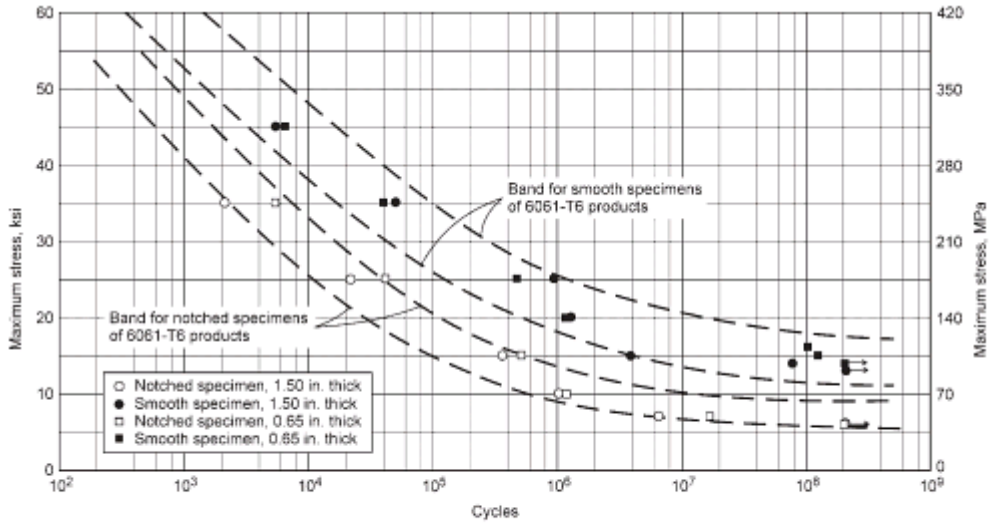

B11 Rotating-beam ($R = -1.0$) fatigue curves for 3/4 in. diam 6061-T91 rolled and drawn rod, smooth and sharply notched specimens, effect of drawing. Stress concentration factor, $K_t = 12$.

Figure 2-23 Effect of Surface Finish on 6061-T6 Fatigue Curves [23]

Research by Colakoglu [24] determined the largest factors on damping for aluminum are frequency, amplitude of strain or stress, and temperature. In addition, damping is affected by corrosion fatigue, grain size, and porosity. If the maximum stress amplitude is over the critical stress level, damping increases permanently with the number of fatigue cycles. Figure 2-24 below is the resulting data of the measured damping factors vs. number of fatigue cycles. The linear curve-fit of the measured results (solid lines) up the crack initiation are shown for the first

mode (59.9 Hz) of the test specimen as listed in Table 2-2. Above a critical stress level, plastic strain damping occurs, even though the stress amplitude may be within the elastic limit. Damping was shown to not only be a function of the stress amplitude but also the number of fatigue cycles above a certain stress level. The research performed by Colakoglu will be relevant for the alteration of the damping values as cycles are completed on the test specimens conducted in this research.

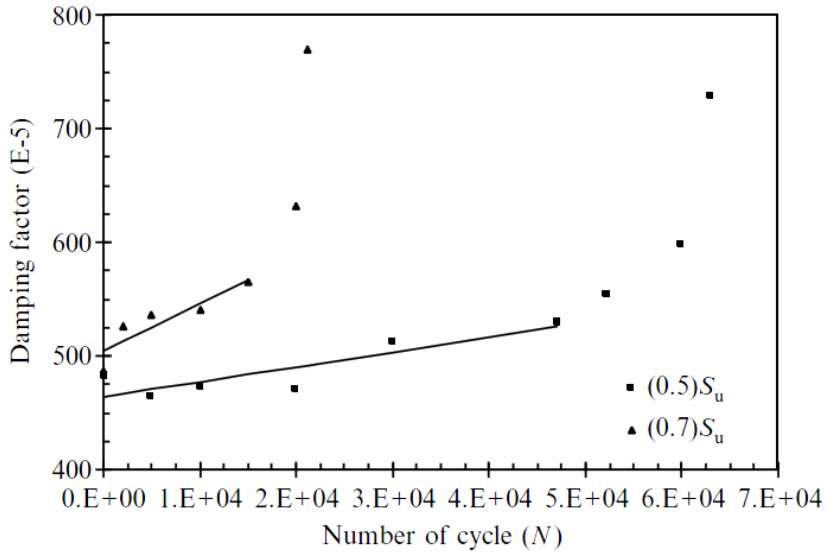

Figure 2-24 Damping factors of 6061-T6511 Al alloy under bending vibration load. [24]

$$S_u \propto Damping\ factor$$

$$S_u \propto Damping\ factor \frac{d}{dN}$$

Colakoglu tested the first the bending mode of the 6061-T6 specimens and determined the damping values of the specimens before fatigue cycles are as listed in Table 2-2.

Table 2-2 Modal Damping Values 6061-T6 [24]

Material	f_1 (Hz)	ζ_1 (10^{-5})	f_2 (Hz)	ζ_2 (10^{-5})	f_3 (Hz)	ζ_3 (10^{-5})
6061-T6511 Al alloy	59.9	480	168.9	152	308.5	92

2.11 Summary

This section has reviewed the methods in which cyclic damage can be determined from stochastic events. This approach is shown to be applicable for both numerical as wells as experimental approaches. The development of the specimens Frequency Response Function (FRF) enables spectral methods of stress response from load functions (PSD's) to determine the damage by application of statistical evaluation of damage under stochastic load events. Spectral damage presents benefits over traditional time series methods of which are: reduced mathematically intensive calculations, and greatly reduces the amount of data required to specify design load requirements. Because of these advantages PSD vibration design requirements are becoming more prevalent. As well the use of numerical simulation of fatigue is becoming widely used to reduce the cost of testing and time to market of aerospace and automotive products. Therefore, there is a need to research the best methods for numerical approaches compared to experimental testing.

Chapter 3 - Objectives

This research provides guidance to the areas of analysis that are critical in building confidence of numerical simulation models for spectral calculation of fatigue damage under high cycle low stress amplitude stochastic vibrations. The aggregation of this guidance will be justified through the use of aluminum 6061-T6 specimens subjected to stochastic loading. Therefore, the objectives of this research are as follows:

1. Evaluate the most representative method for determining damping values for structures under stochastic loading.
2. Determine the accuracy of applying spectral methods of counting stress cycles from PSD (Power Spectral Density) stochastic vibrations.
3. Validate numerical fatigue simulation models under random spectral vibration to physical shake table durability testing under an equivalent time domain loading for aluminum 6061-T6 specimens.
4. Develop guidance on the combination of mathematical models that provide the highest accuracy for fatigue life estimation.

Chapter 4 - Experimental and Numerical Methods

4.1 Materials

The research conducted used test specimens constructed of Aluminum 6061-T6. The test specimens used various sized cantilevered masses that will be constructed of Steel A-36. The material properties for each of these are in Table and Table 4-2.

Table 4-1 Test Sample Material Properties - Aluminum 6061-T6 [19]	
Yield Strength	276 MPa
Ultimate Strength	310 MPa
Modulus of Elasticity	68.9 GPa
Elastic Poisson's Ratio	0.3
Density	2.77 g/cc

Table 4-2 Test Mass Material Properties - Steel ASTM A-36 [25]	
Yield Strength	250 MPa
Ultimate Strength	475 MPa
Modulus of Elasticity	200 GPa
Elastic Poisson's Ratio	0.3
Density	7.85 g/cc

4.2 Design of Test Specimens

Developing the geometry of the test specimens required iterative calculation steps. A critical portion of this testing is evaluating the effect of damping on the stress response. Since damping has the most effect at the natural frequency as shown in the Figure 2-10A the specimens were designed to have natural frequencies in the 0-80Hz planned test frequencies. Parametric models are created for a cantilevered beam with a mass attached at the free end. The specimen parameters that are adjusted to develop the desired natural frequencies are: specimen length, cross sectional area, and the size of the cantilevered masses. Part of this research was to develop an S-N curve from the fatigue results. Therefore, the added masses must have enough separation in the resulting stress to produce the SN. The goal was to have the cycles in the range of 400k to

1M cycles. It was determined that approximately twenty percent difference in the masses would provide an adequate stress range.

4.3 Test Specimens Fabrication

The test samples and shake table mounting apparatus are designed specifically for this validation test. The setup was designed to allow for twelve samples to be mounted to the shake table at one time. There are twelve of each test configuration fabricated to make a total of thirty-six data points, four additional specimens were manufactured for the mounting of strain gages. The test setup and specimens were manufactured at Paccar Technical Center's machine shop in Mt. Vernon, Washington.

Test Specimen Fabrication

The vibration test specimens are fabricated from four 3.65M long by 25.4mm round bars of extruded 6061-T6 aluminum. A total of 40 parts were machined using a manually operated center lathe. A trace template was used to automate the manufacturing of the radius and minor diameter of the test specimens. The feed rate and radius of the tool were selected to ensure the desired surface finish of a R_a value of 3.2μm was achieved. The approximate surface finish can be determined by applying the equation $\mathrm{Ra} = f^2/32r$ where f is the feed rate of the cutting tool and r is the radius of the cutting tool. The ends of the specimens are cut to finalize the length of the part. Samples are then mounted in a vertical mill and the flat faces are machined tangent to the part. Two holes are machined at each end of the specimen, two of which are threaded for mounting of test masses to the cantilevered end. These flat faces and holes are designed to mount the test specimens to the shake table fixture. Dimensions of the specimen are found in Figure 4-1, as well final machined examples are displayed in Figure 4-2.

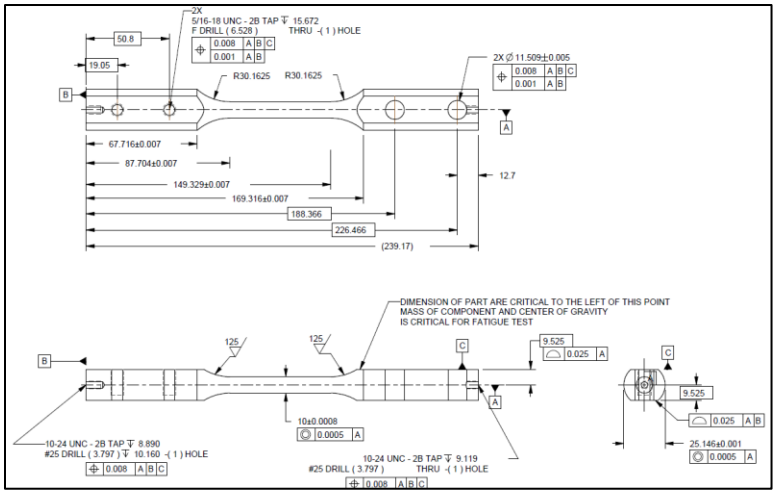

Figure 4-1 Vibration Test Sample Dimensions

Figure 4-2 Test Specimens - Completed Fabrication

Nine of the specimens are placed back in the lathe and emery cloth was used to polish the samples to a mirror finish. These sets of specimens were polished in the expected failure location and are to be used to determine baseline data. The surface profile parameters are measured using a Mitutoyo CS-5000 CNC3V-3100 series surface tactile analyzer [26]. Each sample was measured along the top edge as shown in Figure 4-3 to determine the roughness in the area of expected fracture. The values determined for both the polished and unpolished samples are shown in Table 5-5.

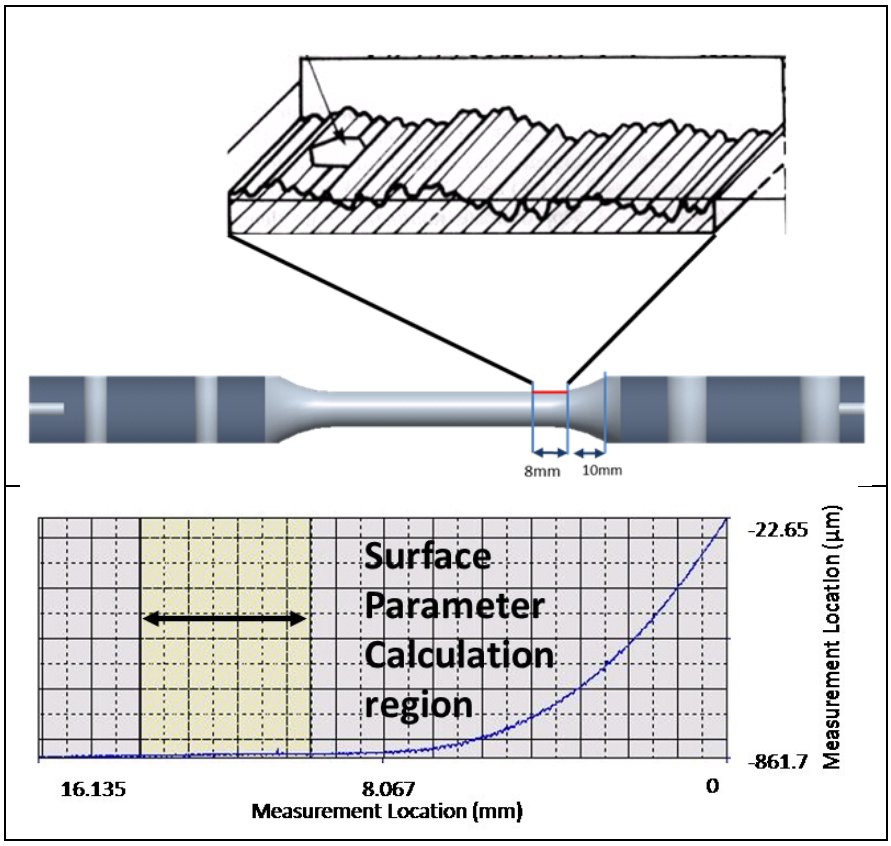

Figure 4-3 Specimen Surface Measurement Location

Test Mass Fabrication

Twelve specimens of each mass configuration are fabricated from one 3.65m long 12.7mm x 19.05mm hot rolled flat bar A-36 steel [25]. Using a vertical end mill, each sample was machined on all sides to ensure accurate mass was achieved for each specimen. Holes are drilled maintaining tight tolerances to ensure masses are located uniformly on each test sample. The parts were painted in a light coating of blue spray paint to keep the parts from rusting. The dimensions of these drawings are shown in Figure 4-4 through Figure 4-6, as well in Appendix A.

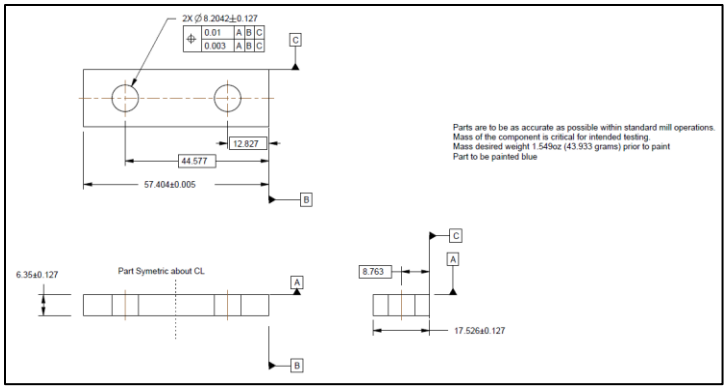

Figure 4-4 44g Mass Dimensions

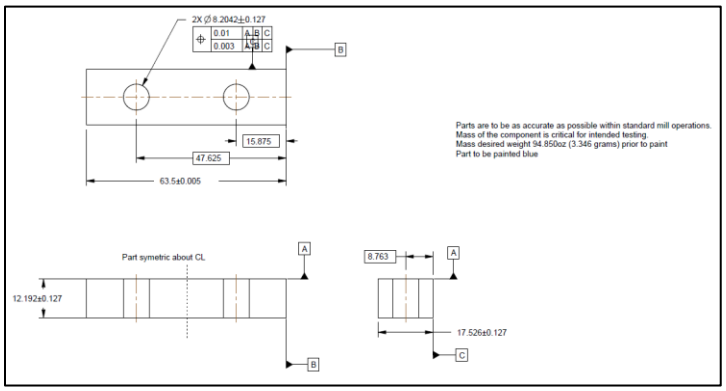

Figure 4-5 95g Mass Dimensions

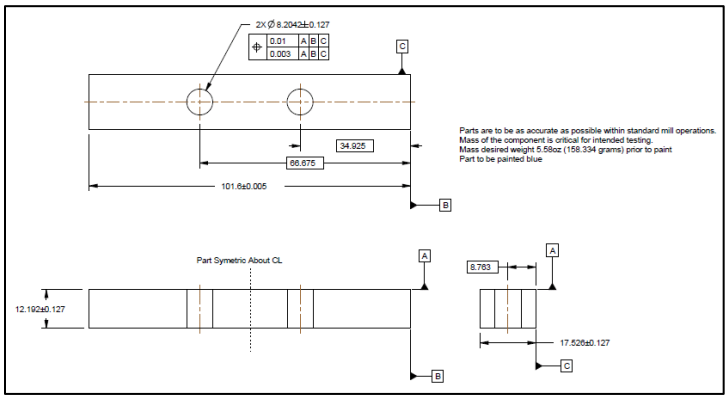

Figure 4-6 158g Test Mass Dimensions

Test Specimen Assembly

Each of the twelve specimens are matched with a specific mass to reduce the total mass variation The +/- weight variation in the added masses allowed for grouping low mass specimens with a heavier masses to provide for more consistent test (see Table 7-1). The masses are bolted to the specimens using two bolts and two washers. The bolts were torqued to 27 N-m to ensure

proper clamp load was achieved for joint integrity. An example of the specimen assembly is shown in Figure 4-7.

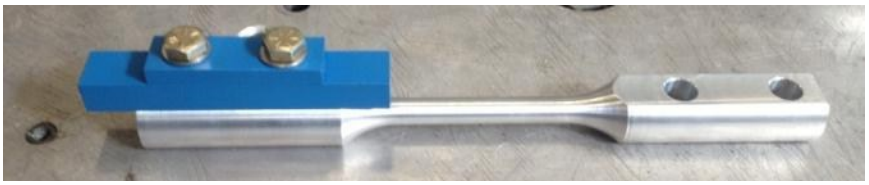

Figure 4-7 Test Specimen Assembly

The test specimen configurations are shown in Table 4-3. The different size masses are grouped to reach the desired total bending moment. Larger bolts are required for the thicker stacked masses.

Table 4-3 Test Specimen Configuration Matrix						
Test Specimen Assembly Name	Added Mass (qty 1)			Bolts (qty 2)		Washer (qty 2)
	44 g	95 g	158 g	14.3g	17g	1.8g
190g			X	X		X
235g	X		X	X		X
291g		X	X		X	X

4.4 Shake Table Test Fixture

The shake table test fixture was manufactured from one 3.65M long 25.4mm square bar of extruded 6061-T6 aluminum [27]. The apparatus was designed to enable the mounting of up to twelve test samples at one time. This structure mounts directly to the hydraulic shake table. Aluminum was used to keep the overall weight of the system low to ensure proper performance was achieved with the hydraulic rams. Resonance of this mounting fixture was checked by applying the impulse modal test as described in section 4.5 to ensure that no natural resonances would affect the test samples in the desired excitation frequency range (0-80Hz). All mounting

surfaces of the test fixture are machined to ensure proper mounting of the test specimens are achieved.

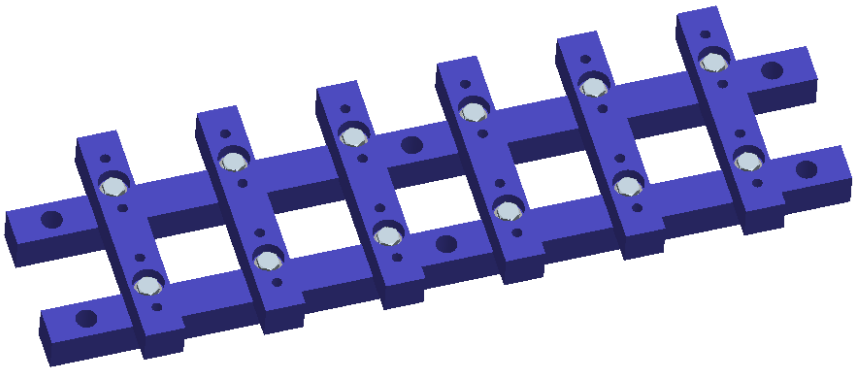

Figure 4-8 Shake Table Test Fixture

4.5 Experimental Modal Analysis - Impulse Method

Experimental modal testing was conducted on the specimen configurations to determine the damping ratios (ζ). To perform the Experimental Modal Analysis (EMA) an impulse method was applied. The impulse function was imparted on the system by using hammer with a force transducer instrumented to the striking end. The force impulse was measured when the hammer was impacted on the specimen as shown in Figure 4-9. A c52323 (Appendix E, Table 7-14) accelerometer was mounted onto to the cantilevered free end of the specimen to measure the acceleration results in the up/down direction. National Instrument LabView Signal Express [28] was used to record and post process the data. To calculate the FRF the acceleration was double integrated to determine the displacement response. The Laplace transform was then applied to both the force input $\{F(\omega)\}$ (Figure 4-10 item 1) as well as the displacement response$\{X(\omega)\}$ (Figure 4-10 item 2). Recording the entire decay response of X(t) is required to develop the correct shape and magnitude of the FRF, the effects of not recording the entire

response decay is discussed in Appendix C. The formulation of the FRF $[H(f)]$ (Figure 4-10 item 3) was then calculated by applying equation (2.26). Since the specimen is essentially a Single Degree of Freedom (SDOF) due to the large separation in the eigenmodes, only one impulse location impulse and response location is required. Therefore, the resulting matrix from equation (4.1) is a {1 x 1} sized matrix. The location of the response and impulse must not be on a node of the system vibration. To determine the preferred locations FEA modal analysis was used to determine where the nodes of vibration occurred to ensure this location was not used to excite or measure the response.

$$\underset{(rx1)}{\{X\ (j\omega)_1\}} = \underset{(rxn)}{[H\ (j\omega)_{11}]}\underset{(nx1)}{\{F\ (j\omega)_1\}} \tag{4.1}$$

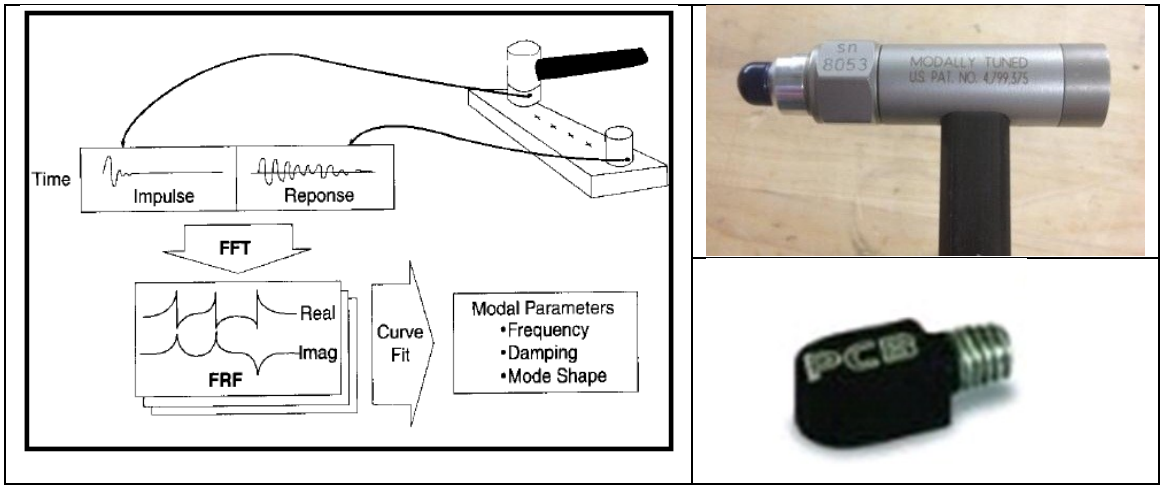

Figure 4-9 Rover Hammer Modal Analysis Schematic

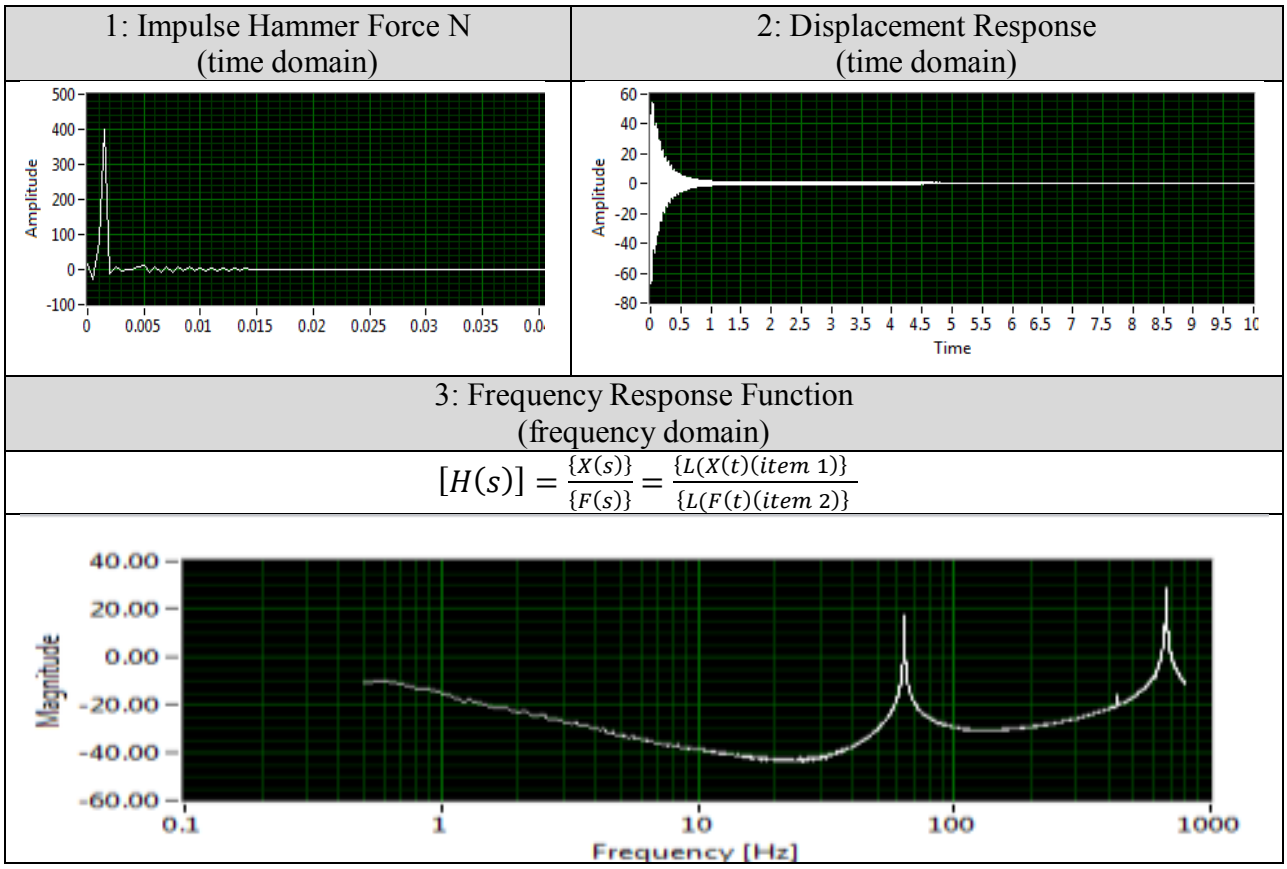

Figure 4-10 EMA data display - National Instruments GUI [28]

Free Boundary Condition Modal Test

To validate the FEA model a free boundary EMA was completed. The 190g specimen assembly was hung freely with a rubber band as demonstrated in Figure 4-11to simulate near free boundary conditions. The impulse hammer was once again used to measure the FRF of the system as depicted by Figure 4-9.

Figure 4-11 Free Boundary Conditions EMA

Cantilevered Boundary Conditions Impulse EMA Damping Determination

The specimens were mounted to the test fixture as intended during the fatigue testing. The constrained cantilevered boundary conditions are used to determine the FRF of each of the specimen configurations. The c52323 (Appendix E, Table 7-14) accelerometer was mounted to the tip of the free end to measure the vertical vibration response as shown in Figure 4-12. The specimen was lightly struck five times ensuring there was no double hits, similar force, and in the approximately same location as shown in Figure 4-12. To reduce the error in FRF five impulse events are averaged together prior to calculating the FRF $[H(\omega)]$ (Figure 4-10 item 3). Using methods described for equation (2.43) the damping values of each of the specimen configurations are determined using the curve fitting function in the software ME'scope [29].

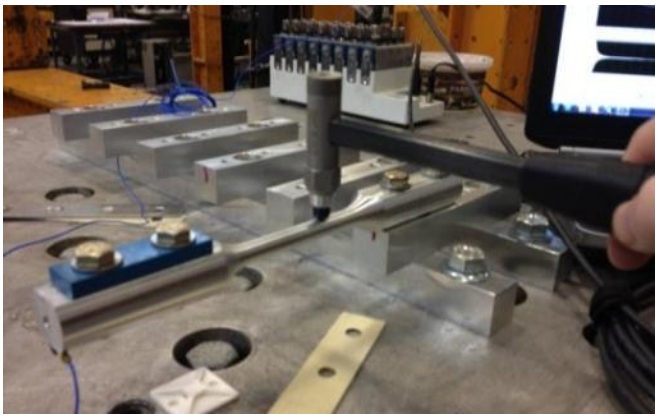

Figure 4-12 Constrained Modal Test Impulse Impact Location

Test Fixture and Shake Table Natural Frequencies

Validating the natural frequencies of the mounting fixture is required to ensure no interactions effect the specimen excitation. Adequate stiffness must be provided to ensure excitation energy is transferred directly to the specimen being tested. A resonance in the test structure would cause for a change in the excitation imposed on the test specimen. To ensure interaction would not occur modal testing was conducted on the mounting fixture and shake table. Impulse modal testing as shown in Figure 4-9. However, the base accelerometer shown in Figure 4-13 was used to measure the response function. A secondary method used the impulse hammer to impulse the shake table base right under the location of the specimen impulse method.

4.6 Experimental Modal Analysis – Forced Response

Typical methods of measuring FRF's by means of a shake table are not used on the shake table setup. The shake table used in this test had a displacement control system and no force transducer in line to measure the force input into the specimen. One could apply F=ma to calculate the expected force input based from the double integral of displacement. However, for this analysis a modified version of the FRF equation (2.65) is applied. The shake table was used

to develop normalized stress response from the base accelerations. Dividing this stress response magnitude by the base acceleration normalized the data to unit load acceleration (i.e. 1g). Three methods of excitation are used to measure the stress response at the specimen free end accelerations. These responses were then used to determine the system gain over the desired frequency intervals. The response function was calculated using the excitation input acceleration over the strain response of the specimen measured. This method does not directly calculate a standard FRF, however, applying this mathematical method does allow for the formation of a modified FRF for the response stress per unit load of acceleration input in the form of equation (2.65). The max stress value at the Eigenmode was compared to the numerical modal response function to calculate a correction factor to apply to the damping value. The numerical stress response function under a 1g load input then correlated to the shake table test stress determined.

This test was done by mounting a strain gauged sample to table using 27Nm torque onto the mounting bolts. A 352c23 accelerometer (Appendix E, Table 7-14) was mounted to the tip as shown in

To measure the acceleration vertical response. A 7292A-30M1 accelerometer (Appendix E, Table 7-16) was used to record the base acceleration of the specimen mounting fixture. The data rate of recording was 512 samples per second for all sensors. This provides accurate reading up to 512/2 Hz reading to ensure no Nyquist error occurs.

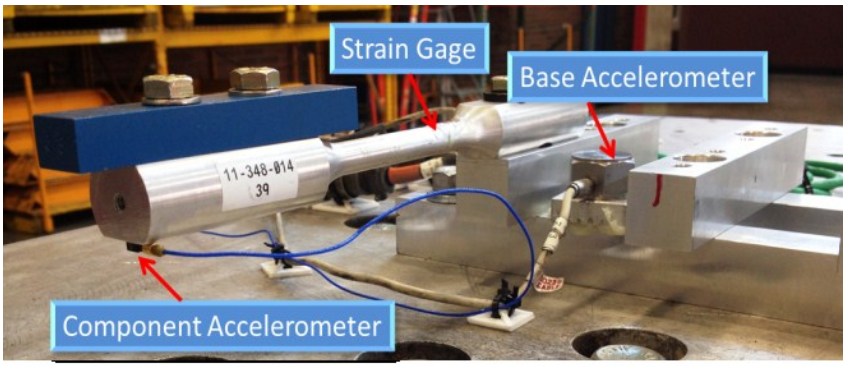

Figure 4-13 Shake Table Specimen Measurement Locations

4.6.1 Shake Table Sweep Stress Response

Sine sweep method is used to determine the stress response of the specimen as it nears resonance but not allowed to reach steady state resonance amplitudes. The rate of this sweep profile has a substantial effect on the resonance magnitude. If the sweep is slow enough the stress value will be the same as a constant frequency dwell on the Eigenmode frequency. The three test configurations from Table 4-3 are individually excited with a sinusoidal frequency sweep rate of 0.1 Hz/sec, which was chosen based on a few sweep rate comparisons which will later be discussed and shown in Figure 6-2. The frequency range was set to +/- 5 Hz from natural frequency of each specimen. The shake profile ran one sweep up and one sweep down. Small displacement sweeps are initially used and slowly increased the displacement amplitude to provide a max strain level of (±4000) μstrain to avoid yielding the specimen or overloading the strain gage. The gain of the modified FRF $|H(\omega)|$ was then calculated (see Figure 4-14). The resulting magnitude of this function is the stress response from a unit load input (I.E. 1g). This value was then used to adjust the damping values in FEA to obtain the same $|H(\omega)|$ stress value from equation (2.65).

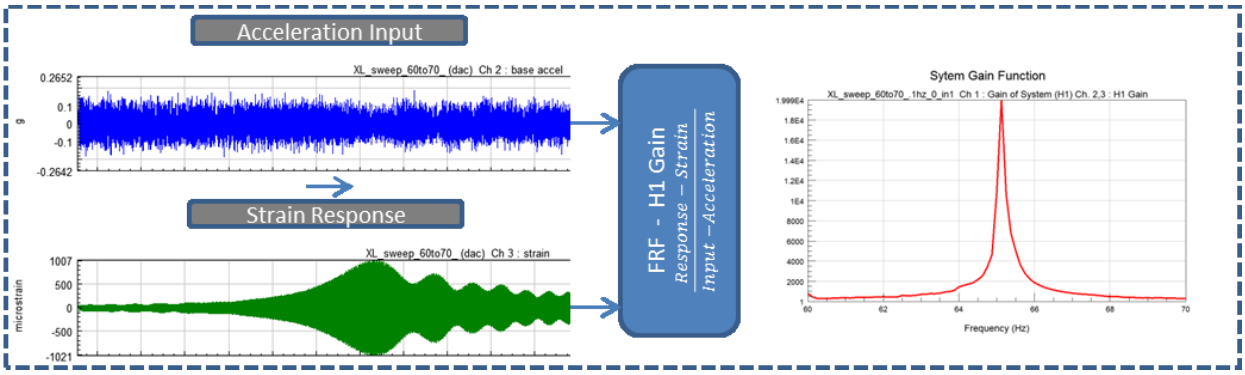

Figure 4-14 Strain Gain (H1) Process Diagram

4.6.2 Shake Table Dwell Stress Response

The objective of this test is to determine the max resonance peak stress or gain from FRF. The three specimen configurations from Table 4-3 are individually excited with a sinusoidal constant frequency excitation. This was done at intervals of 0.1 Hz around the natural frequency of each specimen. The shake profile was initiated with small displacements and was slowly ramped up to provide a max strain level of (±4000) μstrain to avoid yielding the specimen or overloading the strain gage. It is important to induce adequate vibration levels to obtain consistent strain measurements. To normalize the system response the RMS peak stress value was divided by the RMS base acceleration. This develops the stress response from 1g loading that will be used to develop the correction factor for the damping applied to the numerical models.

4.6.3 Shake Table PSD Stress Response

The third method applies the actual 600 second PSD (Power Spectral Density) excitation used in the fatigue testing. The table acceleration and specimen stress are recorded at a sample rate 512 samples/sec. Strain data was then used to calculate the Gain of the FRF $|H(f)|$. This calculation results in the stress response from a unit load input (I.E. 1g).

4.7 Experimental Shake Table Testing

Shake table testing was used to develop the experimental (S-N) fatigue curve for these test specimens. Test configurations (190g, 235g, and 291g) outlined in Table 4-3 are used to generate higher and lower stress values under the same applied PSD excitation file. The following sections cover the processes used to experimentally determine the fatigue life results. The PSD function was defined by using the numerical fatigue models discussed in section 2.9 to ensure the cycles to failure were in the desired range of 400k to 1M. This PSD function was adjusted after the numerical models were updated with experimental damping values.

4.7.1 Shake Table Machine

The shake table used in the experiment was a Pegasus Model 244.21str (Appendix F, Table 7-17).The shake apparatus uses a valve actuated hydraulic ram to displace the table on a vertical axis. The system uses a 3000 PSI and 100 gal/min flow rate to actuate the movement of the table. This particular model can perform up to ~80 Hz vibrations (dependent on force required to shake at the given frequency). Since hydraulics is used to operate the table this enables large forcing functions upwards of 10,000 lbf however has a limited frequency range. Performance curves and shake table specification are listed in Appendix F .

The table and mounting structure weighs approximately 400 lbs. and was considered to be massive enough that the addition or removal of test samples during testing would not affect the levels of vibration of the other test samples. This assumption was determined to be inaccurate as the interaction between specimens was significant. Going forward one sample at a time was determined to be required for proper results, see further discussion on this in Appendix F.

Figure 4-15 Vibration Test Machine [30]

4.7.2 Shake Table Shake Profile

Hydraulics in the shake table are controlled by MTS Remote Parameter Control (RPC) Systems [31]. The hydraulic ram uses displacement methods to operate the table. Therefore a time series displacement file must be generated to control this system. To replicate a PSD function on the shake table a time series displacement file was generated. The below steps are required to provide the correct replication of a PSD file.

1. PSD load profile must be converted to a time series displacement load file
2. Tune shake table to provide acceleration response desired
3. Run system in an open loop feedback to continuously adjust the load profile for system fluctuations in acceleration output.

Generation of time Series file from PSD function

The desired PSD function (Table 4-4) was generated to provide a load spectrum to break the specimens in the range of 4k-1M cycles depending on mass configuration.

Table 4-4 PSD Excitation Load Profile

Frequency	*g^2/Hz*
5	*0.05*
60	*0.08*
80	*0.08*

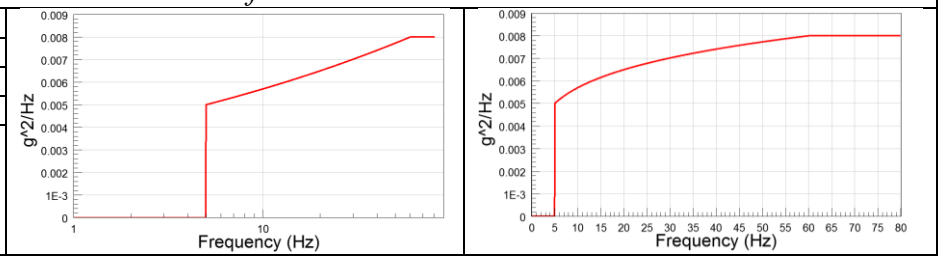

Time domain vibration signal is required to operate the shake table, hence, an equivalent PSD load profile was calculated by using the Inverse Fourier function from equation (2.4) . The function applied white noise (random sinusoidal data) of 1g RMS magnitude to re-create the phase and sign for a random time series data. This is required since a PSD does not contain phase or sign to convert to a time series. The length and sample rate of the white noise function is critical in the generating a representative time series load profile as shown in Figure 4-17. The time series generation uses the PSD function to modify the magnitude of the randomized white noise to generate a representative time series acceleration data. Figure 4-16 shows the process steps used to generate the time series data from the PSD function.

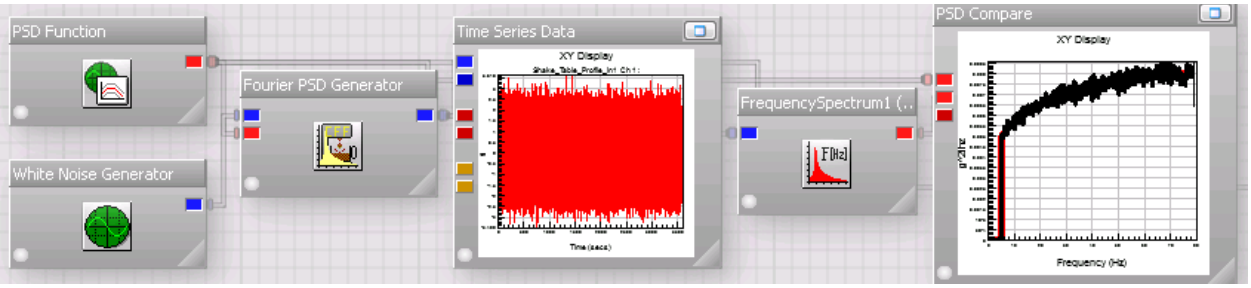

Figure 4-16 Time Series Generation from PSD Process Diagram - nCode [22]

To ensure the time series adequately represents the PSD function the time series file is processed through a forward Fourier analysis to re-generate the PSD function by applying equation (2.5). The original and regenerated PSD file are then compared for residuals as shown in Figure 4-17. The longer the length or higher the sample rate the lower the residuals will be when compared to initial PSD file. The ideal length would have been 3600 seconds as the earliest a sample broke at ~3600 second. This would have created the best fit of PSD regeneration. The life was however not known at the time of generation of the time series. The reproducibility of the time series on the hydraulic shake is difficult due to the valve operation and hydraulic fluid changes. For this reason it was chosen to use a mid-length file of 600 seconds which was assumed to be much shorter than any of the fatigue failures. This also allows for averaging of the block cycles for any system variations that may occur during testing. This choice in length of time series had a negative impact to the residuals from the initial PSD function. The effects of the time series length can be seen in Figure 4-17. Adjusting the sample rate also has the same effect as this provides more or less data points per second, therefore improving the PSD replication. In this testing the maximum sample rate of the controller was used at 512 samples per second.

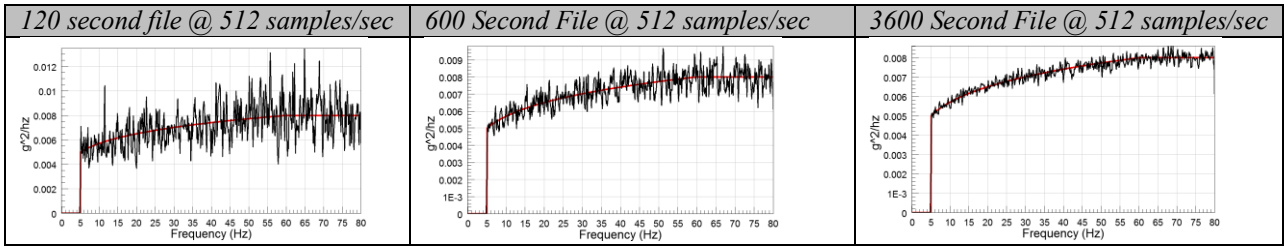

Figure 4-17 Time Series Duration Effects on PSD Replication

4.7.3 Shake Table Testing

Shake Table Tuning

Developing a displacement load profile that will induce the desired acceleration from the time series excitation required tuning the shake table response. This method of tuning is discussed in Appendix F. During the initial testing it was determined the system must stay in open/iterative loop in order to accommodate for system changes (oil pressure, oil temperature, change in specimen vibration response). This improved the reproducibly of the system response.

Specimen Fatigue Testing

Six specimens were originally mounted to the device and the time series equivalent 600 second excitation was applied to the test specimens. During this testing it was determined that the specimens influenced each other. It was therefore decided that each specimen must be tested individually. This particular issue is further discussed in Appendix F. Each of the individual specimens were then mounted to the shake table and the 600 second excitation block was repeated until the specimen ultimately failed. This process demonstrated in Figure 4-18 was repeated for each test specimen.

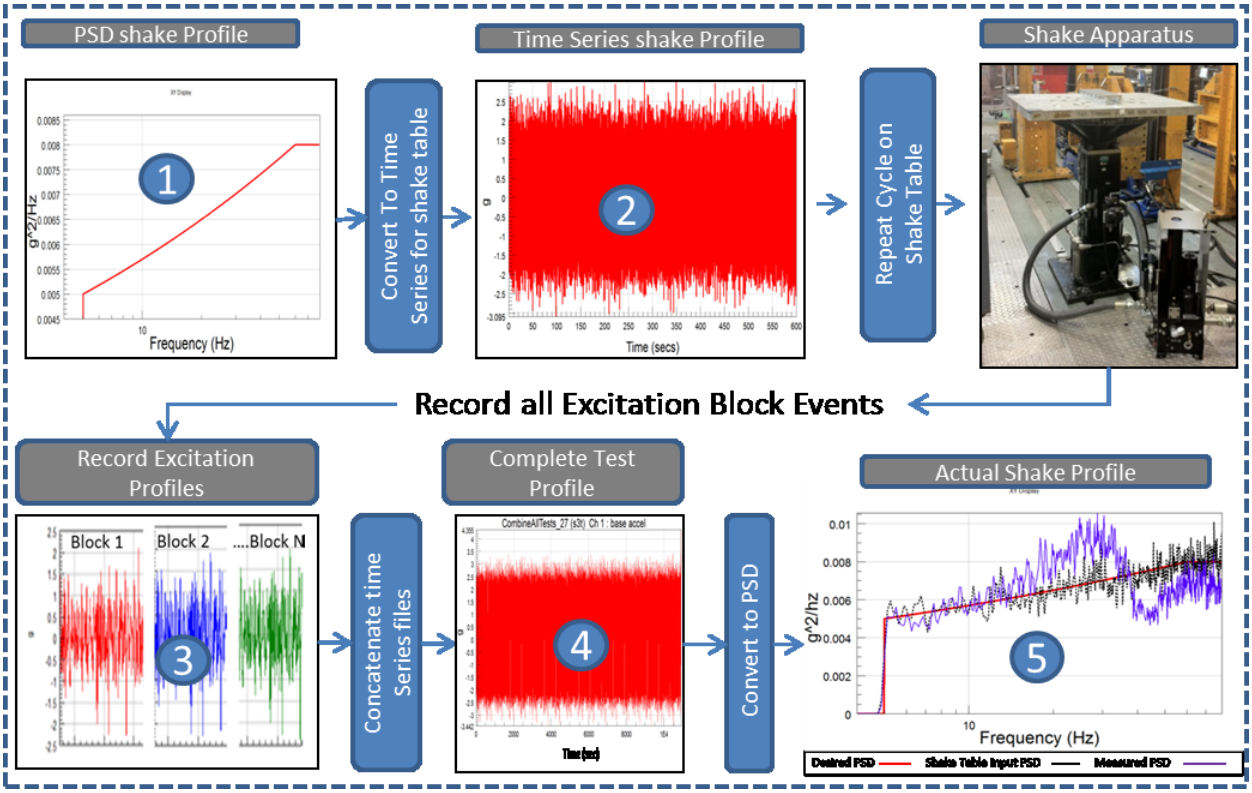

Figure 4-18 Experimental PSD Load Cycle Generation

Shake Table Data Collection

Base excitation was measured during every cycle of the fatigue testing. Accelerometer type 7292A-30M1 (Table 7-16) was attached to the specimen mounting fixture as is shown in . Acceleration data was recorded at 512 samples per second for each excitation block shown in (item 3) of Figure 4-18. Specimen base acceleration block repeat data till failure of the specimen was concatenated to one time series file shown in Figure 4-18 item 4. This file was then processed to generate the actual PSD of acceleration for each test specimen as shown by Figure 4-18 item 5.

The time series cycle count till failure of the specimen was recorded by the MTS (RPC) Systems [31]. To automate the detection of specimen failure a trip wire was integrated to stop the shake table when activated. When the specimen broke ~80% the tip would bend to the table base prior to breaking off completely. This provided a method for a trip wire system to be developed. This was accomplished by using an electrically isolated base plate under the specimen's cantilevered end (see Appendix F, Figure 7-39). The entire table and specimen are grounded to the trip wire setup. When the specimen broke and rotated down to the contact pad the circuit was then closed notifying the machine that the specimen had been broken. At this time, the hydraulics were shut off and the RPC system logged the time series cycles till failure. This setup did not work to stop the machine for the samples that broke off completely. For this reason the apparatus was checked often for specimen failure. Typically the broken specimen would vibrate on the table loudly notifying the operator the specimen had broken.

Four of the remaining specimens were instrumented with strain gage type EA-13-045AL350, details of strain gage are in the Appendix E, Figure 7-27. Strain gage location was the highest stressed area of the specimen. Maximum stress occurs in the location as shown in Figure 4-19. This location has the smallest cross sectional area and longest distance from the cantilevered mass.

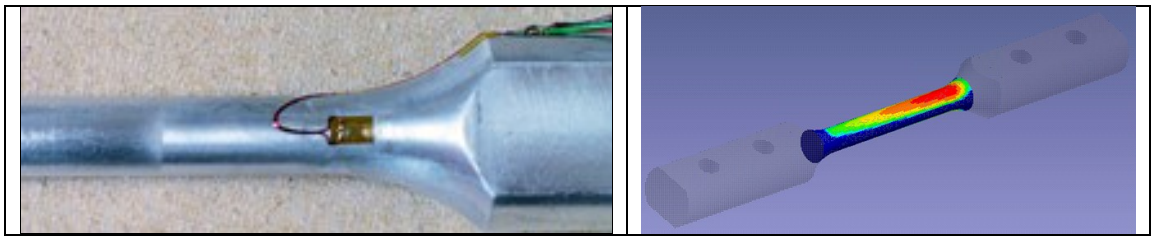

Figure 4-19 Specimen Strain Gage Location

4.7.4 Specimen Stress Evaluation and stress Cycle Counting

Stress Measurements

To develop an S-N curve stress must be determined for each specimen. Strain data was collected for one full excitation block event for each of the three specimen configurations (195g, 235g, and 291g). To determine the stress Hook's Law was applied to the data values. Stochastic vibration do not induce constant amplitude stress cycles, hence RMS stress is calculated by applying equation (4.2) to determine the average stress from a complete excitation block event. The time series data was processed through nCode glyphworks [32]. The strain/stress data was noted to have mean drift as the strain gage began to fail. Corrections are applied to the data to account for this (details are in Appendix B). The strain gage also must be zeroed out to set baseline of voltage at which no stress is applied to the part. This strain reading was set to zero when specimen assembly was mounted to test fixture. To account for the 1g load of the cantilevered mass an offset amount of strain should be added to the data during the post processing (details in Appendix B).

$$RMS\ strain = \sqrt[2]{\frac{1}{t_2 - t_1}\int_{t_1}^{t_2}[\varepsilon(t)]^2 dt} \tag{4.2}$$

$$\varepsilon(t) = time\ series\ of\ strain$$

$$RMS\ stress = RMS\ strain * Material\ \ Modulous\ of\ Elasticity$$

Stress Cycle Counting

Evaluation of stress cycles from a complete excitation block event can be determined by applying deterministic rainflow cycle counting from section 2.9.1. Methods of applying filters to remove stress ranges that are below the approximate fatigue limit should be applied to only count the cycles that contribute to damage. Aluminum has no defined fatigue limit; therefore this research used S-N curve stress values intercepts at approximately 1X10^8 cycles. This value is

often time used for approximation of the fatigue limit on non-ferrous metals. Figure 4-20 below shows this process of determining the stress cycles. The far right chart shows the effect of filtering the stress range values to the range distribution defined by the green solid and dashed black lines, details can be found in Appendix B. Stress cycle filtration was applied to remove the stress ranges that are below the published MIL-HDBK-5J stress intercept of 86.6 MPa [19] at 1E8 cycles. The total specimen stress cycles are determined by equation (4.3).

$$Total\ Stress\ cycles = \#\ of\ block\ repeats * \frac{stress\ cycles > stress\ filter}{block\ cycle} \qquad (4.3)$$

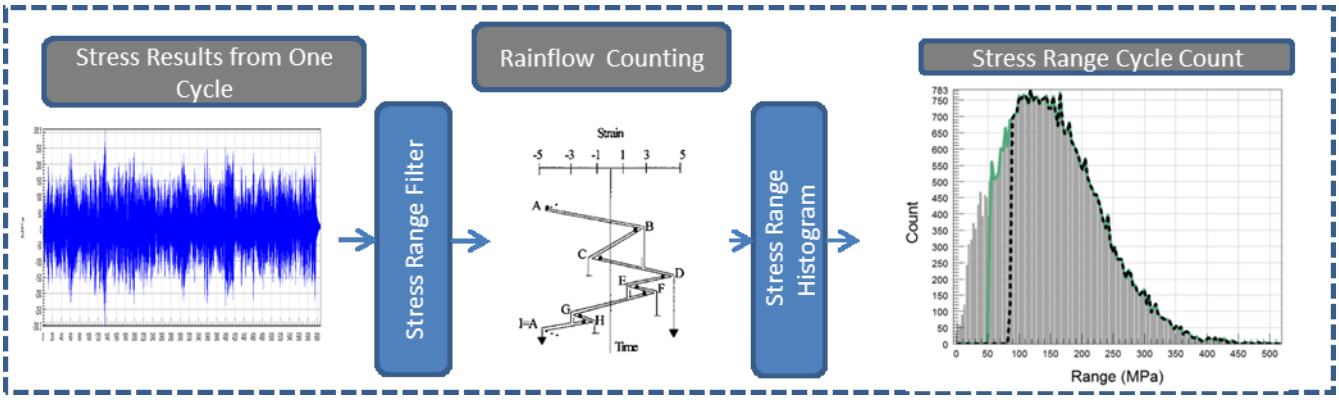

Figure 4-20 Deterministic Rainflow Stress Counting Method

4.8 Numerical Fatigue Analysis Methods

The numerical simulation steps proposed to calculate the fatigue life under stochastic vibrations are outlined in into seven steps, as well Figure 4-21 displays these steps in a process diagram.

1. Generate parametric geometry of specimens
2. Create 3D mesh of specimens
3. Apply boundary conditions and material properties
4. Calculate stress FRF of system $H(\omega)$ by equation (2.65)
5. Calculate stress PSD function $G(\omega)$ by equation (2.71)
6. Rainflow count occurrences of stress amplitudes from PSD loading by applying equation (2.78)
7. Determine damage calculation by using equation (2.79)

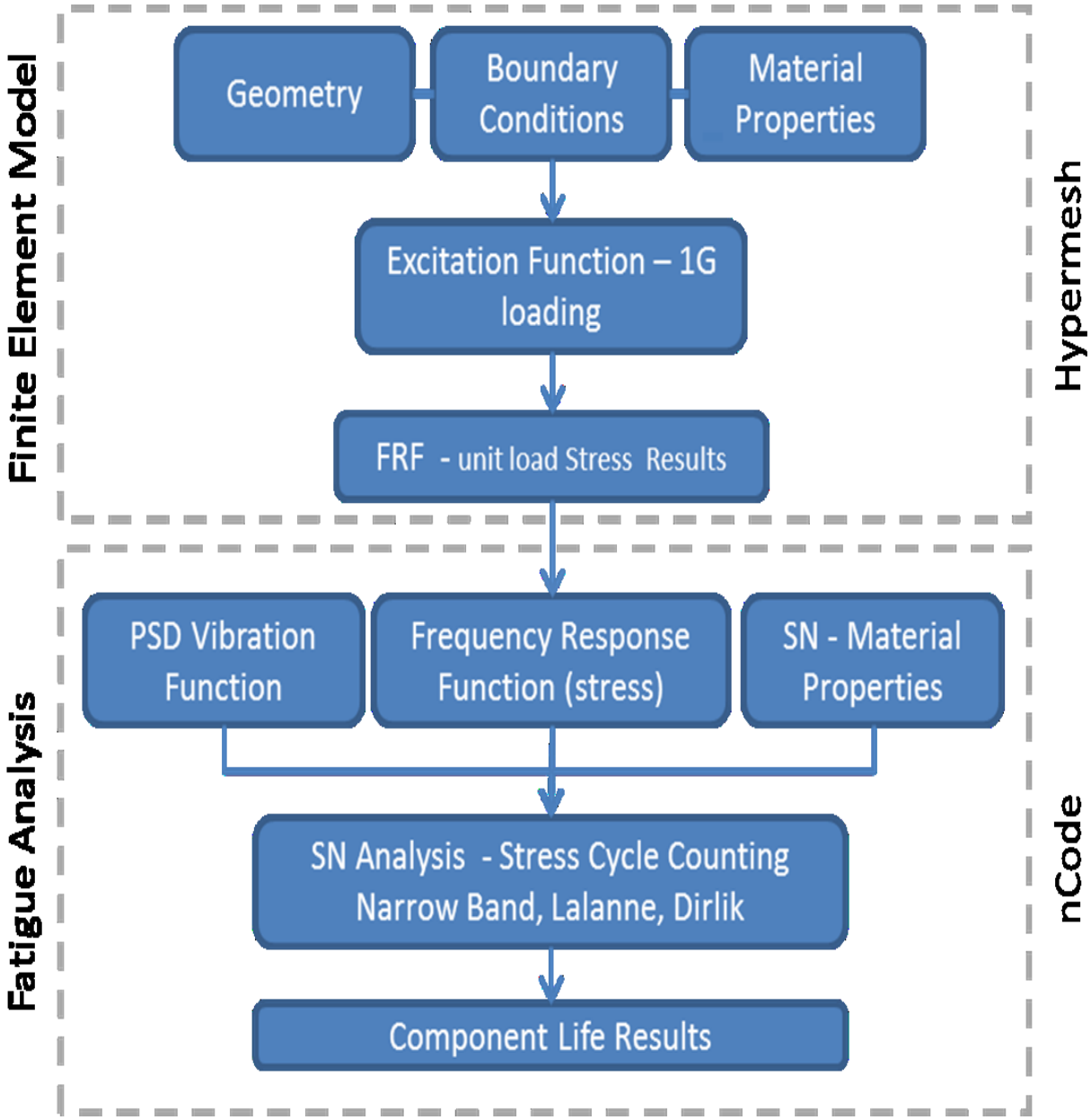

Figure 4-21 Numerical Fatigue Calculation Process Diagram

Specimen Model

The Finite Element Analysis model was created using Creo Elements/Pro [33]. The 3D data was imported into Hypermesh [34] using the solver Radios – Bulk Data. The mesh was created using a mixture of tetra, penta, hexa elements. See Table 4-5 for model properties, the mesh density and specimen geometry is shown in Figure 4-22.

Table 4-5 FEA model Properties: Test Coupon

Number of Elements	40437
Max element edge length in critical stress region	1mm
Max element edge length in no critical stress region	3.1mm
Material Applied	6061-T6 Aluminum

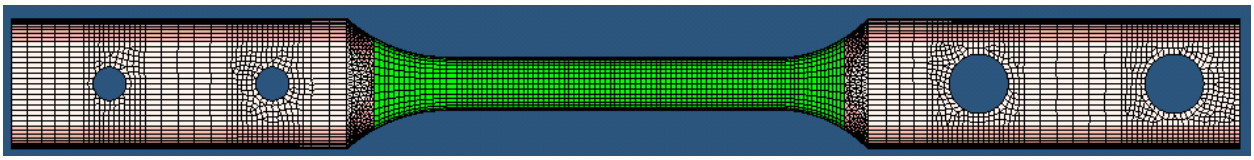

Figure 4-22 FEA model of Test Sample

Two component layers are created for modal evaluation and FRF data export. The Green surface (minor diameter of specimen) is setup as surface stress elements. This layer will export a smaller subset of the surface stress data.

Test Mass Modeling

The various masses, bolts, and washers were modeled in Hypermesh [34]. The masses are constrained to the test sample using rigid elements that connect the bolt to the threaded section of specimen. The model must include the inertial properties of the mass and geometry to develop a representative modal behavior. See Table 4-6 for model properties, as the mesh density on model geometries for each specimen configuration is shown in Figure 4-23.

Table 4-6 FEA Test Mass Properties	190g Mass	235g Mass	291g Mass
Number of Elements	2536	3790	2341
Max element edge length	1.8mm	0.87mm	1.94mm
Min element edge length	3.17mm	3.04mm	3.04mm

195g mass	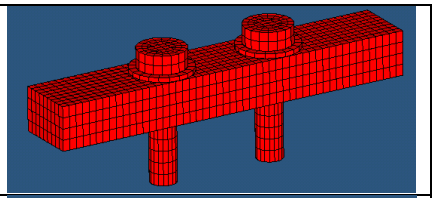
235g mass	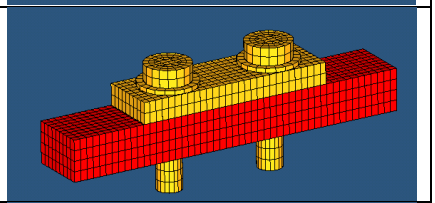
291g mass	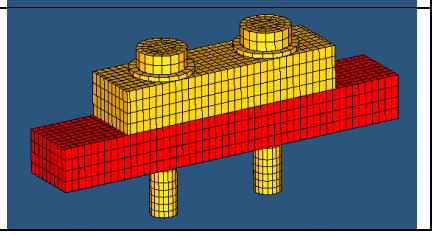

Figure 4-23 FEA Mass and Bolt Modeling

Specimen Assembly Modeling

Assemblies of each of the test configurations were created form Table 4-3. Model geometry included the complete assembly of the specimen, masses, bolts, and washers. The 3D geometry is displayed in Figure 4-24.

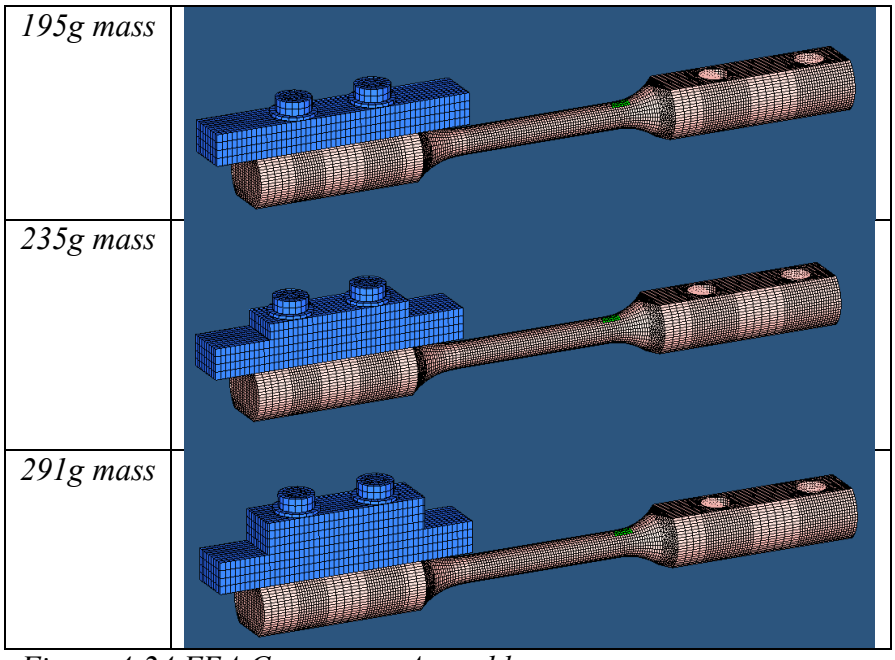

Figure 4-24 FEA Component Assembly

Model Constraints

The model constraints are applied at non cantilevered end of the test specimen. The top elements are constrained around the washer surface areas and the bottom elements are constrained around the mating surface areas. These constraints are then rigidly connected to the forcing function node (green triangle in Figure 4-25). This green triangle was used to excite the structure for calculation of the FRF. The various masses, bolts, and washers are constrained to the test sample using rigid elements that connect the bolt to the threaded section of the test sample as displayed in Figure 4-26.

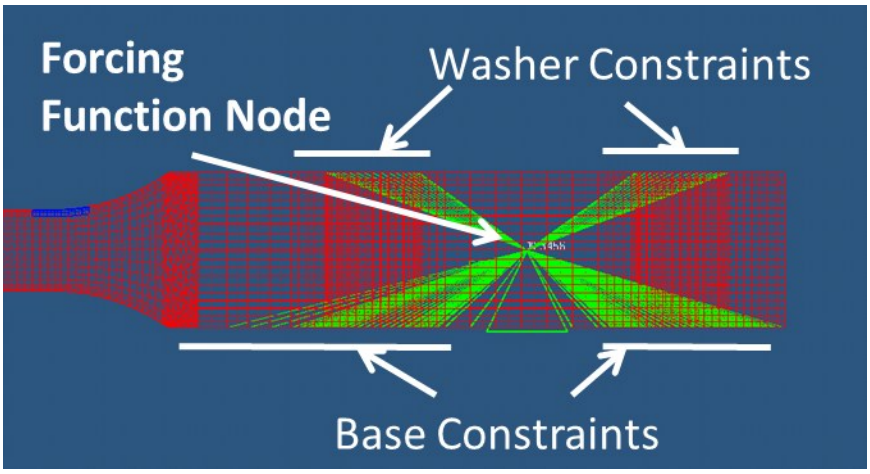

Figure 4-25 Numerical Boundary Conditions of vibration Specimen

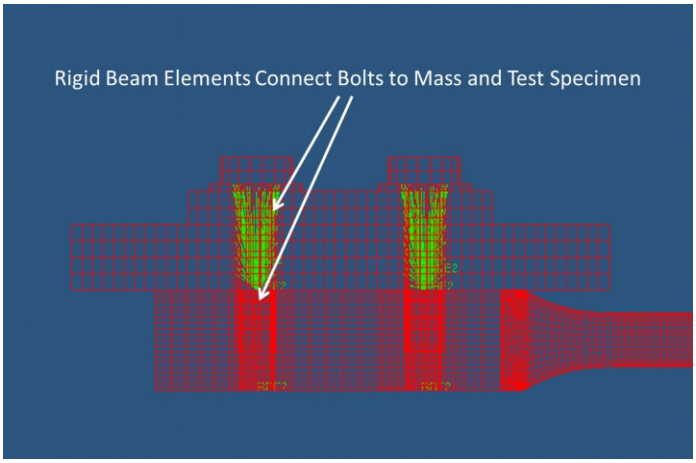

Figure 4-26 Numerical Boundary Conditions of Cantilevered Mass

Model Damping Methods

Damping was initially applied to the model using published values from Colakoglu [24]. Free boundary conditions are used to determine the damping ratio (ζ) of 0.48 % @ 59.9Hz and 0.152% @ 168.2Hz for aluminum 6061-T6. The actual component damping should be tested if possible as many contributing factors will affect this value. The model damping applied in this case was hysteretic damping as described in chapter 2.7.3.The determined damping ratio (ζ) evaluated in sections 4.5 and 4.6 are later applied to the models for comparisons in life estimation accuracies.

It was determined for such structures, applying hysteretic damping was the best representation of the physical response of the structure (see section 2.7.3 for explanation of this damping method). The damping method chosen affects the FRF shape and magnitude as shown in Figure 4-27. The damping methods as discussed in section 2.7 diverge as frequency increases. Proportional viscous and structural are both acceptable methods as the proportional method applied the same damping effect at the natural frequencies. Applying viscous damping equation (2.49) results in too much damping resulting in a low peak stress.

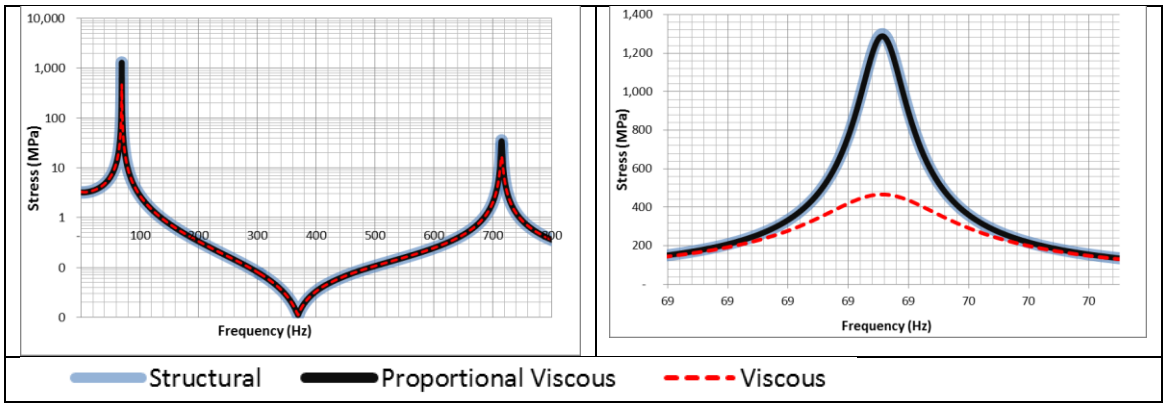

Figure 4-27 Numerical FRF Effects from Various Damping Methods

4.8.1 Stress Transfer Function

Stress FRF's where solved to determine the response stress given a 1g excitation across the frequency domain. This was calculated by applying a 1g (32.2ft/sec^2, 9.81 m/sec^2) sinusoidal excitation to the specimen modal at the constrained end. The stress tensor matrix $[\sigma(\omega)]$ equation (2.67) is then solved. From this the stress FRF is formed by using one the yield criterion. In this analysis absolute max principle equation (2.70) was used to develop the stress FRF $H(\omega)$ for equation (2.71), this process is demonstrated in Figure 4-28 . The frequency resolution of the output FRF is vital for ensuring the proper shape as well as the magnitude. For this analysis 0.1 Hz resolution was used. Appendix C, Figure 7-19 demonstrates that $\Delta f < 0.5$ Hz

converges to the same shape and magnitude, therefore, 0.1Hz was chosen. Adding finer resolution would make the model larger and would not obtain any significant differences in the accuracy of the FRF shape and magnitude.

$$[H(\omega)] = \frac{\{\sigma(\omega)\}}{\{F(\omega)\}} \tag{4.4}$$

Where:

$F(\omega)$ = Spectral Force input derived from a 1g unit excitation loading.

$\sigma(\omega)$ = absolute max principle spectral stress response of each element.

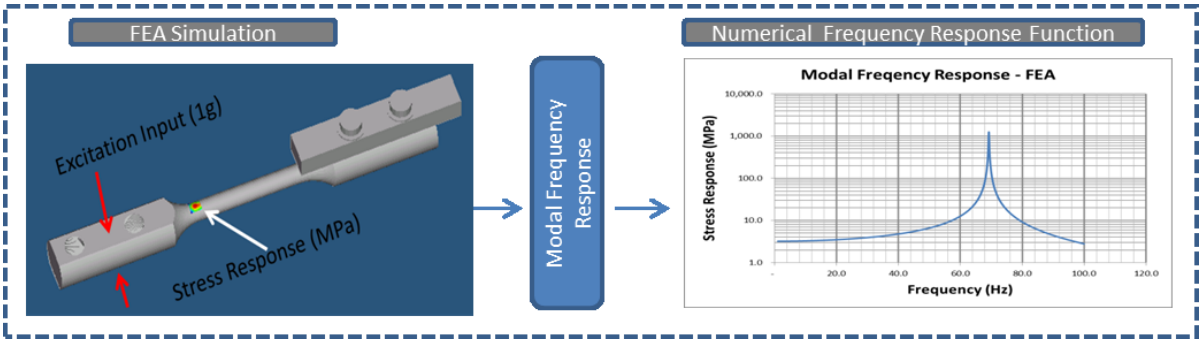

Figure 4-28 Numerical Stress Response FRF process diagram - Hypermesh [34]

Stress FRF's are calculated for each of the variants of damping as well as the specimen configurations as shown in Table 4-7. These values derived for these configurations will be discussed in the results section.

Table 4-7 Numerical FRF model configurations

	Damping Methods and values applied			
Mass Configuration	**Impulse**	**Sweep**	**Dwell**	**PSD**
190g	X	X	X	X
235g	X	X	X	X
291g	X	X	X	X

See section 4.6 for details of damping measurement methods

4.8.2 Numerical Shake Table

Stress response PSD functions $G(\omega)$ (Figure 4-29) are calculated in the frequency domain by multiplying the squared stress FRF $|H(\omega)|^2$by the PSD excitation load $W(\omega)$ as derived in equation (2.71). This was completed for each of the configurations outlined in Table 4-7. The process was calculated for two versions of the PSD excitation. The first function used was the target PSD excitation as shown in Figure 4-29 Item 1. Upon completion of the experimental testing the actual PSD excitation are used as calculated in Figure 4-18 item 5.

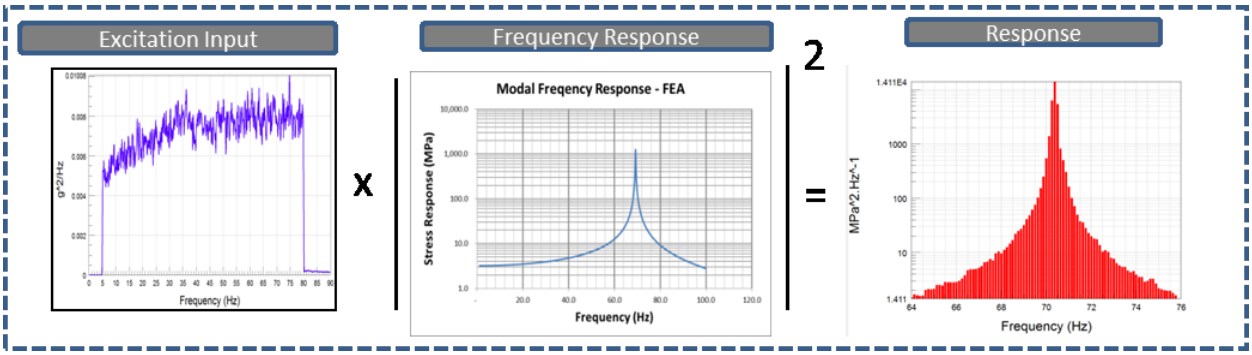

Figure 4-29 Stress PSD Function Process Diagram –nCode [22]

Stress Accumulation Methods

The resulting stress PSD functions $G(\omega)$ are used to determine the damage from each PSD load excitation cycle. For this research the Lalanne method [14] from section 2.9.2 was applied to evaluate the statistical stress range distribution equation (2.78). This method was chosen as it included the irregularity factor (γ) to adjust for the bandwidth of the signal as calculated by equation (2.75)

Damage Determination

The Damage to the specimen was determined by applying Miner's rule equation (2.79). This calculation summates the damage of each stress range from the Stress PSD $G(\omega)$ from equation (2.71). Summing up the damage of each stress range multiplied by the occurrences of each stress range is the total damage from one cycle of the PSD vibration loading. The inverse of the damage is the number of times the PSD excitation cycle can occur before specimen failure. Since this process is completed thousands of times the correct S-N values are crucial. For this evaluation the published values for Aluminum 6061-T6 SN curves from Table 4-1 are applied for damage calculation.

The process diagram to calculate damage in the frequency domain by applying PSD excitations is shown in Figure 4-30. This process was repeated for each specimen assembly, surface finishes, damping methods, and different material SN curves.

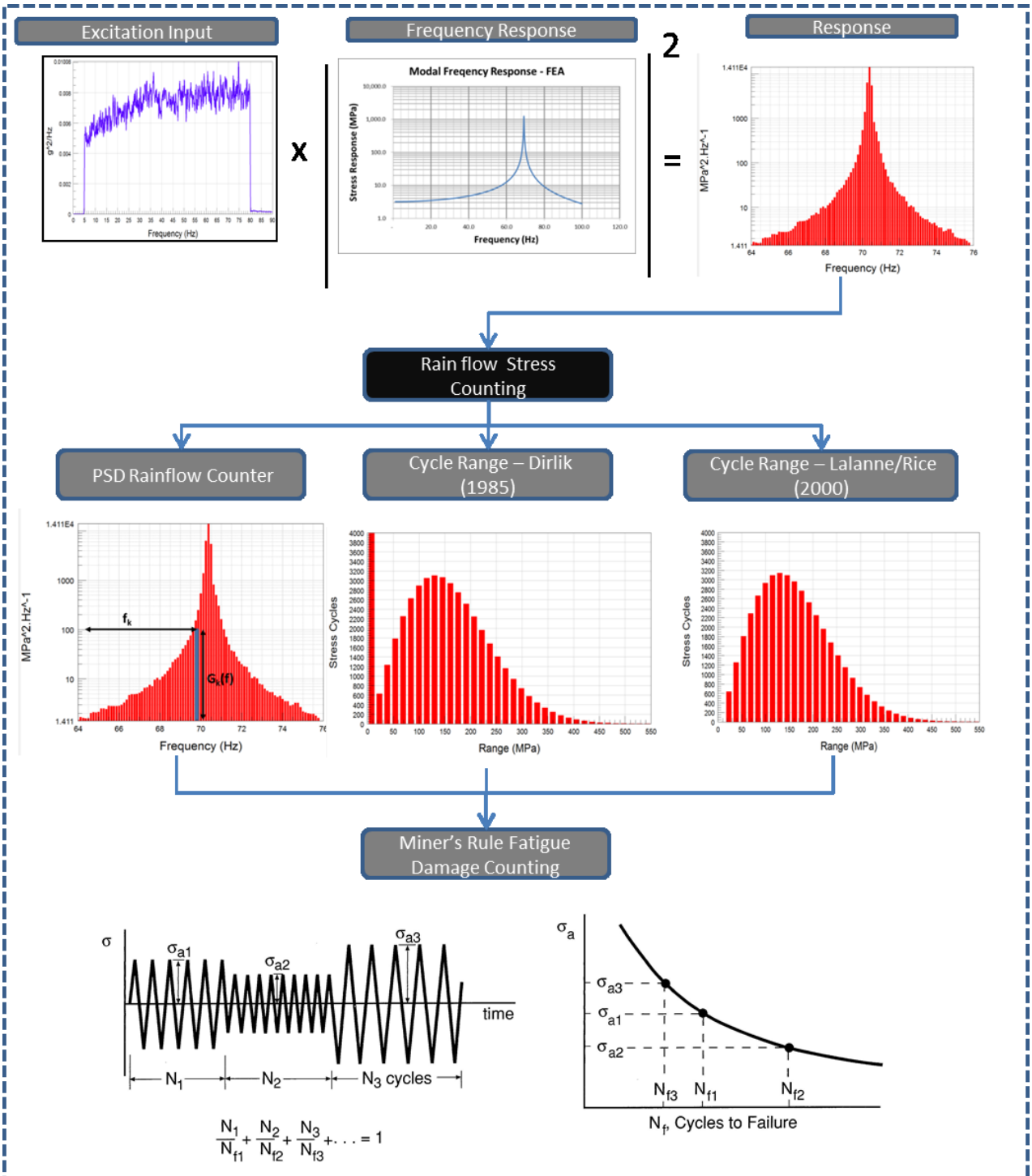

Figure 4-30 Spectral Methods for PSD Fatigue Damage Process Diagram

Chapter 5 - Results

In this chapter, both results of the experimental and numerical methods are presented, as well additional information pertinent to the results is given. Experimental results are presented in section 5.1 through 5.3. Numerical validation and results are presented in section 5.4 through 5.6.

5.1 Specimen Measurements

Manufactured specimens, masses, and assemblies are all evaluated for variations in mass, geometry, and surface finishes as shown in the Table 5-1 through Table 5-5. The tabular data for each specimen in located in the tables in Appendix A. Examples of a typical machined and polished specimen are displayed in Figure 5-1.

Table 5-1 Specimen Mass Variations				
	Specimen	44 gram mass	95 gram mass	158 gram mass
Mean	178.91	44.39	95.015	158.56
Std Dev	0.32	0.16	0.16	0.18

Table 5-2 Added Mass Variations			
Specimen Configuration	190g	235g	291g
Mean (gram)	158.6	203.0	253.6
Std Dev	0.16	.024	0.06
Includes configuration masses and 2 washers and 2 bolts			

Table 5-3 Complete Specimen Assembly Mass Variations			
Specimen Configuration	190g	235g	291g
Mean (gram)	337.33	381.94	432.49
Std Dev	0.06	0.17	0.19
Includes mass of specimen, weights, 2 washers, and 2 bolts			

Table 5-4 Test Specimen Dimension Variations					
Sample #	Dim 1 (mm)	Dim 2 (mm)	Dim 3 (mm)	Dim 4 (mm)	Dim 5 (mm)
Mean	67.3164	168.9227	25.1841	19.0056	10.0711
Std Dev	1.2686	16.9687	0.0792	0.0466	0.0315

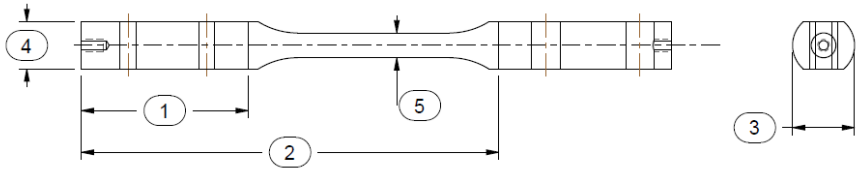

Table 5-5 Specimen Surface Finish Parameters					
	Surface Parameter	**Min**	**Max**	**Mean**	**Std Dev**
Machined Surface Finish					
Mean Deviation of the Roughness Profile	Ra (µm)	0.075	4.401	2.47	1.356
RMS Deviation of the Roughness Profile	Rq (µm)	0.098	5.079	2.921	1.555
Skewness of the roughness profile	Rsk	0.976	1.099	-0.203	0.535
Kurtosis of the Roughness Profile	Rku	1.864	6.669	2.7195	1.220
Maximum Valley Depth of the Roughness profile	Rv (µm)	0.214	10.321	5.974	2.674
Polished Surface Finish					
Mean Deviation of the Roughness Profile	Ra (µm)	0.049	0.1	0.0735	0.015
RMS Deviation of the Roughness Profile	Rq (µm)	0.057	0.117	0.0875	0.017
Skewness of the roughness profile	Rsk	-0.299	0.426	-0.0355	0.227
Kurtosis of the Roughness Profile	Rku	2.331	3.374	2.6105	0.383
Maximum Valley Depth of the Roughness profile	rv (µm)	0.103	0.239	0.1975	0.046

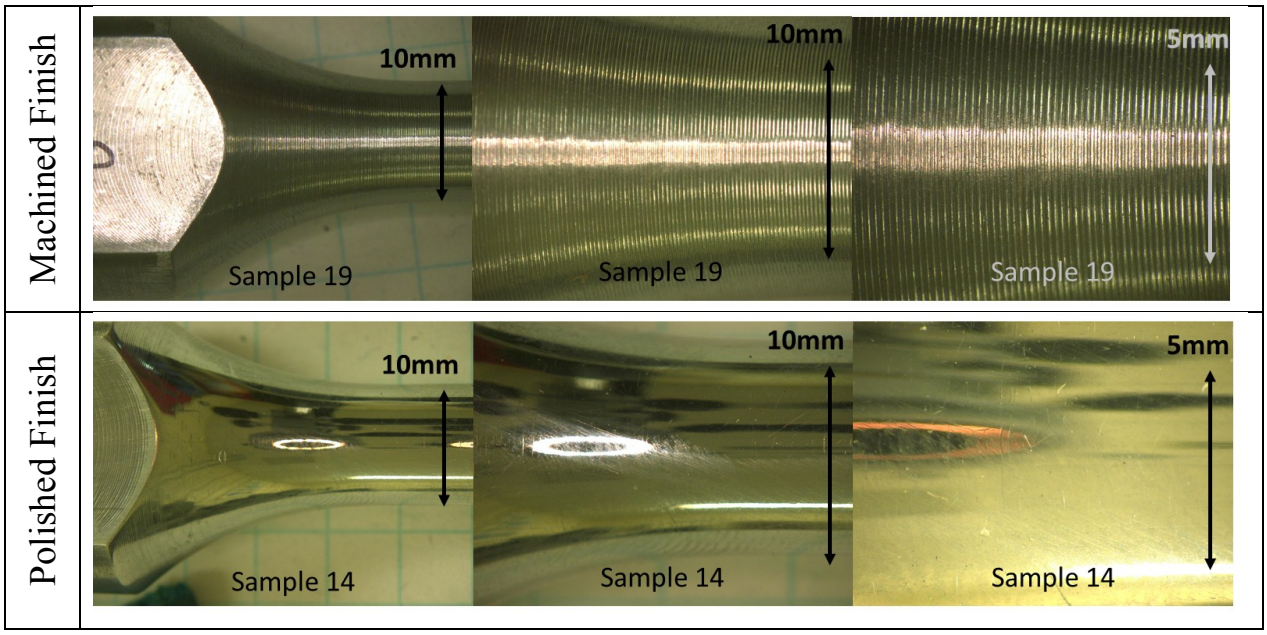

Figure 5-1 Specimen Surface Finish Pictures

5.2 Shake Table Testing

Shake Table Test Fixture

Validating the natural frequencies of the mounting fixture was required to ensure no interactions occur between the specimens and natural resonance of the table or mounting fixture. The testing methods described in section 4.5 developed the FRF (Frequency Response Function) shown in Figure 5-2 A and B. Figure 5-2 B is applying the impulse load on the test specimen in the location shown in Figure 4-12. The resulting FRF shows no natural frequencies other than the specimen resonance existing in the test profile frequency range of (0-80Hz). Figure 5-2 B is the FRF developed when striking the table assembly with the impulse hammer directly under the specimen impact location. Testing shows striking the table did not cause resonance to occur in the specimen. This is due to the impulse energy provided by the small hammer was inadequate to excite the specimen. It is also noted no major resonance peaks exist in the 0-200Hz range as

shown in. Modal testing applied validates the table and mounting fixture for concerns of resonance in the frequency range of the PSD (Power Spectral Density) shake profile (0-80 Hz).

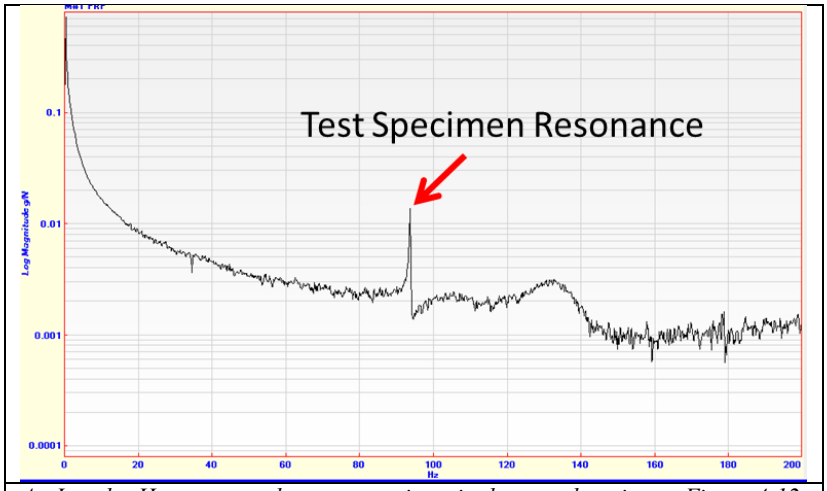

A - Impulse Hammer struck on test specimen in the same location as Figure 4-12

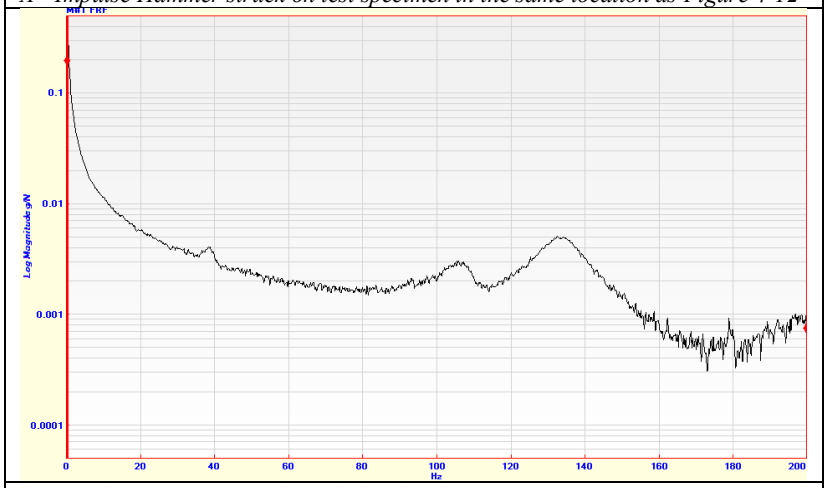

B - Impulse Hammer struck on shake table base Figure 4-12

Figure 5-2 Shake Table Resonance Check

Shake Table Excitation Reproducibility

Acceleration profiles are recorded for the complete block repeats until specimen failure. Fluctuations in oil pressure, temperature, or flow-rate in the system are shown to affect the reproducibility of each block cycle. Figure 5-3 displays the PSD of block cycles 1, 4, 12, and 16 of the total 18.4 repeated blocks of the specimen 27.

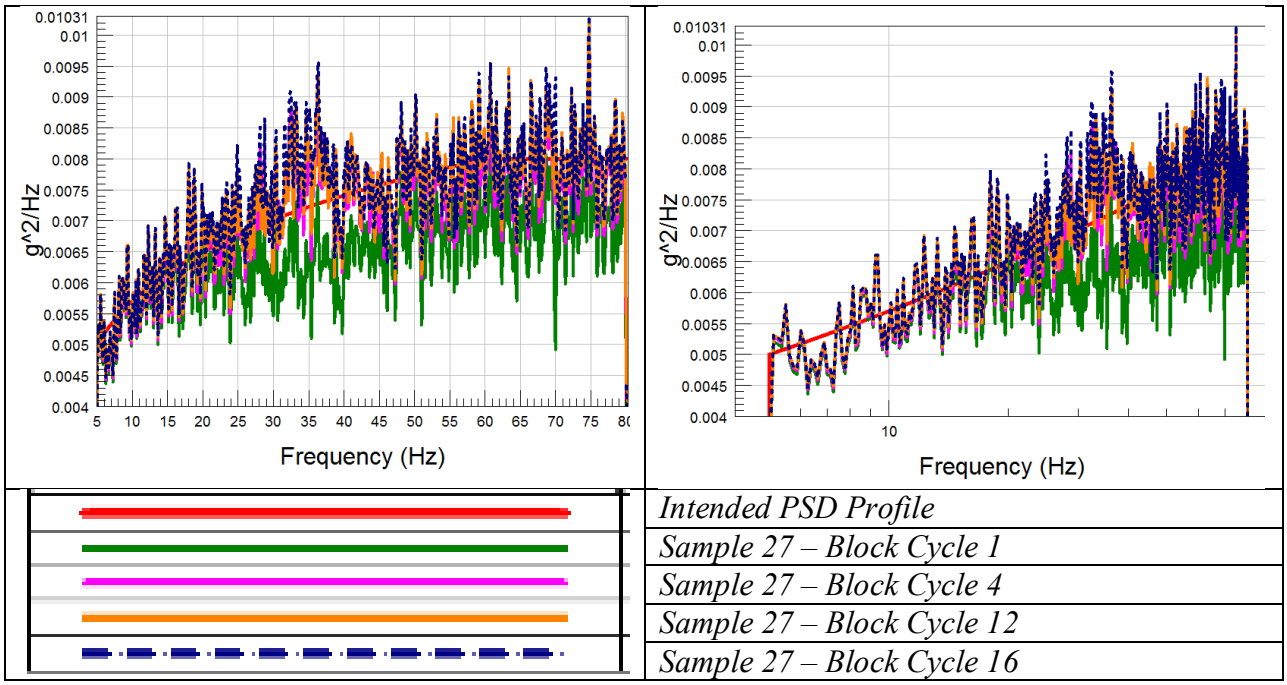

Figure 5-3 Hydraulic Shake Table Run Variations

Impulse Response Modal Analysis

Experimental modal analysis was conducted on each of the specimen configurations (190g, 235g, and 291g) from Table 4-3. The damping ratio (ζ) and damped natural frequency (ω_d) for the free boundary conditions are shown in Table 5-6, Table 5-8 shows the results for the cantilevered constrained boundary conditions. The damping ratio is shown in % of damping which is determined by equation (2.46). The free boundary condition experiment is used to validate the unconstrained numerical model. The unconstrained model allows for the mass and stiffness of the system to be checked without the influences of constrained boundary conditions.

Table 5-6 Free Boundary Condition Mode 1 Natural Frequency Determination		
Specimen Configuration	Impulse Test (Hz)	Damping ratio (ζ)
190g mass	371.15	0.327%

Constrained boundary condition modal testing was used to validate the numerical model, as well as providing damping values for the specimens. Modal testing of the constrained boundary conditions results are tabulated in Table 5-7for the damped natural frequency (ω_d)and damping ratios (ζ) for all three specimen assembly configurations. Samples 24, 41, and 42 were randomly chosen specimens to determine the variation of damping within the sample set. The identical masses are used to illuminate the mass variations as a factor. The results show a significant difference in the determined damping value of sample 41 when compared to samples 24 and 42. The statistical means and standard deviations are shown in Table 5-7. The applied damping values for the numerical models are the mean values from the three tests and are displayed Table 5-8.

Table 5-7 Impulse Hammer EMA Damping Values

Modal Impulse Damping Values				
	291 g mass	235g mass	190g mass	Mean Specimen Values
Speciment 24	0.121	0.115	0.121	0.121
Specimen 41	0.150	0.209	0.252	0.209
Specimen 42	0.109	0.106	0.129	0.109
Mean	**0.121**	**0.115**	**0.129**	**0.12**
Standard Dev	0.021	0.057	0.073	0.055

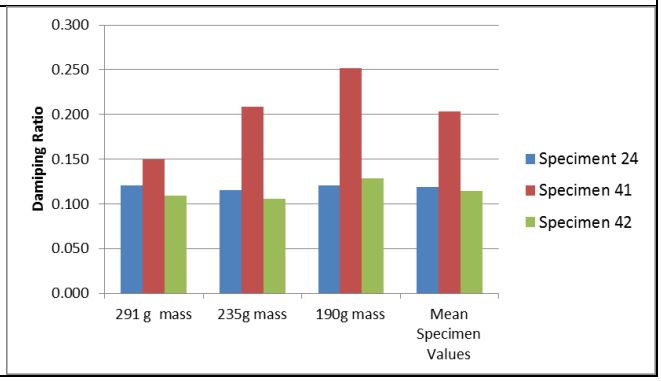

Table 5-8 Cantilevered Boundary Condition Mode 1 Natural Frequency Determination		
Specimen Configuration	Impulse Test (Hz)	Damping ratio (ζ)
190g	69.3	0.129%
235g	64.1	0.115%
291g	58.6	0.121%
Average	Not Applicable	**0.120%**

The average value of all three masses was used as no trend was shown with increasing mass.

Forced Response Modal Testing

Three methods are used to develop damping correction factors. The stress values determined in these tests are used to tune the damping values in the numerical model. The details of this analysis are discussed in section 4.6 and the results are shown in Table 5-9 through Table 5-11. The details and on the signal processing is located in Appendix B for details on calculation.

Table 5-9 FRF stress magnitude: Sine Sweep (0.1 Hz/sec) Constant			
Specimen Configuration	Specimen Number	FRF Peak Strain μ(mm/mm)/1g	FRF Peak Stress (MPa)/1g
190g mass	3	18074	1246
235g mass	37	19437	1340
291g mass	37	21526	1484
Note: 1g unit load is scaled value, component cannot survive a 1g loading at resonance			

Table 5-10 FRF stress magnitude: Dwell Frequency Constant Amplitude			
Specimen Configuration	Specimen Number	Max Strain μ(mm/mm)/1g	RMS Stress (MPa)/1g
190g mass	3	37511	2586
235g mass	37	25152	1734
291g mass	37	18422	1270
Note: 1g unit load is scaled value, component cannot survive a 1g loading at resonance			

Table 5-11 FRF Stress Magnitude: PSD Acceleration Block Loading			
Specimen Configuration	Specimen Number	FRF Peak Strain μ(mm/mm)/1g	FRF Peak Stress (MPa)/1g
190g mass	37	13583	936
235g mass	37	14679	1012
291g mass	26	15187	1047

5.3 Experimental Fatigue Results

To compare the numerical methods the experimental data must be evaluated for stress and stress cycles until specimen failure. Section Appendix B discussed the methods to evaluate the RMS stress values from measured strain data, as well as the methods in which to apply stress cycle counting. More details on the analysis used to determine these values are covered in Appendix B. The values determined for specimen stress levels are shown in Table 5-12. The

applied stress cycle counting methods and stress filtering methods are shown in Table 5-13 and Figure 5-4.

Specimen Stress

Table 5-12 Experimental Specimen RMS Stress Values for 1 Block Excitation

Specimen Configuration	Specimen Number	RMS base acceleration g's	RMS response acceleration g's	RMS strain μ(mm/mm)	RMS Stress (MPa)
190g	37	0.6731	25.95	905	62.42
235g	37	0.7556	28.1	1022	70.43
291g	26	0.7412	22.13	1064	73.38

Rainflow Stress Cycle Counting

Stress amplitudes below each of materials stress intercept at 1E8 cycles that are listed in material properties Table 4-1 are filtered from the stress cycle count. The 1E8 intercept is typically used for the approximate endurance limit of non-ferrous materials. The result of removing the lower stress range greatly reduce the stress cycles that will later be applied to plot the S-N data. The graphical from of Table 5-13 is shown in Figure 5-4 which displays the total stress cycles counted for damage. As well each of the specimen configurations is plotted in 3D histograms in Figure 5-5 through Figure 5-7. Histogram plots demonstrate both the near zero mean stress as well as the range of which stress cycles that will be included in the damage calculations.

Table 5-13 Rainflow Count of Stress From One Block Cycle Excitation

		MIL-HDBk-5J	Steinberg
	ALL Stress Cycles	> 86.6 MPa	>120 MPa
Specimen Configuration	Stress Cycles Per Block Cycle		
190g (#37 specimen)	46132	16096	5414
235g (#37 specimen)	38816	17766	8548
291g (#26 specimen)	35123	17927	8701
Filtered for stress intercept @ 1E8 cycles			

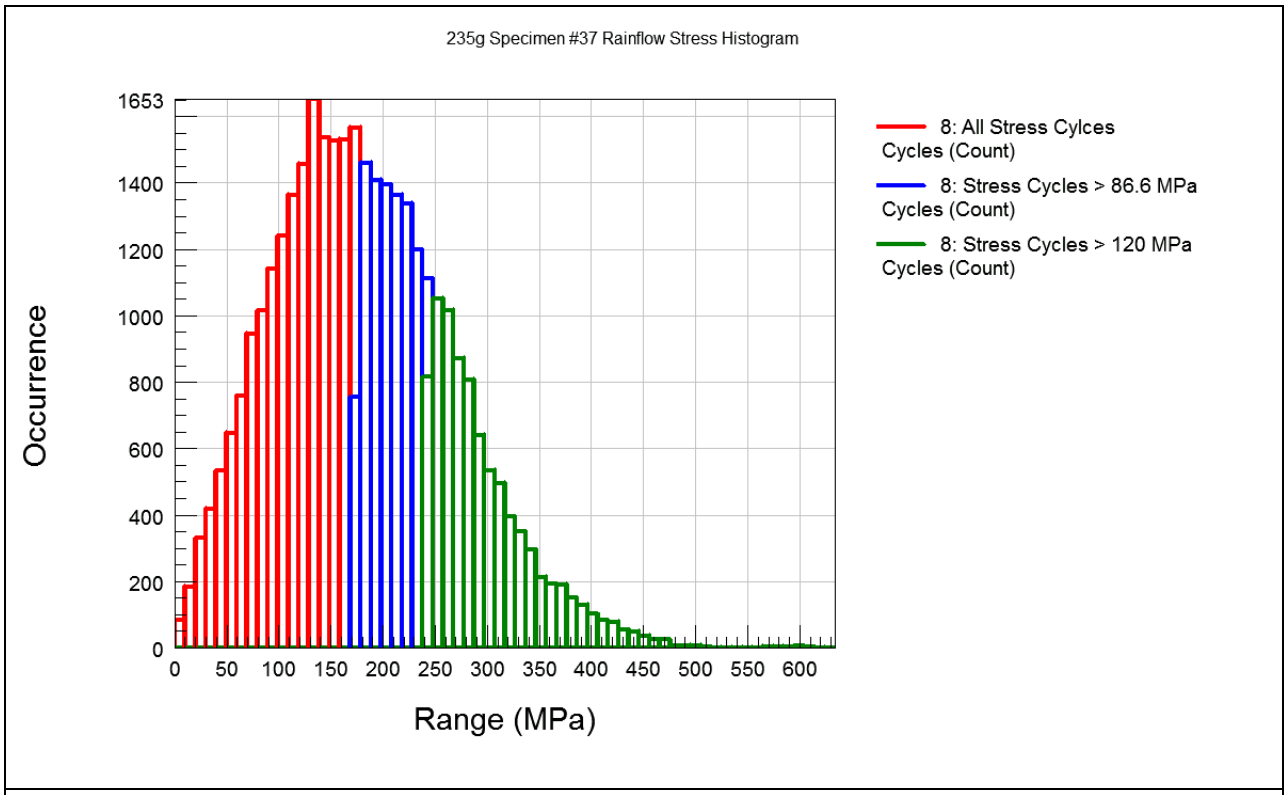

Results for 235g specimen assembly (#37)

Figure 5-4 Block Cycle Rainflow Count Histogram Results

190 g Speciment Configuration (Specimenh #37)		
	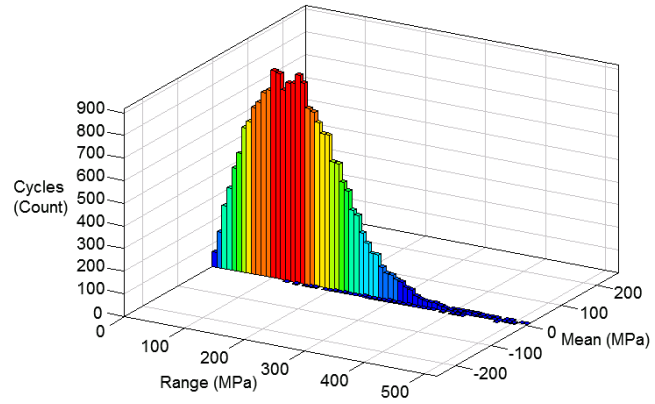	No Stresss Filtering
	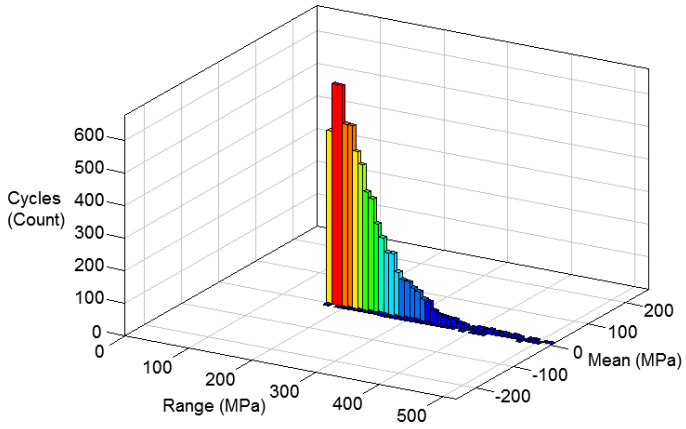	Stress Amplitude > 86.6MPa Stress Range > 173.2 MPa
	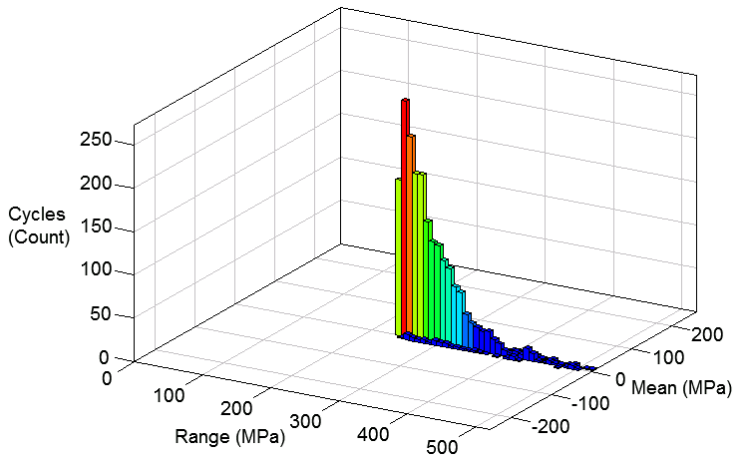	Stress Amplitude > 120 MPa Stress Range > 240 MPa

Figure 5-5 Block Cycle Rainflow Count Histogram Results (190g Specimen)

235 g Speciment Configuration (Specimen #37)	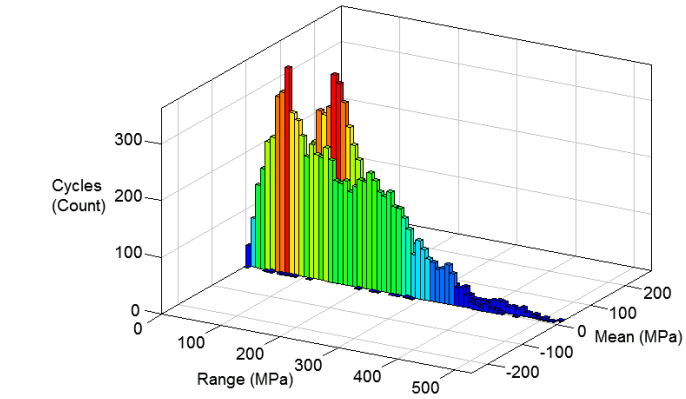	No Stresss Filtering
	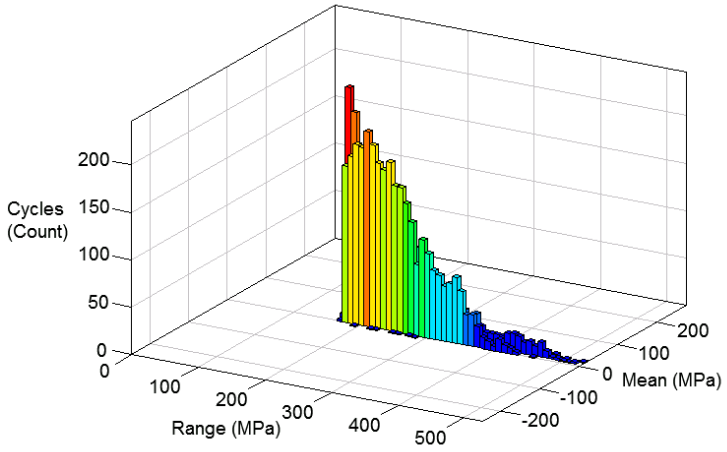	Stress Amplitude > 86.6MPa Stress Range > 173.2 MPa
	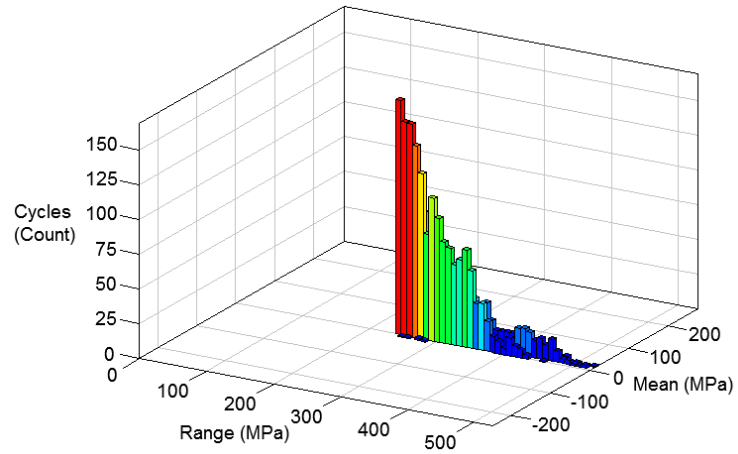	Stress Amplitude > 120 MPa Stresss Range > 240 MPa

Figure 5-6 Block Cycle Rainflow Count Histogram Results (235g specimen)

291 g Speciment Configuration (Specimen #26)	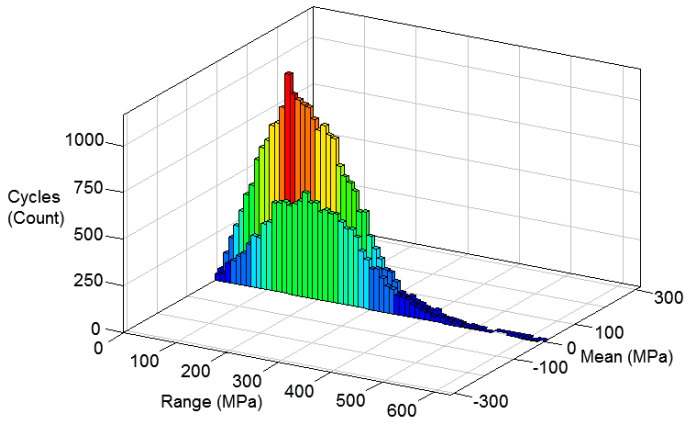	No Stresss Filtering
	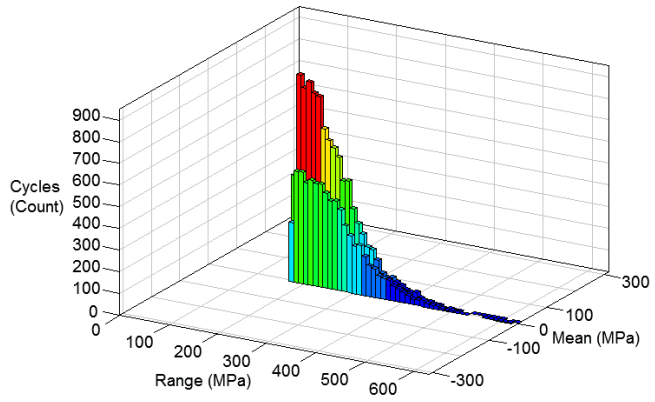	Stress Amplitude > 86.6MPa Stress Range > 173.2 MPa
	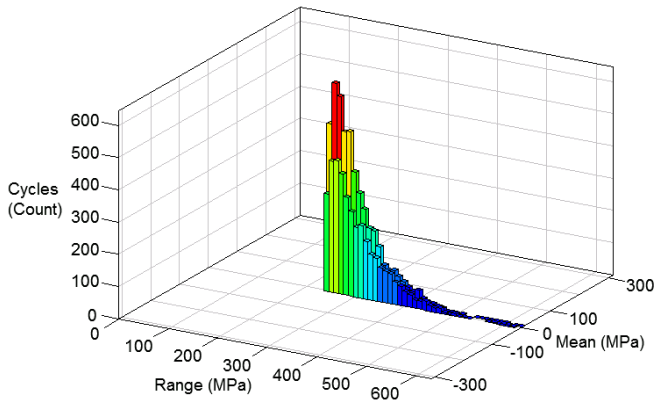	Stress Amplitude > 120 MPa Stress Range > 240 MPa

Figure 5-7 Block Cycle Rainflow Count Histogram Results (291g specimen)

Specimen total stress cycles are calculated by applying equation (4.3). The stress range distributions show that stress amplitudes are mostly reversible [R = -1 equation (2.80)]. The nature of random vibration makes each sequential peak and valley not always equal in magnitudes. However, over the test period the mean loading is near zero. The test specimens have a mean stress value of 1g due to the static stress of the cantilevered mass. The largest static stress is 4.43MPa for the 291g specimen configuration (see Appendix B, Table 7-7 for 190g and 235g). The stress amplitudes are random, therefore no direct stress ratio can be calculated. The mean stress is a constant 4.43MPa for each stress range hence a stress ratio exists for each stress range as shown in Figure 5-8. The occurrences of each stress range are displayed in Figure 5-9. See Appendix B for the 190g and 235g specimen configuration stress range histogram.

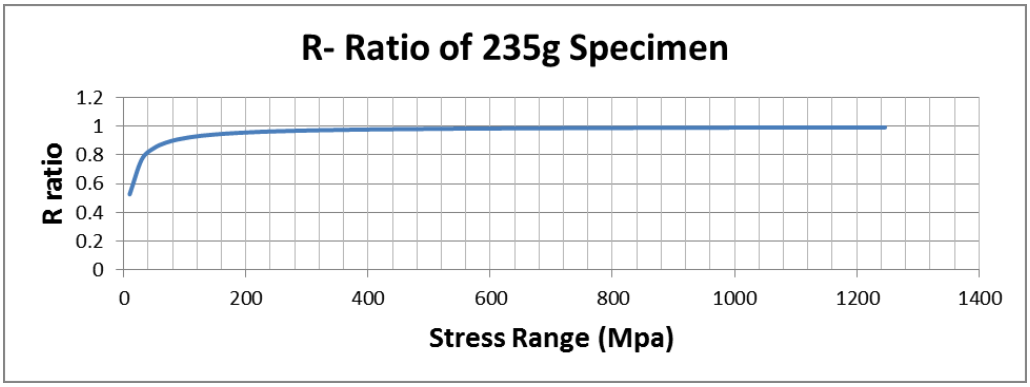

Figure 5-8 Compressive Stress Ratio Specimen Loading

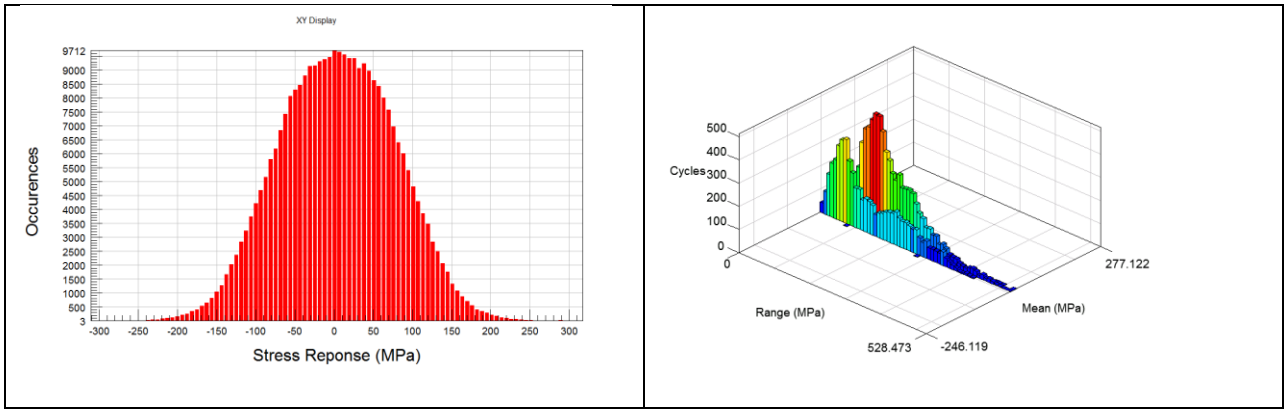

Figure 5-9 Experimental 291g Strain gage Stress Histogram

Fatigue Specimen Failure Results

The tabulated data for specimen stress and non-filtered stress cycles to failure are displayed in Table 5-14 and Figure 5-10. These stress cycles are then filtered for stress amplitudes that were below the approximate fatigue limit for each S-N curve applied that are shown in Table 5-13. Results of only counting stress cycles above 86.6 MPa for MIL-HDBK-5J [19] are shown in Table 5-15 and Figure 5-11 . Results of 120Mpa and higher stress amplitudes for Steinberg [18] stress intercept are shown in Table 5-16 and Figure 5-12. The experimental 86.6 MPa and higher stress cycle data point are overlaid with the S-N materials curve in Figure 5-13. The specimens were well below both MIL-HDBK-5J [19] and Steinberg [18] material S-N curves, but above the S-N curve established by Yahr [20]. It should also be noted that the 190g specimen configuration does not have all twelve data points. Tests attempted with six specimens mounted to the table at one time led to large vibration interactions between these specimens. Iterative acceleration table adjustment controls were not used, leading to random and shifting excitation events. This is shown and discussed in Appendix F, Figure 7-37.

Table 5-14 Experiment Specimen Life Results (non-filtered stress)									
Stress Cycle Filtering: All Stress Cycles									
		Specimen Number	Strain gage RMS μ(mm/mm)	RMS Stress (MPa)	Mean Stress (MPa)	Block Cycles until Failure (600 sec/block)	Time to Failure (seconds)	Stress Cycles	
190 g Configuration	Polished	25	905.43	62.42	88.29	37.05	22228	1709037	46132 stress cycles per block
		26	905.43	62.42	88.29	18.60	11157	857825	
		27	905.43	62.42	88.29	18.35	11011	846568	
		Mean	905.43	62.42	88.29	24.66	14799	1137810	
	Machined	33	905.43	62.42	88.29	16.63	9975	766945	
		34	905.43	62.42	88.29	19.45	11670	897267	
		35	905.43	62.42	88.29	12.99	7796	599408	
		36	905.43	62.42	88.29	24.32	14594	1122084	
		Mean	905.43	62.42	88.29	18.35	11009	846426	
235 g Configuration	Polished	1	1021.61	70.43	99.62	18.25	10951	708457	38816 stress cycles per block
		2	1021.61	70.43	99.62	18.74	11244	727412	
		3	1021.61	70.43	99.62	14.72	8834	571501	
		Mean	1021.61	70.43	99.62	17.24	10343	669123	
	Machined	4	1021.61	70.43	99.62	7.43	4460	288532	
		5	1021.61	70.43	99.62	8.44	5064	327607	
		6	1021.61	70.43	99.62	8.98	5389	348632	
		7	1021.61	70.43	99.62	8.31	4983	322367	
		8	1021.61	70.43	99.62	12.75	7651	494969	
		9	1021.61	70.43	99.62	12.08	7245	468703	
		10	1021.61	70.43	99.62	8.21	4928	318809	
		11	1021.61	70.43	99.62	6.52	3910	252951	
		12	1021.61	70.43	99.62	9.09	5454	352837	
		Mean	1021.61	70.43	99.62	9.09	5454	352823	
291 g Configuration	Polished	13	1064.40	73.38	103.79	13.16	7894	464588	35123 stress cycles per block
		14	1064.40	73.38	103.79	11.84	7101	417918	
		15	1064.40	73.38	103.79	10.94	6564	386313	
		Mean	1064.40	73.38	103.79	11.98	7186	422940	
	Machined	16	1064.40	73.38	103.79	8.30	4977	292913	
		17	1064.40	73.38	103.79	7.97	4779	281260	
		18	1064.40	73.38	103.79	11.70	7017	412974	
		19	1064.40	73.38	103.79	8.66	5195	305743	
		20	1064.40	73.38	103.79	7.39	4433	260897	
		21	1064.40	73.38	103.79	11.28	6766	398202	
		22	1064.40	73.38	103.79	12.08	7250	426687	
		23	1064.40	73.38	103.79	10.86	6514	383371	
		24	1064.40	73.38	103.79	8.86	5317	312923	
		Mean	1064.40	73.38	103.79	9.68	5805	341663	

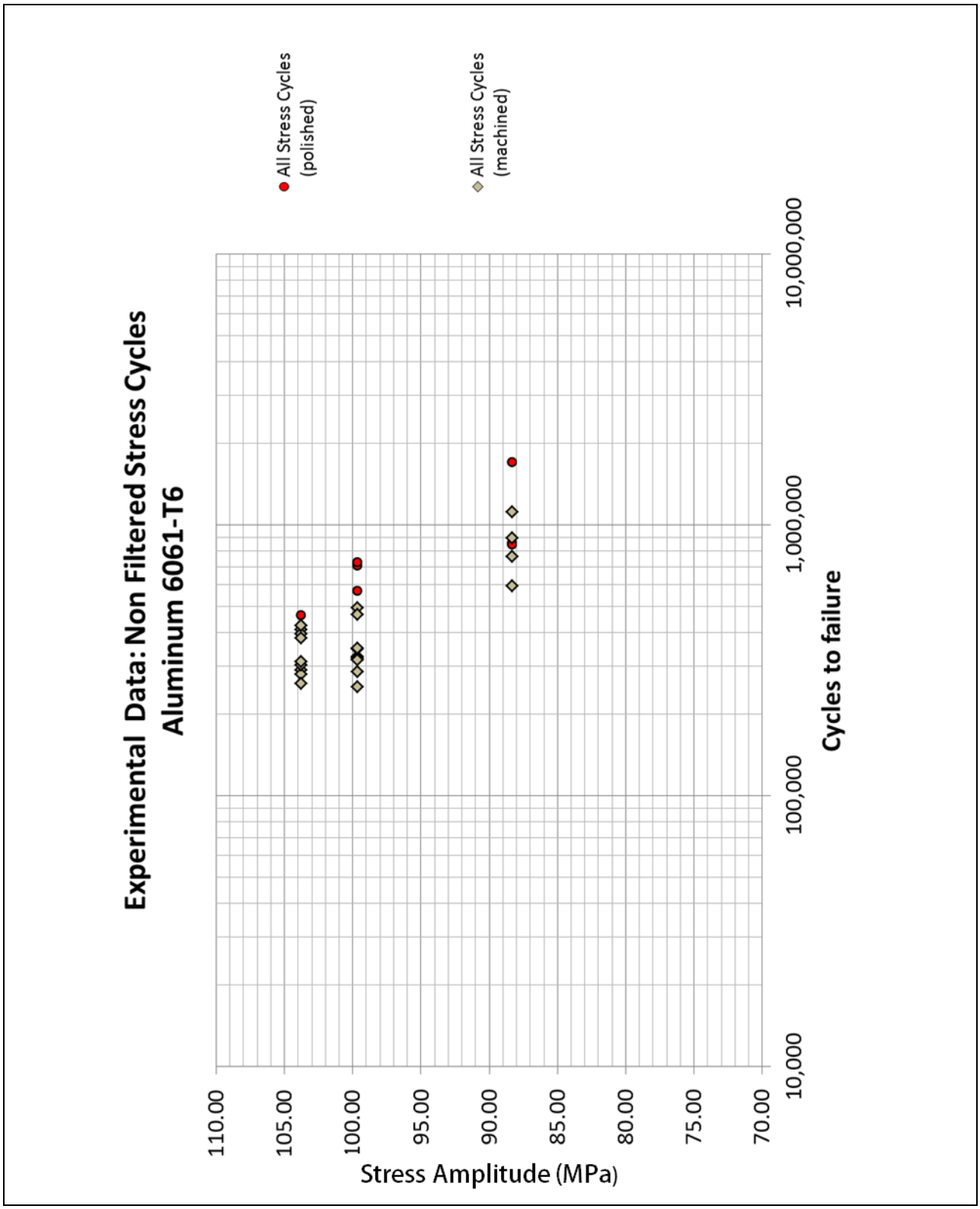

Figure 5-10 Experimental S-N: Non-Filtered Stress Cycles

Table 5-15 Experiment Specimen Life Results (>86.6 MPa Stress Range Filtered)									
Stress Cycle Filtering: Only stress cycles > 86.6 MPa cycles (1E10^8 Fatigue Limit) - MIL-HDBK-5J									
		Specimen Number	Strain gage RMS μ(mm/mm)	RMS Stress (MPa)	Mean Stress (MPa)	Block Cycles Until Failure (600 sec/block)	Time to Failure (seconds)	Stress Cycles	
190 g Configuration	Polished	25	905.43	62.42	88.29	37.05	22228	596303	16096 stress cycles per block
		26	905.43	62.42	88.29	18.60	11157	299305	
		27	905.43	62.42	88.29	18.35	11011	295378	
		Mean	905.43	62.42	88.29	24.66	14799	396995	
	Machined	33	905.43	62.42	88.29	16.63	9975	267596	
		34	905.43	62.42	88.29	19.45	11670	313067	
		35	905.43	62.42	88.29	12.99	7796	209141	
		36	905.43	62.42	88.29	24.32	14594	391508	
		Mean	905.43	62.42	88.29	18.35	11009	295328	
235 g Configuration	Polished	1	1021.61	70.43	99.62	18.25	10951	324442	17766 stress cycles per block
		2	1021.61	70.43	99.62	18.74	11244	333122	
		3	1021.61	70.43	99.62	14.72	8834	261722	
		Mean	1021.61	70.43	99.62	17.24	10343	306429	
	Machined	4	1021.61	70.43	99.62	7.43	4460	132135	
		5	1021.61	70.43	99.62	8.44	5064	150029	
		6	1021.61	70.43	99.62	8.98	5389	159658	
		7	1021.61	70.43	99.62	8.31	4983	147630	
		8	1021.61	70.43	99.62	12.75	7651	226674	
		9	1021.61	70.43	99.62	12.08	7245	214645	
		10	1021.61	70.43	99.62	8.21	4928	146000	
		11	1021.61	70.43	99.62	6.52	3910	115840	
		12	1021.61	70.43	99.62	9.09	5454	161584	
		Mean	1021.61	70.43	99.62	9.09	5454	161577	
291 g Configuration	Polished	13	1064.40	73.38	103.79	13.16	7894	235860	17927 stress cycles per block
		14	1064.40	73.38	103.79	11.84	7101	212166	
		15	1064.40	73.38	103.79	10.94	6564	196121	
		Mean	1064.40	73.38	103.79	11.98	7186	214716	
	Machined	16	1064.40	73.38	103.79	8.30	4977	148704	
		17	1064.40	73.38	103.79	7.97	4779	142789	
		18	1064.40	73.38	103.79	11.70	7017	209656	
		19	1064.40	73.38	103.79	8.66	5195	155218	
		20	1064.40	73.38	103.79	7.39	4433	132451	
		21	1064.40	73.38	103.79	11.28	6766	202157	
		22	1064.40	73.38	103.79	12.08	7250	216618	
		23	1064.40	73.38	103.79	10.86	6514	194627	
		24	1064.40	73.38	103.79	8.86	5317	158863	
		Mean	1064.40	73.38	103.79	9.68	5805	173454	

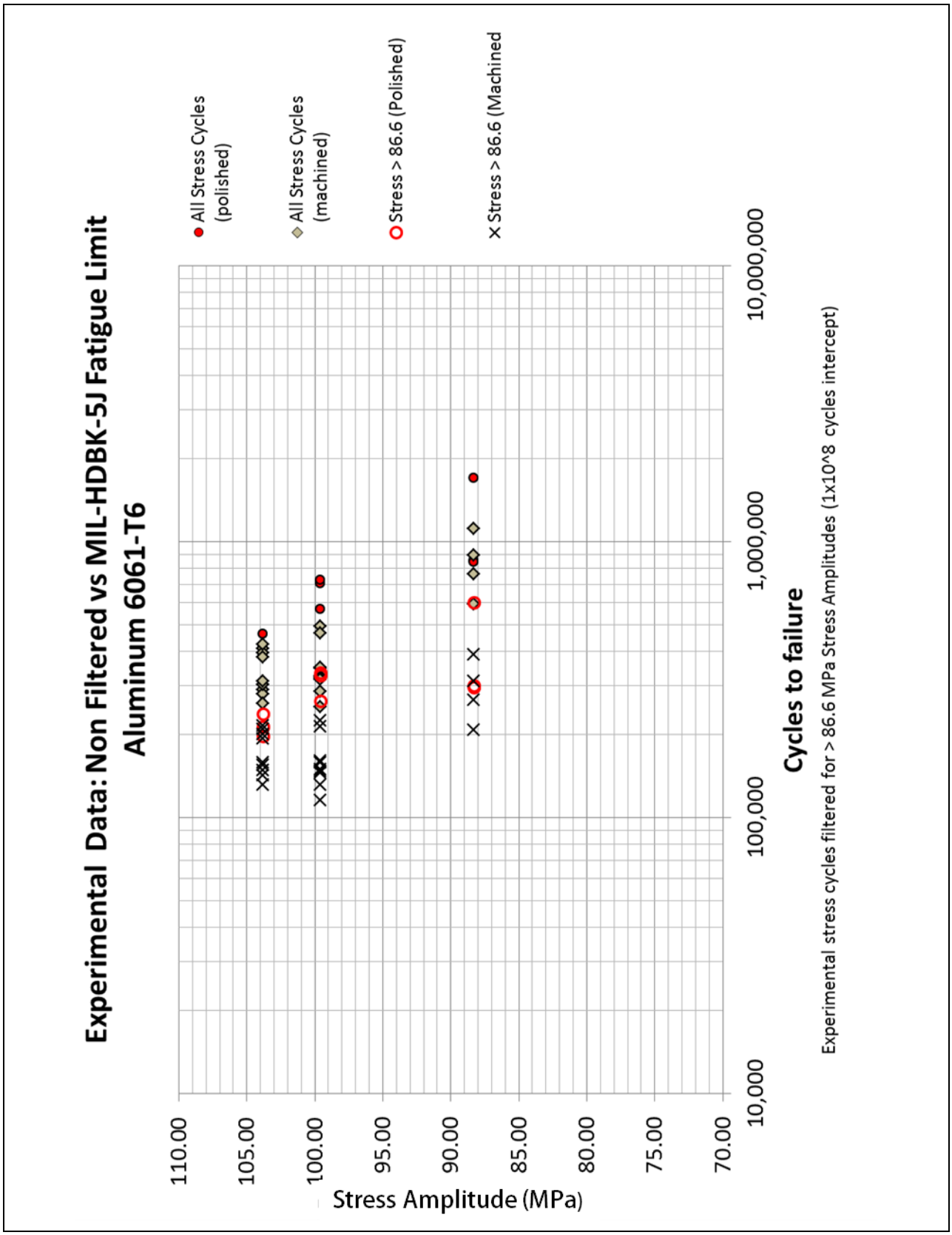

Figure 5-11 Experimental S-N: Stress Amplitude > 86.6 MPa (MIL-HDBK-5J)

Table 5-16 Experiment Specimen Life Results (>120 MPa Stress Range Filtered)									
Stress Cycle Filtering: Only stress cycles > 120 MPa cycles (1E10^8 Fatigue Limit) - Steinberg									
		Specimen Number	Strain gage RMS μ(mm/mm)	RMS Stress (MPa)	Mean Stress (MPa)	Block Cycles until Failure (600 sec/block)	Time to Failure (seconds)	Stress Cycles	
190 g Configuration	Polished	25	905.43	62.42	88.29	37.05	22228	200571	5414 stress cycles per block
		26	905.43	62.42	88.29	18.60	11157	100673	
		27	905.43	62.42	88.29	18.35	11011	99352	
		Mean	905.43	62.42	88.29	24.66	14799	133532	
	Machined	33	905.43	62.42	88.29	16.63	9975	90008	
		34	905.43	62.42	88.29	19.45	11670	105302	
		35	905.43	62.42	88.29	12.99	7796	70346	
		36	905.43	62.42	88.29	24.32	14594	131687	
		Mean	905.43	62.42	88.29	18.35	11009	99336	
235 g Configuration	Polished	1	1021.61	70.43	99.62	18.25	10951	156015	8548 stress cycles per block
		2	1021.61	70.43	99.62	18.74	11244	160190	
		3	1021.61	70.43	99.62	14.72	8834	125855	
		Mean	1021.61	70.43	99.62	17.24	10343	147353	
	Machined	4	1021.61	70.43	99.62	7.43	4460	63540	
		5	1021.61	70.43	99.62	8.44	5064	72145	
		6	1021.61	70.43	99.62	8.98	5389	76775	
		7	1021.61	70.43	99.62	8.31	4983	70991	
		8	1021.61	70.43	99.62	12.75	7651	109001	
		9	1021.61	70.43	99.62	12.08	7245	103217	
		10	1021.61	70.43	99.62	8.21	4928	70208	
		11	1021.61	70.43	99.62	6.52	3910	55704	
		12	1021.61	70.43	99.62	9.09	5454	77701	
		Mean	1021.61	70.43	99.62	9.09	5454	77698	
291 g Configuration	Polished	13	1064.40	73.38	103.79	13.16	7894	114476	8701 stress cycles per block
		14	1064.40	73.38	103.79	11.84	7101	102976	
		15	1064.40	73.38	103.79	10.94	6564	95189	
		Mean	1064.40	73.38	103.79	11.98	7186	104214	
	Machined	16	1064.40	73.38	103.79	8.30	4977	72175	
		17	1064.40	73.38	103.79	7.97	4779	69303	
		18	1064.40	73.38	103.79	11.70	7017	101758	
		19	1064.40	73.38	103.79	8.66	5195	75336	
		20	1064.40	73.38	103.79	7.39	4433	64286	
		21	1064.40	73.38	103.79	11.28	6766	98118	
		22	1064.40	73.38	103.79	12.08	7250	105137	
		23	1064.40	73.38	103.79	10.86	6514	94464	
		24	1064.40	73.38	103.79	8.86	5317	77105	
		Mean	1064.40	73.38	103.79	9.68	5805	84187	

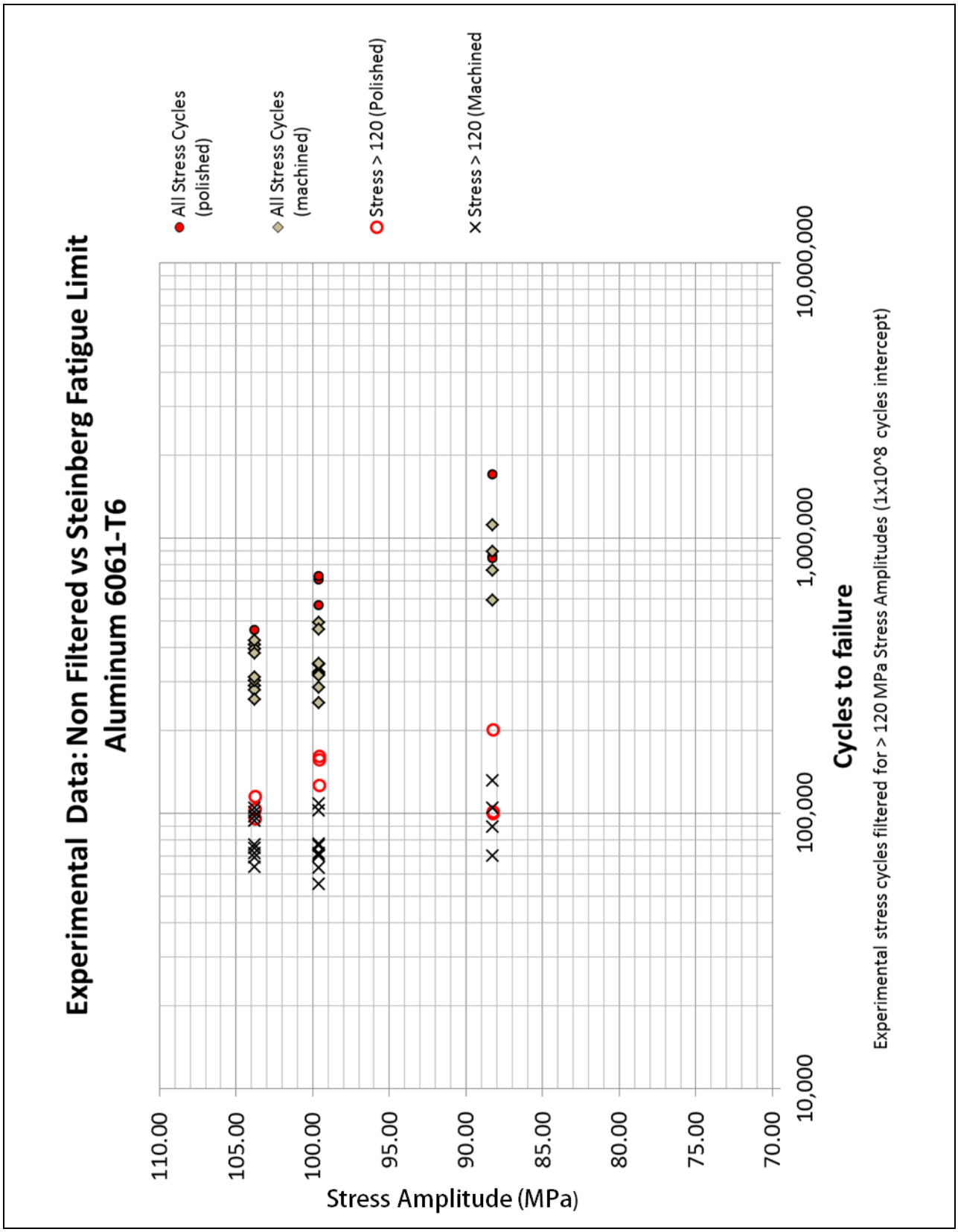

Figure 5-12 Experimental S-N: Stress Amplitude > 120 MPa (Steinberg)

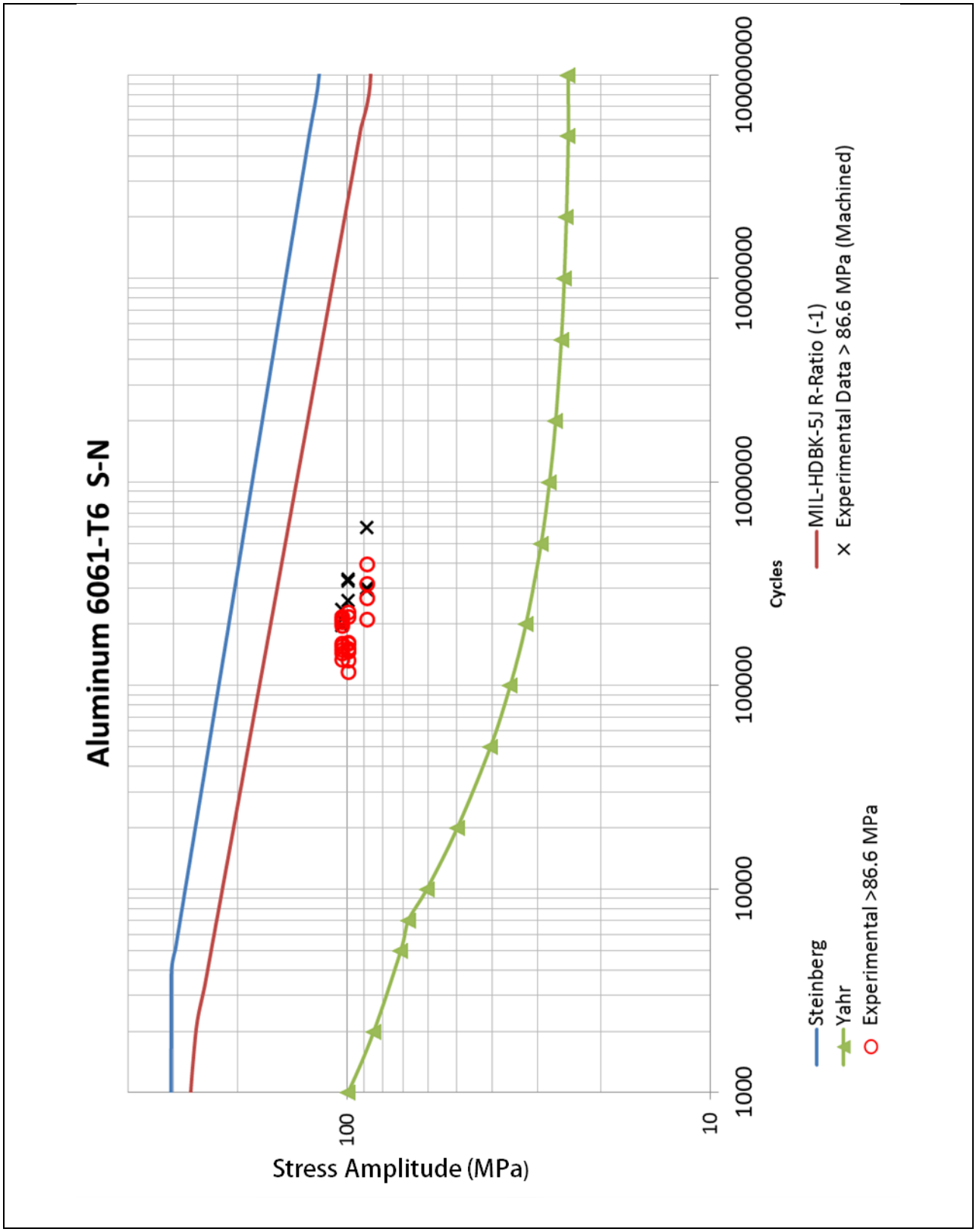

Figure 5-13 Experimental S-N: >86.6 MPa Stress Cycles vs. Published S-N Curves

5.4 Numerical Model Validation

Validation and fine-tuning of numerical specimens and assemblies are important steps in developing a model that was representative of the experimental system. Critical components necessary for calculating numerical fatigue include system validation for natural frequencies, damping, and stress responses. Validation steps or methods applied to tune the models are:

- Validation of system mass (Table 5-17)
- Natural frequencies for free boundary conditions (Table 5-18)
- Natural frequencies for cantilevered constrained boundary conditions (Table 5-19)
- Tuning model with experimental damping values (Table 5-24)

Validation of System Mass

Table 5-17 FEA Test Mass Accuracy

Specimen Configuration	Model Mass (g)	Actual Mean Mass (g)	% Error
190g	190.8	190.77	.016%
235g	232.7	235.16	-1.046%
291g	288.1	291.15	-1.047%

Mass calculation includes bending moment portion of specimen, masses, 2 bolts, and 2 washers

See Appendix I for % error definition

Free Boundary Conditions Natural Frequencies

Modal testing outlined in section 4.5 concludes that the FEA model correlates with a 1.1% error in the specimen assembly's natural frequency. Therefore, the model is acceptable to use for the further investigations under the fatigue loading system constraints.

Table 5-18 Free Boundary Condition Mode 1 Natural Frequency Determination

Specimen	Impulse Test (Hz)	FEA Modal (Hz)	% Error
190g mass	371.15	375.1	1.1%

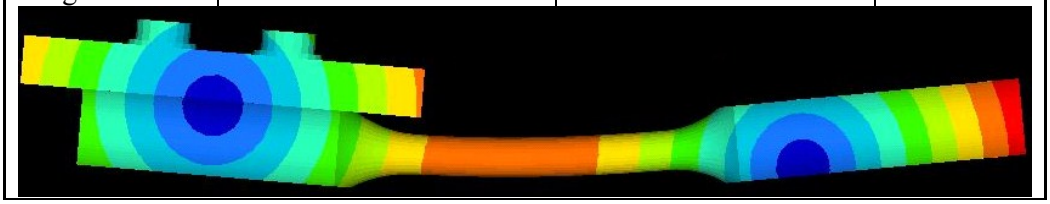

See Appendix I for % error definition

Cantilevered Boundary Conditions Natural Frequencies

Modal testing outlined in section 4.5 concludes that the FEA model correlates all specimen configurations with good results. Results validate the model for correct stiffness and boundary constraints. Hence, the numerical linear frequency response function should represent the physical specimen's response to excitation frequencies. Calculating the numerical frequency response functions are highlighted in section 4.8.1.

Table 5-19 Clamped Boundary Condition Mode 1 Natural Frequency Determination

Specimen Configuration	Impulse Test (Hz)	FEA Modal (Hz)	% Error
190g mass	69.3	69.2	0.1%
235g mass	64.1	64.3	-0.3%
291g mass	58.6	59.0	-0.6%

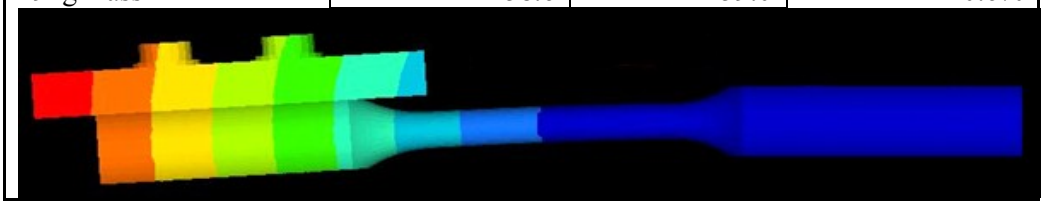

See Appendix I for % error definition

5.5 Applying Experimental Damping Values to Numerical Models

Modal testing with impulse (section 4.5) and forced (section 4.6) response functions are used to develop correction factors for the applied damping ratio (ζ). Damping ratio values are directly measured from the impact model test as shown in Table 5-8. The forced response methods used the determined normalized stress response values from Table 5-9 though Table 5-11 to apply a correction factor for the damping value in the numerical models to produce the same FRF peak stress, as calculated and displayed in Table 5-20 through Table 5-23. A summary of all the resulting damping ratio (ζ) values for each of the methods is shown in Table 5-24.

Table 5-20 Impulse Hammer Damping Ratios

Specimen configuration	**Damping Ratio ζ fraction of critical damping**	**Uniform Structural equivalent viscous damping gi=2 x c/c0**	**Method of damping Determination**
190g	0.121%	0.242%	Impulse Modal Test
235g	0.121%	0.242%	Impulse Modal Test
291g	0.121%	0.242%	Impulse Modal Test

Table 5-21 Forced Response Sine Frequency Sweep 0.1 Hz/sec Constant Amplitude Damping Ratio Correction Factors

Specimen configuration	**Damping Ratio ζ fraction of critical damping**	**Uniform Structural equivalent viscous damping gi=2 x c/c0**	**Method of damping Determination**	1 G max stress response		**Correction Factor**
				Analytical Stress Approximation (MPa)	**Testing** Sine Dwell Peak Stress (MPa)	
190g	0.121%	0.242%	Impulse Modal Test	1288	1246	0.97
	0.125%	0.250%	Correction Factor			
235g	0.121%	0.242%	Impulse Modal Test	1498	1340	0.89
	0.135%	0.271%	Correction Factor			
291g	0.121%	0.242%	Impulse Modal Test	1727	1484	0.86
	0.141%	0.282%	Correction Factor			

Table 5-22 Forced Response Sine Frequency Dwell Constant Amplitude Damping Ratio Correction Factors

Specimen configuration	**Damping Ratio ζ fraction of critical damping**	**Uniform Structural equivalent viscous damping gi=2 x c/c0**	**Method of damping Determination**	1 G max stress response		**Correction Factor**
				Analytical Stress Approximation (MPa)	**Testing** Sine Dwell Peak Stress (MPa)	
190g	0.121%	0.242%	Impulse Modal Test	1288	2586	2.01
	0.060%	0.120%	Correction Factor			
235g	0.121%	0.242%	Impulse Modal Test	1498	1734	1.16
	0.105%	0.209%	Correction Factor			
291g	0.121%	0.242%	Impulse Modal Test	1727	1270	0.74
	0.164%	0.329%	Correction Factor			

Table 5-23 Forced Response PSD Block Cycle Damping Ratio Correction Factors						
Specimen configuration	**Damping Value ζ fraction of critical damping**	**Uniform Structural equivalent viscous damping gi=2 x c/c0**	**Method of damping Determination**	1 G max stress response **Analytical** Stress Approximation (MPa)	1 G max stress response **Testing** PSD Block Cycle FRF peak Stress (MPa)	**Correction Factor**
190g	0.121%	0.242%	Impulse Modal Test	1288	937	0.73
	0.166%	0.332%	Correction Factor			
235g	0.121%	0.242%	Impulse Modal Test	1498	1012	0.68
	0.179%	0.358%	Correction Factor			
291g	0.121%	0.242%	Impulse Modal Test	1727	1047	0.61
	0.200%	0.399%	Correction Factor			

Table 5-24 Experimental Damping Method Comparison				
	Damping Methods and values applied			
Mass Configuration	**Impulse**	**Sweep**	**Dwell**	**PSD**
190g	0.121%	0.125%	0.060%	0.166%
235g	0.121%	0.135%	0.105%	0.179%
291g	0.121%	0.141%	0.164%	0.200%

5.6 Numerical Shake Table

The numerical simulation completed for each of the damping values and specimen configurations are shown in Table 4-7. These configurations are calculated for fatigue damage by using aluminum 6061-T6 S-N curves published by Steinberg [18] and MIL-HDBK-5J [19].

The fatigue results of each of these configurations are plotted by using the mean peak of the stress function versus the cycles to failure. The charts are displayed by the S-N material used to calculate the cycle stress damage, as well as the damping determination methods. The numerical results of using MIL-HDBK-5J [19] are compared to the filtered experimental Stress cycles from the published stress intercept of 86.6 MPa at 1E8 cycles. Similarly, numerical results using Steinberg [18] are compared to the filtered experimental stress cycles from the published stress intercept of 120 MPa at 1E8 cycles. Each of these S-N materials is applied to the four different damping methods (impulse, sine, sweep, and PSD). The tabular data for all specimens are displayed in Table 5-25 through Table 5-32.

Table 5-25 Experimental vs. Numerical Specimen Life: (Method: Impulse – SN: Steinberg)										
Damping Method: Impulse Forced Response										
SN Material: Aluminum 6061-T6 Steinberg										
Stress Cycle Filtering: Only stress cycles > 120 MPa cycles (1E10^8 Fatigue Limit)										
		Specimen Number	Experimental				Numerical			
			RMS Stress (MPa)	Max Stress Cycle (MPa)	Block Cycles Until Failure 600 sec block	Total Stress Cycles > 86.6MPa	RMS Stress (MPa)	Max Stress Cycle (MPa)	Block Cycles Until Failure 600 sec block	Total Stress Cycles
190 g Configuration	Polished	25	62.4	263.3	37.0	200571	58.2	268.3	16.7	90376
		26	62.4	263.3	18.6	100673	62.2	286.7	4.7	25694
		27	62.4	263.3	18.4	99352	61.3	282.8	4.7	25700
		Mean	62.4	263.3	24.7	133532	60.6	279.3	8.7	47257
	Machined	33	62.4	263.3	16.6	90008	65.4	301.6	1.4	7711
		34	62.4	263.3	19.5	105302	59.5	274.2	15.8	85449
		35	62.4	263.3	13.0	70346	58.4	269.4	16.3	88048
		36	62.4	263.3	24.3	131687	57.8	266.5	29.8	161150
		Mean	62.4	263.3	18.3	99336	60.3	277.9	15.8	85589
235 g Configuration	Polished	1	70.4	277.1	18.3	156015	64.4	295.9	1.5	13190
		2	70.4	277.1	18.7	160190	63.2	290.2	2.8	23815
		3	70.4	277.1	14.7	125855	64.5	296.6	1.5	13190
		Mean	70.4		17.2	147353	64.0	294.2	2.0	16731
	Machined	4	70.4	277.1	7.4	63540	65.6	301.4	1.5	13172
		5	70.4	277.1	8.4	72145	64.5	296.5	1.5	13190
		6	70.4	277.1	9.0	76775	65.3	300.2	1.5	13087
		7	70.4	277.1	8.3	70991	63.0	289.4	2.8	23823
		8	70.4	277.1	12.8	109001	62.7	288.1	2.8	23840
		9	70.4	277.1	12.1	103217	63.4	291.4	2.8	23806
		10	70.4	277.1	8.2	70208	65.1	299.1	1.5	13181
		11	70.4	277.1	6.5	55704	64.6	296.7	1.5	13164
		12	70.4	277.1	9.1	77701	63.6	292.3	2.8	23644
		Mean	70.4	277.1	9.1	77698	64.2	295.0	2.1	17879
291 g Configuration	Polished	13	73.4	317.4	13.2	114476	82.1	375.8	0.0	222
		14	73.4	317.4	11.8	102976	79.4	363.5	0.0	355
		15	73.4	317.4	10.9	95189	78.9	361.0	0.0	355
		Mean	73.4	317.4	12.0	104214	80.1	366.8	0.0	311
	Machined	16	73.4	317.4	8.3	72175	79.7	364.8	0.0	355
		17	73.4	317.4	8.0	69303	77.9	356.5	0.1	576
		18	73.4	317.4	11.7	101758	77.9	356.3	0.1	576
		19	73.4	317.4	8.7	75336	78.2	357.9	0.1	576
		20	73.4	317.4	7.4	64286	81.1	371.1	0.0	355
		21	73.4	317.4	11.3	98118	79.3	362.7	0.0	355
		22	73.4	317.4	12.1	105137	81.0	370.5	0.0	355
		23	73.4	317.4	10.9	94464	78.3	358.4	0.1	576
		24	73.4	317.4	8.9	77105	78.5	359.3	0.1	576
		Mean	73.4	317.4	9.7	84187	79.1	361.9	0.1	478

Table 5-26 Experimental vs. Numerical Specimen Life: (Method: Impulse – SN: MIL-HDBK-5J)										
Damping Method: Impulse Forced Response										
SN Material: SN Material: Aluminum 6061-T6 MIL-HDBK-5J										
Stress Cycle Filtering: Only stress cycles > 86.6 MPa cycles (1E10^8 Fatigue Limit)										
		Specimen Number	Experimental (86.6> MPa cycles)				Numerical			
			RMS Stress (MPa)	Max Stress Cycle (MPa)	Block Cycles Until Failure 600 sec block	Total Stress Cycles > 86.6MPa	RMS Stress (MPa)	Max Stress Cycle (MPa)	Block Cycles Until Failure 600 sec block	Total Stress Cycles
190 g Configuration	Polished	25	62.4	263.3	37.0	596303	58.2	268.3	38.1	613258
		26	62.4	263.3	18.6	299305	62.2	286.7	19.8	318540
		27	62.4	263.3	18.4	295378	61.3	282.8	22.7	365379
		Mean	62.4	263.3	24.7	396995	60.6	279.3	26.9	432392
	Machined	33	62.4	263.3	16.6	267596	65.4	301.6	11.6	187036
		34	62.4	263.3	19.5	313067	59.5	274.2	28.6	459541
		35	62.4	263.3	13.0	209141	58.4	269.4	35.0	563360
		36	62.4	263.3	24.3	391508	57.8	266.5	38.1	612936
		Mean	62.4	263.3	18.3	295328	60.3	277.9	28.3	455718
235 g Configuration	Polished	1	70.4	277.1	18.3	324442	64.4	295.9	15.1	268240
		2	70.4	277.1	18.7	333122	63.2	290.2	18.3	325123
		3	70.4	277.1	14.7	261722	64.5	296.6	14.8	262552
		Mean	70.4		17.2	306429	64.0	294.2	16.1	285305
	Machined	4	70.4	277.1	7.4	132135	65.6	301.4	12.6	223800
		5	70.4	277.1	8.4	150029	64.5	296.5	14.8	263440
		6	70.4	277.1	9.0	159658	65.3	310.8	12.5	222911
		7	70.4	277.1	8.3	147630	63.0	289.4	18.8	333656
		8	70.4	277.1	12.8	226674	62.7	288.1	19.6	348765
		9	70.4	277.1	12.1	214645	63.4	291.4	17.6	312324
		10	70.4	277.1	8.2	146000	65.1	299.1	13.6	241576
		11	70.4	277.1	6.5	115840	64.6	296.7	14.5	256863
		12	70.4	277.1	9.1	161584	63.6	292.3	16.5	292771
		Mean	70.4	277.1	9.1	161577	64.2	296.2	15.6	277345
291 g Configuration	Polished	13	73.4	317.4	13.2	235860	82.1	375.8	1.5	26980
		14	73.4	317.4	11.8	212166	79.4	363.5	2.1	37432
		15	73.4	317.4	10.9	196121	78.9	361.0	2.2	39995
		Mean	73.4	317.4	12.0	214716	80.1	366.8	1.9	34802
	Machined	16	73.4	317.4	8.3	148704	82.1	375.8	1.5	26873
		17	73.4	317.4	8.0	142789	77.9	356.5	2.5	44871
		18	73.4	317.4	11.7	209656	77.9	356.3	2.5	45033
		19	73.4	317.4	8.7	155218	78.2	357.9	2.4	43150
		20	73.4	317.4	7.4	132451	81.1	371.1	1.7	30350
		21	73.4	317.4	11.3	202157	79.3	362.7	2.1	37898
		22	73.4	317.4	12.1	216618	81.0	370.5	1.7	30817
		23	73.4	317.4	10.9	194627	78.3	358.4	2.4	42541
		24	73.4	317.4	8.9	158863	78.3	358.4	2.4	42541
		Mean	73.4	317.4	9.7	173454	79.3	363.1	2.1	38230

Table 5-27 Experimental vs. Numerical Specimen Life: (Method: Sweep – SN: Steinberg)										
Damping Method: Sine Sweep 0.1hz Constant Amplitude Forced Response										
SN Material: Aluminum 6061-T6 Steinberg										
Stress Cycle Filtering: Only stress cycles > 120 MPa cycles (1E10^8 Fatigue Limit)										
			Experimental				Numerical			
		Specimen Number	RMS Stress (MPa)	Max Stress Cycle (MPa)	Block Cycles Until Failure 600 sec block	Total Stress Cycles > 86.6MPa	RMS Stress (MPa)	Max Stress Cycle (MPa)	Block Cycles Until Failure 600 sec block	Total Stress Cycles
190 g Configuration	Polished	25	62.4	263.3	37.0	200571	57.3	264.1	31.7	171872
		26	62.4	263.3	18.6	100673	61.2	282.2	4.8	25759
		27	62.4	263.3	18.4	99352	60.4	278.3	8.8	47804
		Mean	62.4	263.3	24.7	133532	59.6	274.9	15.1	81812
	Machined	33	62.4	263.3	16.6	90008	64.4	296.8	1.4	7738
		34	62.4	263.3	19.5	105302	58.5	269.9	16.4	88535
		35	62.4	263.3	13.0	70346	57.5	265.1	30.8	166511
		36	62.4	263.3	24.3	131687	56.9	262.3	31.0	167865
		Mean	62.4	263.3	18.3	99336	59.3	273.5	19.9	107662
235 g Configuration	Polished	1	70.4	277.1	18.3	156015	60.9	279.6	9.5	81044
		2	70.4	277.1	18.7	160190	59.7	274.2	9.5	81428
		3	70.4	277.1	14.7	125855	61.0	280.3	9.5	80992
		Mean	70.4		17.2	147353	60.5	278.0	9.5	81155
	Machined	4	70.4	277.1	7.4	63540	61.9	284.6	5.1	43296
		5	70.4	277.1	8.4	72145	61.0	280.1	9.3	79864
		6	70.4	277.1	9.0	76775	61.7	283.6	5.1	43330
		7	70.4	277.1	8.3	70991	59.5	273.5	9.4	80531
		8	70.4	277.1	12.8	109001	59.3	272.3	17.5	149505
		9	70.4	277.1	12.1	103217	59.9	275.3	9.4	80351
		10	70.4	277.1	8.2	70208	61.5	282.7	5.1	43364
		11	70.4	277.1	6.5	55704	61.0	280.4	5.1	43441
		12	70.4	277.1	9.1	77701	60.1	276.2	9.4	80266
		Mean	70.4	277.1	9.1	77698	60.7	278.7	8.4	71550
291 g Configuration	Polished	13	73.4	317.4	13.2	114476	72.3	343.5	0.2	1593
		14	73.4	317.4	11.8	102976	73.1	334.3	0.2	1592
		15	73.4	317.4	10.9	95189	72.3	331.1	0.2	1593
		Mean	73.4	317.4	12.0	104214	72.6	336.3	0.2	1593
	Machined	16	73.4	317.4	8.3	72175	73.1	334.3	0.2	1591
		17	73.4	317.4	8.0	69303	71.4	326.7	0.3	2704
		18	73.4	317.4	11.7	101758	71.4	326.7	0.3	2704
		19	73.4	317.4	8.7	75336	71.7	328.3	0.3	2703
		20	73.4	317.4	7.4	64286	74.2	339.7	0.1	950
		21	73.4	317.4	11.3	98118	72.7	332.5	0.2	1591
		22	73.4	317.4	12.1	105137	74.2	339.5	0.1	950
		23	73.4	317.4	10.9	94464	71.8	328.7	0.2	1592
		24	73.4	317.4	8.9	77105	72.0	329.6	0.2	1592
		Mean	73.4	317.4	9.7	84187	72.5	331.8	0.2	1820

Table 5-28 Experimental vs. Numerical Specimen Life: (Method: Sweep – SN: MIL-HDBK-5J)											
Damping Method: Sine Sweep 0.1hz Constant Amplitude Forced Response											
SN Material: SN Material: Aluminum 6061-T6 MIL-HDBK-5J											
Stress Cycle Filtering: Only stress cycles > 86.6 MPa cycles (1E10^8 Fatigue Limit)											
			Experimental (86.6> MPa cycles)					Numerical			
		Specimen Number	RMS Stress (MPa)	Max Stress Cycle (MPa)	Block Cycles Until Failure 600 sec block	Total Stress Cycles > 86.6MPa		RMS Stress (MPa)	Max Stress Cycle (MPa)	Block Cycles Until Failure 600 sec block	Total Stress Cycles
190 g Configuration	Polished	25	62.4	263.3	37.0	596303		57.3	264.1	44.5	716272
		26	62.4	263.3	18.6	299305		61.2	282.2	23.2	372622
		27	62.4	263.3	18.4	295378		60.4	278.3	26.5	427188
		Mean	62.4	263.3	24.7	396995		59.6	274.9	31.4	505361
	Machined	33	62.4	263.3	16.6	267596		64.4	296.8	13.6	219228
		34	62.4	263.3	19.5	313067		58.5	269.9	34.3	551610
		35	62.4	263.3	13.0	209141		57.5	265.1	40.8	656878
		36	62.4	263.3	24.3	391508		56.9	262.3	45.2	728183
		Mean	62.4	263.3	18.3	295328		59.3	273.5	33.5	538975
235 g Configuration	Polished	1	70.4	277.1	18.3	324442		60.9	279.6	26.3	468220
		2	70.4	277.1	18.7	333122		59.7	274.2	31.9	567410
		3	70.4	277.1	14.7	261722		61.0	280.3	25.7	457376
		Mean	70.4		17.2	306429		60.5	278.0	28.0	497669
	Machined	4	70.4	277.1	7.4	132135		61.9	284.6	21.4	379873
		5	70.4	277.1	8.4	150029		61.0	280.1	24.9	442622
		6	70.4	277.1	9.0	159658		61.7	283.6	22.1	393027
		7	70.4	277.1	8.3	147630		59.5	273.5	31.4	557811
		8	70.4	277.1	12.8	226674		59.3	272.3	32.8	582520
		9	70.4	277.1	12.1	214645		59.9	275.3	29.4	522792
		10	70.4	277.1	8.2	146000		61.5	282.7	22.8	405293
		11	70.4	277.1	6.5	115840		61.0	280.4	24.7	438534
		12	70.4	277.1	9.1	161584		60.1	276.2	28.5	506972
		Mean	70.4	277.1	9.1	161577		60.7	278.7	26.4	469938
291 g Configuration	Polished	13	73.4	317.4	13.2	235860		75.1	343.5	3.6	65290
		14	73.4	317.4	11.8	212166		72.8	333.2	4.9	88183
		15	73.4	317.4	10.9	196121		72.3	331.1	5.2	93758
		Mean	73.4	317.4	12.0	214716		73.4	335.9	4.6	82410
	Machined	16	73.4	317.4	8.3	148704		73.1	334.3	4.7	83683
		17	73.4	317.4	8.0	142789		71.4	326.7	5.8	104640
		18	73.4	317.4	11.7	209656		71.4	326.7	5.9	104891
		19	73.4	317.4	8.7	155218		71.7	328.3	5.6	99925
		20	73.4	317.4	7.4	132451		74.2	339.7	4.0	71744
		21	73.4	317.4	11.3	202157		72.7	332.5	4.9	88237
		22	73.4	317.4	12.1	216618		74.2	339.5	4.0	72031
		23	73.4	317.4	10.9	194627		71.8	328.7	5.5	98760
		24	73.4	317.4	8.9	158863		72.0	329.6	5.4	95999
		Mean	73.4	317.4	9.7	173454		72.5	331.8	5.1	91101

Table 5-29 Experimental vs. Numerical Specimen Life: (Method: Dwell – SN: Steinberg)										
Damping Method: Sine Dwell Frequency Constant Amplitude Forced Response										
SN Material: Aluminum 6061-T6 Steinberg										
Stress Cycle Filtering: Only stress cycles > 120 MPa cycles (1E10^8 Fatigue Limit)										
			Experimental (86.6> MPa cycles)					Numerical		
		Specimen Number	RMS Stress (MPa)	Max Stress Cycle (MPa)	Block Cycles Until Failure 600 sec block	Total Stress Cycles > 86.6MPa	RMS Stress (MPa)	Max Stress Cycle (MPa)	Block Cycles Until Failure 600 sec block	Total Stress Cycles
190 g Configuration	Polished	25	62.4	263.3	37.0	200571	79.1	364.7	0.035	189
		26	62.4	263.3	18.6	100673	84.8	391.0	0.014	75
		27	62.4	263.3	18.4	99352	83.4	384.6	0.022	118
		Mean	62.4	263.3	24.7	133532	82.4	380.1	0.024	127
	Machined	33	62.4	263.3	16.6	90008	89.0	410.5	0.010	53
		34	62.4	263.3	19.5	105302	80.8	372.5	0.035	189
		35	62.4	263.3	13.0	70346	79.4	366.1	0.035	189
		36	62.4	263.3	24.3	131687	78.6	362.4	0.057	307
		Mean	62.4	263.3	18.3	99336	82.0	377.9	0.034	184
235 g Configuration	Polished	1	70.4	277.1	18.3	156015	68.6	315.1	0.494	4225
		2	70.4	277.1	18.7	160190	67.2	309.0	0.867	7407
		3	70.4	277.1	14.7	125855	68.7	315.7	0.494	4225
		Mean	70.4		17.2	147353	68.2	313.3	0.618	5286
	Machined	4	70.4	277.1	7.4	63540	69.9	321.3	0.286	2444
		5	70.4	277.1	8.4	72145	68.7	315.7	0.493	4216
		6	70.4	277.1	9.0	76775	69.6	319.7	0.493	4212
		7	70.4	277.1	8.3	70991	67.1	308.1	0.864	7385
		8	70.4	277.1	12.8	109001	66.8	306.7	0.864	7389
		9	70.4	277.1	12.1	103217	67.5	310.2	0.864	7381
		10	70.4	277.1	8.2	70208	69.3	318.4	0.493	4213
		11	70.4	277.1	6.5	55704	68.7	315.9	0.493	4216
		12	70.4	277.1	9.1	77701	67.7	311.2	0.863	7379
		Mean	70.4	277.1	9.1	77698	68.4	314.1	0.635	5426
291 g Configuration	Polished	13	73.4	317.4	13.2	114476	68.8	314.9	0.538	4680
		14	73.4	317.4	11.8	102976	66.9	306.3	0.943	8208
		15	73.4	317.4	10.9	95189	66.5	344.5	0.944	8212
		Mean	73.4	317.4	12.0	104214	67.4	321.9	0.808	7033
	Machined	16	73.4	317.4	8.3	72175	67.2	285.2	0.940	8181
		17	73.4	317.4	8.0	69303	65.6	300.4	1.671	14539
		18	73.4	317.4	11.7	101758	65.6	300.4	1.671	14539
		19	73.4	317.4	8.7	75336	66.0	302.0	0.942	8193
		20	73.4	317.4	7.4	64286	68.1	311.8	0.537	4673
		21	73.4	317.4	11.3	98118	66.8	305.7	0.941	8185
		22	73.4	317.4	12.1	105137	68.2	312.1	0.537	4672
		23	73.4	317.4	10.9	94464	66.1	302.3	0.942	8193
		24	73.4	317.4	8.9	77105	66.3	303.3	0.941	8191
		Mean	73.4	317.4	9.7	84187	66.7	302.6	1.014	8819

Table 5-30 Experimental vs. Numerical Specimen Life: (Method: Dwell – SN: MIL-HDBK-5J)											
Damping Method: Sine Dwell Frequency Constant Amplitude Forced Response											
SN Material: SN Material: Aluminum 6061-T6 MIL-HDBK-5J											
Stress Cycle Filtering: Only stress cycles > 86.6 MPa cycles (1E10^8 Fatigue Limit)											
			Experimental (86.6> MPa cycles)					Numerical			
		Specimen Number	RMS Stress (MPa)	Max Stress Cycle (MPa)	Block Cycles Until Failure 600 sec block	Total Stress Cycles > 86.6MPa		RMS Stress (MPa)	Max Stress Cycle (MPa)	Block Cycles Until Failure 600 sec block	Total Stress Cycles
190 g Configuration	Polished	25	62.4	263.3	37.0	596303		79.1	364.7	1.9	29906
		26	62.4	263.3	18.6	299305		84.8	391.0	0.9	15038
		27	62.4	263.3	18.4	295378		83.4	384.6	1.1	17722
		Mean	62.4	263.3	24.7	396995		82.4	380.1	1.3	20889
	Machined	33	62.4	263.3	16.6	267596		89.0	410.5	0.6	9355
		34	62.4	263.3	19.5	313067		80.8	372.5	1.5	24144
		35	62.4	263.3	13.0	209141		79.4	366.1	1.8	28538
		36	62.4	263.3	24.3	391508		78.6	362.4	2.0	31548
		Mean	62.4	263.3	18.3	295328		82.0	377.9	1.5	23396
235 g Configuration	Polished	1	70.4	277.1	18.3	324442		68.6	315.1	8.1	144857
		2	70.4	277.1	18.7	333122		67.2	309.0	9.9	175627
		3	70.4	277.1	14.7	261722		68.7	315.7	8.0	142119
		Mean	70.4		17.2	306429		68.2	313.3	8.7	154201
	Machined	4	70.4	277.1	7.4	132135		69.9	321.3	6.6	116824
		5	70.4	277.1	8.4	150029		68.7	315.7	7.8	138351
		6	70.4	277.1	9.0	159658		69.6	319.7	6.9	122334
		7	70.4	277.1	8.3	147630		67.1	308.1	9.9	175236
		8	70.4	277.1	12.8	226674		66.8	306.7	10.3	183271
		9	70.4	277.1	12.1	214645		67.5	310.2	9.2	164055
		10	70.4	277.1	8.2	146000		69.3	318.4	7.2	127329
		11	70.4	277.1	6.5	115840		68.7	315.9	7.8	137800
		12	70.4	277.1	9.1	161584		67.7	311.2	9.0	159380
		Mean	70.4	277.1	9.1	161577		68.4	314.1	8.3	147175
291 g Configuration	Polished	13	73.4	317.4	13.2	235860		68.8	314.9	8.6	153599
		14	73.4	317.4	11.8	212166		66.9	306.3	11.3	201679
		15	73.4	317.4	10.9	196121		66.5	304.6	11.9	213331
		Mean	73.4	317.4	12.0	214716		67.4	308.6	10.6	189536
	Machined	16	73.4	317.4	8.3	148704		67.2	307.3	10.6	189668
		17	73.4	317.4	8.0	142789		65.6	300.4	13.2	236816
		18	73.4	317.4	11.7	209656		65.6	300.4	13.2	237174
		19	73.4	317.4	8.7	155218		66.0	302.0	12.5	224625
		20	73.4	317.4	7.4	132451		68.1	311..8	9.2	164642
		21	73.4	317.4	11.3	202157		66.8	305.7	11.1	199528
		22	73.4	317.4	12.1	216618		68.2	312.1	9.1	163548
		23	73.4	317.4	10.9	194627		66.1	302.3	12.4	222474
		24	73.4	317.4	8.9	158863		66.3	303.3	12.0	215303
		Mean	73.4	317.4	9.7	173454		66.7	304.2	11.5	205975

Table 5-31 Experimental vs. Numerical Specimen Life: (Method: PSD – SN: Steinberg)										
Damping Method: PSD Excitation Block Cycle Forced Response										
SN Material: Aluminum 6061-T6 Steinberg										
Stress Cycle Filtering: Only stress cycles > 120 MPa cycles (1E10^8 Fatigue Limit)										
		Specimen Number	Experimental (86.6> MPa cycles)				Numerical			
			RMS Stress (MPa)	Max Stress Cycle (MPa)	Block Cycles Until Failure 600 sec block	Total Stress Cycles > 86.6MPa	RMS Stress (MPa)	Max Stress Cycle (MPa)	Block Cycles Until Failure 600 sec block	Total Stress Cycles
190 g Configuration	Polished	25	62.4	263.3	37.0	200571	49.7	229.1	2595.0	14051925
		26	62.4	263.3	18.6	100673	53.0	244.5	430.1	2328992
		27	62.4	263.3	18.4	99352	52.3	241.4	443.1	2399387
		Mean	62.4	263.3	24.7	133532	51.7	238.3	1156.1	6260101
	Machined	33	62.4	263.3	16.6	90008	55.8	257.3	58.7	317590
		34	62.4	263.3	19.5	105302	50.8	234.3	1058.0	5729070
		35	62.4	263.3	13.0	70346	49.9	230.0	1193.0	6460095
		36	62.4	263.3	24.3	131687	49.3	227.5	1785.0	9665775
		Mean	62.4	263.3	18.3	99336	51.5	237.3	1023.7	5543132
235 g Configuration	Polished	1	70.4	277.1	18.3	156015	52.3	244.7	248.8	2126742
		2	70.4	277.1	18.7	160190	52.2	240.0	479.3	4097056
		3	70.4	277.1	14.7	125855	53.4	245.4	247.8	2118194
		Mean	70.4		17.2	147353	52.6	243.4	325.3	2780664
	Machined	4	70.4	277.1	7.4	63540	49.3	227.5	1785.0	15258180
		5	70.4	277.1	8.4	72145	53.3	245.0	225.3	1925864
		6	70.4	277.1	9.0	76775	53.9	247.8	219.3	1874576
		7	70.4	277.1	8.3	70991	52.1	239.4	417.5	3568790
		8	70.4	277.1	12.8	109001	51.9	238.3	687.8	5879314
		9	70.4	277.1	12.1	103217	52.4	240.9	408.4	3491003
		10	70.4	277.1	8.2	70208	53.8	247.4	220.2	1882270
		11	70.4	277.1	6.5	55704	53.4	245.4	224.4	1918171
		12	70.4	277.1	9.1	77701	52.6	241.8	403.3	3447408
		Mean	70.4	277.1	9.1	77698	52.5	241.5	510.1	4360620
291 g Configuration	Polished	13	73.4	317.4	13.2	114476	61.9	283.5	5.6	48421
		14	73.4	317.4	11.8	102976	60.5	276.7	10.3	89968
		15	73.4	317.4	10.9	95189	60.2	275.3	10.4	90142
		Mean	73.4	317.4	12.0	104214	60.9	278.5	8.8	76177
	Machined	16	73.4	317.4	8.3	72175	60.7	277.6	10.2	88663
		17	73.4	317.4	8.0	69303	59.3	271.4	19.0	165667
		18	73.4	317.4	11.7	101758	59.3	271.4	19.0	165667
		19	73.4	317.4	8.7	75336	59.7	273.2	10.3	89185
		20	73.4	317.4	7.4	64286	61.5	281.2	5.5	47856
		21	73.4	317.4	11.3	98118	60.4	276.3	10.2	88837
		22	73.4	317.4	12.1	105137	61.6	281.8	5.5	48047
		23	73.4	317.4	10.9	94464	59.7	273.3	10.3	89185
		24	73.4	317.4	8.9	77105	60.0	274.4	10.2	89098
		Mean	73.4	317.4	9.7	84187	60.2	275.6	11.1	96912

Table 5-32 Experimental vs. Numerical Specimen Life: (Method: PSD – SN: MIL-HDBK-5J)											
Damping Method: PSD Excitation Block Cycle Forced Response											
SN Material: SN Material: Aluminum 6061-T6 MIL-HDBK-5J											
Stress Cycle Filtering: Only stress cycles > 86.6 MPa cycles (1E10^8 Fatigue Limit)											
			Experimental (86.6> MPa cycles)					Numerical			
		Specimen Number	RMS Stress (MPa)	Max Stress Cycle (MPa)	Block Cycles Until Failure 600 sec block	Total Stress Cycles > 86.6MPa		RMS Stress (MPa)	Max Stress Cycle (MPa)	Block Cycles Until Failure 600 sec block	Total Stress Cycles
190 g Configuration	Polished	25	62.4	263.3	37.0	596303		49.7	229.1	180.1	2898890
		26	62.4	263.3	18.6	299305		53.0	244.5	95.1	1530247
		27	62.4	263.3	18.4	295378		52.3	241.4	107.7	1733539
		Mean	62.4	263.3	24.7	396995		51.7	238.3	127.6	2054225
	Machined	33	62.4	263.3	16.6	267596		55.8	257.3	54.6	878037
		34	62.4	263.3	19.5	313067		50.8	234.3	135.8	2185837
		35	62.4	263.3	13.0	209141		49.9	230.0	162.4	2613990
		36	62.4	263.3	24.3	391508		49.3	227.5	180.3	2902109
		Mean	62.4	263.3	18.3	295328		51.5	237.3	133.3	2144993
235 g Configuration	Polished	1	70.4	277.1	18.3	324442		53.3	244.7	97.7	1737071
		2	70.4	277.1	18.7	333122		52.2	240.0	118.4	2104678
		3	70.4	277.1	14.7	261722		53.4	245.4	95.1	1690498
		Mean	70.4		17.2	306429		53.0	243.4	103.7	1844082
	Machined	4	70.4	277.1	7.4	132135		54.1	248.4	80.0	1421369
		5	70.4	277.1	8.4	150029		53.3	245.0	91.4	1624015
		6	70.4	277.1	9.0	159658		53.9	247.8	82.0	1457276
		7	70.4	277.1	8.3	147630		52.1	239.4	114.6	2037130
		8	70.4	277.1	12.8	226674		51.9	238.3	119.9	2131342
		9	70.4	277.1	12.1	214645		52.4	240.9	107.6	1912698
		10	70.4	277.1	8.2	146000		53.8	247.4	83.3	1480563
		11	70.4	277.1	6.5	115840		53.4	245.4	89.9	1597707
		12	70.4	277.1	9.1	161584		52.6	241.8	104.0	1848704
		Mean	70.4	277.1	9.1	161577		53.1	243.8	97.0	1723423
291 g Configuration	Polished	13	73.4	317.4	13.2	235860		61.9	283.5	24.1	432579
		14	73.4	317.4	11.8	212166		60.5	276.7	30.5	547491
		15	73.4	317.4	10.9	196121		60.2	275.3	32.1	576174
		Mean	73.4	317.4	12.0	214716		60.9	278.5	28.9	518748
	Machined	16	73.4	317.4	8.3	148704		60.7	277.6	28.5	510023
		17	73.4	317.4	8.0	142789		59.3	271.4	35.4	634795
		18	73.4	317.4	11.7	209656		59.3	271.4	35.0	627445
		19	73.4	317.4	8.7	155218		59.7	273.2	33.3	596611
		20	73.4	317.4	7.4	132451		61.5	281.2	25.1	449430
		21	73.4	317.4	11.3	202157		60.4	276.3	29.8	534225
		22	73.4	317.4	12.1	216618		61.6	281.8	24.6	440108
		23	73.4	317.4	10.9	194627		59.7	273.3	33.1	593204
		24	73.4	317.4	8.9	158863		60.0	274.4	31.9	571692
		Mean	73.4	317.4	9.7	173454		60.2	275.6	30.7	550837

Chapter 6 - Discussion

In this chapter, the numerical and experimental results are discussed. Experimental damping evaluation and the material S-N curves applied for stress damage calculations are shown to be the most significant effect to numerical correlation with the experimental testing. The discussion provides guidance for developing numerical models for fatigue prediction under the stochastic excitations.

6.1 Specimen Variations

Variations in the specimen mass induce differences in fatigue life results. Mass variations of each specimen assembly affect the undamped natural frequency (ω_n), damping ratio (ζ), and resulting stress levels under the same excitation. Specifically, the damping ratio (ζ) needs to be evaluated since this has the greatest effect on stress response in resonance. To evaluate the effects of the mass variations within each configuration the following methods are applied to numerically compare the effects of mass variations. The damping coefficient and stiffness are assumed to be equivalent for each specimen. Therefore, equation (2.11) can be reduced to equation (6.1). $M_{baseline}$ is the mean value of the specimen mass from Table 5-3. $M_{compare}$ is the mean mass plus three standard deviations (3σ) of the specimen mass variations. A baseline multiplier can be calculated for the system variance by applying equation (6.1). The results of this comparison shown in Table 6-1 show little effect to damping ratio (ζ) based on the system mass variations. Therefore, the variation in damping values experimentally determined shown in Table 5-7 can be contributed to stiffness and boundary condition variations.

$$damping\ baseline\ multiplier = \frac{\frac{c}{2\sqrt{k\ M_{compare}}}}{\frac{c}{2\sqrt{k\ M_{baseline}}}} \rightarrow \sqrt{\frac{M_{baseline}}{M_{compare}}} \qquad (6.1)$$

Table 6-1 Effects of Specimen Mass variation on Damping (Theoretical Comparison)				
Mass Configuration	$M_{baseline}$ Complete assembly Baseline Mean Value	Std 3σ	$M_{compare}$ Mean +3σ	Baseline Multiplier
190g	373.33	0.18	373.35	1.0000
235g	381.94	0.05	381.99	0.9999
291g	432.49	0.57	433.06	0.9993

6.2 Experimental Damping Evaluation

Methods of damping evaluation determine that the measured damping ratio (ζ) is not consistent between approaches. The selected method is dependent upon the application of the damping ratio (ζ) for numerical modeling. Characteristics of each method are discussed in Table 6-2 . Figure 6-1 demonstrates that the mass of the cantilevered specimen has a significant effect on the measured damping ratio (ζ) on most of the measurement methods.

Table 6-2 Summary of Effect of Mass for Various Methods on Damping Determination	
Impulse Response • Mass has little effect damping value • Damping values in lower end of measurements values	**Forced Response: Sweep 0.1 Hz/sec Response** • Mass has little effect damping value • Damping values in lower end of measurement values • Requires selection of proper sweep rate. No way to really determine this. • Correlates well with impact tests
Forced Response: Sine Dwell Constant Frequency and Amplitude • Mass has a large effect on damping value measured • Large spread in values determined	**Forced Response: PSD Excitation Block Cycle FRF Gain** • Mass has a large effect on damping value measured • Damping values are high end of measurements values

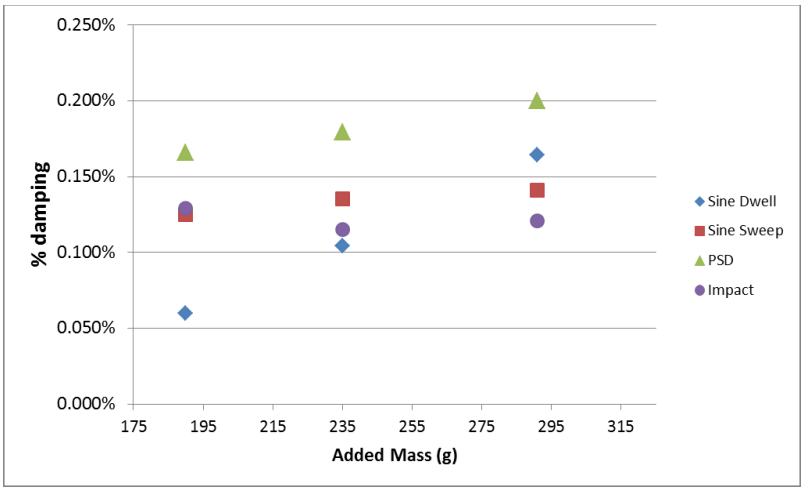

Figure 6-1 Damping Methods and Added Mass Trends

Increased system mass was evaluated for the effects the damping ratio (ζ) by applying equation (6.2) to the values listed in Table 5-24. This calculation shows the damping ratio (ζ) trend for each of the four methods of evaluation. Values are compared with the theoretical viscous damping from equation (2.11). The baseline multipliers are displayed in Table 6-3. Experimental damping methods increased the damping ratio (ζ) with added mass, whereas applying the viscous numerical calculation from equation (6.1) has the inverse effect on added mass. In turn, differences in damping ratio (ζ) affect the stress response as shown in Figure 2-10. The damping ratio (ζ) is plotted versus the added cantilevered mass in Figure 6-1.

$$damping\ baseline\ multiplier = \frac{compare\ damping\ ratio}{baseline\ damping\ ration} \qquad (6.2)$$

Table 6-3 Effects of Increasing Specimen Mass on Damping (Theoretical Comparison)

		Baseline Multiplier			
Mass Configuration	**Theoretical correction factor for damping with increasing mass**	**Impact**	**Sweep**	**Dwell**	**PSD**
190g	Baseline	baseline	baseline	baseline	baseline
235g	0.89	1.00	1.08	1.74	1.28
291g	0.81	1.00	1.13	2.74	1.26

Forced response constant amplitude frequency sweep continued discussion

The sweep rate that is chosen for the constant amplitude frequency sweep is critical in obtaining the desired FRF shape and magnitude. If a slow enough rate is applied, full resonance is achieved. The sweep rates evaluated ranged from 0.05 to 1 Hz/sec. The gain of the FRF for each of these tested sweep rates are displayed in Figure 6-2. This method is not advised since the sweep rate is difficult to determine.

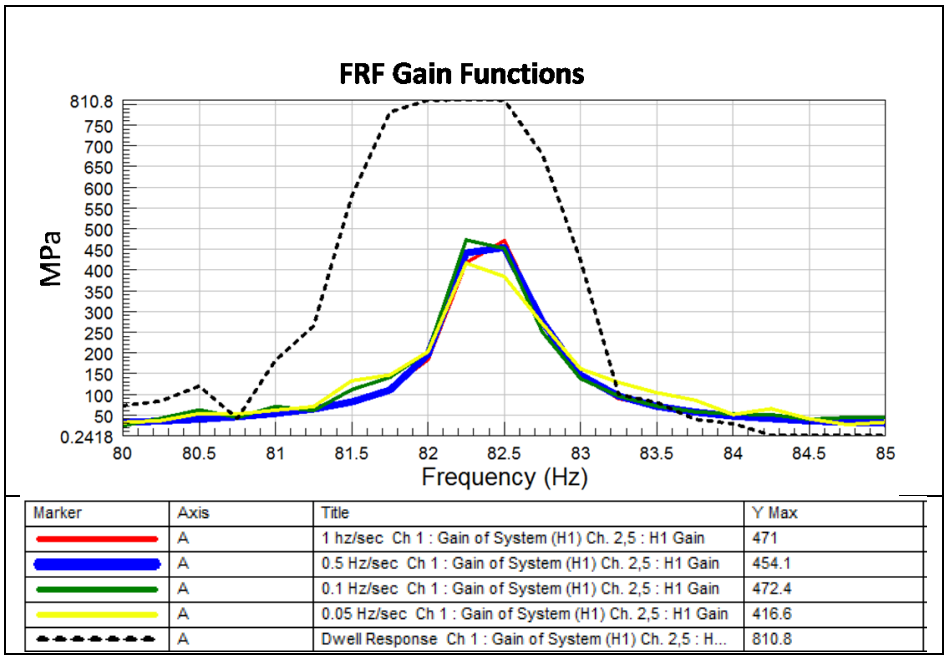

Marker	Axis	Title	Y Max
	A	1 hz/sec Ch 1 : Gain of System (H1) Ch. 2,5 : H1 Gain	471
	A	0.5 Hz/sec Ch 1 : Gain of System (H1) Ch. 2,5 : H1 Gain	454.1
	A	0.1 Hz/sec Ch 1 : Gain of System (H1) Ch. 2,5 : H1 Gain	472.4
	A	0.05 Hz/sec Ch 1 : Gain of System (H1) Ch. 2,5 : H1 Gain	416.6
	A	Dwell Response Ch 1 : Gain of System (H1) Ch. 2,5 : H...	810.8

Figure 6-2 Frequency Sweep Rate Effects to the FRF magnitude
Note time series is too short to adequately define the FRF shape as well the peak, however the function trend shows the response stress is less than the dwell FRF magnitude for each of the sweep rates.

6.3 Experimental Fatigue Testing

Fatigue life results can be contributed to the specimen variants of mass, stiffness, surface finish, surface flaws, and damping. Variation in excitation of the samples has great influence on the results. This section discusses the major system variants that are evaluated to have the greatest effects on fatigue life.

Variation in shake table excitation block events

Variations in the excitation cause deviations in the resulting stress, altering the specimen life. Figure 6-3 displays the specimen RMS acceleration versus the number of block repeats the specimen survived. It also shows that the RMS acceleration variance greatly impacts the specimen life.

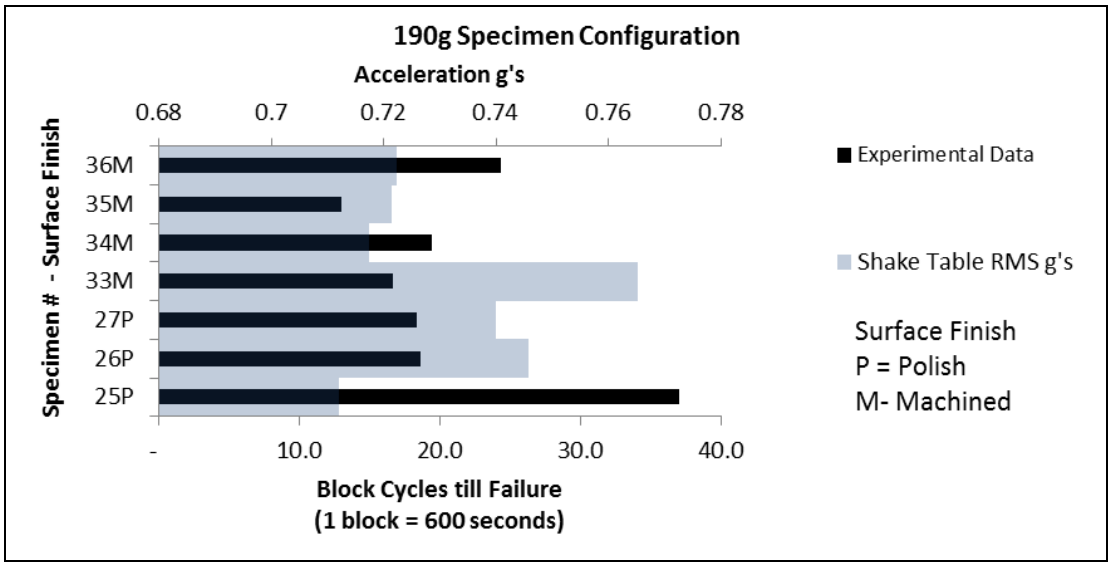

Figure 6-3 Effects of Variations of Excitation Variations on Fatigue Life

Surface Finish Effects

Surface roughness (μm) is plotted against stress cycles to failure to evaluate correlation of specimen failure. The variation in RMS acceleration of each specimen complicates the comparison of the surface finish results. An alternate method is to compare the mean and standard deviation of each configuration and the corresponding surface finish. Figure 6-4 shows a polished surface nearly doubles the life of the specimens.

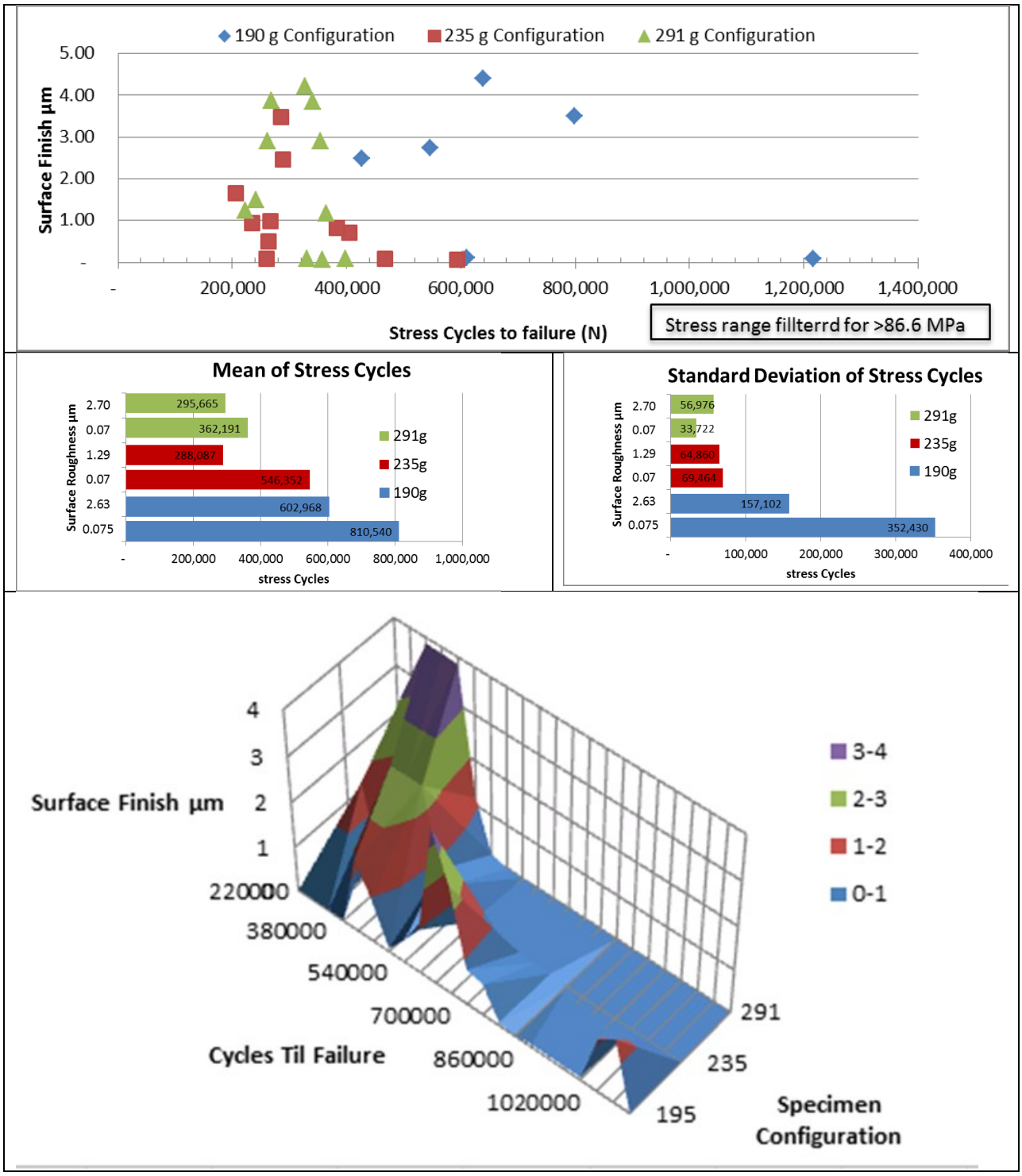

Figure 6-4 Effects of Surface Roughness on Fatigue Life

Experimental S-N Curve

The experimental S-N plotted data from Figure 5-12 is compared to published S-N values for aluminum 6061-T6 in Figure 6-5. The experimental values are within the range of published S-N curves that have been established by Yahr [20], Steinberg [18], and MIL-HDBK-5J [19]. Methods of fatigue testing cause differences in the associated S-N curves. Yahr and Steinberg used rotating bending with fully reversed stresses. This approach applies stress across the entire circumference of the specimen fatigue zone. MIL-HDMK-5J applies axial fully reversed loading, making it a function of the cross sectional area. Neither of these methods represents the cyclic stress reversals applied in this experiment. Only the top and bottom surfaces are exposed to the peak stress. This variation in specimen loading alters the resulting fatigue life of the specimens. As well the chosen specimen dimensions and surface finishes will affect the experimental S-N curve.

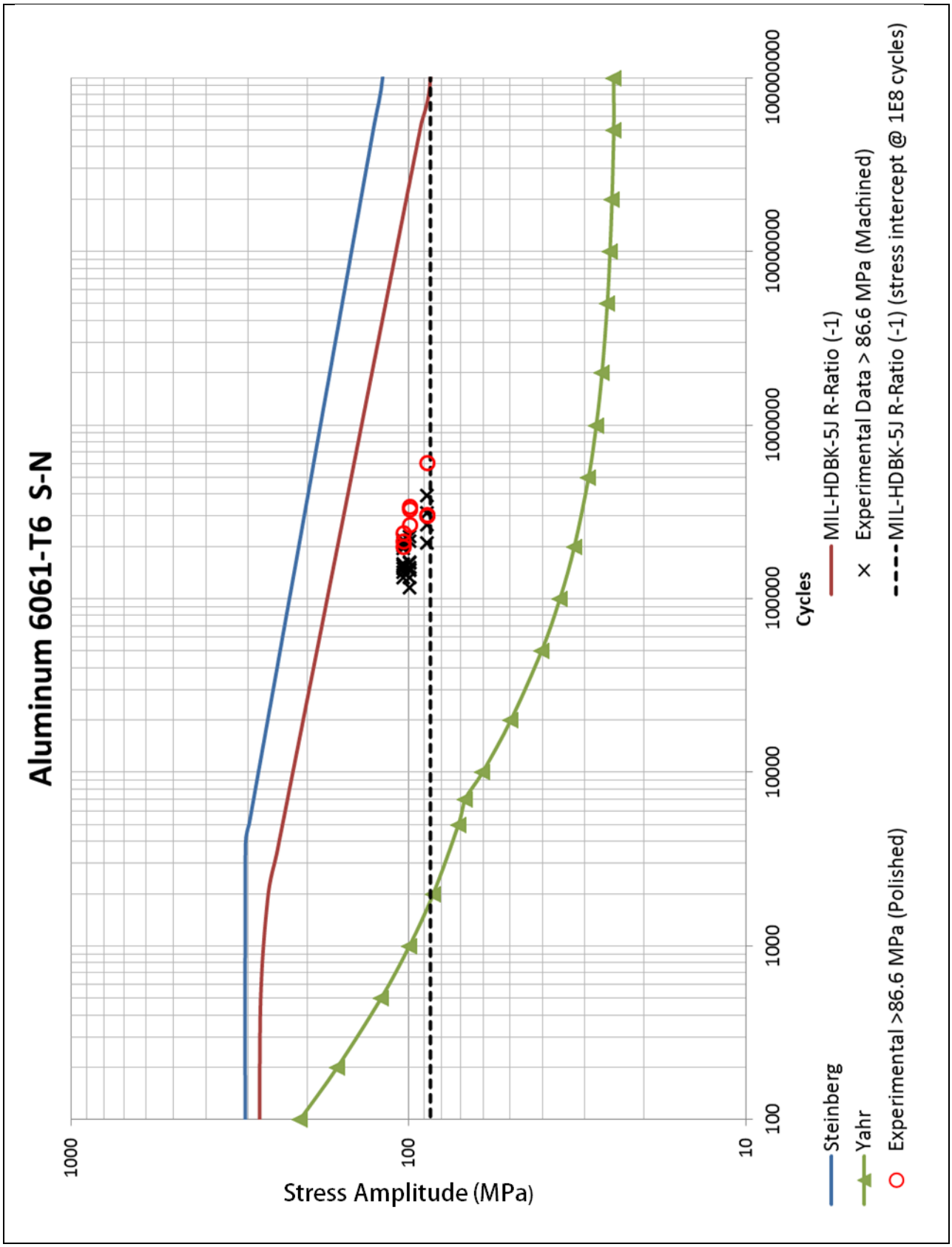

Figure 6-5 Experimental S-N Curve vs. Published 6061-T6 S-N Curves [19], [20], [18]

Specimen Fracture Surface Review

During the testing, specimens did not vibration vertically, but rather on a tilted plane or a circular pattern when viewing specimens down the central axis at the cantilevered end. Crack developed at angles on some specimens (see Appendix G for specimen images). These angles are then measured for further analysis. By applying trigonometric functions, the component vectors of stress can be determined (tabular calculation in Table 7-9). Analysis shows that stress component vectors can be used to develop correction factors for stress at crack initiation. Figure 6-6 demonstrates the results of applying this correction factor hypothesis. The modified data develops a better curve fit noted by the reduced r-squared. This interaction of out-of-plane vibration correlates to the proposed calculation adjustment. The origin for the out-of-plane vibration is contributed to crack initiation on the side of the specimen. This unidirectional reduction in stiffness causes out-of-plane vibration. Increasing out-of-plane vibration further increases the stress values at the crack surface due to the stress component vector proposed above.

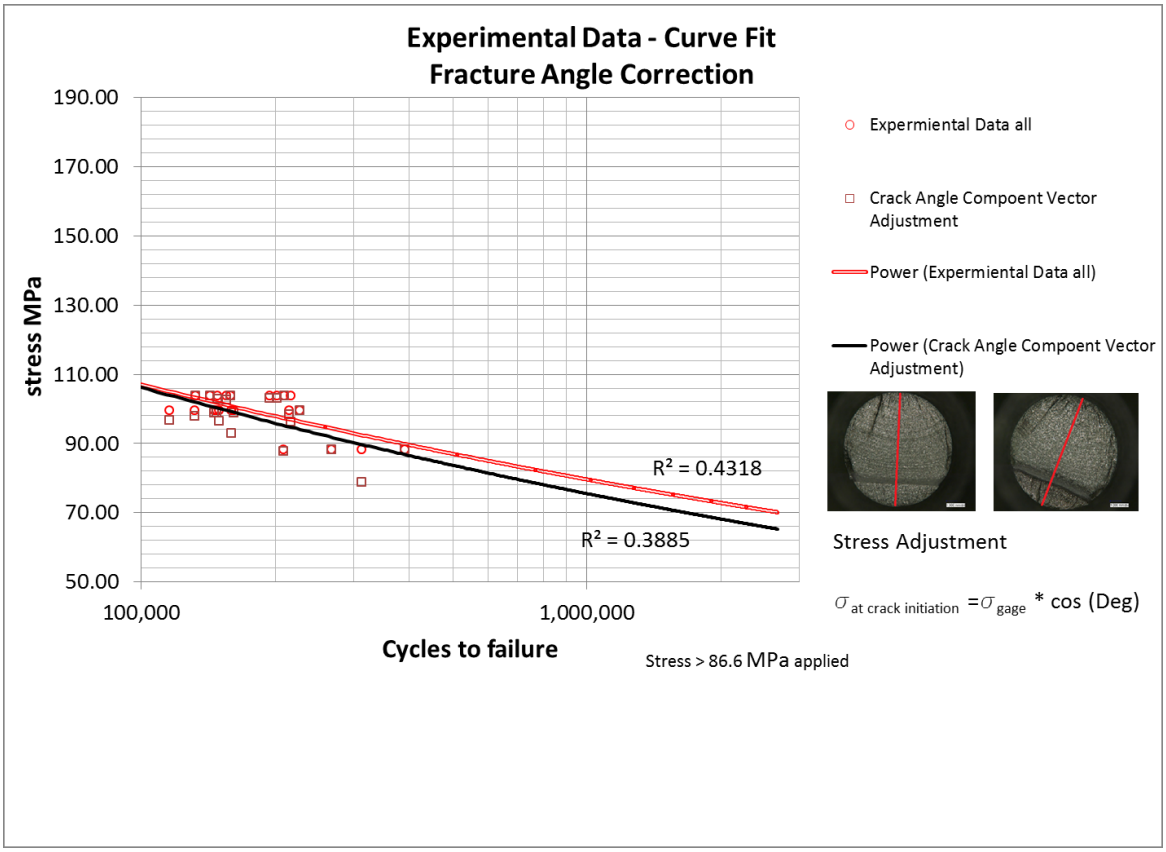

Figure 6-6 Fracture Angle Effects to Experimental Data Curve Fitting

6.4 Numerical Model Damping

Four methods of measuring damping are investigated in this research. Each of these damping values is used in the numerical simulation to evaluate which process provides the highest level of experimental prediction for fatigue life. The resulting stress transfer functions $H(\omega)$ are shown in Figure 6-7. Each of the experimental damping ratios (ζ)listed in Table 5-24 are used to calculate numerical stress transfer functions $H(\omega)$ displayed in Figure 6-7. Experimental methods of determining damping are shown to have significant effects on the magnitude of the stress FRF. The effects of varying stress magnitudes on the life are shown in Table 5-25 through Table 5-32.

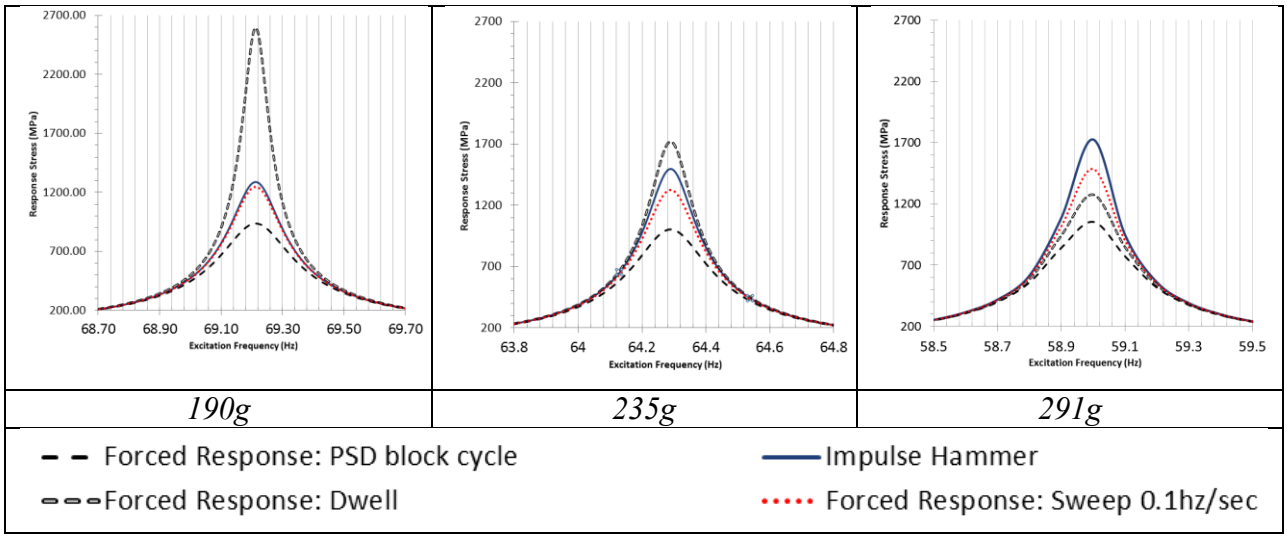

Figure 6-7 FEA FRF Stress Plots

6.5 Numerical Spectral Damage Calculations

The various applied experimental methods of determination of damping ratio (ζ) generated different stress PSD's functions $G(f)$ that are used to calculate spectral damage, as discussed in section 2.9.2. The stress range differences in applying the four different damping evaluation methods are displayed in Figure 6-8. The increased width and shift of the stress distribution for constant amplitude sine dwell damping method result in reduced specimen life. Alternatively, applying the PSD forced response method statistically lowers stress magnitudes ultimately leading to longer life estimation compared to the other three methods.

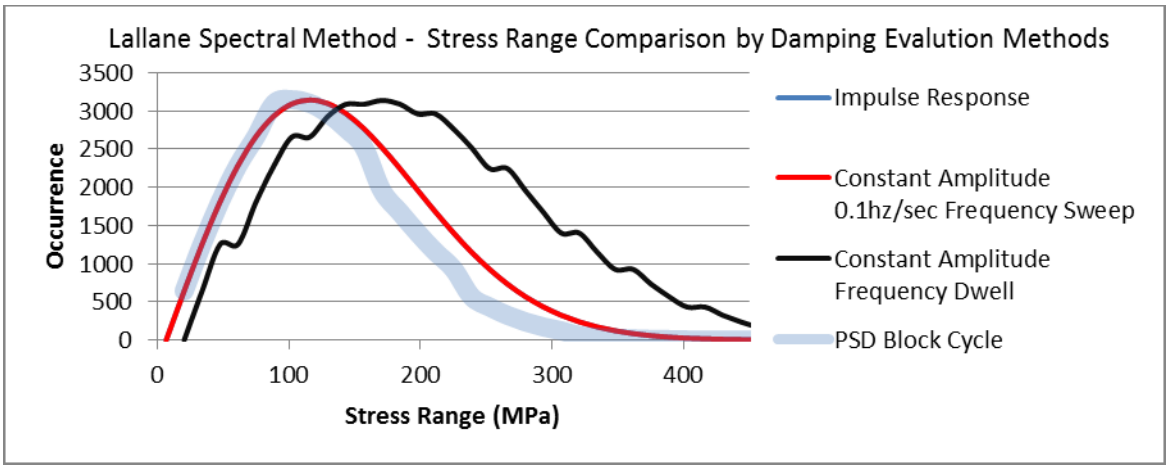

Figure 6-8 Stress Histogram Comparison of Damping Evaluation Methods

Figure 6-9 displays the probability stress distribution differences in spectral damage calculations discussed in section 2.7. For this analysis, the Lalanne [14] method is applied. However, either narrow band or Dirlik method [13] could have been applied with similar results. As discussed in section 2.7, the Lalanne and narrow band methods are similar when the irregularity factor (γ) is near 1. The time series signal used in this experiment equates to an irregularity factor (γ) of 0.998. Therefore, either the Lalanne or narrow band methods could be applied with similar results (see Appendix B for calculations).

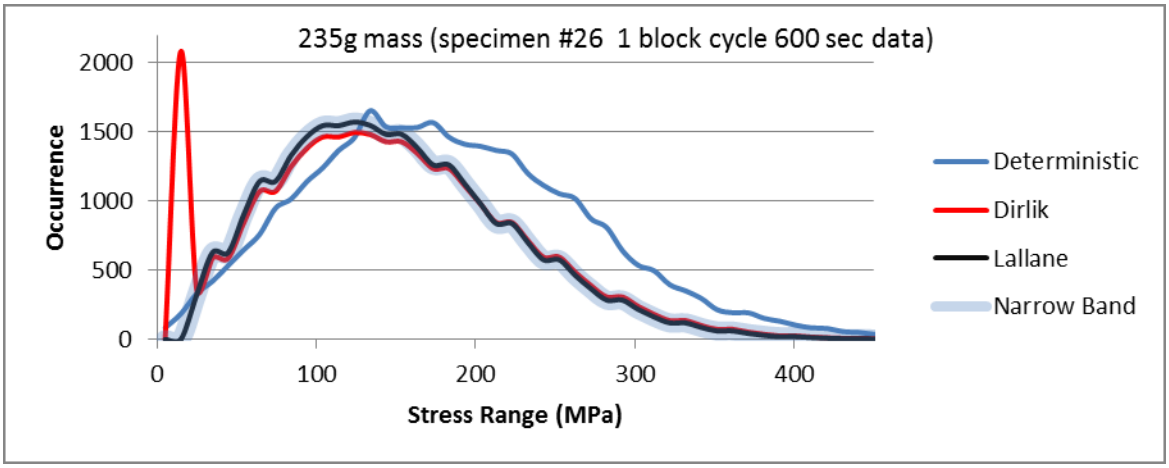

Figure 6-9 Stress Cycle Counting Method Comparisons (experimental testing)

Table 6-4 Life Results Comparison for Spectral Damage Methods	
Method of Damage Counting	*Numerical Block Cycle Repeats*
Deterministic - Rainflow	*27.0*
Spectral - Dirlik	*29.9*
Spectral - Lalanne	*39.1*
Spectral - Narrow Band	*39.1*
Specimen 37 test excitation – Impulse damping determination for 190g specimen	

6.6 Numerical Comparison to Experimental Fatigue Results

Comparing numerical results of damping determination and S-N material selection validate the importance in developing a representative model for estimating fatigue life. Determining what stress range is beyond the fatigue limit of the material needs to be considered for filtering out the stresses that don't significantly induce damage. S-N curves that are extrapolated at either end of the cycle range need to be evaluated carefully. These extrapolated curves can result in premature numerical specimen failure. At the higher stress amplitudes, if the S-N curves are extrapolated, the curve does not determine ultimate failure of the part, but rather sum up damages from high stress loading. Numerical methods used allow for ultimate strength modification of the S-N curve to account for this concern. If the S-N curve from Figure 6-10 A is used instead of Figure 6-10B, the stress ranges that are above 610MPa would count damage rather determining ultimate failure.

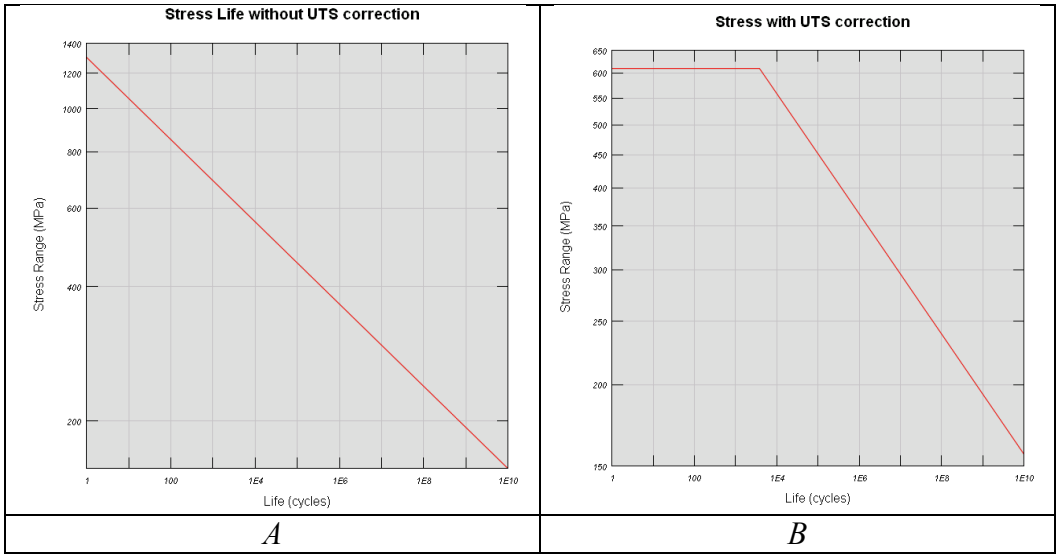

Figure 6-10 S-N Curve Ultimate Strength Correction

Experimental verse Numerical Stress Cycle Comparison

To improve the correlation of numerical versus experimental values, stress range filtering is applied to the measured strain data from section 4.7.4 . For this evaluation, material MIL-HDBK-5J [19] S-N curve is used to define the 86.6MPa stress intercept at 1E^8 cycles since aluminum does not have a defined fatigue limit. Figure 6-12 and Figure 6-13 display the highest correlation of numerical to experimental fatigue data based on the applied methods. This was accomplished by applying either the impulse forced response or constant amplitude sine sweep methods for determining the damping values. Applying MIL-HDBK-5J (R=-1) SN curve for damage calculations proves to be the most accurate. All other damping evaluation methods and S-N materials used to calculate damage are displayed in Appendix G, Figure 7-45through Figure 7-52.

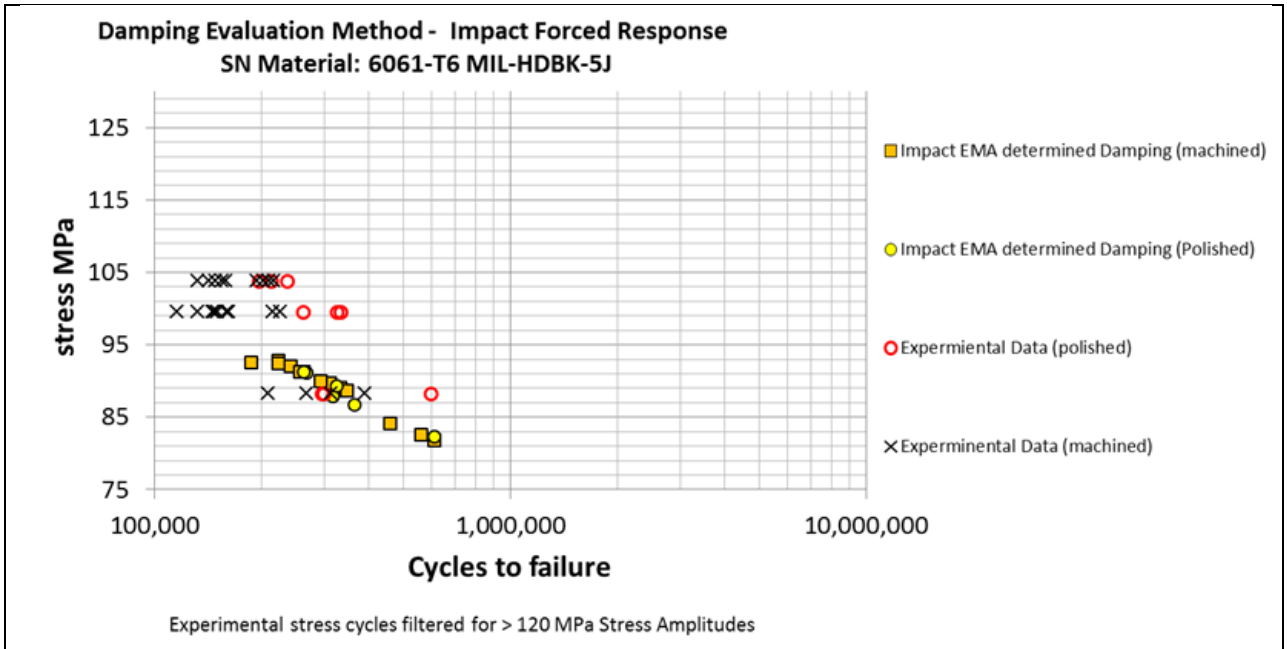

Figure 6-11 Numerical vs. Experimental S-N Impulse Damping Evaluation (MIL-HDBK-5J)

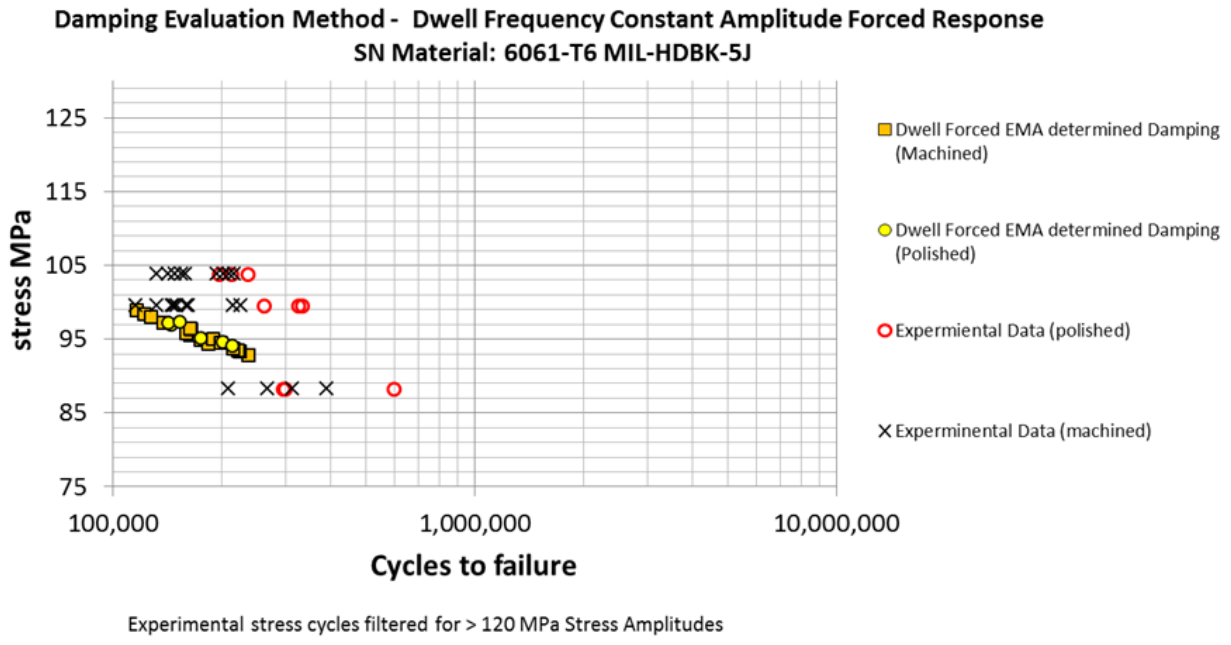

Figure 6-12 Numerical vs. Experimental S-N Dwell Damping Evaluation (MIL-HDBK-5J)

Experimental verse Numerical Specimen Block Repeat Life Comparison

To evaluate the accuracy of the numerical models, the block cycle repeats are compared to the experimental versus the numerical models. The mean values for each specimen configuration are calculated to show the trend of correlation by the mass size plotted in Figure 6-13. These data graphs display important attributes to compare the presented methods of evaluation. The columns represent the damping evaluation methods applied (Impulse, Sine Sweep, Sine Dwell, PSD Gain). The grouping of columns by specimen number are denoted by surface finish (M=machined or P = Polished). From the prior discussions on shake table excitation reproducibility (Appendix F and sections 6.3) the RMS acceleration that each test specimen experienced is plotted in the background blue columns. From this, the variations correlate well with the life variances between specimens. The higher RMS stress levels cause for earlier fatigue failure as one would expect. See 0, Figure 7-53 through Figure 7-59 for all other damping evaluation methods and S-N material curves used to calculate damage.

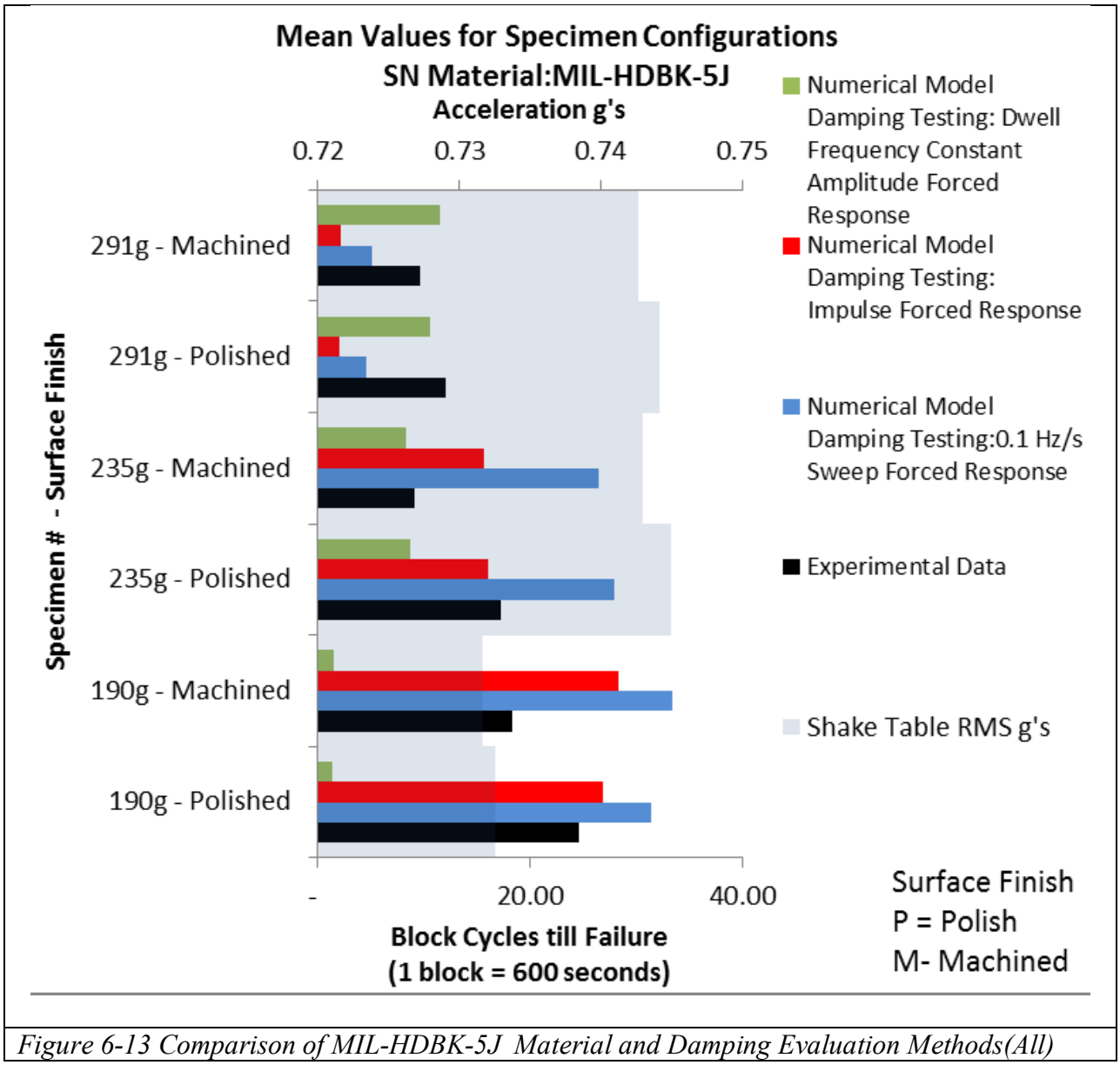

Figure 6-13 Comparison of MIL-HDBK-5J Material and Damping Evaluation Methods(All)

Table 6-5 summarizes the advantages and issues of each of the four applied damping evaluation methods. Table 6-6 shows the experimental versus numerical correlation for each of the damping determination approaches.

Table 6-5 Damping Evaluation Methods and Correlation of Numerical to Experimental Results	
Impulse Response • Consistent correlation under most configurations • Damping value represents the correct stress response well	**Forced Response: Sweep 0.1 Hz/sec Response** • Consistent correlation under most configurations • Damping value is high - consistent overshoot on life prediction
Forced Response: Sine Dwell Constant Frequency and Amplitude • Inconsistent correlation results • Overdamped on low mass • Acceptable on 295g mass (with MIL-HDBK-5J) • Large spread in values determined • Method is too dependent on mass	**Forced Response: PSD Excitation Block Cycle FRF Gain** • Extremely high damping • Overshoots life estimation for 190g and 235g (emitted from chart). • Slightly overshoots estimation for 291g • Does not change with increased mass (fundamental wrong $\zeta = \frac{C}{\sqrt{MK}}$)

Table 6-6 Comparison of Damping Methods Verse Experimental Correlation

	Damping Methods and values applied			
Mass Configuration	**Impact**	**Sweep**	**Dwell**	**PSD**
190g Machined	0	-	-	-
190g Polished	+	+	-	-
235g Machined	0	-	+	-
235g Polished	+	-	-	-
291g Machined	-	-	+	-
291g Polished	-	-	+	-

Key: + good correlation, 0 poor correlation, - no correlation

Evaluating Impulse, Sweep, Dwell, and PSD damping determination methods shows that the impulse method of using an impact hammer and the constant amplitude frequency dwell correlate the best to the experimental testing. The impact method is preferred as testing is simplistic and does not require a lot time or equipment. Choosing the damping evaluation method depends on the structure being tested. Table 6-7 and Table 6-8 list a few considerations to note when selecting the method of damping evaluation methods.

Table 6-7 Impulse Response Experimental Modal Analysis Discussion	
Advantages • Easy to set up • Fast measurement time • Minimum equipment • Low cost • FRF's can be leakage free	Disadvantages • Poor RMS to peak levels • Poor for non-linear structures • Multiple impacts occur easy • Sometimes difficult to measure all DOF's

Table 6-8 Forced Response Experimental Modal Analysis Discussion	
Advantages • Gives a good linear representation of a nonlinear system • Relatively fast • Low peak to RMS level	Disadvantages • Requires shake apparatus • Long set up time • Force transducer must be in series with shake input (not always possible)

Chapter 7 - Conclusions and Recommendations

The experimental and numerical study conducted in this research for spectral fatigue analysis under stochastic vibrations provides guidance for the application of spectral damage calculations. The results of the numerical models are correlated to the experimental testing to provide confidence in the methods applied. The focus of this research is to investigate correlation for low stress (62 MPa-73 MPa) amplitude high cycle (342,000 - 1,148,000) fatigue of aluminum 6061-T6. Since aluminum has no well-defined fatigue limit, this extenuates the need for improved analysis under such stress amplitudes. This research delves into the important system parameters to develop representative specimen response to random excitation in the frequency domain. These parameters include the damped natural frequency (ω_d) and damping ratio (ζ) to develop the correct specimen stress response under PSD (Power Spectral Density) represented time domain stochastic vibrations. Statistical methods of stress range cycle counting are evaluated against the deterministic rainflow methods. Based on the experimental evaluation conducted, the following conclusions are given as:

1. Numerical models must represent the physical system for damped natural frequency (ω_d) as well as damping ratio (ζ). To correctly model these values experimental methods of the system response should be conducted. The research demonstrated that applying either the impulse forced response or constant amplitude frequency dwell at damped natural frequency (ω_d) methods of damping evaluation provide the most robust process.
2. Experimentally determined damping is evaluated for the different numerical methods of damping representation. Applying hysteretic (structural) damping was

shown to provide the correct FRF's (Frequency Response Functions). These correct response functions are critical in calculating the stress transfer functions that will develop the stress levels under stochastic PSD vibration profiles.

3. Spectral stress range counting correlates well to the deterministic rainflow stress counting. The results compared in this research validate the application of frequency domain stress counting methods (62 MPa-73 MPa) developed by Bendat [12], Dirlik [13], Lalanne [14], and the excitation block repeats were found to be 39.1, 29.9, and 39.1 respectively.
4. Damage calculations for either deterministic or stochastic are reliant on material S-N curves. Proper selection of the S-N curve is important as the published values for S-N curves of aluminum 6061-T6 are different based on the methods of measurement as well as specimen dimensions, and surface finishes.

The spectral methods of fatigue analysis provide a computational reduced method when compared to deterministic damage evaluations. This research validates the application of spectral damage calculations to improve design efficiency and provide an iterative design process prior to experimental fatigue validation testing.

Based on the preliminary results of this research, the following recommendations are:

- Investigate the application of spectral methods of numerical damage evaluation to MDOF (Multiple Degree of Freedom) systems.
- Further research should also be conducted on the various methods of damping evaluation of different specimen geometries and boundary conditions.

- Examine the effects of damping with increased number of cycles and amplitudes of stress.
- Additionally, research should be conducted on the experimental testing methods for developing aluminum S-N curves for various specimen geometries and cyclic stress applications.

References

References

[1] D. C. Montgomery and G. C. Runger, in *Applied Statistics and Probability for Engineers*, Danvars, MA, John Wiley & Sons, 2003.

[2] S. M. Kumar, Analyzing Random Vibration Fatigue, vol. II, 2008, pp. 39-42.

[3] D. J. Ewins, "Damping Measurement," in *Encyclopedia of Vibrations*, London UK, Academic Press, 2001, pp. 332-335.

[4] P. W. Spenc and C. J. Kenchington, "The Role of Damping in Finite Element Analysis," NAFEMS, Glasgow, 1993.

[5] D. Ewins, Modal Testing - Theory, practice and application, Hertfordshire, England: Research Studies Press LTD., 2000.

[6] J. F. Doyle, "Wave Propogation in Structures," Spinger Verlag, New York, 1989.

[7] S. Gopalakrishnan, A. Chakraborty and D. R. Mahapatra, "Spectral Finite Element Method," Springer Verlag, New York, 2007.

[8] A. Sondipon, Doubly Spectral Stochastic Finite-Element Method for LInear Structural Dynamics, 2001, pp. 264-276.

[9] C. Amzallag, J. P. Gerey, J. L. Robert and J. Bahuaudt, Standardization of the rainflow counting method for fatigue analysis, vol. 16, 1994, pp. 287-293.

[10] R. Sunder, S. Seetharam and T. A. Bhaskaran, Cycle Counting for Fatigue Crack Growth Analysis, vol. 6, 1984, pp. 147-155.

[11] S. Clarke, D. Goodpasture, R. Bennet, H. Deatherage and E. Burdette, "Effect of Cycle-Counting Methods on Effective Stress Range and Number of Stress Cyles for Fatigue Prone Details," Transportation Research Record.

[12] J. S. Bendat, "Probability functions for random responses," NASA report on contract NAS-5-4590, 1964.

[13] T. Dirlik, "Application of Computer Fatigue Analysis," Phd Thesis, Warwick University, 1985.

[14] C. Lalanne, "Mechanical Vibration and Shock," *Hermes Penton Science,* Vols. 3,4, and 5, 2002.

[15] S. Rice, "Mathematical Analysis of Random Noise," Selected papers on stochastic processes, Dover, New York, 1954.

[16] A. Halfpenny, "Rainflow Cycle Counting and Fatigue Analysis from PSD," nCode International Ltd., Sheffield UK, 2007.

[17] N. E. Dowling, "Engineering Methods for Deformation, Fracture, and Fatigue," in *Mechanical Behavior of Materials*, Upper Saddle River, New Jersey, Prentice Hall, 1999.

[18] D. S. Steinberg, Vibration Analysis for Electronic Equipment, 3rd Edition, New York: John Wiley and Sons, 1988.

[19] Department of Defense, Metalic Materials and Elements for Aerospace Vehicle Structures, Department of Defense United States, 2003.

[20] G. Yahr, "Fatigue Design Curves for 6061-T6 Aluminum," Oak Ridge National Labratory, Oak Ridge, Tennessee, 1993.

[21] Criteria of the ASME Boiler and Pressure Vessel Code for Design by Analysis in Sections III and VIII, Division 2, ASME, 1969.

[22] H. U. K. Ncode, Practicle Fatigue Thoery, Detroit, MI: HBM United, 2011.

[23] G. Kaufman, Properties of Aluminum Alloys: Fatigue Data and the Effects of Temperature, Materials Park, OH: ASM International, 2008.

[24] M. Colakoglu and K. L. Jerina, "Material Damping in 6061-t6511 aluminum to assess fatigue damage," *Fatigue Fracture Engineering Material Structure,* vol. 26, pp. 79-84, 2002.

[25] Matweb - Online Material Data, "ASTM A36 Steel Bar," [Online]. Available: http://www.matweb.com/search/DataSheet.aspx?MatGUID=d1844977c5c8440cb9a3a967f8909c3a&ckck=1. [Accessed 10 July 2012].

[26] Mitutoyo - Product Sheet, "Surface Roughness Testers," [Online]. Available: http://www.mitutoyo.com/pdf/2068_SV-3100.pdf. [Accessed 10 July 2012].

[27] Matweb - Online Material Data, "Aluminum 6061-T6," [Online]. Available: http://www.matweb.com/search/DataSheet.aspx?MatGUID=1b8c06d0ca7c456694c7777d9e10be5b&ckck=1. [Accessed 10 July 2012].

[28] National Instruments, "LabView Signal Express Product Sheet," [Online]. Available: http://sine.ni.com/nips/cds/print/p/lang/en/nid/14216. [Accessed 10 July 2012].

[29] Vibrant Technology Inc., "ME'scope VES 5.0 Product Sheet," [Online]. Available: http://vibetech.com/img/en-us/MEScopeVES.pdf. [Accessed 30 April 2012].

[30] MTS, "Spec Sheet: Series 244 Hydraulic Actuators," [Online]. Available: http://www.mts.com/ucm/groups/public/documents/library/dev_002093.pdf. [Accessed 19th July 2012].

[31] MTS RPC - Program Data Sheet, "MTS," [Online]. Available: http://www.mts.com/ucm/groups/public/documents/library/cm3_002017.pdf. [Accessed 29 July 2012].

[32] nCode 8 Software, Sheffield, England: HBM United Kingdom Limited, 2012.

[33] *Creo Elements/Pro 5.0,* 140 Kendrick Street, Needham, MA 02494 USA: Parametric Technologies Corporation, 2011.

[34] Hyperworks V10.0, Altair Engineering Inc., 2009.

[35] R. D. Blevins, in *Formulas for Natural Frequency and Mode Shapes*, Malabar, Florida, Krieger Publishing Company, 1993, pp. 157-158.

[36] D. A. Halfpenny, "Methods for Accelerating Dynamic Durability Tests," nCode International Ltd, Sheffield , 2006.

[37] D. A. Halfpenny, "Accelerated Vibration Testing Based on Fatigue Damage Spectra," nCode International, Sheffield.

[38] E. Macha, T. Lagoda, A. Nieslony and D. Kardas, "Fatigue Life Under Variable-Amplitude Loading According to the Cycle-Counting and Spectral Methods," *Materials Science,* vol. 42, no. 3, pp. 416-425, 2006.

[39] J. Minderhoud and P. Van Baren, "Using Kurtosion to Accelerate Structural Life Testing," Vibration Research Corporation, Jenison, Michigan, 2010.

[40] D. A. Halfpenny, "Accelerated Testing - Virtual and Physical," nCode International, Rotherham, 2007.

[41] S. Lepi and L. S. Parfitt, "Computing Fatigue Damage Caused by Random Vibration," PACCAR Inc., Mt. Vernon, 2009.

[42] C. S. Kraaij, "Model updating of a clamped - free beam system using FEM tools," Technische Universiteit Eindhoven, Eindhoven, 2007.

[43] K. Shye and M. H. Richardson, "Vibetech," [Online]. Available: http://www.vibetech.com/assets/papers/paper31.pdf. [Accessed 1 April 2012].

[44] M. Richardson and R. Potter, "Identification of the Modal Properties of an Elastic Structure From Measured Transfer Function Data," in *International Instrumentation Symposium*, ISA ASI 74250, 1974.

[45] B. J. Schwarz and M. H. Richardson, "Experimental Modal Testing," in *CSI Reliability Week* , Orlando, 1999.

[46] M. A. Peres, R. W. Bono and D. L. Brown, "Practical Aspects of Shaker Measurements for Modal Testing," [Online]. Available: http://www.modalshop.com/filelibrary. [Accessed 4 April 2012].

[47] M. H. Richardson and D. L. Formenti, "Parameter Estimation from Frequency Response Measurements using Rational Fraction Polynomials," in *IMAC Conferance*, Orlando, 1982.

[48] Altair Engineering Inc., "HyperWorks 10 Online Help and Documentation," [Online]. Available: http://www.altairhyperworks.com/hwhelp/Altair/hw10.0/pdf10.aspx. [Accessed 29 April 2012].

[49] J. S. Hoksbergen, "A comparison Study on the Vibration Characteristics of Magnesium Plate versus Carbon Fiber Reinforced Plastic Plate," University of Washington, Seattle, 2006.

[50] G. A. Lesieutre, "Damping in FE Models," in *Encyclopedia of Vibrations*, Academic Press, 2002, pp. 321-326.

[51] A. Halfpenny, "A frequency domain approach for fatigue life estimation from finite Element Analysis," in *International Conference on Damage Assessment of Structures*, Dublin, 1999.

[52] H. Bachmann, Vibration Problems in Structres, Berlin: Birkhauser Verlag, 1995.

[53] M. M. Rahman, Finite Element Based Vibration Fatigue Analysis for a new piston engine component, vol. 34, 2009, pp. 231-246.

[54] M. M. Rahman, A. K. Arfinn and S. Abdullah, Finite Element Based Vibration Fatigue Analysis for a new two stroke linear generator engine component, vol. 2, 2007, pp. 63-74.

[55] C. C. Kennedy and C. D. Pancu, Use of vectors in Vibration Measurments and Analysis, vol. 14, 1947, pp. 603-625.

[56] R. E. Bishop and M. L. Gladwell, An investigation into the theory of resonance testing, vol. 255, Kenneth Mason Press, 1963, p. 241.

[57] L. Yung-Lii, Fatigue Analysis in teh Frequency Domain, Amsterdam, Boston, Heidelberg, London, New York, Oxford, Paris, San Diego, San Franscico, Singapore, Sydney, Tokyo: Elsevier Butterworth Heinemann, 2005, pp. 369-394.

[58] J. W. Miles, Structural Fatigue Under Random Loading, 1954, p. 753.

[59] M. Shariyat, A fatigue model developed by modification of Gough's theory, for random non-proportional loading conditions and three-dimensional stress fields, vol. 30, 2007, pp. 1248-1258.

[60] T. J. George, J. Seidt, S. Herman and N. Theodore, Development of a novel vibration-based

fatigue testing methodology, vol. 26, 2004, pp. 477-486.

[61] T. Lagoda, E. Macha and A. Nieslony, Fatigue Life calculation by means of the cycle counting and spectral methods under multiaxial random loading, 2005, pp. 409-420.

Appendix A Vibration Test Samples

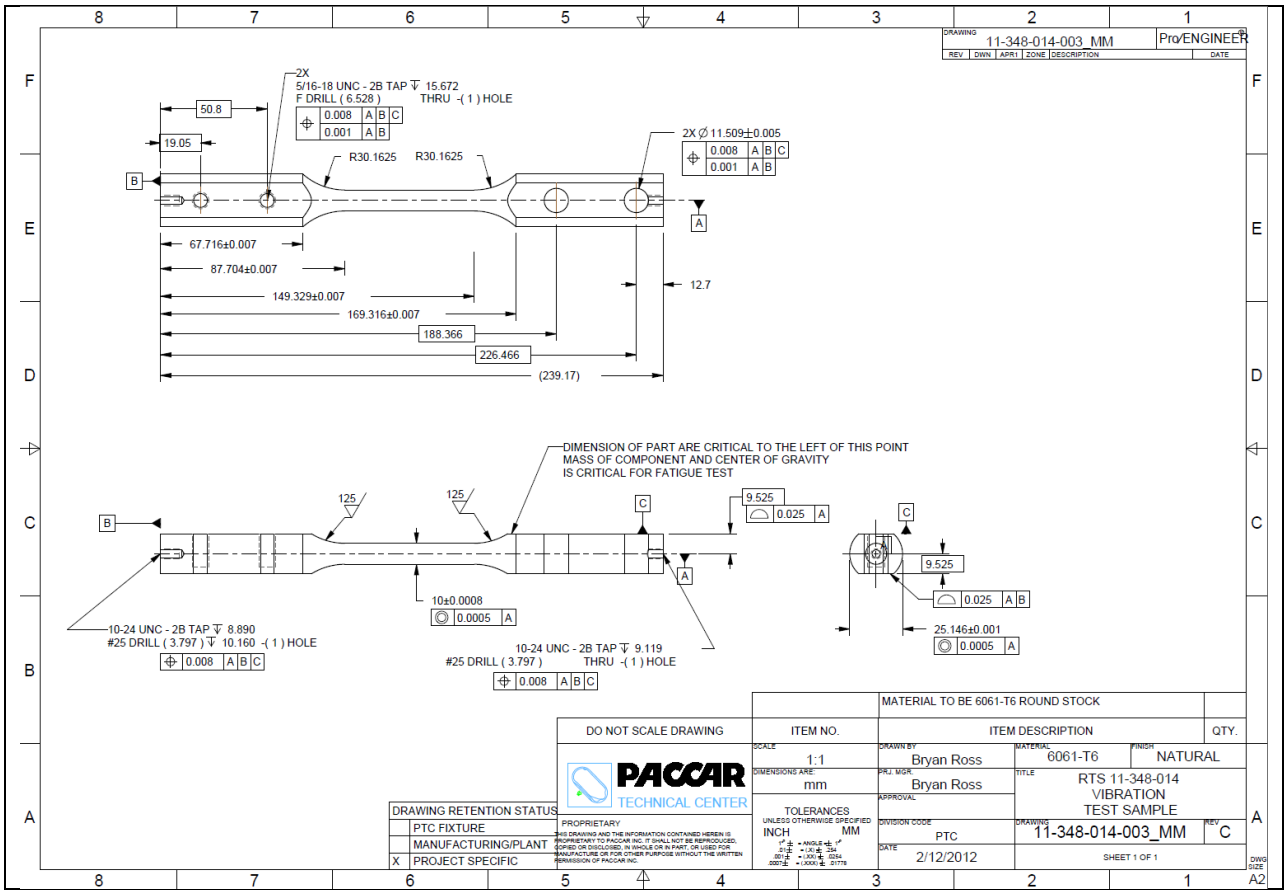

Figure 7-1 Vibration Sample Drawing 11-348-014-003

Figure 7-2 Test Specimen Machining Process 1

Figure 7-3 Test Specimens - Completed Fabrication

Table 7-1 Mass balancing of test samples

291g Specimen Part Mass Variation				Mean variation		0.005
Total added mass (g) =			291.15	Standard deviation		0.192
Specimen Number	Mass (g)	Medium Mass Specimen #	Large Mass Specimen #	Added Mass	Total	Difference
13	178.82	33	43	253.615	432.44	-0.05
14	179.02	24	53	253.690	432.71	0.23
15	178.91	25	49	253.531	432.44	-0.04
16	178.90	21	48	253.574	432.47	-0.01
17	179.12	31	50	253.751	432.87	0.39
18	178.55	29	44	253.611	432.16	-0.32
19	178.90	28	52	253.631	432.53	0.05
20	179.00	32	51	253.638	432.64	0.16
21	178.69	23	47	253.644	432.33	-0.15
22	178.70	27	45	253.578	432.28	-0.20
23	178.89	26	40	253.611	432.50	0.02
24	179.00	20	46	253.549	432.55	0.07

235g Specimen Part Mass Variation				Mean variation		0.079
Total added mass (g) =			235.16	Standard deviation		0.168
Specimen Number	Mass (g)	Small Mass Specimen #	Large Mass Specimen #	Added Mass	Total	Difference
1	178.88	9	51	203.065	381.95	0.09
2	179.94	4	42	202.533	382.47	0.62
3	178.80	8	53	203.073	381.87	0.02
4	178.91	1	49	203.015	381.93	0.07
5	178.98	13	52	202.977	381.96	0.10
6	178.84	3	40	202.997	381.84	-0.02
7	179.00	2	46	202.925	381.93	0.07
8	178.35	14	50	203.604	381.95	0.10
9	178.91	7	47	202.924	381.83	-0.02
10	178.75	6	45	203.126	381.88	0.02
11	179.04	12	48	202.914	381.95	0.10
12	179.10	5	43	202.851	381.95	0.10

190g Specimen Part Mass Variation				Mean variation		-0.138
Total added mass (g) =			190.77	Standard deviation		0.061
Specimen Number	Mass (g)	Large Mass Specimen #		Added Mass	Total	Difference
25	178.62	51		158.704	337.32	-0.14
26	178.70	49		158.586	337.29	-0.18
27	178.76	40		158.508	337.27	-0.20
28	178.84	43		158.495	337.34	-0.13
29	179.06	44		158.354	337.41	-0.05
30	178.91	45		158.447	337.36	-0.11
31	179.03	47		158.415	337.45	-0.02
32	178.68	46		158.610	337.29	-0.18
33	178.76	52		158.556	337.32	-0.15
34	178.56	50		158.835	337.40	-0.07
35	178.73	48		158.559	337.29	-0.18
36	178.55	41		158.874	337.42	-0.04

Table 7-2 Specimen Dimension Variations

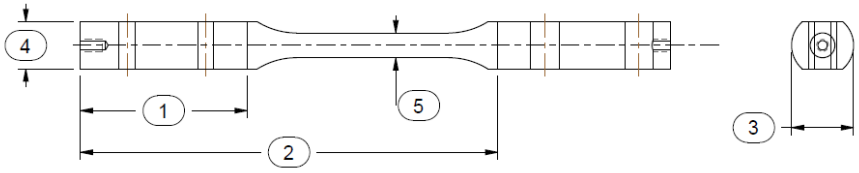

Sample #	Dim 1 (mm)	Dim 2 (mm)	Dim 3 (mm)	Dim 4 (mm)	Dim 5 (mm)
Mean	67.3164	168.9227	25.1841	19.0056	10.0711
Std Dev	1.2686	16.9687	0.0792	0.0466	0.0315
1	2.6445	6.651	0.9905	0.748	0.3955
2	2.634	6.6595	0.9905	0.749	0.3965
3	2.6415	6.651	0.9905	0.749	0.394
4	2.657	6.651	0.99	0.7475	0.397
5	2.656	6.6595	0.9925	0.749	0.396
6	2.649	6.645	0.992	0.745	0.397
7	2.65	6.6525	0.98	0.747	0.3955
8	2.655	6.652	0.9905	0.7485	0.3965
9	2.66	6.659	0.991	0.7458	0.396
10	2.3525	6.6415	0.99125	0.75	0.3965
11	2.6474	6.645	0.9925	0.749	0.395
12	2.647	6.651	0.99515	0.75	0.3965
13	2.6495	6.653	0.99515	0.7495	0.3945
14	2.65	6.6545	0.9915	0.745	0.3965
15	2.6505	6.545	0.9915	0.7455	0.3925
16	2.6505	6.651	0.9895	0.7465	0.397
17	2.6505	6.47	0.9895	0.745	0.397
18	2.65	2.6375	0.9895	0.7485	0.397
19	2.651	6.6492	0.993	0.7515	0.397
20	2.651	6.6505	0.995	0.7465	0.396
21	2.645	6.6505	0.9935	0.7495	0.397
22	2.64	6.6505	0.9925	0.748	0.3965
23	2.64	6.6505	0.995	0.746	0.3975
24	2.6545	6.652	0.995	0.749	0.396
25	2.6505	6.6485	No data	No data	0.3945
26	2.653	6.6485	No data	No data	0.395
27	2.6415	6.6415	No data	No data	0.3935
28	2.6525	6.649	No data	No data	No data
29	2.665	6.6535	No data	No data	No data
30	2.6525	6.6465	No data	No data	No data
31	2.6505	6.6465	No data	No data	No data
32	2.6575	6.661	No data	No data	No data
33	2.649	6.53	No data	No data	No data
34	2.6305	6.6425	No data	No data	No data
35	2.6545	6.654	No data	No data	No data
36	2.6485	6.6445	No data	No data	No data

Mean Deviation of the Roughness Profile	Ra (µm)
RMS Deviation of the Roughness Profile	Rq (µm)
Skewness of the roughness profile	Rsk
Kurtosis of the Roughness Profile	Rku
Maximum Valley Depth of the Roughness profile	rv (µm)

Table 7-3 Surface Finish Parameter Data

Machined Surface Finish						
		Ra (µm)	Rq (µm)	Rsk	Rku	Rv (µm)
Min		**0.075**	**0.098**	**-0.976**	**1.864**	**0.214**
Max		**4.401**	**5.079**	**1.099**	**6.669**	**10.321**
Mean		**2.47**	**2.921**	**-0.203**	**2.719**	**5.97**
Std Dev		**1.355**	**1.555**	**0.535**	**1.219**	**2.674**
Specimen Number	4	0.945	1.175	0.122	2.775	2.739
	5	0.988	1.218	-0.607	3.095	3.51
	6	3.477	4.4	-0.249	3.558	9.466
	7	0.503	0.655	-0.745	3.967	2.253
	8	0.711	0.863	-0.31	2.673	2.365
	9	0.809	0.997	-0.269	2.659	2.572
	10	0.075	0.098	1.099	6.267	0.214
	11	1.652	2.012	-0.45	2.501	4.867
	12	2.463	2.997	-0.976	2.848	7.764
	17	1.483	1.873	-0.903	3.351	5.294
	18	2.903	3.516	-0.923	2.766	8.732
	19	2.903	3.516	-0.923	2.766	8.732
	20	1.234	1.691	-0.178	6.669	4.588
	21	3.847	4.481	0.266	2.153	8.059
	22	1.172	1.479	0.528	3.835	2.847
	23	4.212	4.868	0.203	1.891	8.365
	24	3.87	4.483	-0.715	2.226	10.321
	28	0.738	0.975	-0.042	4.451	2.754
	29	2.935	3.384	-0.46	1.972	6.898
	30	4.188	4.869	0.631	2.188	6.438
	31	0.657	0.843	-0.228	3.729	2.291
	32	3.73	4.354	0.507	2.139	6.611
	33	2.731	3.23	-0.07	2.251	6.733
	34	4.401	5.079	0.442	1.973	7.478
	35	2.477	2.845	0.008	1.864	5.51
	36	3.489	4.049	0.087	1.867	6.975
Polished Surface Finish						
		Ra (µm)	Rq (µm)	Rsk	Rku	Rv (µm)
Min		**0.049**	**0.057**	**-0.299**	**2.331**	**0.103**
Max		**0.1**	**0.117**	**0.426**	**3.374**	**0.239**
Mean		**0.0735**	**0.087**	**-0.0355**	**2.610**	**0.197**
Min		**0.014908**	**0.017**	**0.226**	**0.383**	**0.0460**
Specimen Number	2	0.065	0.076	0.018	2.706	0.187
	3	0.073	0.087	0.426	2.515	0.133
	13	0.089	0.103	-0.299	3.282	0.227
	14	0.061	0.072	-0.089	2.472	0.16
	15	0.074	0.088	-0.25	3.374	0.239
	25	0.076	0.093	-0.186	2.94	0.226
	26	0.1	0.117	0.19	2.355	0.208
	27	0.049	0.057	0.043	2.331	0.103

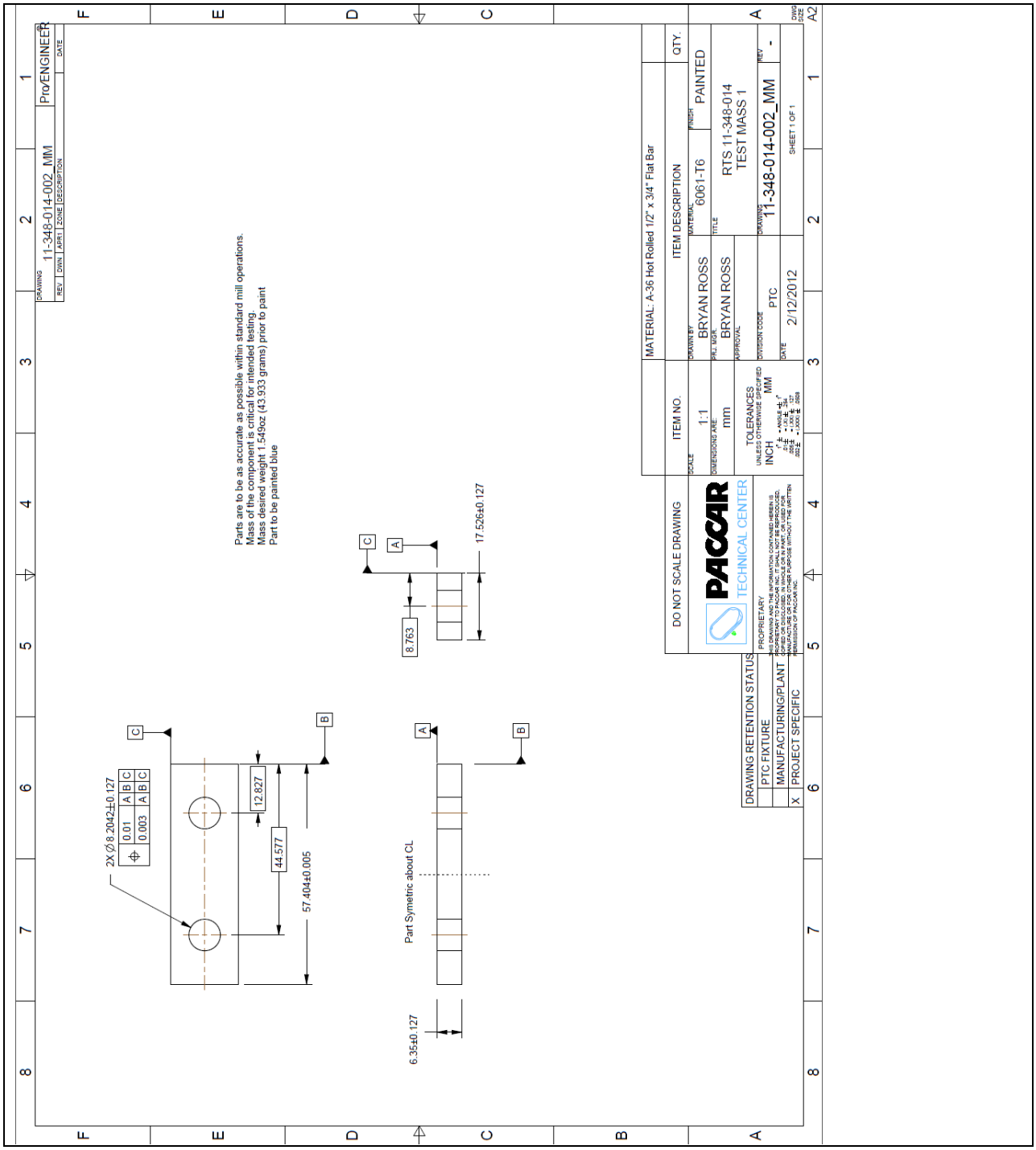

Figure 7-4 44g Mass Drawing

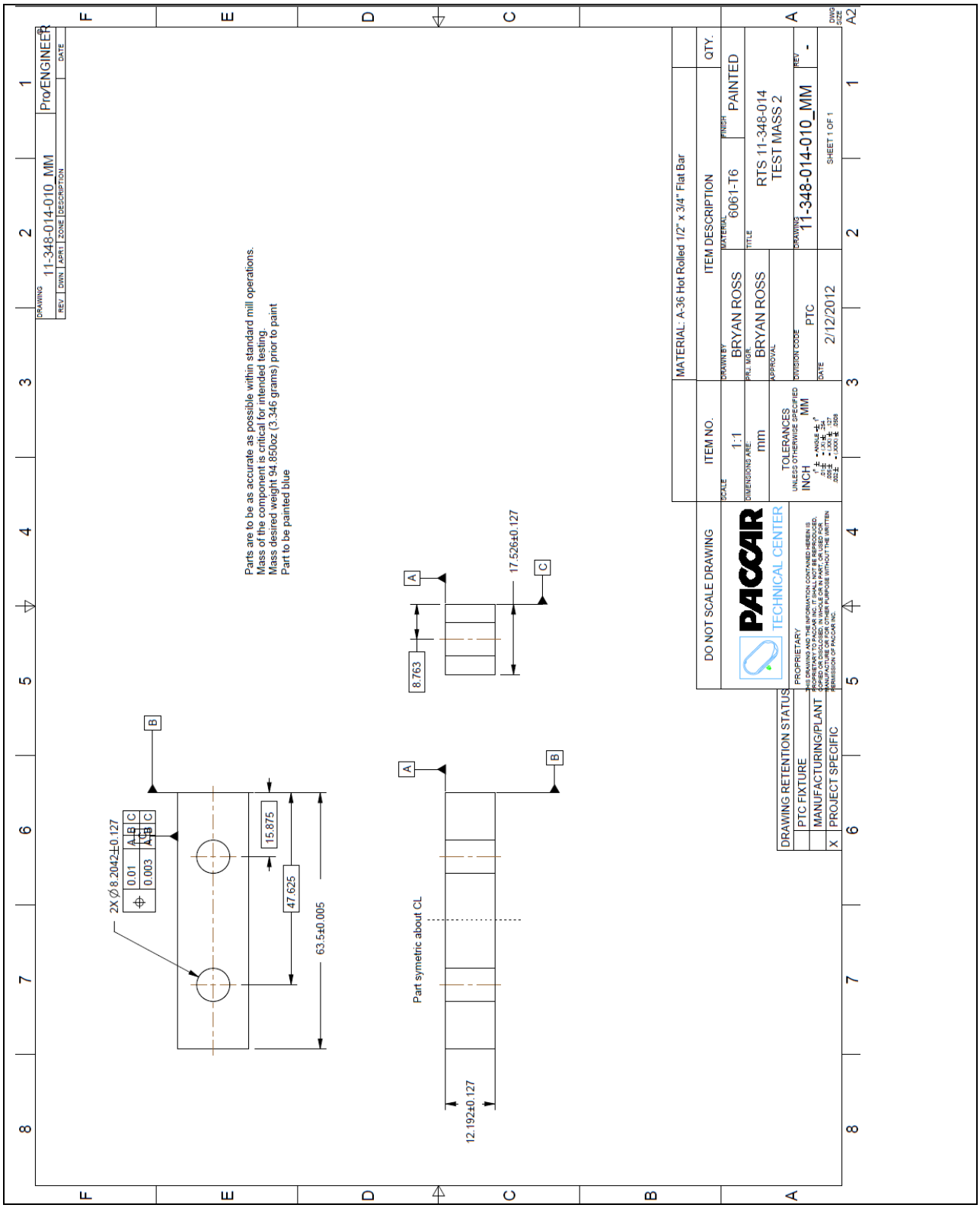

Figure 7-5 95g Mass Drawing

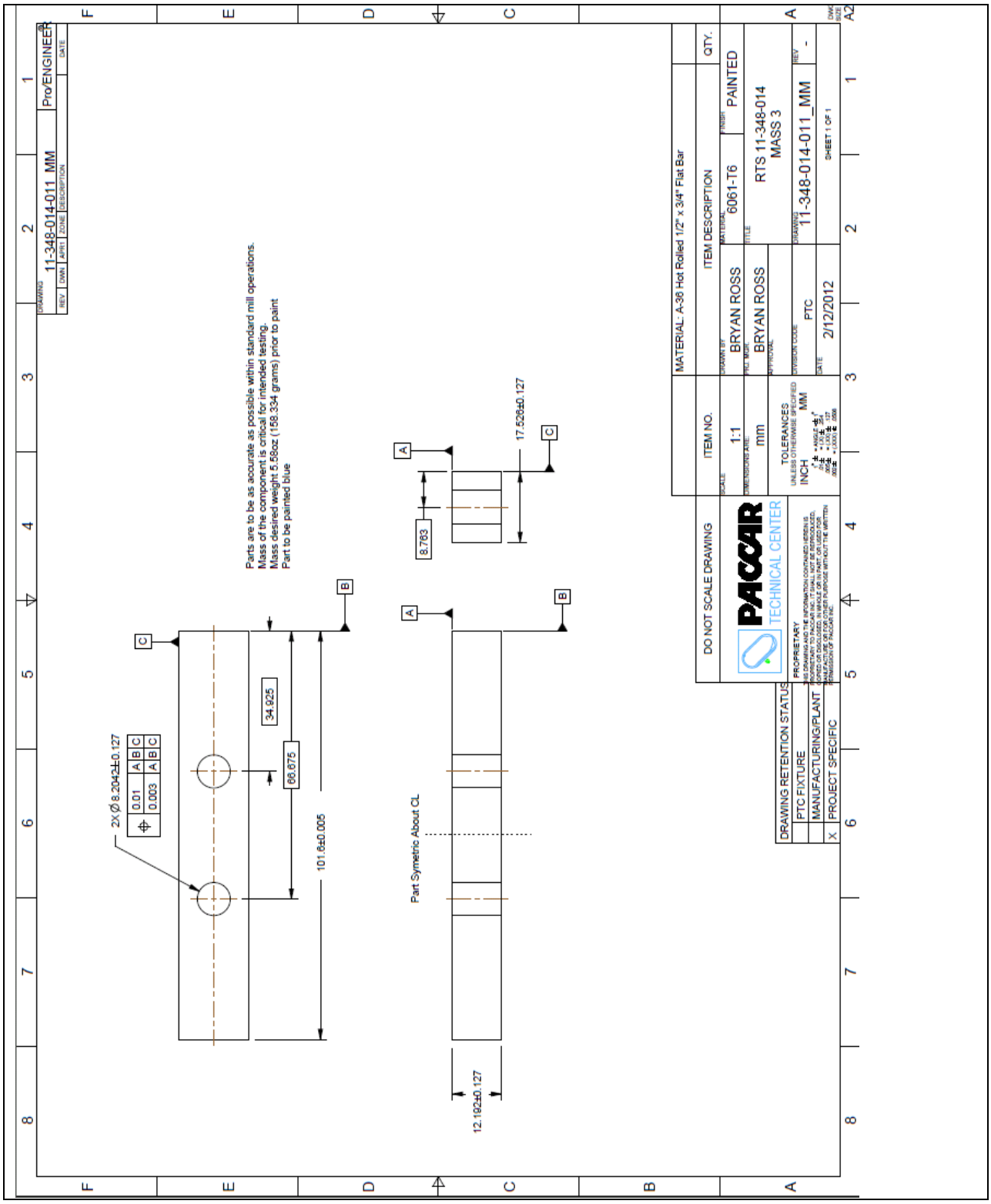

Figure 7-6 158g Mass Drawing

Fundamental Cantilevered Beam with Concentrated Mass Natural Frequency Calculations

The fundamental first mode of natural frequency can be derived by applying the energy (Rayleigh) technique. The derived formula for a Single Degree of Freedom (SDOF) beam with a concentrated mass is shown in equation (7.1).

Fundamental Frequency [35]

$$\omega_1 = \frac{1}{2\pi}\left[\frac{3EI}{L^3(M + .024\,M_B}\right]^{1/2} \tag{7.1}$$

Where:
E = modulus of elasticity of beam = 68950 (N/m^2)
I = 2nd moment of inertia of beam = 4.9E-10 (m^4)
L= length of beam = .01925 (m)
M = mass of beam = .02316(kg)
M_1 = mass of concentrated mass = 0.190 (kg)
M_2 = mass of concentrated mass = 0.235 (kg)
M_3 = mass of concentrated mass = 0.291 (kg)

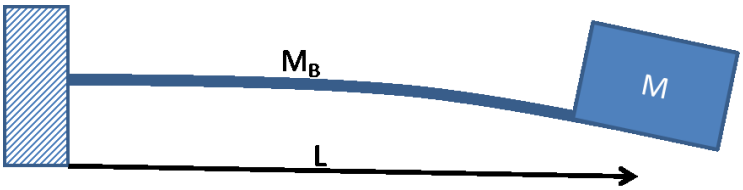

Figure 7-7 Clamped Beam with Concentrated Mass

Table 7-4 Numerical Cantilevered Beam with Concentrated Mass Natural Frequencies		
Numerical Calculation for 1st mode of vibration using bending beam equation		
Mode 1 Freq (190g mass)	Mode 1 Freq (235g mass)	Mode 1 Freq (291g mass)
71 Hz	66 Hz	61 Hz

Comparison of results from Table 5-20 impulse impact hammer versus hand calculated values form Table 7-5 are shown in Table 7-5. It was shown that the addition of mass reduces the natural frequency as calculated by (7.1). The numerical simplified beam with a concentrated end correlated well to the experimental testing for damped natural frequency (ω_d) as shown in Table 7-5.

Table 7-5 Experimental Specimen Natural Frequencies vs. Hand Calculations			
Specimen	Impulse Test (Hz)	Numerical Base Calculation (Hz)	% Error
190g mass	69.3	71.0	-2.5%
235g mass	64.1	66.0	-3.0%
291g mass	58.6	61.0	-4.0%

Appendix B Stress Calculations

Spectral Stress PSD formation and Spectral Damage Example

The spectral stress PSD was generated by multiplied the square of the stress transfer function $|H(\omega)|^2$ by the PSD excitation load profile $W(\omega)$. This was done at each frequency interval of the functions to derive the response stress function $G(f)$ for the applied excitation.

$$G(\omega) = |H(\omega)|^2 \cdot W(\omega) \qquad (2.71)$$
$$G(\omega) = Stress\ PSD\ \ ((MPa)^2/Hz)$$

$$H(\omega) = Stress\ transfer\ function -\ equations\ \ (2.68) or\ (2.69) or (2.70)$$

$$W(\omega) = PSD\ load\ profile$$

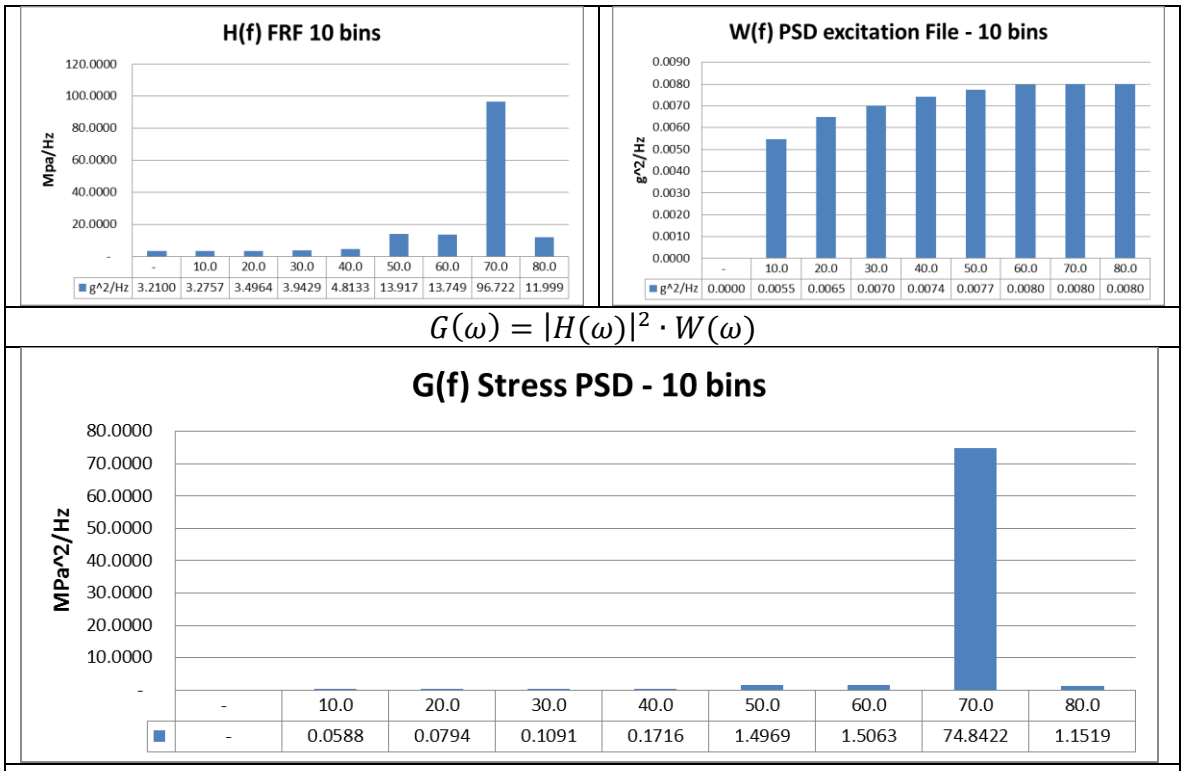

Figure 7-8 G(ω) Stress PSD Process Example

Statistics are then applied to determine the raw moment (m_0), Variance (m_2), and kurtosis (m_4) of the calculated stress probability density function G(ω).

$$M_j = moment\ of\ the\ area\ of\ the\ PSD = \int f^j G_x(\omega) df$$

Where f^j is the frequency of block and j is the moment number $G_x(\omega)df$ is the area of each block. Each of the block values are summed to calculate the total moment (M_j) of the function. A simple example of this is if only 60 Hz and 70 Hz blocks were the function the moments would be calculated at follows:

$$M_0 = 60^1 * 1.5063 * 10 + 70^1 * 74.8422 * 10$$

$$M_2 = 60^2 * 1.5063 * 10 + 70^2 * 74.8422 * 10$$

$$M_4 = 60^4 * 1.5063 * 10 + 70^4 * 74.8422 * 10$$

The moment values can be used statistically to evaluate the expected level crossings $E[0^+]$ as well as the number of peaks$E[P]$:

$$E[0^+] = \sqrt{\frac{M_2}{M_0}} \qquad E[P] = \sqrt{\frac{M_4}{M_2}}$$

Additionally the spectral width parameter (λ) and function irregularity factor (γ) are developed by applying the moments as follows:

$$\gamma = \sqrt{\frac{M_2^2}{M_0 M_4}} \qquad \lambda = \sqrt{1-\gamma}$$

These developed parameters can then be applied to various methods of spectral damage modeling developed by Dirlik [13] , Lalanne, and Rice [14]. The three analysis methods are shown below.

$$N_i = \#\ of\ cycles\ in\ stress\ range\ (stress\ \text{min}\ to\ stress\ \text{max})$$

$$E[P] = expected\ number\ of\ stress\ or\ strain\ peaks$$
$$T = time\ period\ of\ evaluation\ (s)$$
$$S = Stress\ Range\ {}^{N}/_{mm^2}$$

Bendat Narrow Band (1964) [12]

$$N_i = E[P] * T * \int_{stress\ min}^{stress\ max} \frac{S}{4\ m_0} e^{\frac{s^2}{8\ m_0}}\ ds \tag{7.2}$$

Dirlik Method (1985) [13]

$$N_i = E[P] * T * \int_{stress\ min}^{stress\ max} S * P(S)\ ds \tag{7.3}$$

$$P(S) = \frac{\frac{D_1}{Q} e^{\frac{-Z}{Q}*S} + \frac{D_2 Z}{R^2} e^{\frac{-Z^2}{2R^2}*S^2} + D_3 Z e^{\frac{-Z^2}{2}*S^2}}{2\sqrt{M_0}}$$

$$Z = \frac{1}{2\sqrt{M_0}} \qquad \gamma = \frac{M_2}{\sqrt{M_0 M_4}} \qquad X_m = \frac{M_1}{M_2}\sqrt{\frac{M_2}{M_4}} \qquad R = \frac{\gamma - X_m - D_1^2}{1-\gamma-D_1-D_1^2} \qquad E[P] = \sqrt{\frac{M_4}{M_2}}$$

$$D_1 = \frac{2(X_m-\gamma^2)}{1+\gamma^2} \qquad D_2 = \frac{1-\gamma-D_1+D_1^2}{1-R} \qquad D_3 = 1 - D_1 - D_2 \qquad Q = \frac{1.25(\gamma-D_3-D_2R)}{D_1}$$

Lalanne Method (2002) [14]

$$N_i = \frac{1}{rms}\frac{\sqrt{1-\gamma^2}}{\sqrt{2\pi}} * \int_{stress\ min}^{Stress\ max} e^{\frac{-S^2}{2rms^2(1-\gamma^2)}} + \frac{S*\gamma}{2rms}\left[1 + erf\left(\frac{S*\gamma}{rms\sqrt{2(1-\gamma^2}}\right)\right] ds \tag{7.4}$$

$$\text{erf}(x) = \frac{2}{\sqrt{2\pi}}\int_0^x e^{-t^2}\,dt$$

$$\gamma = irregularity\ factor = \frac{M_2}{\sqrt{M_0 M_4}} \quad \text{(adjusts for bandwidth of measurement)}$$

$$S = Stress\ Range\ {}^{N}/_{mm^2}$$

$$rms = .707$$

Table 7-6 Dirlik Hand Calculation Validation	
Hand calculated 235g stress cycle counting	Ncode Dirlik cycle count for 235g specimen
36459 cycles per block	35132 cycles per block

Stress Determination of Shake Table Specimens

Stress was measured on the specimens using the strain gage located as depicted in Figure 7-28. The strain gage was set to zero when installed on the shake fixture. To account for this, the FEA stress of 1G was applied to add a static stress value to the RMS stress measured. These values are shown in Table 7-7.

Table 7-7 Specimen 1g Static Stress	
Specimen Configuration	1 G FEA max stress (MPa)
190g	3.21
235g	3.70
291g	4.44

The strain gages were noted to have drift effects during an entire block event until ultimately failed to read correct strain. First, the strain was converted to stress, secondly, the mean stress values were calculated at 0.1 second intervals. The mean intervals were then subtracted from the stress data at 0.1 second block intervals to account for the drift in data. The results of 190g, 235g, and 291g specimen configuration are as follows:

190g Specimen Stress Results

Specimen #37 strain gage data was corrupt after 330 seconds. Only the first 330seconds were used to adjust for mean drift for a representation of the full block RMS s stress.

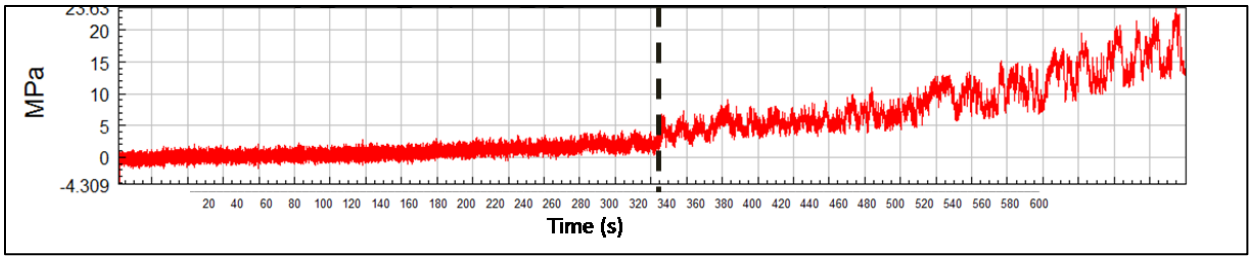

Figure 7-9 Experimental 190g Mean Strain Gage Stress (Drift Detection)

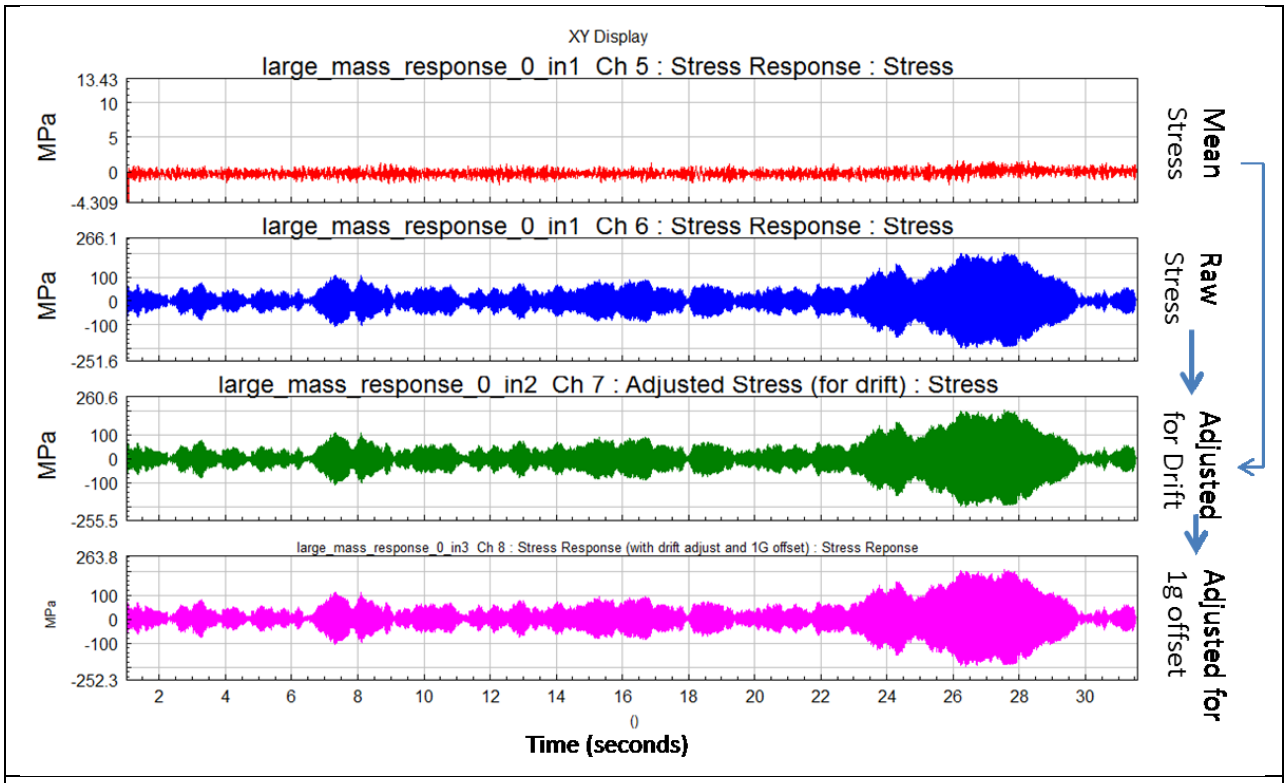

RMS stress 62.42MPa = 59.22+3.2 (1g)
Mean stress 3.2 MPa

Figure 7-10 Experimental 190g Specimen Stress Measurement Adjustments

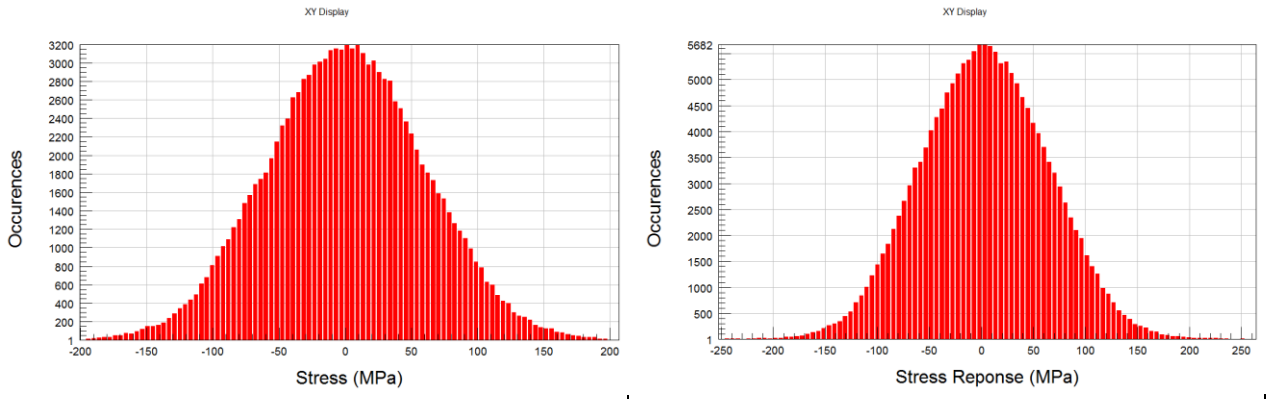

Stress distribution of 0-330seonds prior to drift adjustments	Stress distribution of 0-330seonds after to drift adjustments

Figure 7-11 Experimental 190g Strain gage Stress Histogram

235g Specimen Stress Results

Specimen #37 strain gage data was corrupt after 215 seconds. Only the first 215 seconds were used to adjust for mean drift for a representation of the full block RMS s stress.

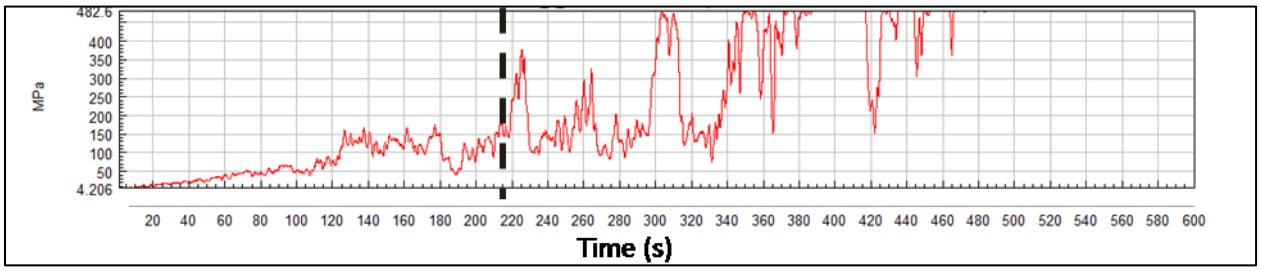

Figure 7-12 Experimental 235g Mean Strain Gage Stress (Drift Detection)

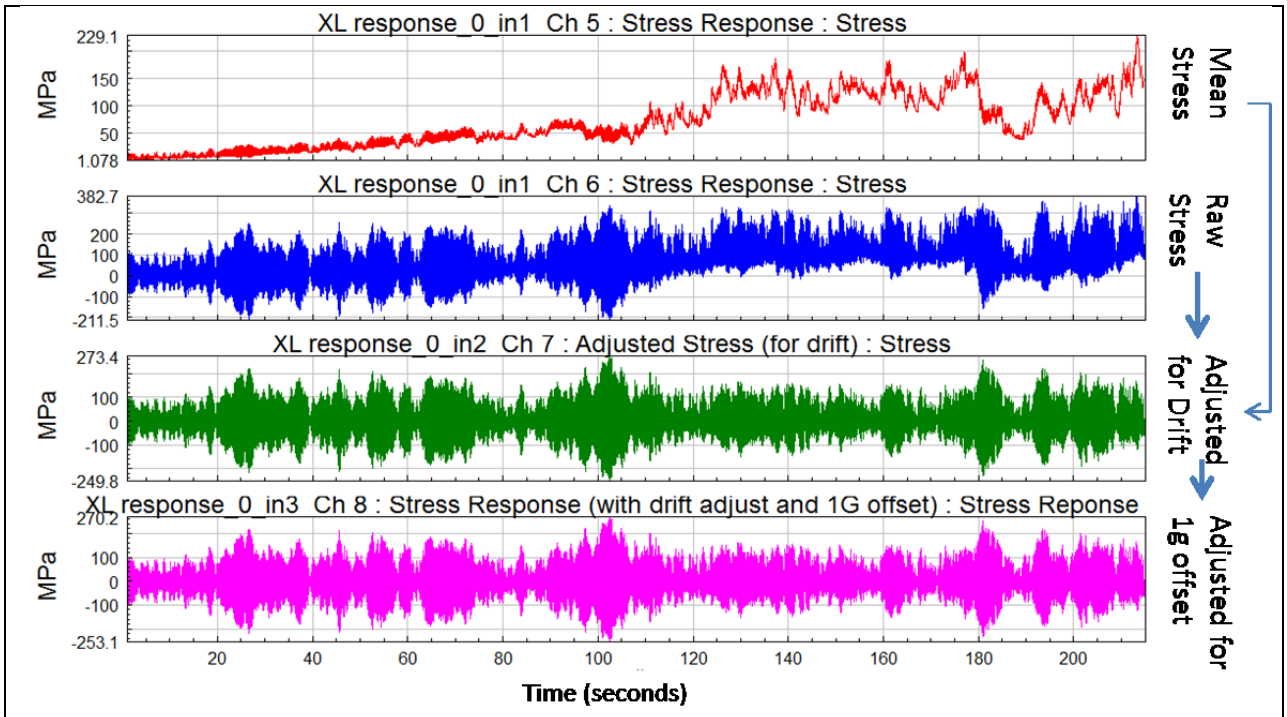

RMS stress 70.43MPa = 66.73 +3.7(1g)
Mean stress 3.7 MPa

Figure 7-13 Experimental 235g Specimen Stress Measurement Adjustments

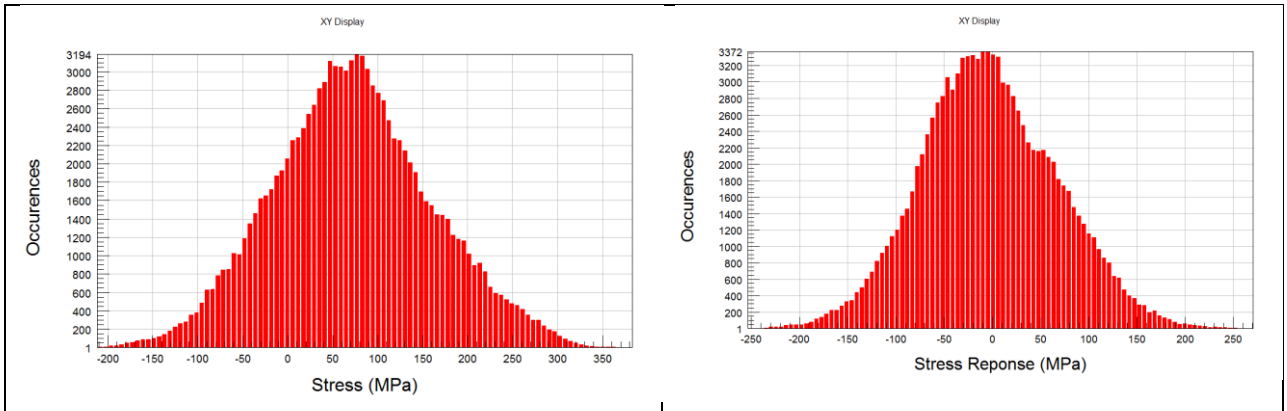

Stress distribution of 0-215seonds prior to drift adjustments	Stress distribution of 0-215seonds after to drift adjustments

Figure 7-14 Experimental 235g Strain gage Stress Histogram

Stress adjustment for 291g specimen configuration

Stress adjustment for 235g configuration specimen #26. Strain gage data was good for all 600 seconds. Strain drift was detected and adjusted. The strain mean stress values were calculated at 0.1 second intervals. The mean intervals were then subtracted from the stress data at 0.1 second block intervals to account for the drift in data.

291g Specimen Stress Results

Specimen #26 strain gage survived the entire 600 second block cycle. The entire 600 seconds were used to adjust for mean drift for a representation of the full block RMS s stress.

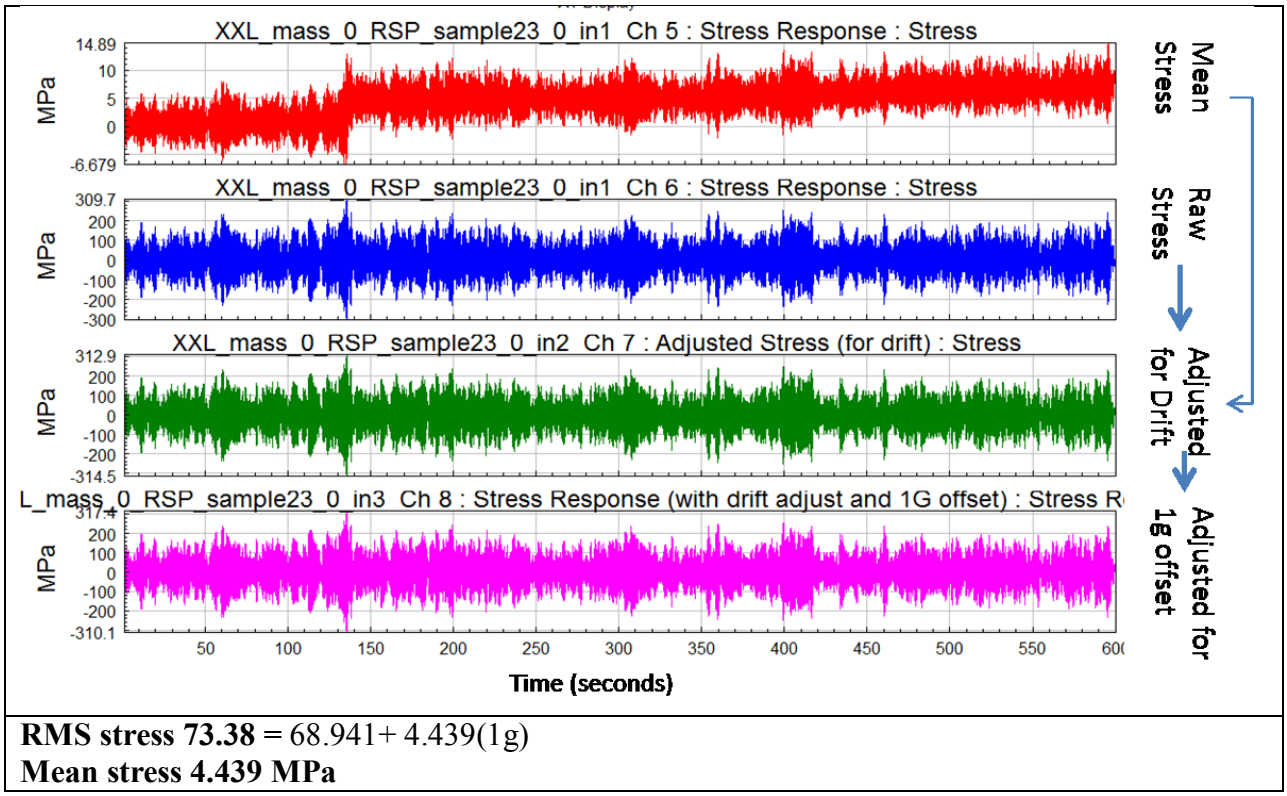

RMS stress 73.38 = 68.941+ 4.439(1g)
Mean stress 4.439 MPa

Figure 7-15 Experimental 291g Specimen Stress Measurement Adjustments

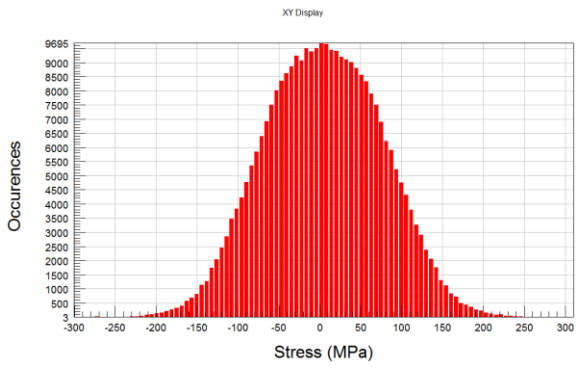

Stress distribution of 0-600 seconds prior to drift adjustments

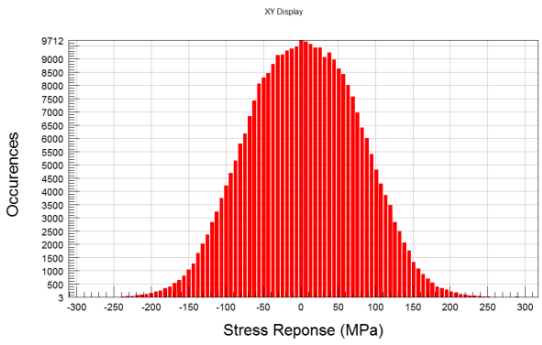

Stress distribution of 0-600seonds after to drift adjustments

Figure 7-16 Experimental 291g Strain gage Stress Histogram

Shake Table g Acceleration Normalizing for Specimen Testing

To use these determined stress values for all specimens, the data was normalized by the base acceleration RMS value. This normalized value was then multiplied by each specimen's recorded RMS acceleration for all block cycles until failure. This method was not applied but was investigated for application.

$$Specimen\ Stress\ (MPa) = \frac{Measured\ RMS\ stress\ \ (MPa)}{measured\ RMS\ accleration\ (g)} * Specimen\ RMS\ \ acceleration(\mathrm{g}) \tag{7.5}$$

Table 7-8 Experimental Specimen Stress Normalized vs. Base Accelerations			
Specimen Configuration	Measured RMS stress (MPa)	Measured RMS base acceleration (g's)	Normalized RMS stress/1g base (MPa)
190g	62.42	0.68	92.16
235g	70.43	0.76	93.21
291g	73.38	0.74	99.00

Adjusting stress for the facture angle of specimens

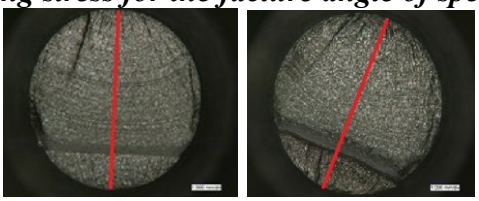

$$\sigma\ at\ crack\ origin = \sigma_{strain\ gage} * \cos\theta$$

Table 7-9 Specimen Stress Adjustment for Fracture Angle

		Specimen Number	Strain gage RMS μ(mm/mm)	RMS Stress (MPa)	Mean Stress (MPa)	Fracture Angle	Adjusted component vector stress	Block Cycles Until Failure (600 sec/block)
190 g Configuration	Polished	25	905.43	62.42	88.29	no data		37.05
		26	905.43	62.42	88.29	no data		18.60
		27	905.43	62.42	88.29	no data		18.35
		Mean	905.43	62.42	88.29			24.66
	Machined	33	905.43	62.42	88.29	0.00	88	16.63
		34	905.43	62.42	88.29	-27.00	79	19.45
		35	905.43	62.42	88.29	7.00	88	12.99
		36	905.43	62.42	88.29	2.00	88	24.32
		Mean	905.43	62.42	88.29			18.35
235 g Configuration	Polished	1	1021.61	70.43	99.62	26.00	90	18.25
		2	1021.61	70.43	99.62	7.50	99	18.74
		3	1021.61	70.43	99.62	7.00	99	14.72
		Mean	1021.61	70.43	99.62			17.24
	Machined	4	1021.61	70.43	99.62	11.00	98	7.43
		5	1021.61	70.43	99.62	14.50	96	8.44
		6	1021.61	70.43	99.62	21.00	93	8.98
		7	1021.61	70.43	99.62	-7.00	99	8.31
		8	1021.61	70.43	99.62	0.00	100	12.75
		9	1021.61	70.43	99.62	9.00	98	12.08
		10	1021.61	70.43	99.62	7.00	99	8.21
		11	1021.61	70.43	99.62	14.00	97	6.52
		12	1021.61	70.43	99.62	7.00	99	9.09
		Mean	1021.61	70.43	99.62			9.09
291 g Configuration	Polished	13	1064.40	73.38	103.79	14.00	101	13.16
		14	1064.40	73.38	103.79	7.00	103	11.84
		15	1064.40	73.38	103.79	7.00	103	10.94
		Mean	1064.40	73.38	103.79			11.98
	Machined	16	1064.40	73.38	103.79	-8.00	103	8.30
		17	1064.40	73.38	103.79	0.00	104	7.97
		18	1064.40	73.38	103.79	0.00	104	11.70
		19	1064.40	73.38	103.79	9.00	103	8.66
		20	1064.40	73.38	103.79	2.00	104	7.39
		21	1064.40	73.38	103.79	7.00	103	11.28
		22	1064.40	73.38	103.79	22.00	96	12.08
		23	1064.40	73.38	103.79	7.00	103	10.86
		24	1064.40	73.38	103.79	3.00	104	8.86
		Mean	1064.40	73.38	103.79			9.68

Appendix C FRF calculations

Spectral Resolution for Impulse Hammer Testing

The spectral resolution of the calculation was critical to ensure the magnitude of the FRF function is accurate. Various intervals are applied to test the effects of frequency sweep rates. It can be seen in Figure 7-19 that the system converged to the same shape function with $\Delta f < 0.5$ Hz.

While determining the damping values from this method, it was established that the frequency resolution was critical in obtaining the correct damping magnitudes. Therefore, various spectral resolutions were used to determine the correct block size. The testing showed that using a value of 0.25 spectral resolutions only recorded a time sample length of four seconds. This caused the time signal to not capture the entire response of the component as shown in Figure 7-17. Since the damping of aluminum is small, a larger time record was required to capture the entire response decay. Using 0.1 Hz spectral resolution established a ten second response file ensuring the response was encompassed in the data set for the FRF calculation. The various spectral resolutions were tested on samples 24,41, and 42 to evaluate difference in the specimens as displayed in Figure 7-18.

0.1 Hz Spectral Resolution	0.25 Hz Spectral Resolution

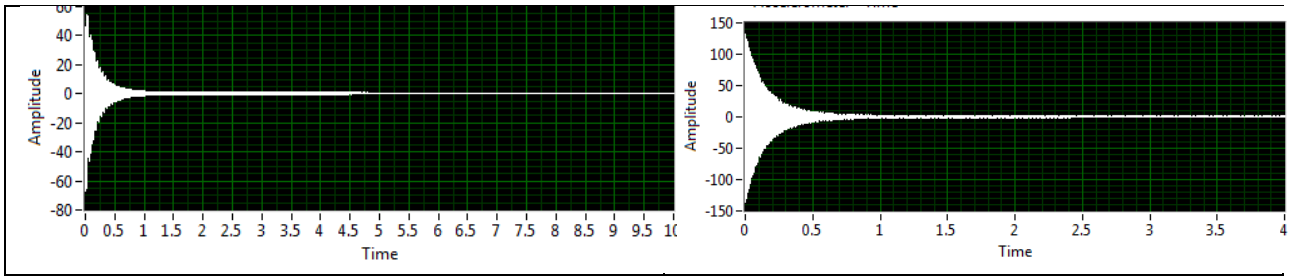

Figure 7-17 Impulse Free Response Method: Spectral Resolution Time Data

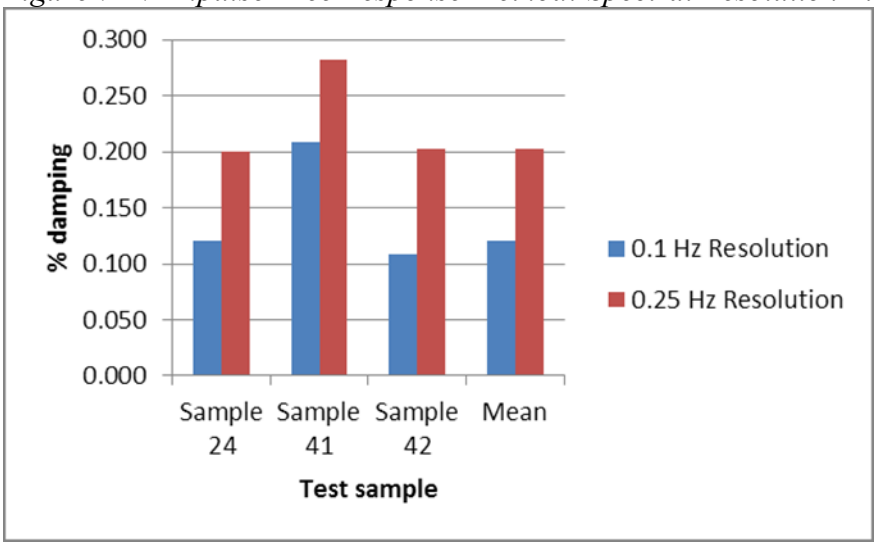

Figure 7-18 Effect of EMA Spectral Resolution

Figure 7-19 shows the evaluation on .01 to 1 Hz spectral resolution for the numerical FRF calculation. Values are shown to converge below .05 Hz spectral resolution.

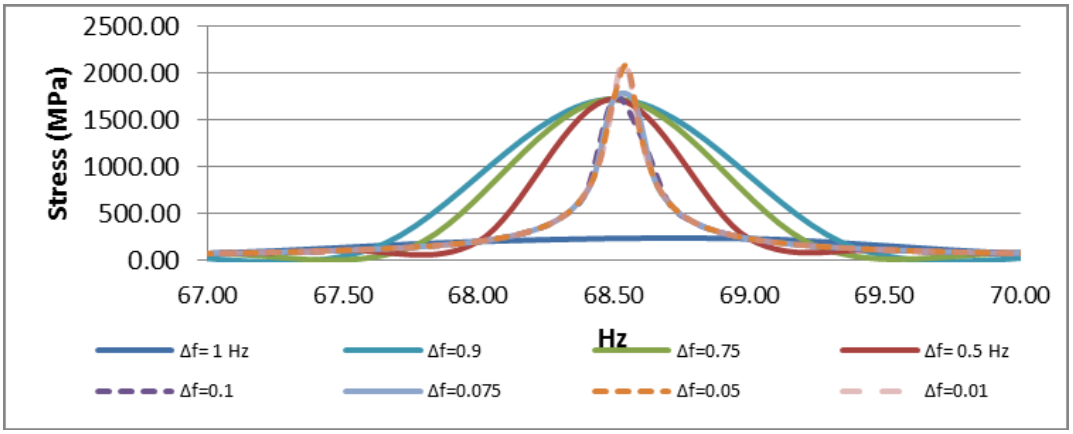

Figure 7-19 Effects of the FRF Shape from varying frequency Interval of calculation

Modal Impulse Damping Values								
	291 g added mass		235g added mass		190g added mass		System Mean Values	
Speciment #	% Damping Value 0.25 Hz	% Damping Value 0.1 Hz	% Damping Value 0.25 Hz	% Damping Value 0.1 Hz	% Damping Value 0.25 Hz	% Damping Value 0.1 Hz	% Damping Value 0.25 Hz	% Damping Value 0.1 Hz
24	0.205	0.121	0.196	0.115	0.200	0.121	0.200	0.121
41	0.239	0.150	0.282	0.209	0.308	0.252	0.282	0.209
42	0.203	0.109	0.196	0.106	0.216	0.129	0.203	0.109
Mean	**0.216**	**0.121**	**0.196**	**0.115**	**0.216**	**0.129**	**0.203**	**0.121**
Standard Dev	0.020	0.021	0.050	0.057	0.058	0.073	0.047	0.055
Lower 1σ	0.195	0.100	0.146	0.058	0.158	0.056		
Lower 1σ	0.236	0.142	0.246	0.172	0.274	0.202		

Table 7-10 Constrained Boundary Condition Modal Results

Specimen #	24	41	42
190g 0.1hz (Resolution)	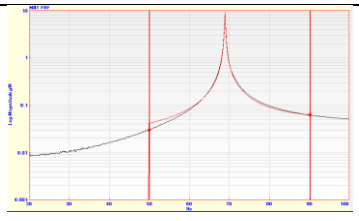	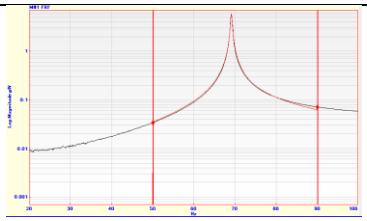	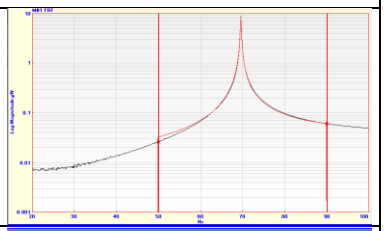
	Select Mode: 1 — Frequency Hz: 69 — Damping Hz: 0.0832 — Damping (%): 0.121 — Residue Mag: 10.3 — Residue Phs (deg): 174	Select Mode: 1 — Frequency Hz: 69.2 — Damping Hz: 0.174 — Damping (%): 0.252 — Residue Mag: 13.3 — Residue Phs (deg): 178	Select Mode: 1 — Frequency Hz: 69.6 — Damping Hz: 0.0901 — Damping (%): 0.129 — Residue Mag: 9.84 — Residue Phs (deg): 177

Specimen #	24	41	42
190g 0.25hz (Resolution)	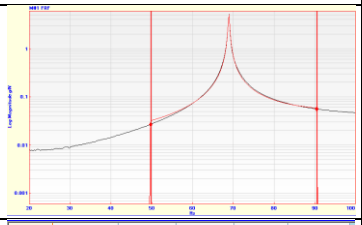	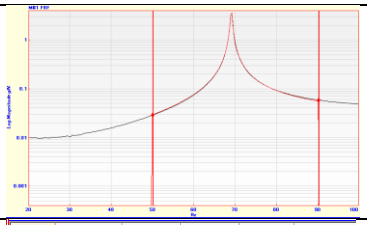	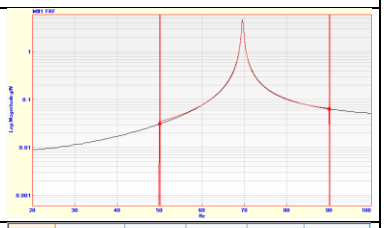
	Select Mode: 1 — Frequency Hz: 69 — Damping Hz: 0.138 — Damping (%): 0.2 — Residue Mag: 9.42 — Residue Phs (deg): 179	Select Mode: 1 — Frequency Hz: 69.2 — Damping Hz: 0.213 — Damping (%): 0.308 — Residue Mag: 10.5 — Residue Phs (deg): 179	Select Mode: 1 — Frequency Hz: 69.6 — Damping Hz: 0.15 — Damping (%): 0.216 — Residue Mag: 10.7 — Residue Phs (deg): 178

Specimen #	24	41	42
235g 0.1hz (Resolution)	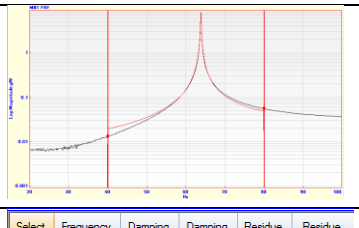	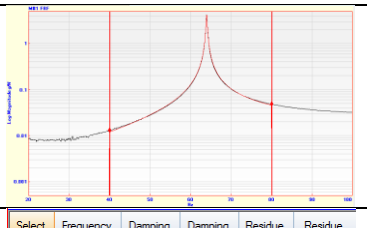	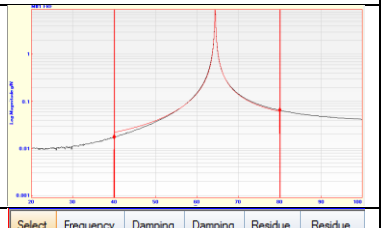
	Select Mode: 1 — Frequency Hz: 63.9 — Damping Hz: 0.0735 — Damping (%): 0.115 — Residue Mag: 7.53 — Residue Phs (deg): 173	Select Mode: 1 — Frequency Hz: 64 — Damping Hz: 0.134 — Damping (%): 0.209 — Residue Mag: 7.09 — Residue Phs (deg): 179	Select Mode: 1 — Frequency Hz: 64.4 — Damping Hz: 0.0685 — Damping (%): 0.106 — Residue Mag: 8.88 — Residue Phs (deg): 175

Specimen #	24	41	42
235g 0.25hz (Resolution)	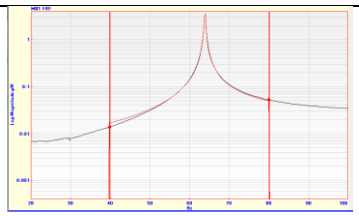	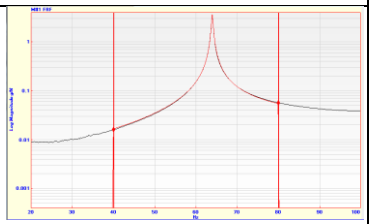	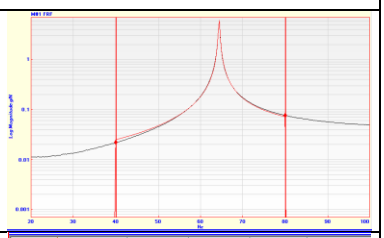

Select Mode	Frequency Hz	Damping Hz	Damping (%)	Residue Mag	Residue Phs (deg)
1	63.9	0.126	0.196	7.37	177

Select Mode	Frequency Hz	Damping Hz	Damping (%)	Residue Mag	Residue Phs (deg)
1	64	0.18	0.282	8.25	178

Select Mode	Frequency Hz	Damping Hz	Damping (%)	Residue Mag	Residue Phs (deg)
1	64.4	0.127	0.196	10.8	179

Specimen #	24	41	42
291g 0.1hz (Resolution)	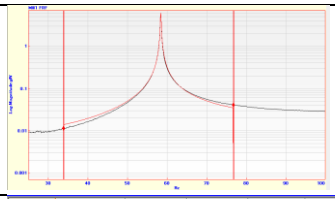	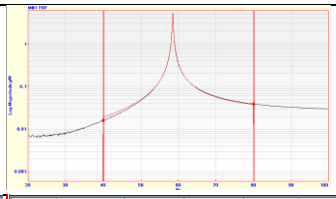	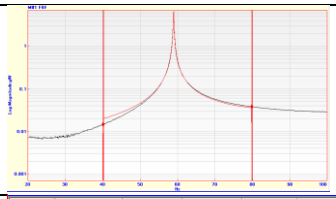

Select Mode	Frequency Hz	Damping Hz	Damping (%)	Residue Mag	Residue Phs (deg)
1	58.4	0.0705	0.121	6.3	173

Select Mode	Frequency Hz	Damping Hz	Damping (%)	Residue Mag	Residue Phs (deg)
1	58.5	0.0879	0.15	6.36	176

Select Mode	Frequency Hz	Damping Hz	Damping (%)	Residue Mag	Residue Phs (deg)
1	59	0.0642	0.109	6.04	174

Specimen #	24	41	42
291g 0.25hz (Resolution)	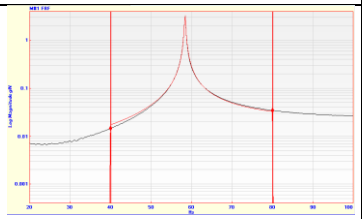	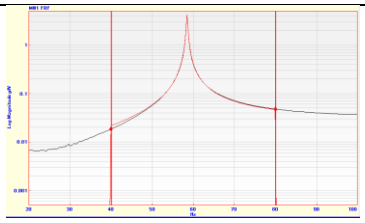	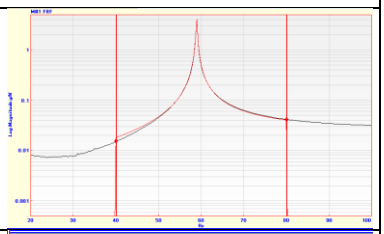

Select Mode	Frequency Hz	Damping Hz	Damping (%)	Residue Mag	Residue Phs (deg)
1	58.4	0.12	0.205	5.64	179

Select Mode	Frequency Hz	Damping Hz	Damping (%)	Residue Mag	Residue Phs (deg)
1	58.5	0.14	0.239	7.69	176

Select Mode	Frequency Hz	Damping Hz	Damping (%)	Residue Mag	Residue Phs (deg)
1	59	0.119	0.203	6.57	179

Forced Response PSD block Cycle FRF stress magnitudes

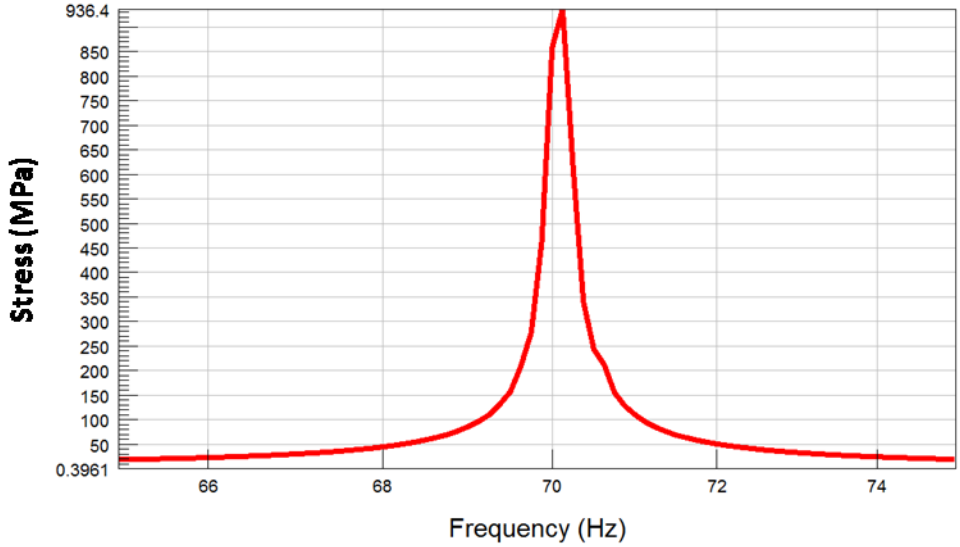

Figure 7-20 Forced Response PSD FRF 190g Specimen Configuration

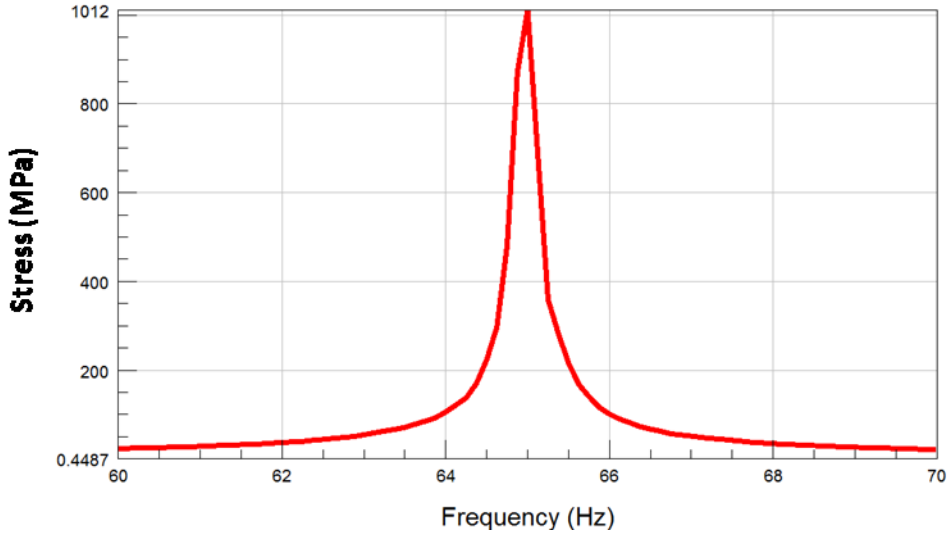

Figure 7-21 Forced Response PSD FRF 235g Specimen Configuration

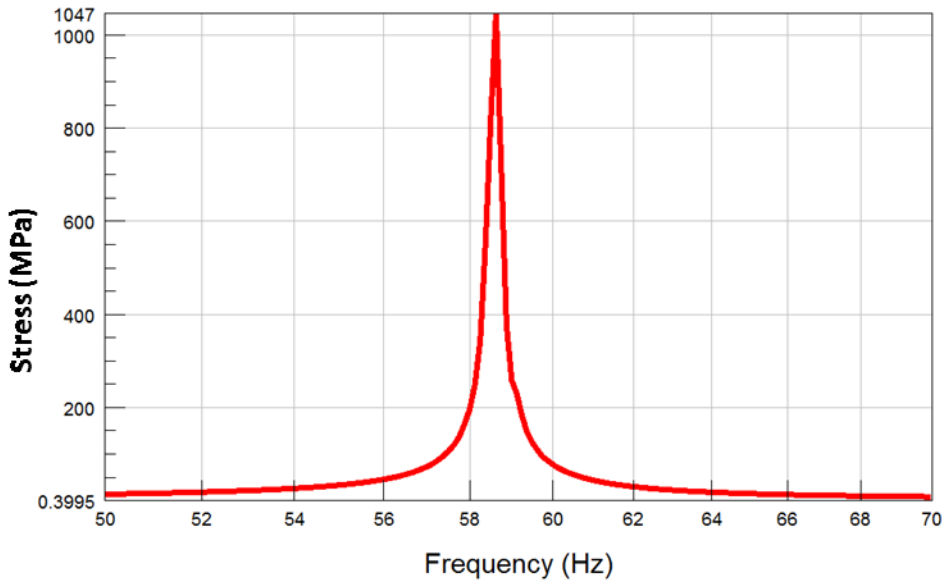

Figure 7-22 Forced Response PSD FRF 291g Specimen Configuration

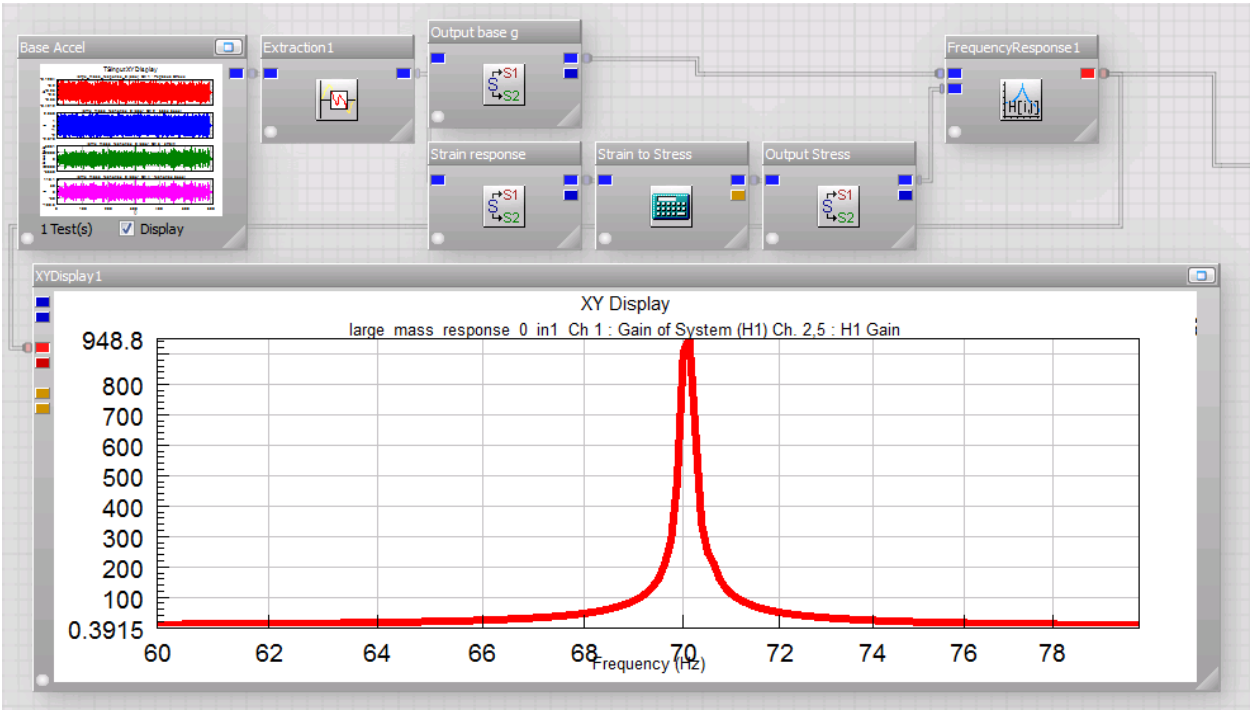

Figure 7-23 FRF Magnitude PSD Process Calculation

Appendix D Aluminum Properties

Table 7-11 Tabulated 6061-T6 SN Curve Data: Yhar [20]

Table 1. Tabulated values of Sa from Fig. 6.

Number of Cycles	Sa			
	Zero mean stress		Maximum mean stress	
	(MPa)	(ksi)	(MPa)	(ksi)
1.0E+01	482.63	70.00	482.63	70.00
2.0E+01	482.63	70.00	482.63	70.00
5.0E+01	482.63	70.00	482.63	70.00
7.0E+01	482.63	70.00	482.63	70.00
1.0E+02	420.28	60.96	420.28	60.96
2.0E+02	325.43	47.20	325.43	47.20
5.0E+02	241.32	35.00	239.94	34.80
1.0E+03	198.91	28.85	184.71	26.79
2.0E+03	168.92	24.50	137.89	20.00
5.0E+03	142.31	20.64	95.01	13.78
7.0E+03	135.83	19.70	75.36	10.93
1.0E+04	120.66	17.50	63.02	9.14
2.0E+04	99.46	14.43	53.37	7.74
5.0E+04	80.64	11.70	49.50	7.18
1.0E+05	71.15	10.32	47.50	6.89
2.0E+05	64.45	9.35	37.68	5.47
5.0E+05	58.50	8.49	30.06	4.36
1.0E+06	55.50	8.05	26.68	3.87
2.0E+06	53.38	7.74	24.48	3.55
5.0E+06	51.50	7.47	22.68	3.29
1.0E+07	50.55	7.33	21.79	3.16
2.0E+07	49.88	7.24	21.18	3.07
5.0E+07	49.28	7.15	20.66	3.00
1.0E+08	48.99	7.11	20.39	2.96
2.0E+08	48.77	7.07	20.21	2.93
5.0E+08	48.59	7.05	20.06	2.91
1.0E+09	48.49	7.03	19.97	2.90

Table 7-12 Aluminum 6061-T6 SN Curve MIL-HDBK-5J [19] [32]

	6061-T6 (R-Ratio Curves)	Description
MaterialType	100	Material Type
UTS	496.42272	Ultimate Tensile Strength (MPa)
E	6.89476E4	Elastic Modulus (MPa)
Nfc	1E30	Cutoff (cycles)
Ne	1E30	Endurance Limit (cycles)
SEls	0.119919	Standard error of log stress
StressType	Range	Type of stress used to describe a fatigue cycle
M1		Mean stress parameter M1
M2		Mean stress parameter M2
M3		Mean stress parameter M3
M4		Mean stress parameter M4
Comments		Comments
References	MIL-HDBK-5J, Figure 3.6.2.2.8, p3-289	References

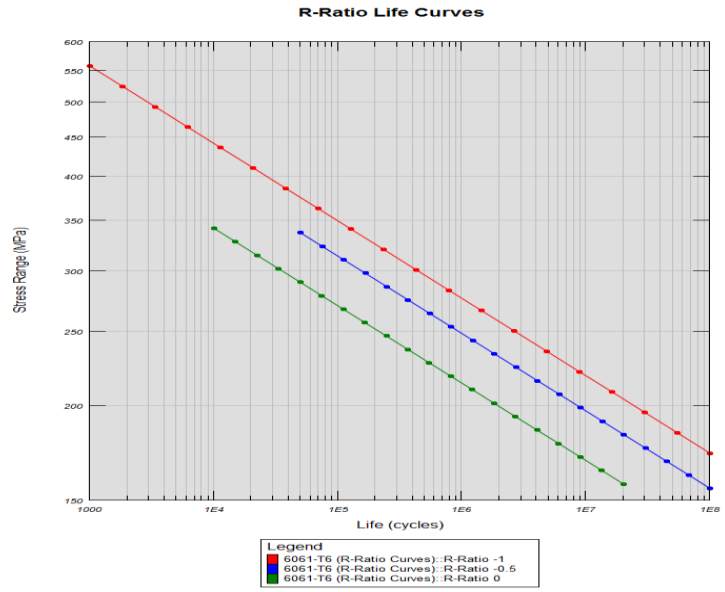

Figure 7-24 Aluminum 6061-T6 SN Curve MIL-HDBK-5J [19] [32]

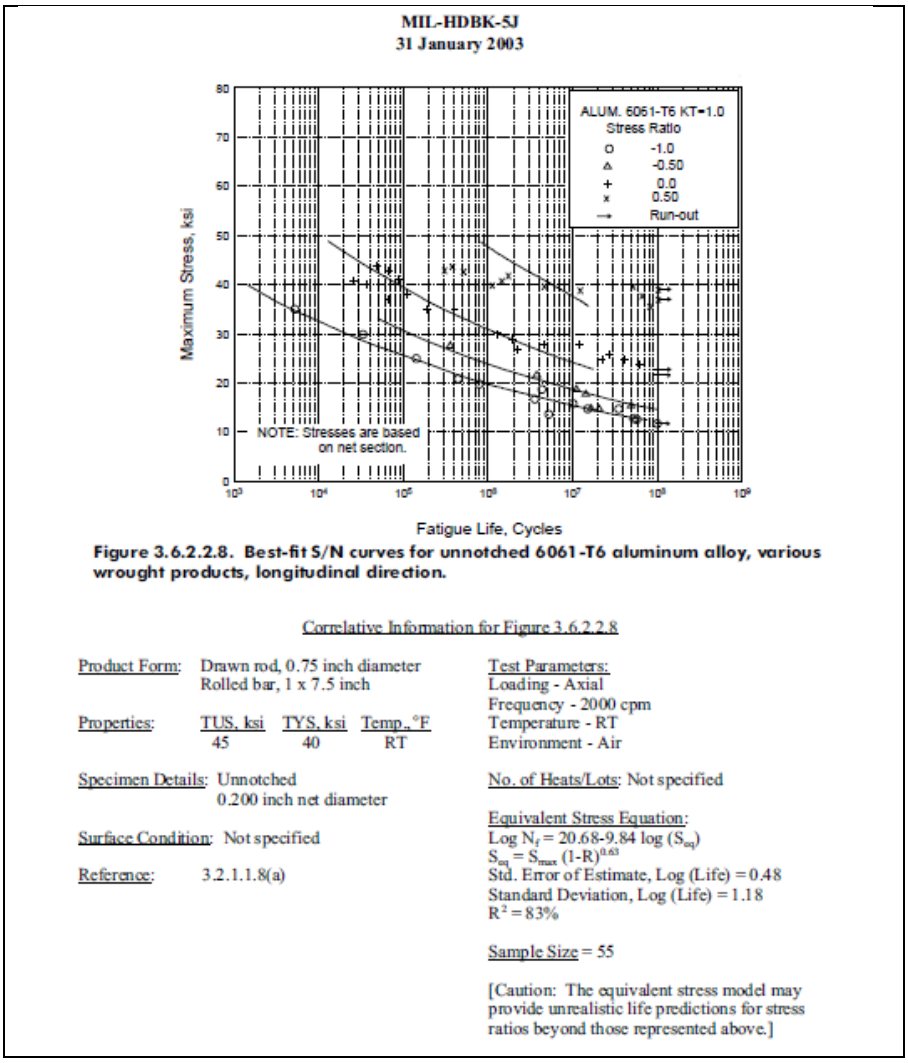

Figure 7-25 Aluminum 6061-T6 SN Curve (Wiley Published) [18]

Table 7-13 Aluminum 6061-T6 S-N Curve Steinberg [18]

	6061_HV_T6::Stress-life (S-N)	Description
MaterialType	104	Material Type
YS	265	Yield Strength (MPa)
UTS	305	Ultimate Tensile Strength (MPa)
E	7.17E4	Elastic Modulus (MPa)
me		Elastic Poisson's Ratio
mp		Plastic Poisson's Ratio
SRI1	1304	Stress Range Intercept (MPa)
b1	-0.0921	First Fatigue Strength Exponent
Nc1	1E6	Fatigue Transition Point (cycles)
b2	-0.0921	Second Fatigue Strength Exponent
SE	0	Standard Error of Log(N)
RR	-1	R-ratio of Test
Nfc	1E30	Fatigue CutOff
M1		Mean stress parameter M1
M2		Mean stress parameter M2
M3		Mean stress parameter M3
M4		Mean stress parameter M4
Comments	2nd Edition, 1988, John Wiley & Sons.T6 material; reversed bending	Comments
References	Vibration Analysis for Electronic Equipment, D S Steinberg:	References

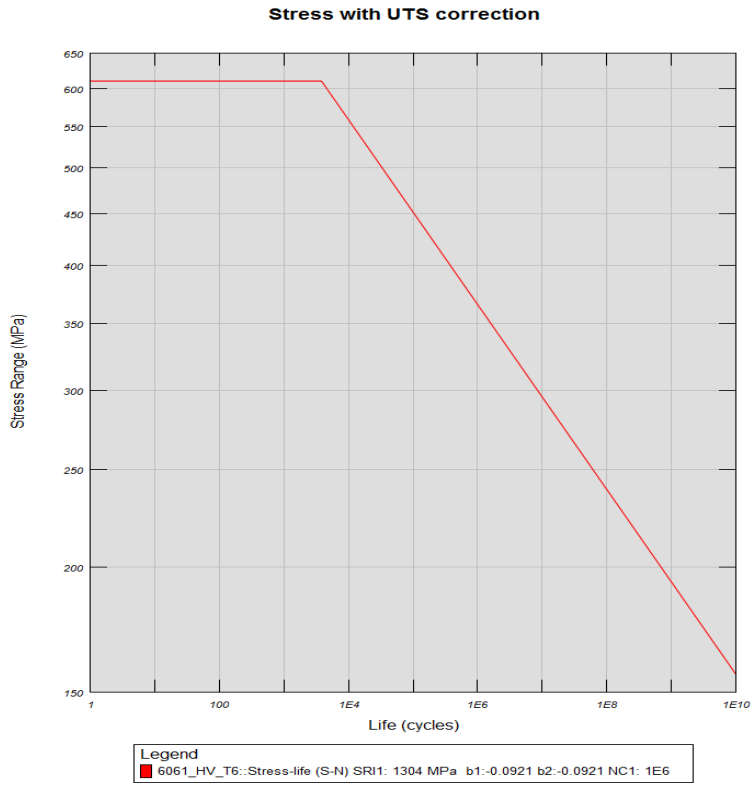

Figure 7-26Aluminum 6061-T6 S-N Curve Steinberg [18]

Appendix E Data Logging Equipment

Figure 7-27 Test Specimen Strain Gage Information

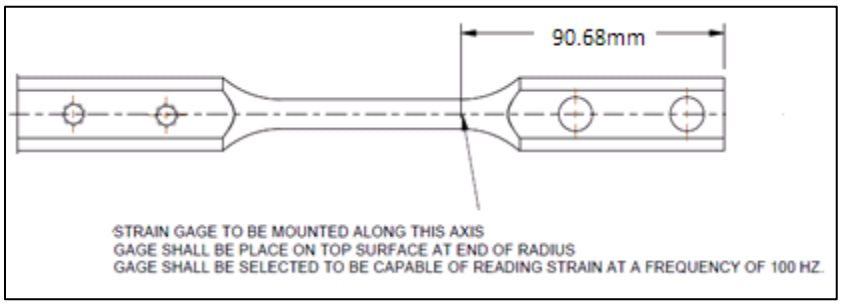

Figure 7-28 Strain Gage Location

Table 7-14 Accelerometer Data Sheet: Modal Test Tip Location

PCB PIEZOTRONICS INC.

Model 352C23

Product Type: Accelerometer, Vibration Sensor

Miniature, lightweight (0.2 gm), ceramic shear ICP® accel., 5 mV/g, 2 to 10k Hz, 10-ft detachable cable

View Spec Sheet (PDF)

View photo and drawing .

PERFORMANCE	ENGLISH	SI	
Sensitivity(± 20 %)	5 mV/g	0.5 mV/(m/s²)	
Measurement Range	± 1000 g pk	± 9810 m/s² pk	
Frequency Range(± 5 %)	2.0 to 10,000 Hz	2.0 to 10,000 Hz	
Frequency Range(± 10 %)	1.5 to 15,000 Hz	1.5 to 15,000 Hz	
Frequency Range(± 3 dB)	0.7 to 25,000 Hz	0.7 to 25,000 Hz	
Resonant Frequency	≥ 70 kHz	≥ 70 kHz	
Broadband Resolution(1 to 10,000 Hz)	0.003 g rms	0.03 m/s² rms	[1]
Non-Linearity	≤ 1 %	≤ 1 %	[2]
Transverse Sensitivity	≤ 5 %	≤ 5 %	
ENVIRONMENTAL			
Overload Limit(Shock)	± 10,000 g pk	± 98,000 m/s² pk	
Temperature Range(Operating)	-65 to +250 °F	-54 to +121 °C	
Temperature Response	See Graph	See Graph	[1]
ELECTRICAL			
Excitation Voltage	18 to 30 VDC	18 to 30 VDC	
Constant Current Excitation	2 to 20 mA	2 to 20 mA	
Output Impedance	≤ 200 ohm	≤ 200 ohm	
Output Bias Voltage	7 to 11 VDC	7 to 11 VDC	
Discharge Time Constant	0.24 to 1.0 sec	0.24 to 1.0 sec	
Settling Time(within 10% of bias)	<3 sec	<3 sec	
Spectral Noise(1 Hz)	1500 µg/√Hz	14,715 (µm/sec^2)/√Hz	[1]
Spectral Noise(10 Hz)	400 µg/√Hz	3924 (µm/sec^2)/√Hz	[1]
Spectral Noise(100 Hz)	120 µg/√Hz	1177 (µm/sec^2)/√Hz	[1]
Spectral Noise(1 kHz)	30 µg/√Hz	294 (µm/sec^2)/√Hz	[1]
Spectral Noise(10 kHz)	20 µg/√Hz	196 (µm/sec^2)/√Hz	[1]
Electrical Isolation(Base)	>10^8 ohm	>10^8 ohm	
PHYSICAL			
Sensing Element	Ceramic	Ceramic	
Sensing Geometry	Shear	Shear	
Housing Material	Anodized Aluminum	Anodized Aluminum	
Sealing	Epoxy	Epoxy	
Size (Height x Length x Width)	.11 in x 0.34 in x 0.16 in	2.8 mm x 8.6 mm x 4.1 mm	
Weight	0.007 oz	0.2 gm	[1]
Electrical Connector	3-56 Coaxial Jack	3-56 Coaxial Jack	
Electrical Connection Position	Side	Side	
Mounting	Adhesive	Adhesive	
SUPPLIED ACCESSORIES:			
Model 030A10 Coax Cable, 10 ft (3 m), 3-56 plug to 10-32 plug. (1)			
Model 039A26 Removal Tool (1)			
Model 080A109 Petro Wax (1)			
Model ACS-1 NIST traceable frequency response (10 Hz to upper 5% point). (1)			

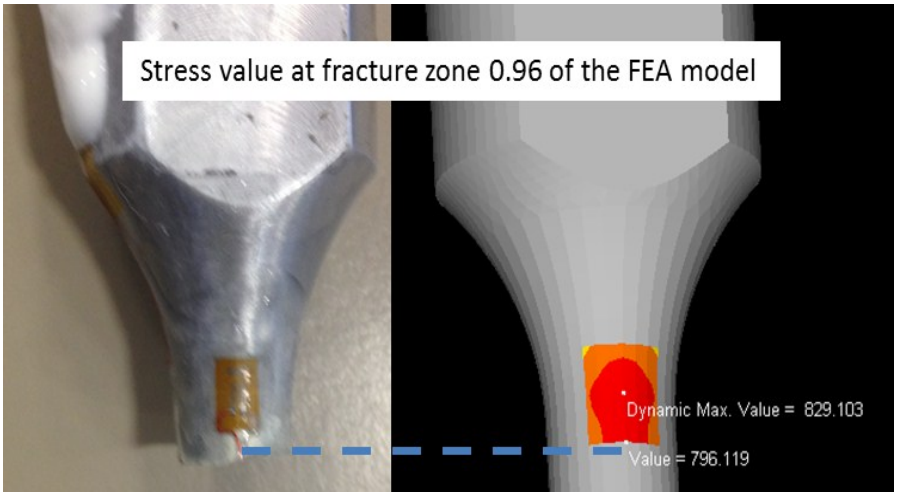

Figure 7-29 Specimen Strain Gage Location vs. Fracture

The fracture locations were offset from the location of the strain gage. The FEA model applied a correction factor of 0.96 to the measured stress to account for the offset as shown in Figure 7-29.

Table 7-15 Specimen Failure Location

Specimen #	Fracture Location
22	15.2
23	19
17	20
38	21.3
14	20.2
20	23
19	20.5
15	20.1
16	20.4
13	20.1
24	22.2
Mean	20.2
Std	1.991892659

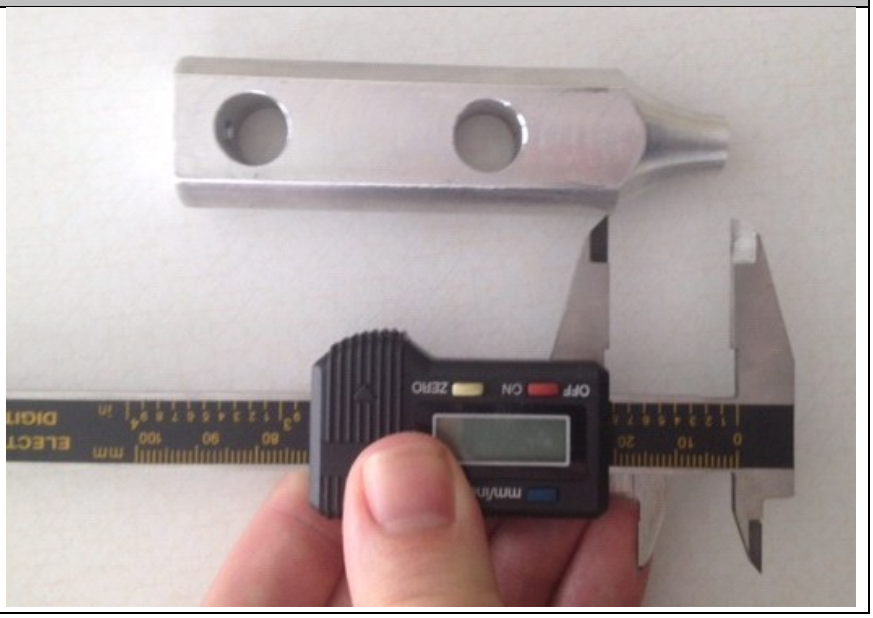

Table 7-16 Accelerometer Data: Shake Table Base Location (3M01)

Variable Capacitance Accelerometer

Model 7292A-XXM1

- 2 to 100 g Full Scale
- Optional Temperature Output (M2) or Simulated Shunt Calibration (M3) also Available
- Overrange Stops
- Gas Damping
- Rugged, Hermetically Sealed

ENDEVCO MODEL 7292A-XXM1

CE

Actual size

DESCRIPTION

The ENDEVCO® Model 7292A-XXM1 MICROTRON® accelerometer utilizes unique variable capacitance microsensors for the measurement of relatively low-level accelerations in rugged aerospace and automotive environments. Since it can respond to DC accelerations (steady-state events), it is ideal for measuring whole-body motion even after being subjected to shock motion. The 7292A-XXM1 series accelerometer is designed to withstand shock levels up to 10,000 g's with immediate recovery.

The 7292A-XXM1 features a rugged hermetic, stainless-steel package provides years of reliable service. The 10-32 mounting stud and 6-pin electrical interface make the 7292A-XM1 series of accelerometers a "plug and play" equivalent to the popular Endevco 2262CA series accelerometer.

The 7292A-XXM1 operates from an 8.5 to 30 vdc source and provides a high level, low impedance output biased at 3.6v. The use of gas damping provides the near-critically damped characteristics found in the 2262 Series of accelerometers without thermally induced changes in frequency response. The output can be fed into either a differential or single-ended amplifier, or standard bridge electronics having 10 Vdc excitation.

ENDEVCO Model 136 Three-Channel System, Model 4430A or the OASIS 2000 Computer-Controlled System are recommended as signal conditioners and power supplies.

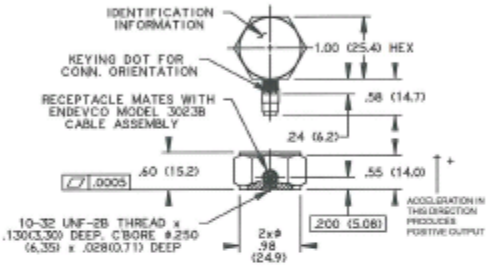

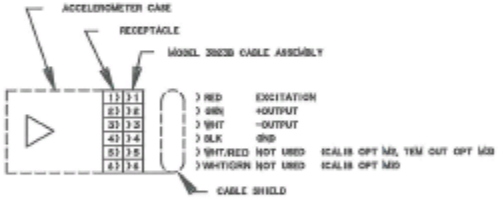

SPECIFICATIONS

PERFORMANCE CHARACTERISTICS: All values are typical at +75°F (+24°C) and 10 Vdc excitation unless otherwise stated. Calibration data, traceable to the National Institute of Standards (NIST), is supplied.

	Units	7292-2M1	-10M1	-30M1	-50M1	-100M1
RANGE	g pk	±2	±10	±30	±50	±100
SENSITIVITY (at 100 Hz) [1] [2]	mV/g	1000 ±100	200 ±20	66 ±8	40 ±4	20 ±2
FREQUENCY RESPONSE (± 5%)	Hz	0 to 15	0 to 500	0 to 800	0 to 1000	0 to 1000
MOUNTED RESONANCE FREQUENCY	Hz	1300	3000	5500	5500	6000
NON-LINEARITY AND HYSTERESIS [3]	% FSO Typ	±0.20	±0.20	±0.20	±0.20	±1
	% FSO (Max)	±0.50	±0.50	±0.50	±0.50	±2
TRANSVERSE SENSITIVITY [4]	% Typ	1	1	1	1	1
ZERO MEASURAND OUTPUT [2]	mV Max	±200	±200	±200	±200	±200
DAMPING RATIO		4.0	0.7	0.7	0.7	0.8
DAMPING RATIO CHANGE	%/°F	+0.04	+0.04	+0.04	+0.04	+0.04
From -65°F to +250°F (-55°C to +121°C)	%/°C	+0.08	+0.08	+0.08	+0.08	+0.08

MEGGITT

ENDEVCO

ENDEVCO MODEL 7292A-XXM1

Variable Capacitance Accelerometer

SPECIFICATIONS

PERFORMANCE CHARACTERISTICS—continued

	Units	7292-2M1	-10M1	-30M1	-50M1	-100M1
THERMAL ZERO SHIFT						
From 32°F to 122°F (0°C to 50°C)	% FSO Max	±2.0	±2.0	±2.0	±2.0	±2.0
From -13°F to +167°F (-25°C to +75°C)	% FSO Max	±4.0	±4.0	±4.0	±4.0	± 4.0
From -65°F to +250°F (-54°C to +121°C)	% FSO Max	±6.0	±6.0	±6.0	±6.0	± 6.0
THERMAL SENSITIVITY SHIFT						
From 32°F to 122°F (0°C to +50°C)	% Max	±2.0	±2.0	±2.0	±2.0	±2.0
From -13°F to +167°F (-25°C to +75°C)	% Max	±4.0	±4.0	±4.0	±4.0	±4.0
From -65°F to +250°F (-54°C to +121°C)	% Max	±8.0	±8.0	±8.0	±8.0	± 8.0
THERMAL TRANSIENT ERROR	Equiv. g/°F	< 0.0006	< 0.0006	< 0.0006	< 0.0006	<0.0006
PER ISA RP 37.2	Equiv. g/°C	< 0.001	< 0.001	< 0.001	< 0.001	<0.001
OVERRANGE (Determined by Electrical clipping or Mechanical stops, whichever is smaller.)						
Electrical clipping	g	-3.5/+3.8	-18/+18	-53/+57	-87/+95	-175/+190
Mechanical stops, typical	g	±4	±30	±90	±200	±200
Recovery Time	µs	< 10	< 10	< 10	< 10	< 10
THRESHOLD (RESOLUTION) [5]	Equiv. g's	0.0005	0.0025	0.0075	0.025	0.013
BASE STRAIN SENSITIVITY, MAX [6]	Equiv. g's	0.01	0.01	0.01	0.01	0.01
MAGNETIC SUSCEPTIBILITY [7]	Equiv. g's	< 0.1	< 0.1	< 0.1	< 0.1	<0.1
WARM-UP TIME (to within 1%)	ms	10	10	10	10	10

ELECTRICAL

EXCITATION [2]	8.5 ± 30.0 Vdc, Calibration
CURRENT DRAIN [8]	4.5 mA Typ, 8 mA (max)
OUTPUT IMPEDANCE/LOAD	50Ω max/10kΩ resistance minimum, 0.1µF capacitance max
RESIDUAL NOISE	100 µV rms typ, 0.5 to 100 Hz, 500µV rms typ, 0.5 Hz to 10 kHz
CASE ISOLATION	100 MΩ

PHYSICAL

CASE MATERIAL	Stainless, type 304
ELECTRICAL, CONNECTIONS	6-pin, 12-45 unsi threaded receptacle (mates to Endevco model 3023B-30 supplied)
MOUNTING/TORQUE	Provision for 10-32 UNF x 1/8" stud. Mounting torque 18 lbf-in (2nm)
MASS	40 grams (cable weighs 18 grams/meter)

ENVIRONMENTAL

ACCELERATION LIMITS (in any direction)	
Static	20 000 g
Sinusoidal/Random Vibration	100 g pk, 20 - 2000 Hz/40 g rms, 20 - 2000 Hz
Shock (half-sine pulse)	5000 g, 150 µsec or longer for the -2 and -10; 10 000 g, 80 µsec or longer for the -30 and -100
Zero Shift	0.1% FSO typical at 5000 g
TEMPERATURE	
Operating	-65°F to +250°F (-55°C to +121°C)
Storage	-100°F to +300°F (-73°C to +150°C)
HUMIDITY/ALTITUDE	Unaffected. Unit is hermetically sealed.
ESD SENSITIVITY	Unit meets Class 2 requirements of MIL-STD-883, Method 3015

CALIBRATION DATA SUPPLIED (noted on shipping box)

SENSITIVITY (at 1g and 5 Hz for 2 g range; 10g and 100 Hz, all other ranges)	
FREQUENCY RESPONSE	1-100 Hz for the -2; all other ranges, 20 - 10,000 Hz
ZERO MEASURAND OUTPUT	mV
MAXIMUM TRANSVERSE SENSITIVITY	% of sensitivity

ACCESSORIES (included)

3023B-30	30" CABLE ASSEMBLY
92981-12	10-32 MOUNTING STUD, HEX SOCKET

OPTIONAL ACCESSORIES

2981-3	10-32 ADAPTOR STUD, SLOT
2981-4	M5 X 0.8 ADAPTOR STUD

NOTES

1. Reference frequency is 5 Hz on the 2 g range, 100 Hz for -10,-30,-100
2. Over the excitation range 10 ± 0.05 Vdc
3. Full scale output (FSO) is nominally 4 volts
4. 1% is typical. 1% maximum available on special order
5. THRESHOLD = $\frac{\text{MAX. RESIDUAL NOISE: 0.5 TO 100 Hz}}{\text{SENSITIVITY}}$
6. Per ISA 37.2 at 250 Microstrain
7. At 100 Gauss, 60 Hz
8. Current drain increases slightly with increasing excitation; typical change is +.05 mA per volt from 8.5 to 30.0 Vdc.
9. Maintain high levels of precision and accuracy using Endevco's factory calibration services. Call Endevco's inside sales force at 800-982-6732 for recommended intervals, pricing and turn-around time for these services as well as for quotations on our standard products.

ENDEVCO CORPORATION, 30700 RANCHO VIEJO ROAD, SAN JUAN CAPISTRANO, CA 92675 USA (800) 982-6732 (949) 493-8181 fax (949) 661-7231
www.endevco.com Email:applications@endevco.com

1002 REV B

Appendix F Shake Table Testing

Shake Table Specifications for Pegasus Machine
Pegasus model 244.21str is a hydraulic ram operated vibration table.

Table 7-17 Pegasus Shake Table Specifications [30]

Components Used in Simulation		
Actuator	Model:	244.21str
	Nominal Rating:	11 kip
	Stroke:	6 in
	Orientation:	VERTICAL
Servovalve	Model:	256.05A01
	Nominal Rating:	50 gpm
	Quantity:	1
Pump	Model:	505.90
	Frequency:	60 Hz
	Nominal Rating:	90 gpm
	Line:	
	Acc Size:	2 gal
	Precharge:	1500 psi
	Hose Length:	120 in
	Hose ID:	1.5 in
	CC:	
	Acc Size:	0.01 gal
	Precharge:	1000.03 psi
	Hose Length:	3 in
	Hose ID:	1.5 in
Frame	Model:	312.21
	Nominal Rating:	22 kip
Load Cell	Model:	661.20-02
	Nominal Rating:	11 kip
Grip	Model:	647.10
	Nominal Rating:	22 kip

The pegassus machine has an alumimum mounting fixture attached to the hydraulic ram. With the added system mass, the hydraulic ram should perform to the 2kip performance curve. The total added mass with all table base construction and vibration fixture and test pieces should be less than 2000 lbs.

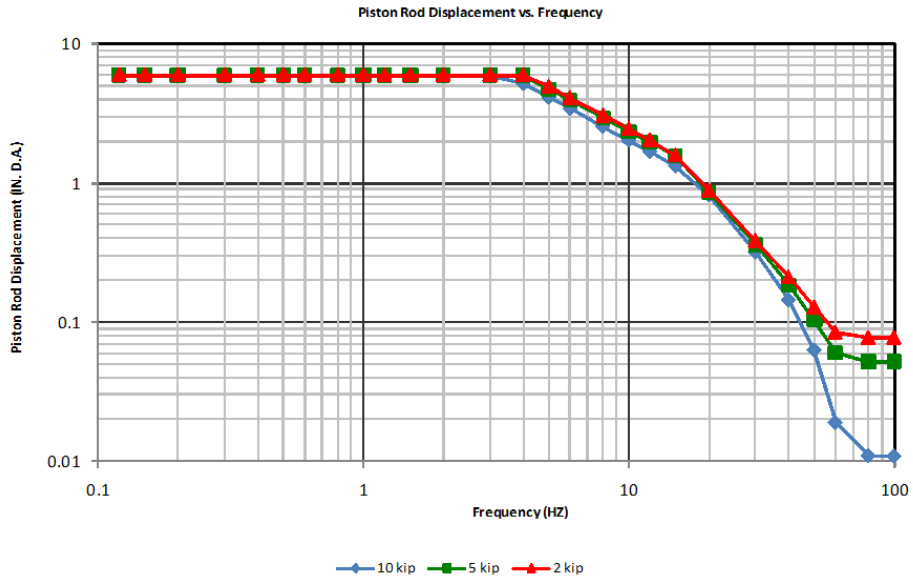

Figure 7-30 Pegasus Shake Table Capability

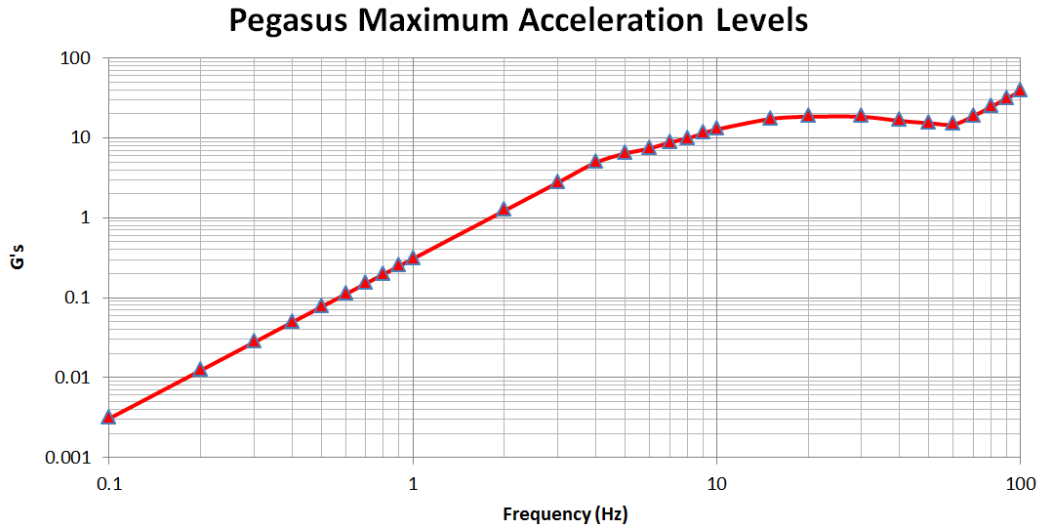

Figure 7-31 Pegasus Maximum Acceleration Profile

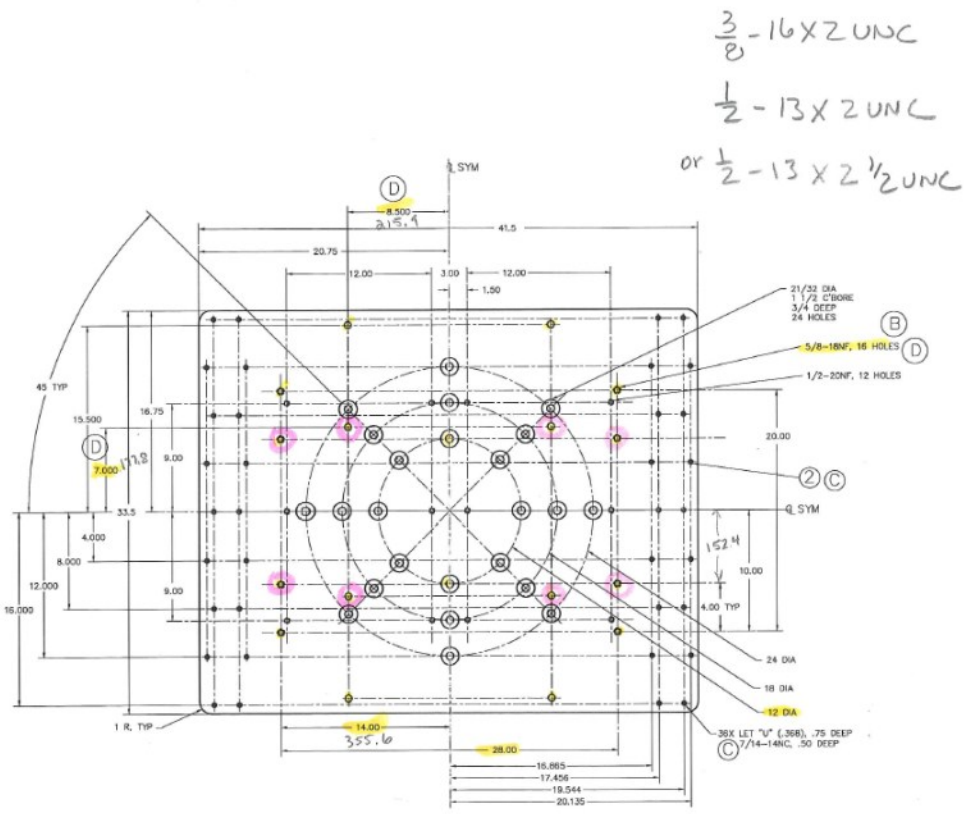

Figure 7-32 Shake Table Mounting Drawing

Figure 7-33 Shake Table Apparatus

Shake Table Calibration

Developing a displacement load file was accomplished first developing the tables FRF with a test specimen mounted to the test fixture (Figure 7-34). The basic principle of [FRF x Excitation = Response] was used to generate the required displacement profile. The table mounted accelerometer is used to tune in the displacements to provide the desired g loads at each time sample. This iterative process is run approximately 8-9 times until the g response matched the desired load profile (Figure 7-35). During the initial testing it was determined the system must stay in open loop to accommodate for system changes. Many variables in the system are noted to affect the response file. Such things as the oil pressure, temperature, specimen changes, other shake rigs transmitting vibration through the floor were possible system changes required a continuously adjusting system.

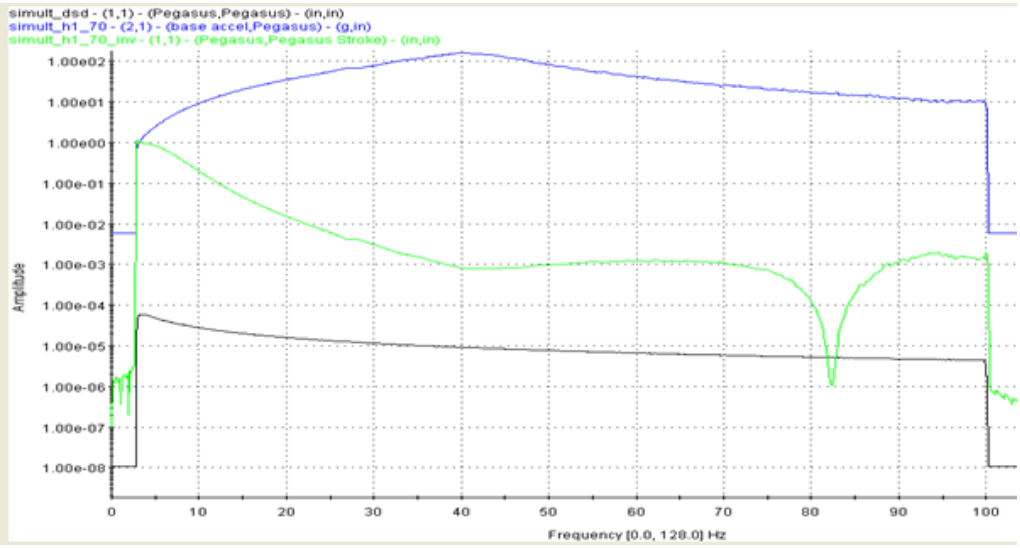

Figure 7-34 Shake Table Tuning: FRF

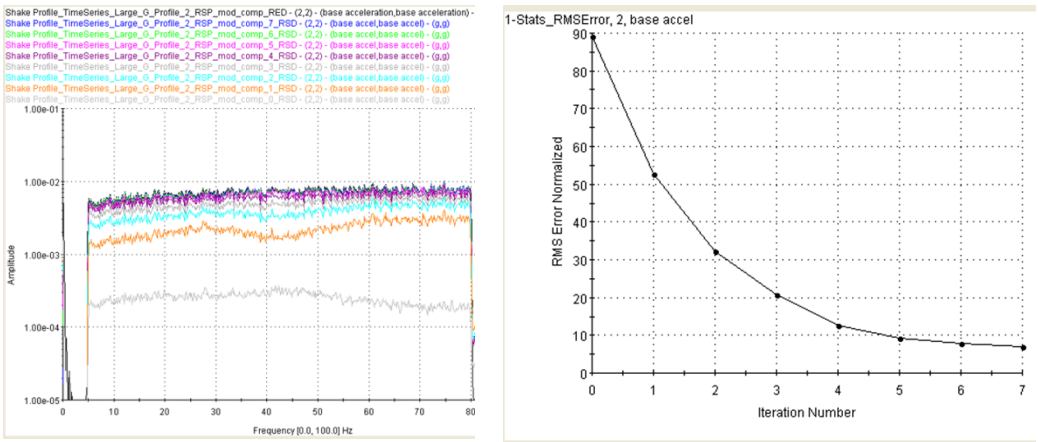

Figure 7-35 Shake Table Tuning: Iterative Runs

Effects of testing more than one specimen at a time on the shake table

Initial testing was attempted with six of the 190g specimen configuration. During this testing it was determined that the specimen vibration affected each other. When viewing the specimens' vibration it was noted that the resonance of each specimen was different. The apparent mass of the resonant specimens caused the shake table to have large residuals in the RMS block repeats. This first test run also did not apply the iterative open loop adjustment for acceleration of the shake table as shown by the block cycle comparison in Figure 7-37. The test setup in Figure 7-36 shows the full potential of twelve specimens at once.

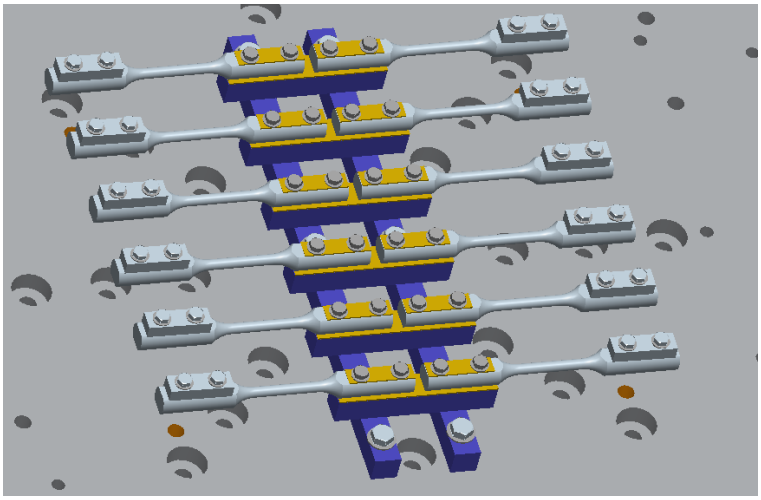

Figure 7-36 Shake Table Mounting Fixture with 12 Specimens Mounted

Table 7-18 Fatigue Life Results for Testing Six Specimens at Once				
Specimen Number	RMS µstrain (strain gage)	RMS Stress (hooks law)	Mean Peak Stress	PSD →Time Series Cycles Until Failure (600 sec/cycle)
28	904.4	62.35	88.19	18.7
29	904.4	62.35	88.19	26.2
30	904.4	62.35	88.19	26.1
31	904.4	62.35	88.19	19.3
32	904.4	62.35	88.19	40.6
38	904.4	62.35	88.19	33.7

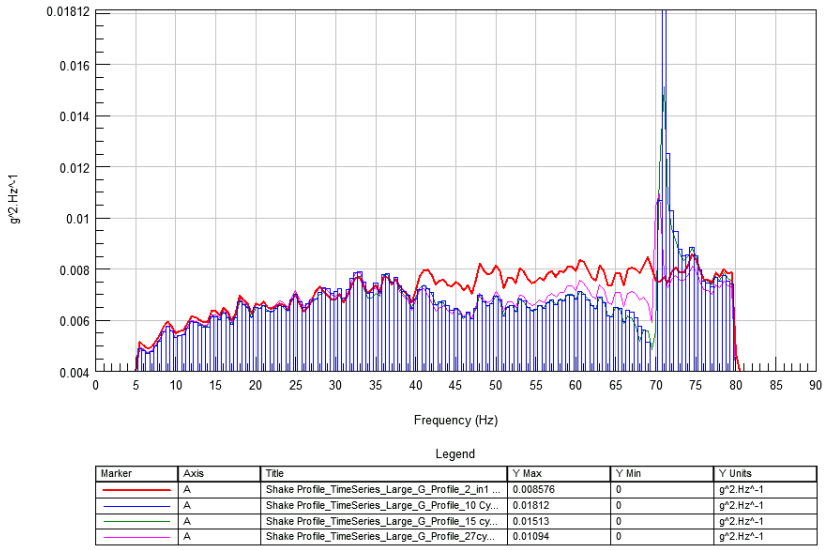

Figure 7-37 Effects of Multiple Samples and non-Iterative Shake Profile

Figure 7-38 Specimen Acceleration PSD's and Stress Histograms display each of the recorded values. The PSD and Histograms are developed from the concatenation of all block cycles. The RMS acceleration values are listed for each of the specimens.

Specimen 1	*RMS acceleration: 0.7441g*
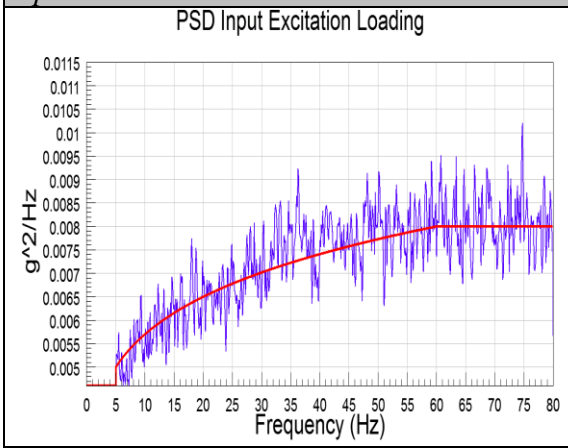	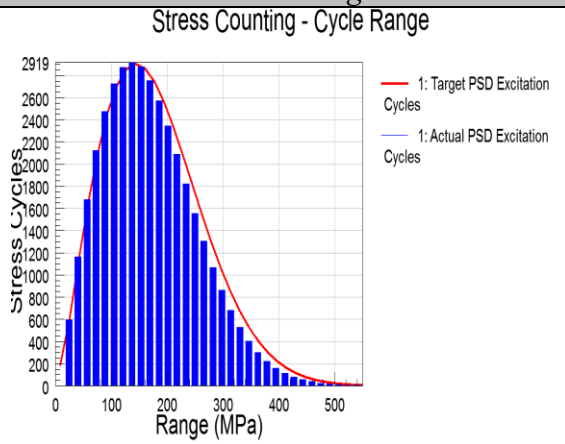
Specimen 2	*RMS acceleration: 0.7363g*
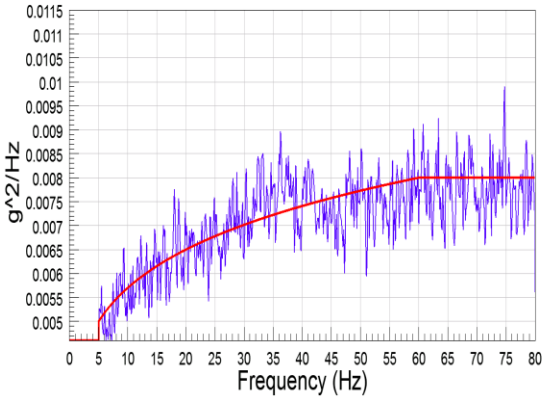	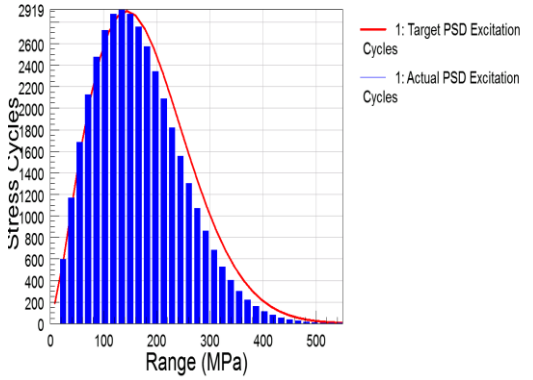
Specimen 3	*RMS acceleration: 0.7545g*
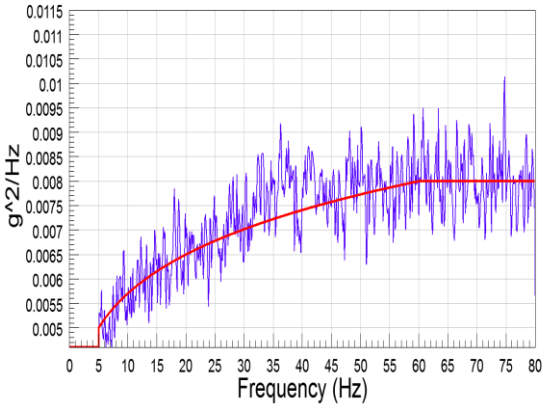	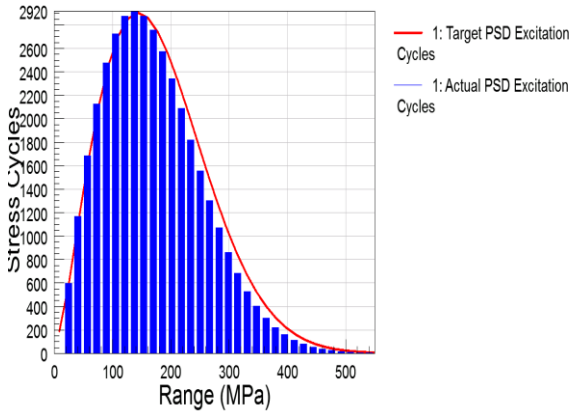

Specimen 4	*RMS acceleration: 0.7505 g*
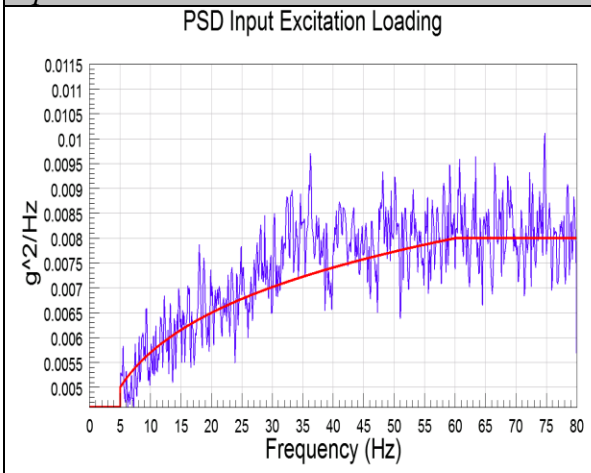	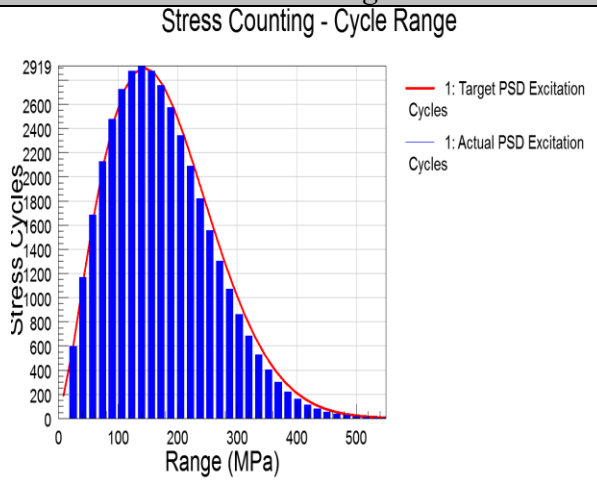
Specimen 5	*RMS acceleration: 0.7509g*
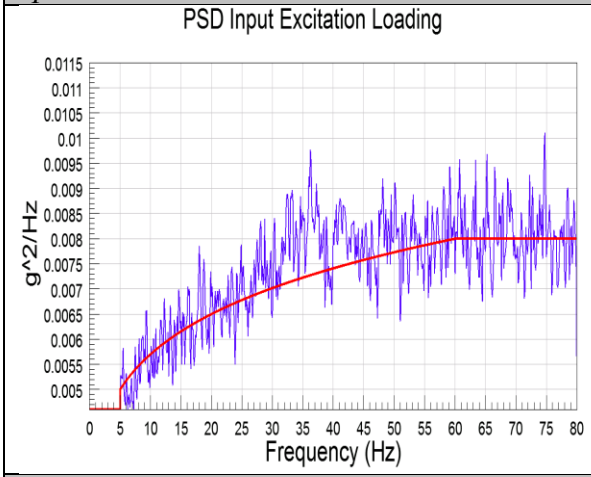	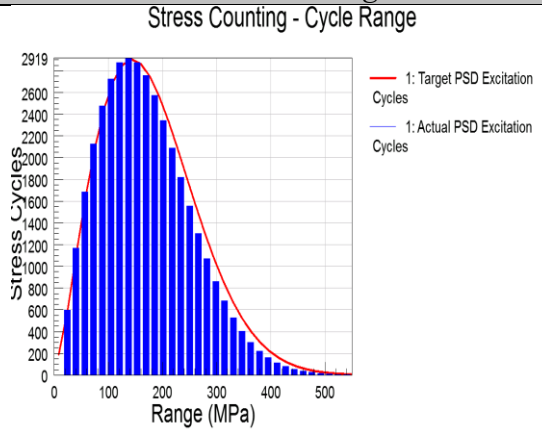
Specimen 6	*RMS acceleration: 0.7522 g*
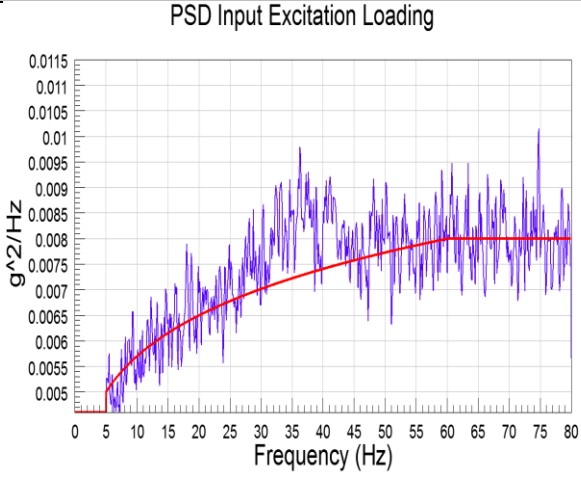	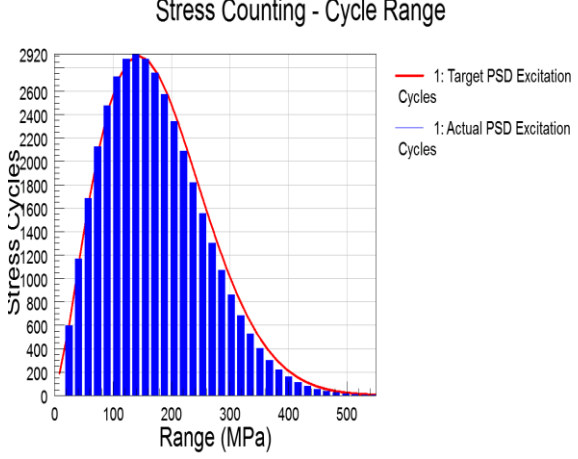

Specimen 7 – 235g	*RMS acceleration: 0.7366 g*
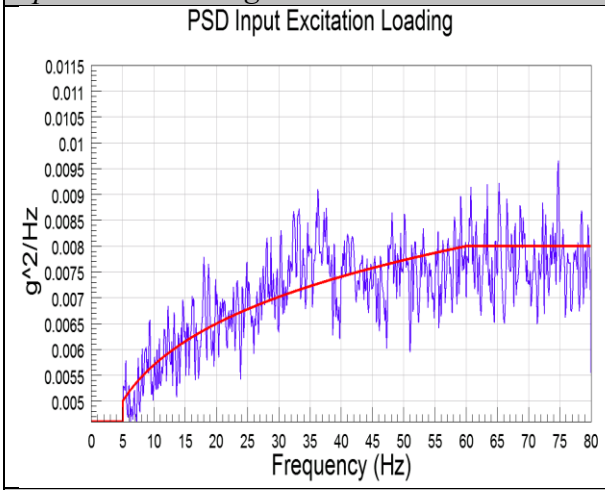	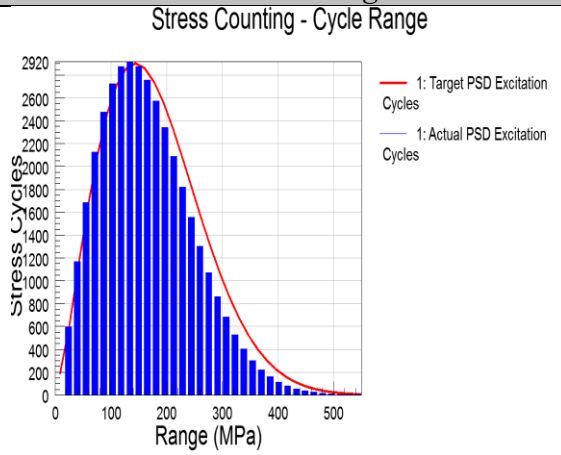
Specimen 8 -235g	*RMS acceleration: 0.7259 g*
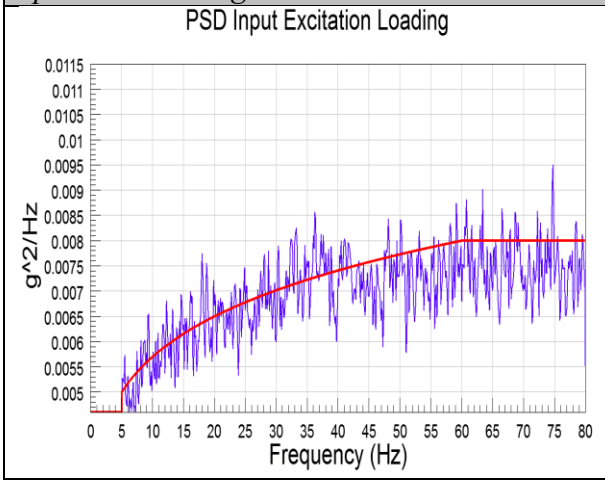	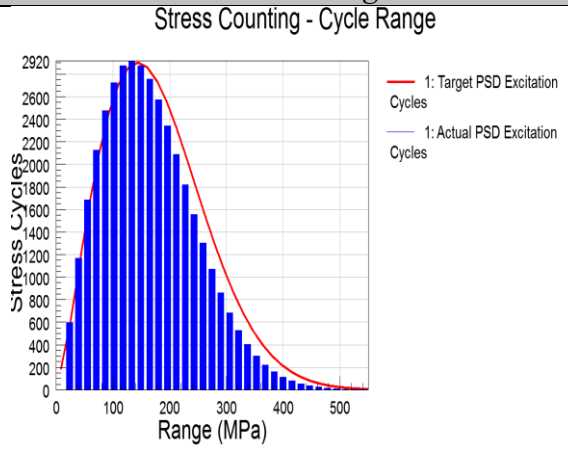
Specimen 9 – 235g	*RMS acceleration: 0.7384g*
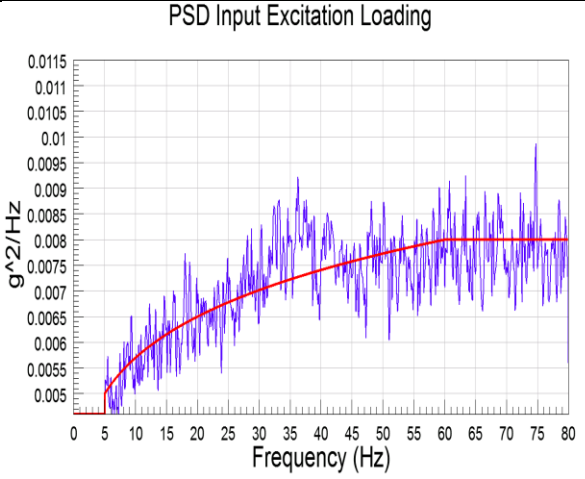	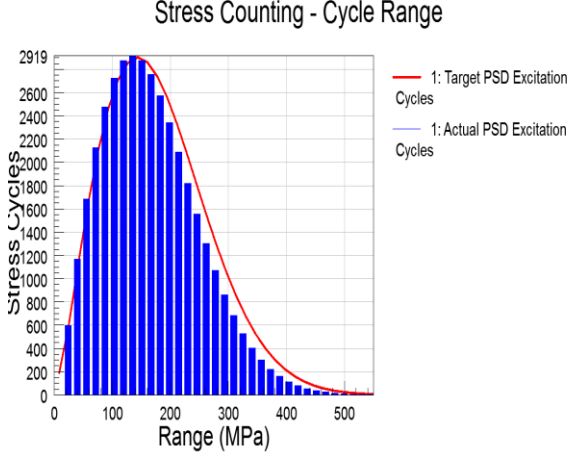

Specimen 10 – 235g	*RMS acceleration: 0.7434g*
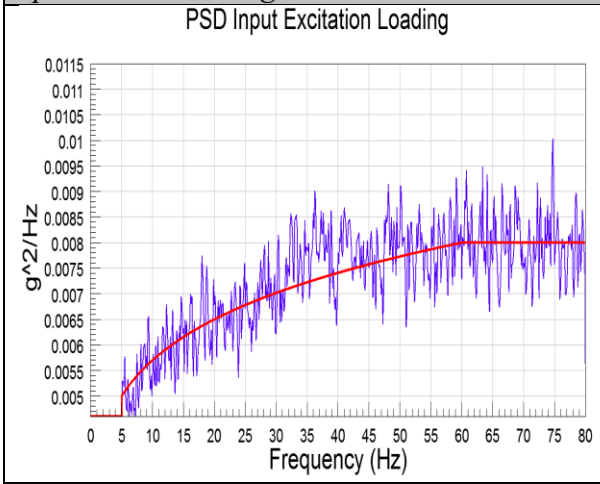	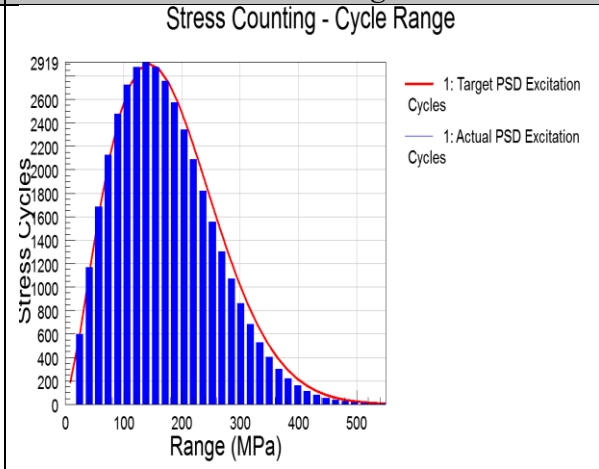
Specimen 11 – 235g	*RMS acceleration: 0.7491g*
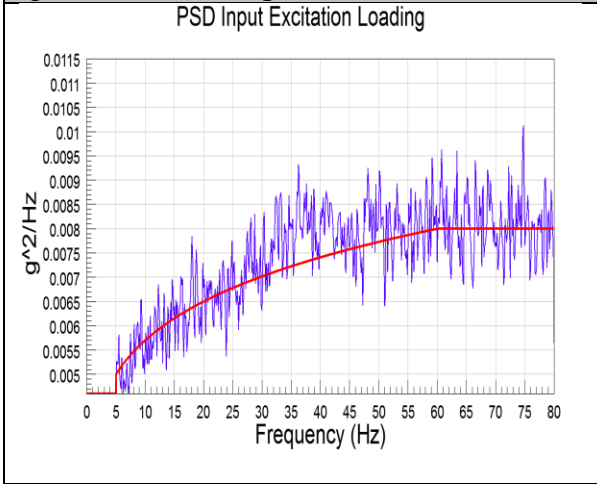	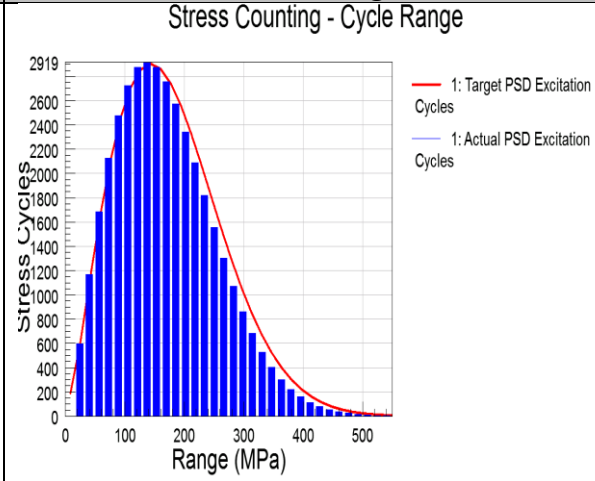
Specimen 12 – 235g	*RMS acceleration: 0.7395g*
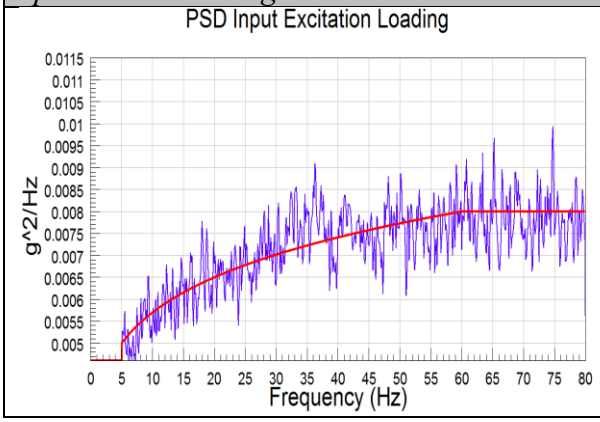	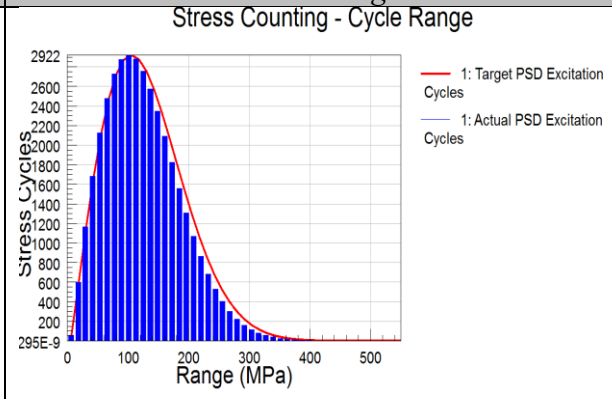

Specimen 13 -291g	*RMS acceleration: 0.7428g*
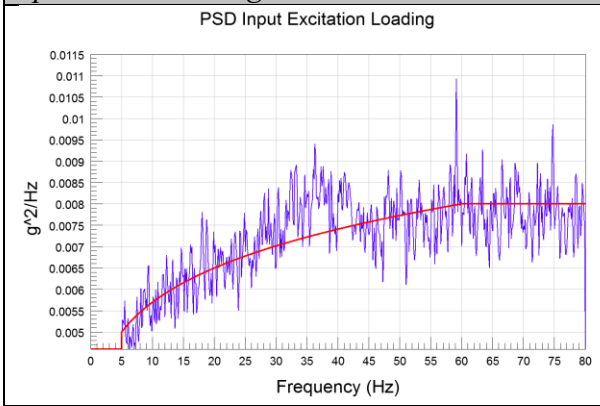	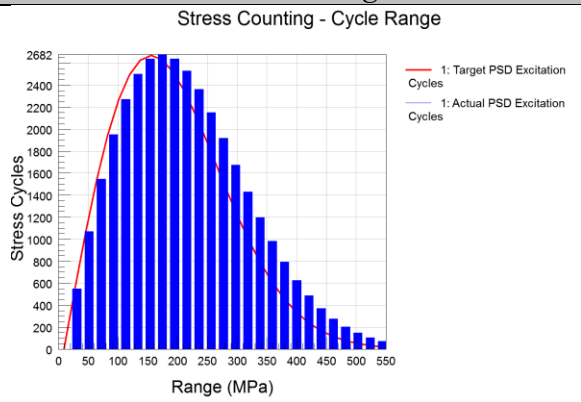
Specimen 14 – 291g	*RMS acceleration: 0.7457g*
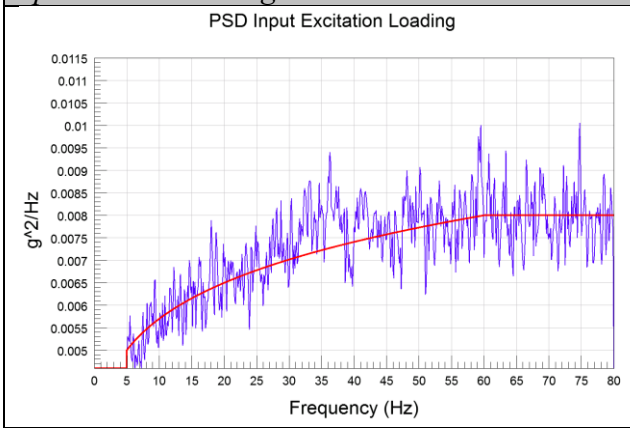	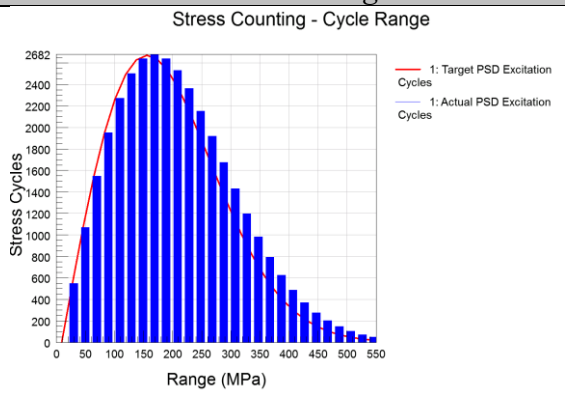
Specimen 15 -291g	*RMS acceleration: 0.744g*
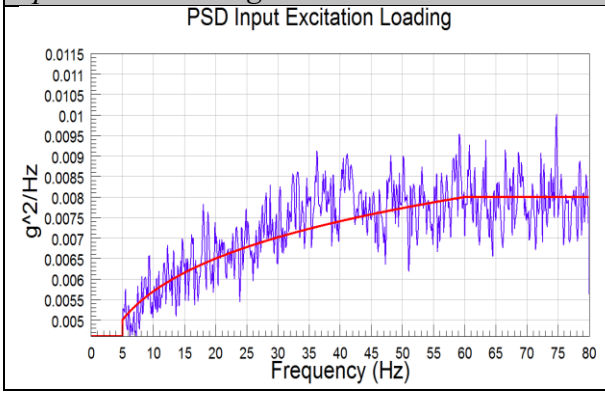	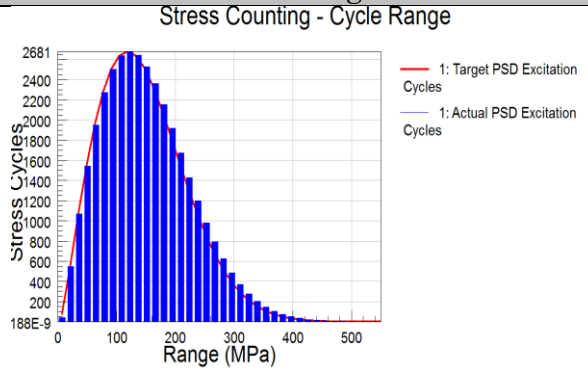

Specimen 16 -291g	*RMS acceleration: 0.7429g*
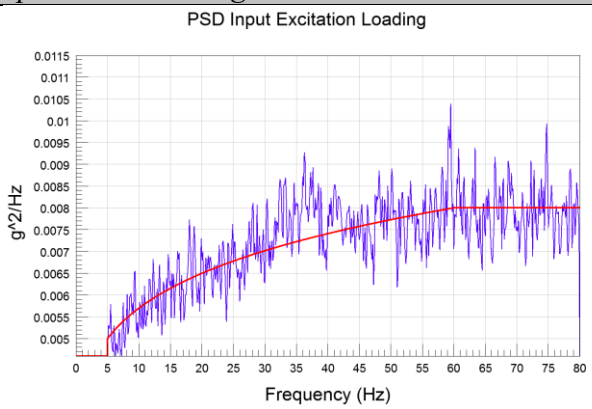	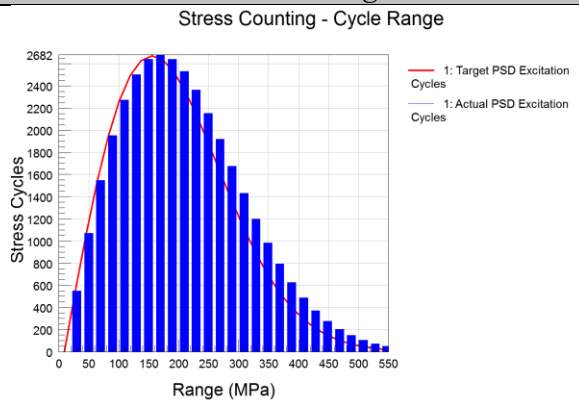
Specimen 17 -291g	*RMS acceleration: 0.7465g*
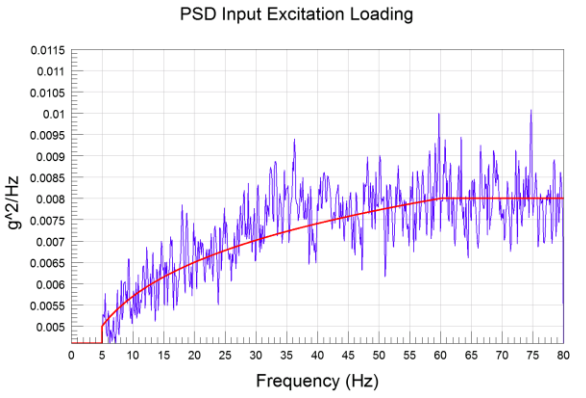	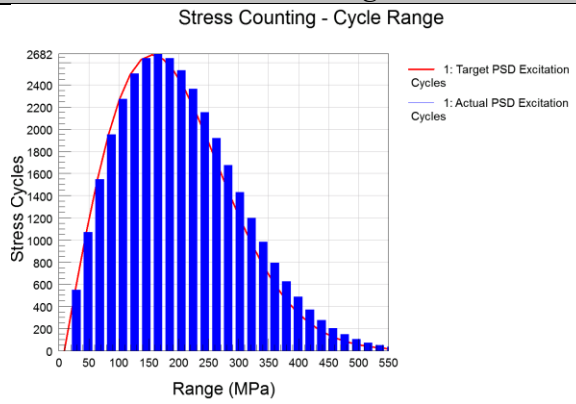
Specimen 18 -291g	*RMS acceleration: 0.7376g*
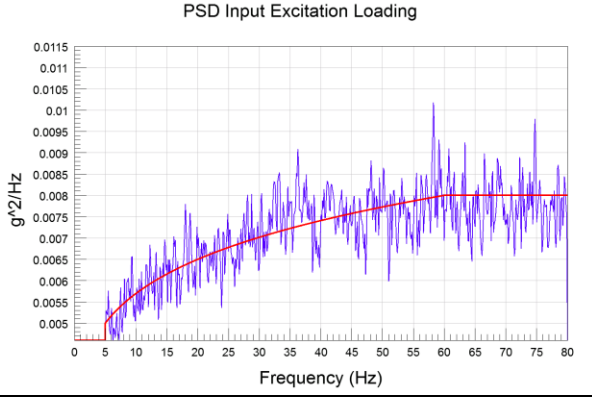	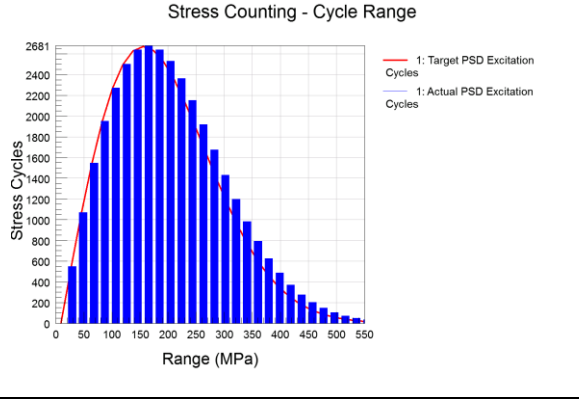

Specimen 19 -291g	*RMS acceleration: 0.7414 g*
PSD Input Excitation Loading	Stress Counting - Cycle Range
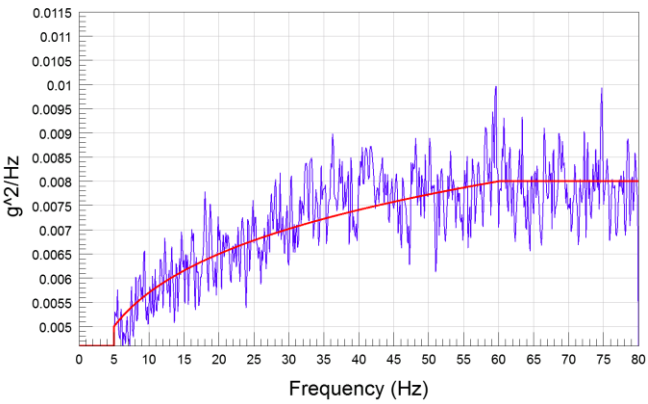	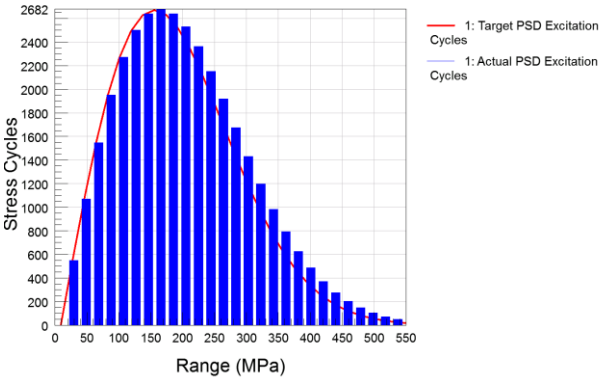
Specimen 20 -291g	*RMS acceleration: 0.7437g*
PSD Input Excitation Loading	Stress Counting - Cycle Range
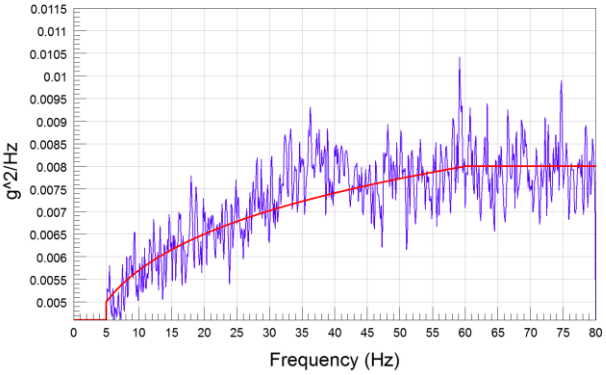	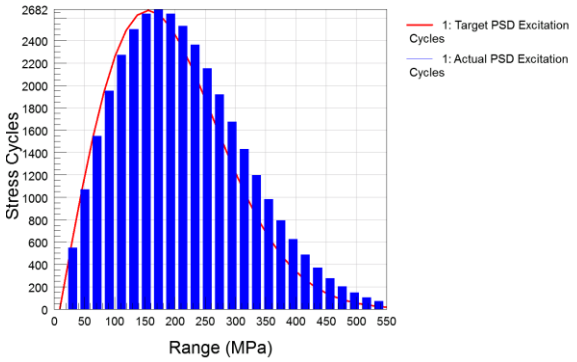
Specimen 21 – 291g	*RMS acceleration: 0.7453 g*
PSD Input Excitation Loading	Stress Counting - Cycle Range
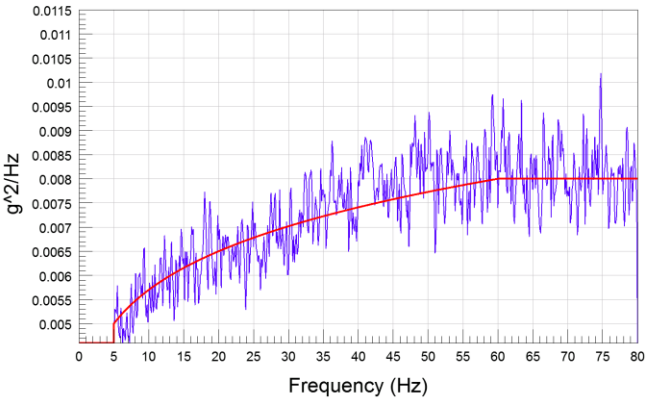	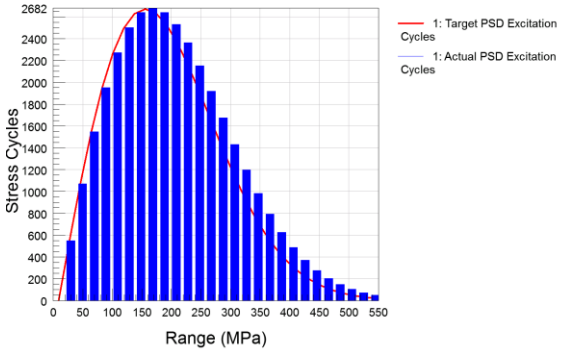

Specimen 22 -291g	*RMS acceleration: 0.7466 g*
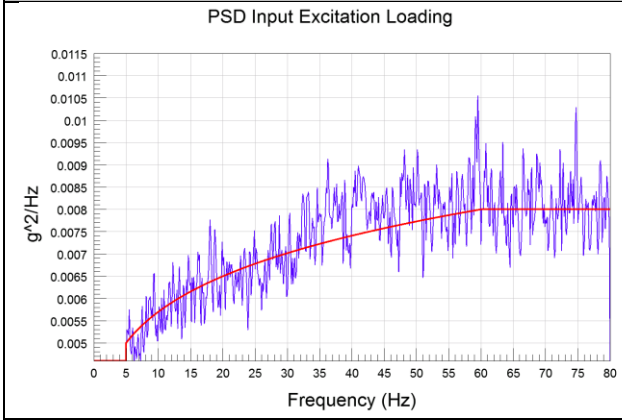	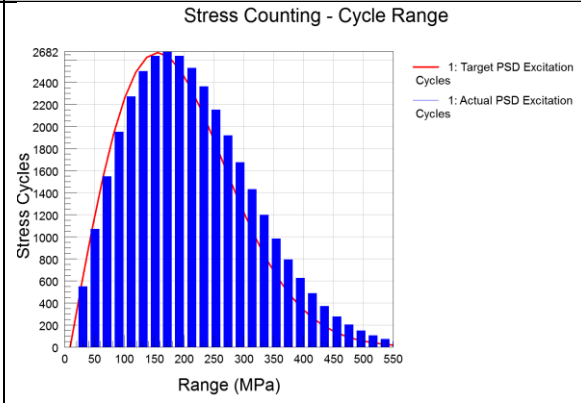
Specimen 23 -291g	*RMS acceleration: 0.7455 g*
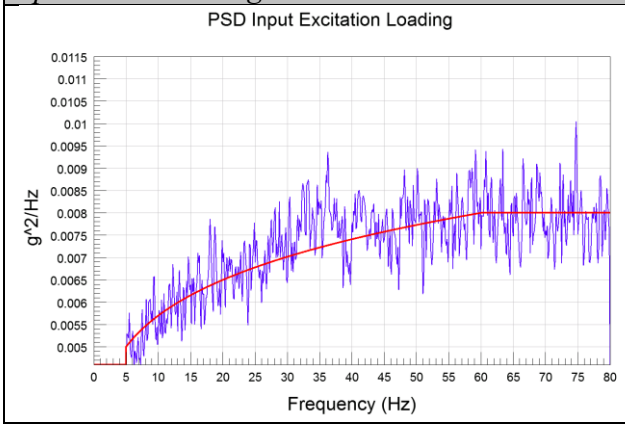	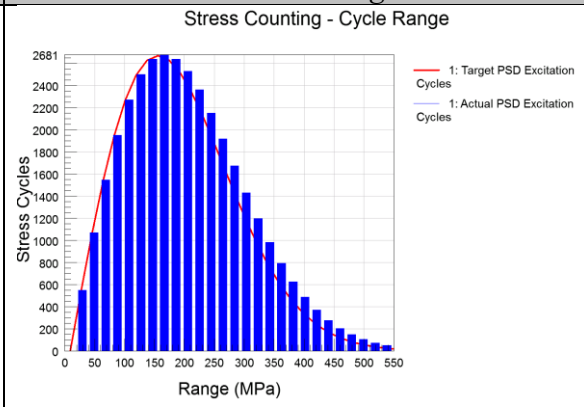
Specimen 24 -291g	*RMS acceleration: 0.7348g*
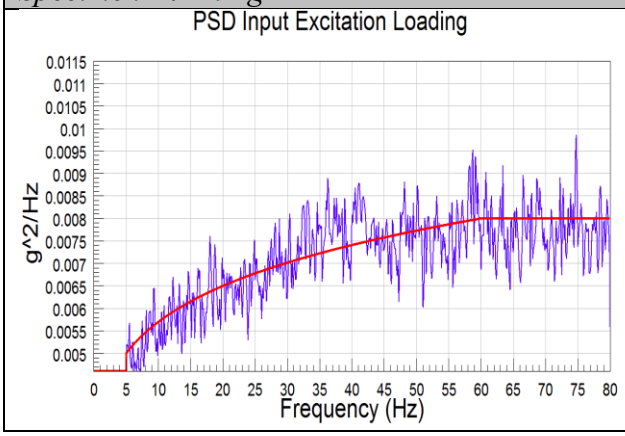	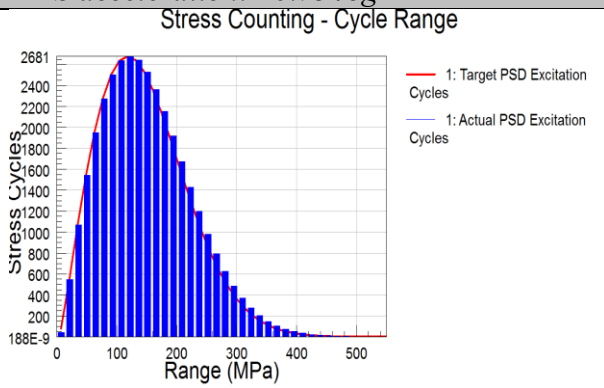

Specimen 25 -190g	*RMS acceleration: 0.712g*
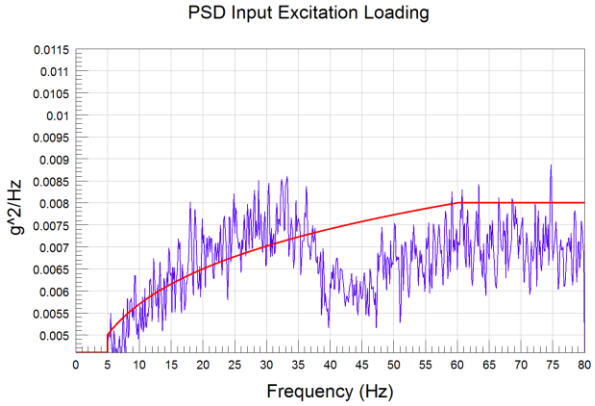	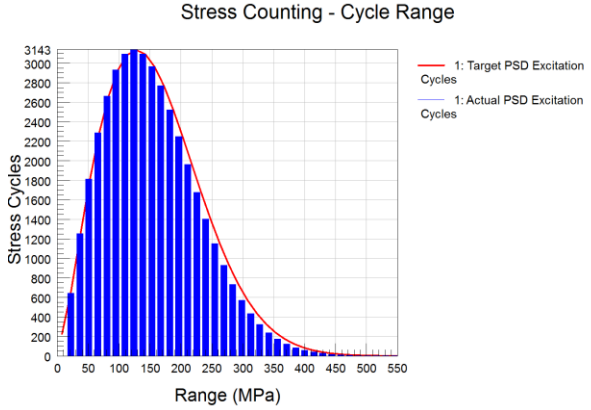
Specimen 26 -190g	*RMS acceleration: 0.7457 g*
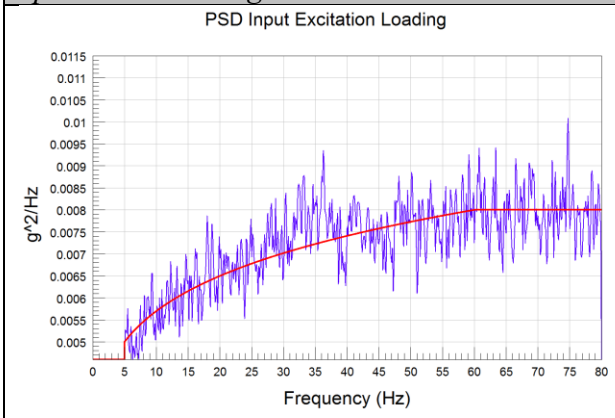	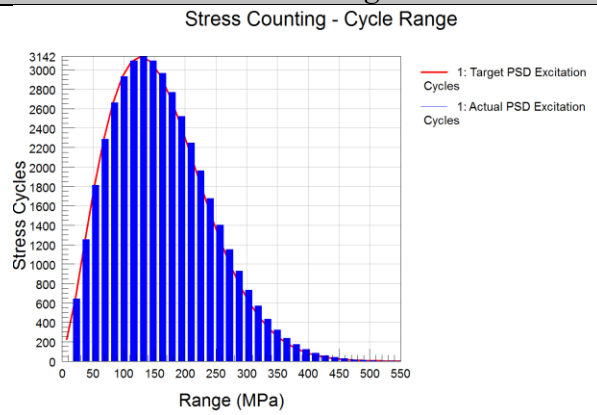
Specimen 27 -190g	*RMS acceleration: 0.74g*
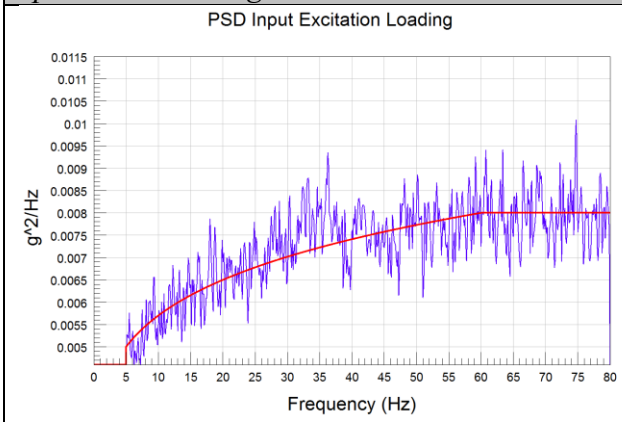	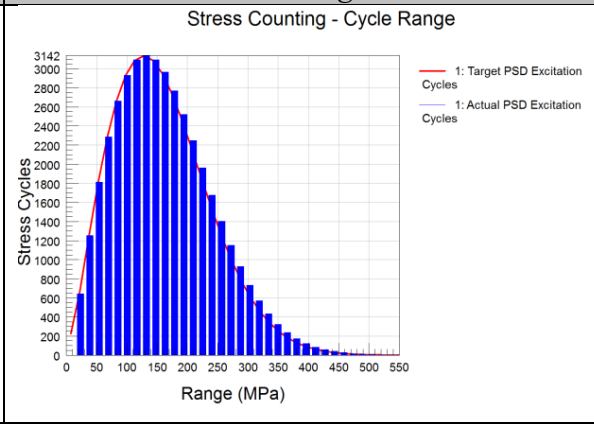

Specimen 33 -190g	*RMS acceleration: 0.7652 g*
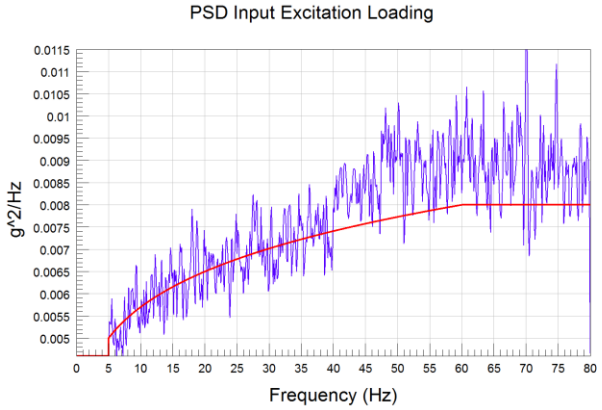	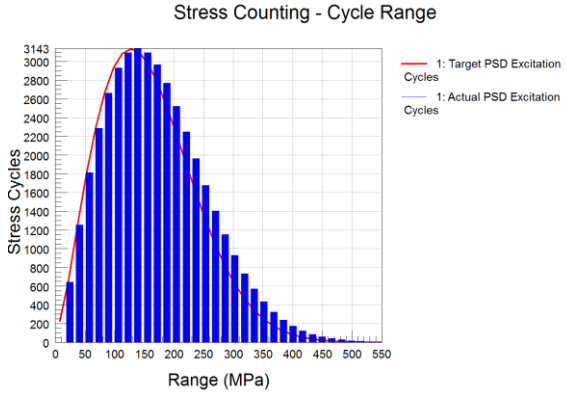
Specimen 34 -190g	*RMS acceleration: 0.7175g*
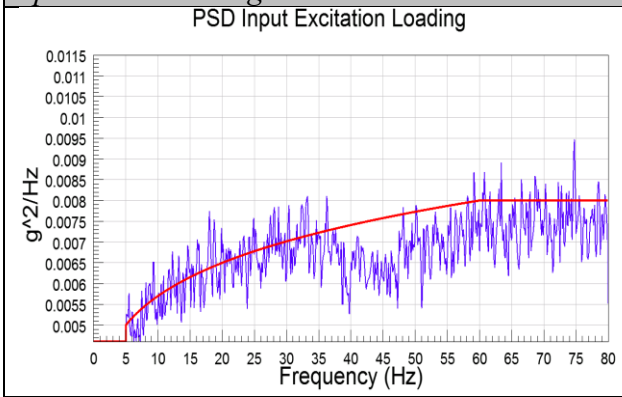	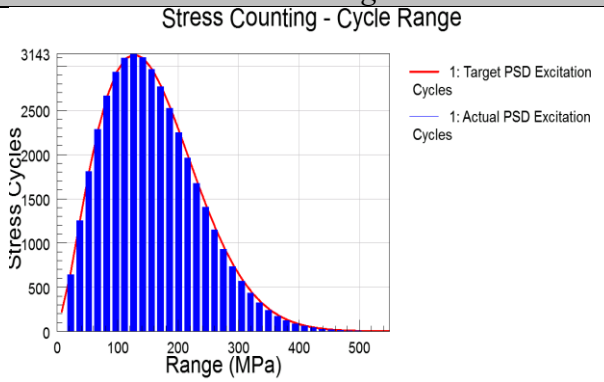
Specimen 35 -190g	*RMS acceleration: 0.7214g*
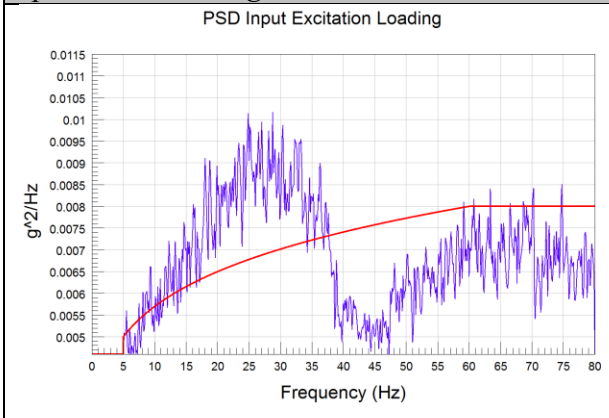	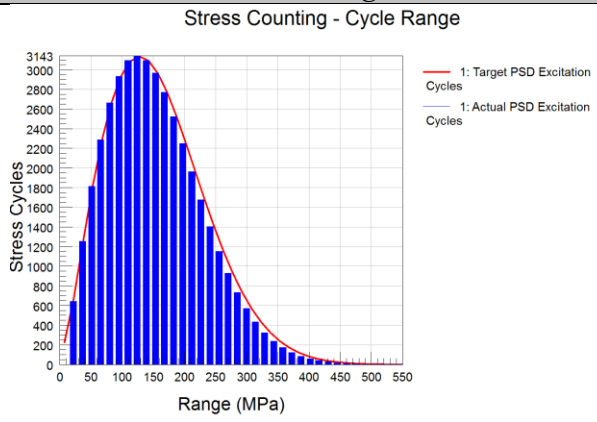

Specimen 36 -190g	*RMS acceleration: 0.7223g*
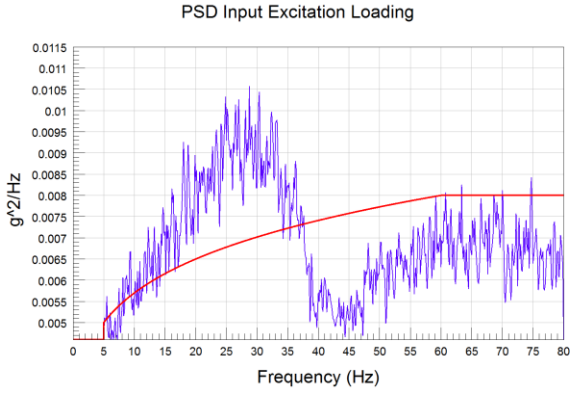	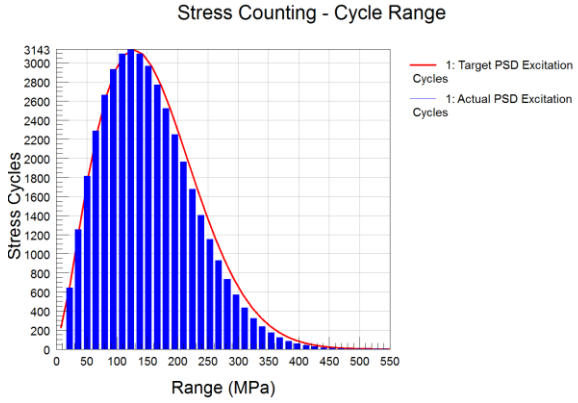

Figure 7-38 Specimen Acceleration PSD's and Stress Histograms

Shake Table specimen Trip System

The isolated pad under the specimen was used to make a system circuit. When the specimen fractured and bent down to the pad the circuit was completed and the monitoring system forced the hydraulics to shut the system down.

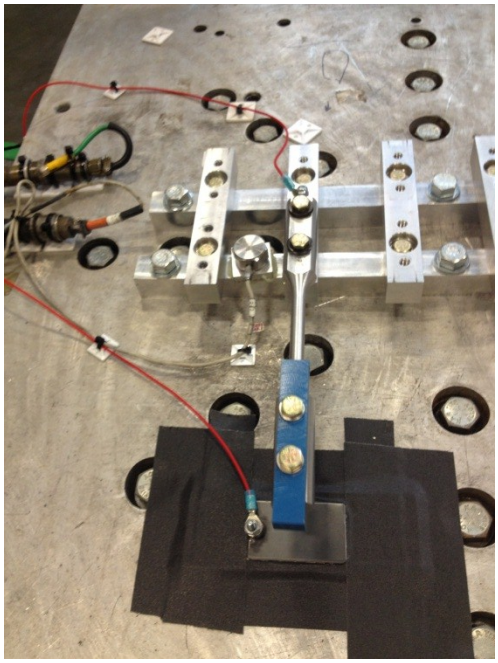

Figure 7-39 Specimen Failure Sensor Apparatus

Appendix G Experimental Results

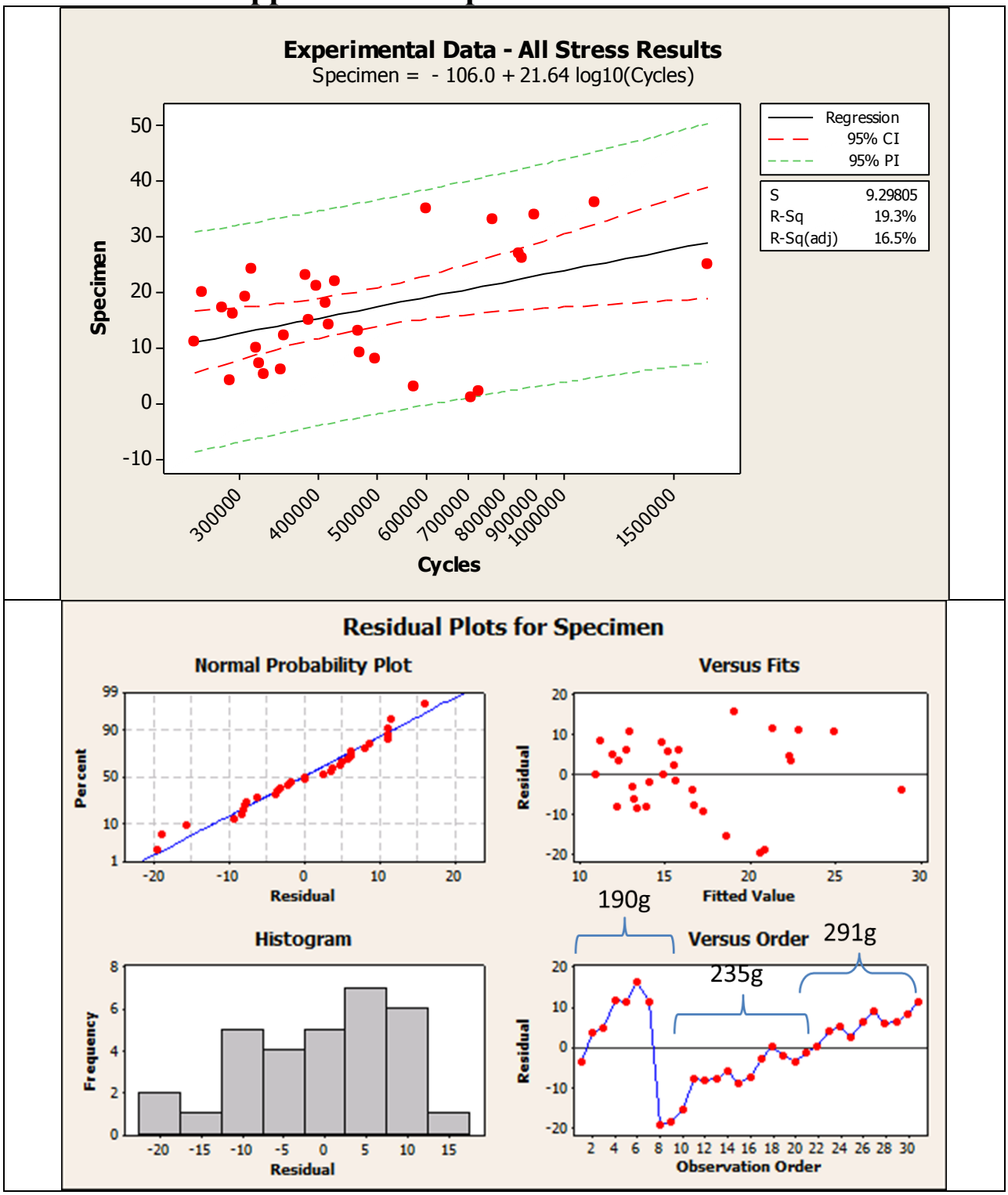

Figure 7-40 Experimental Failure Curve Fit (no stress filtering)

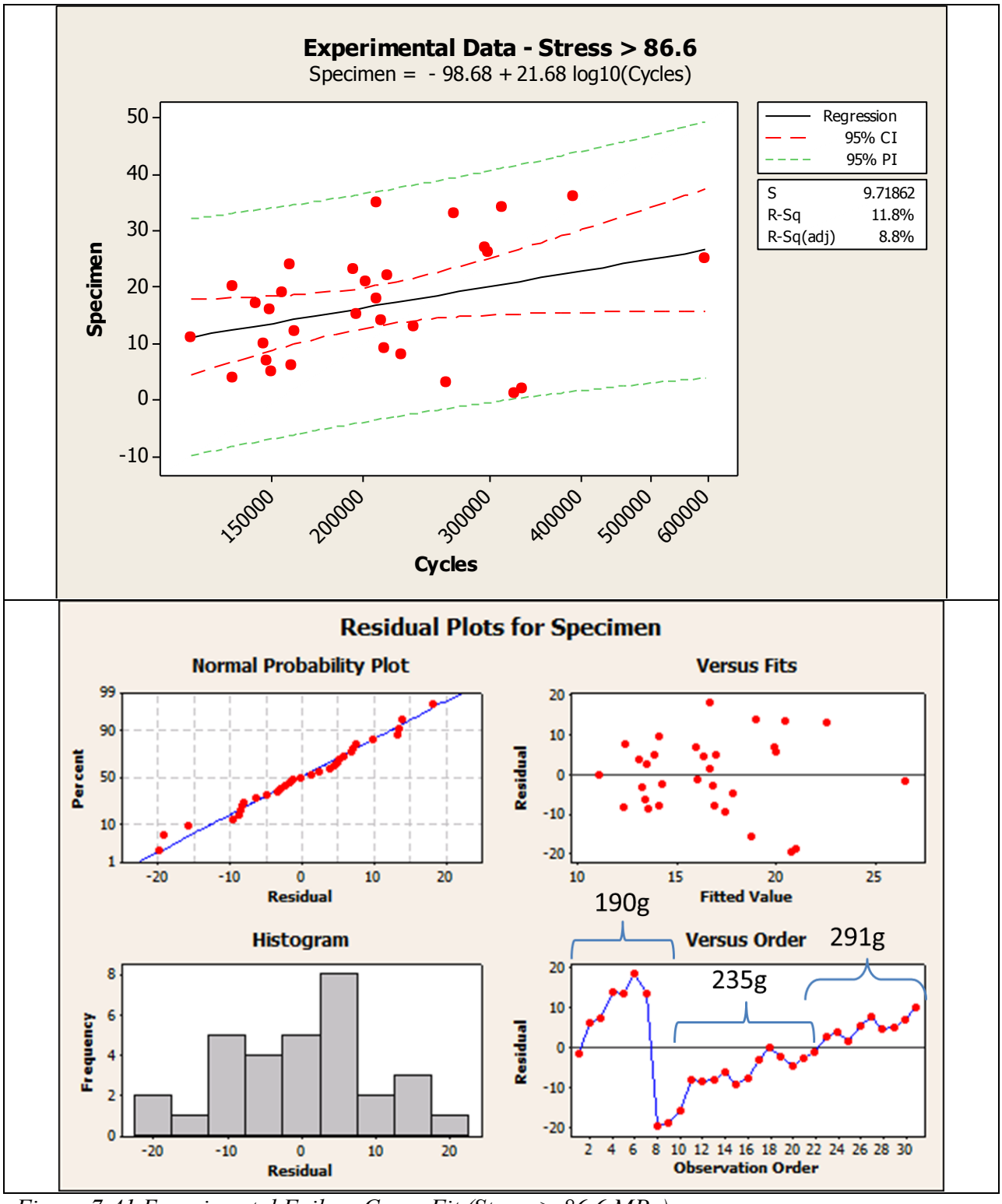

Figure 7-41 Experimental Failure Curve Fit (Stress > 86.6 MPa)

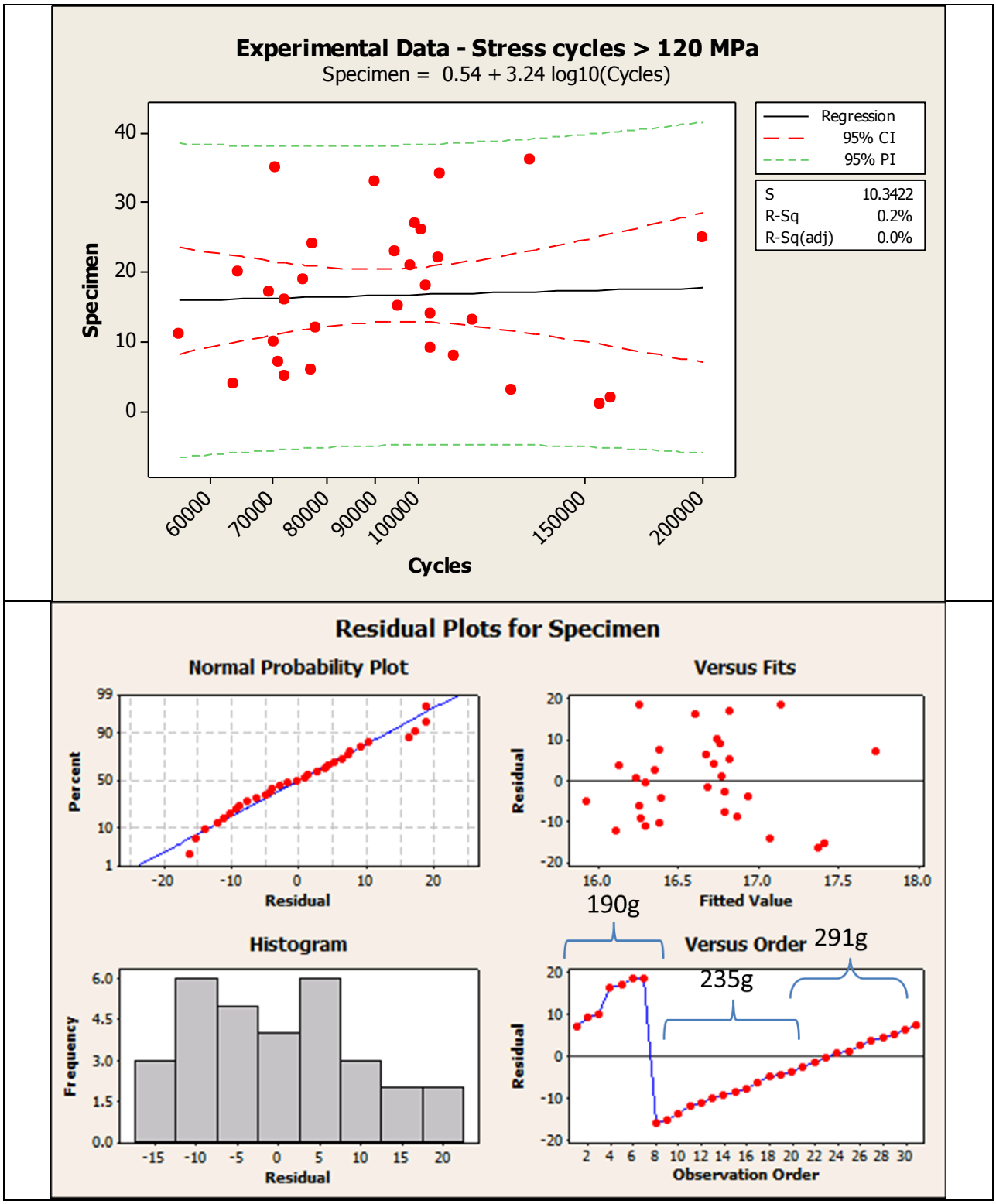

Figure 7-42 Experimental Failure Curve Fit (Stress > 120 MPa)

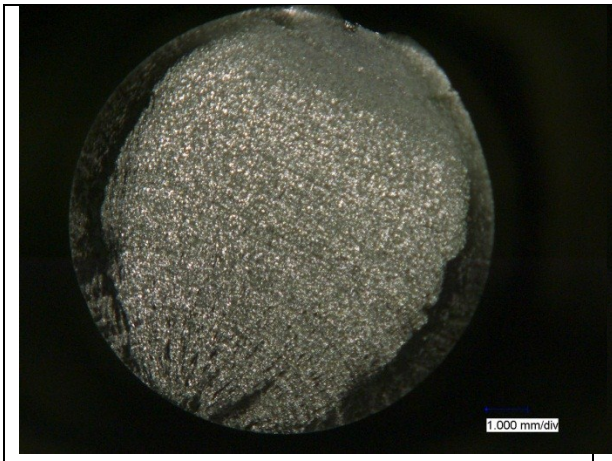	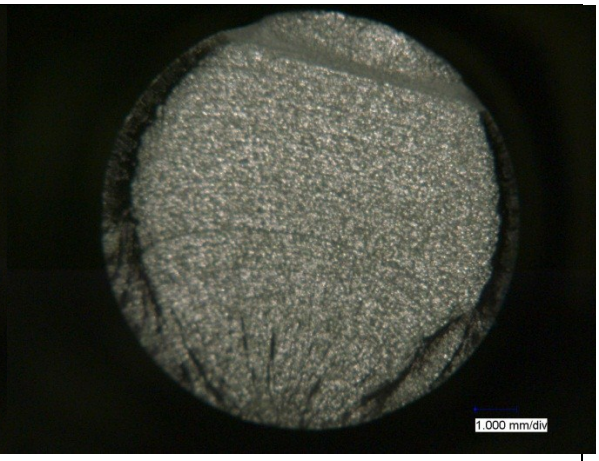
Sample 1	Sample 2
	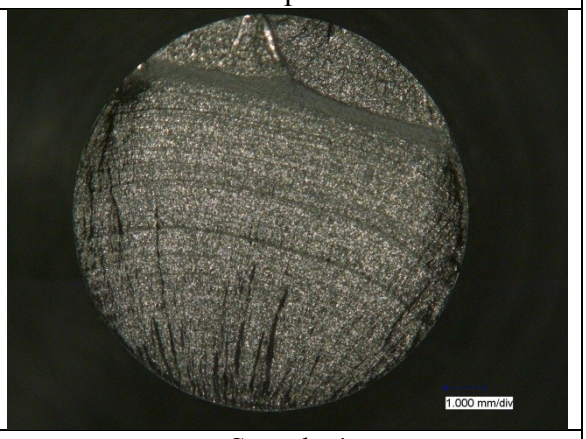
Sample 3	Sample 4
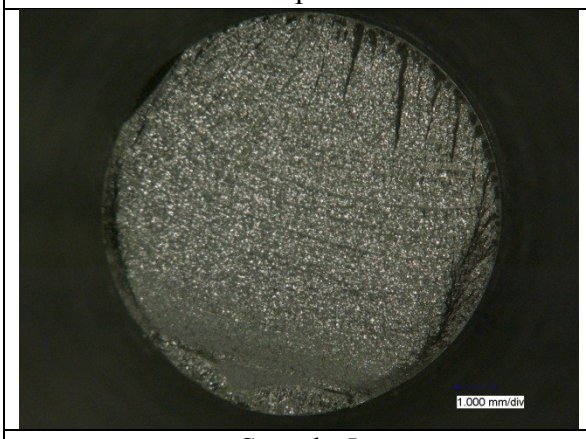	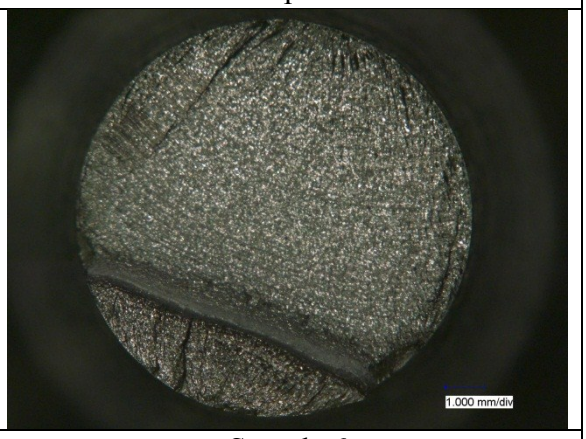
Sample 5	Sample 6

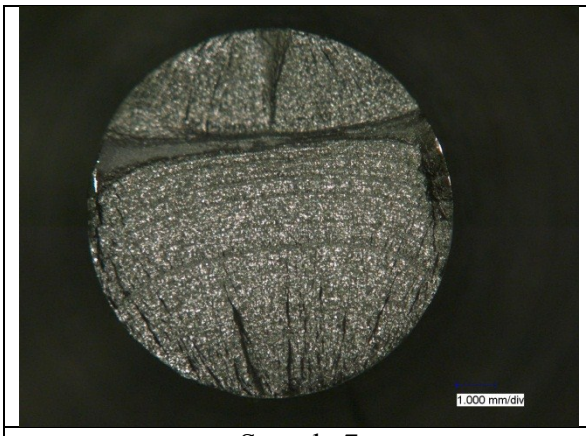

Sample 7

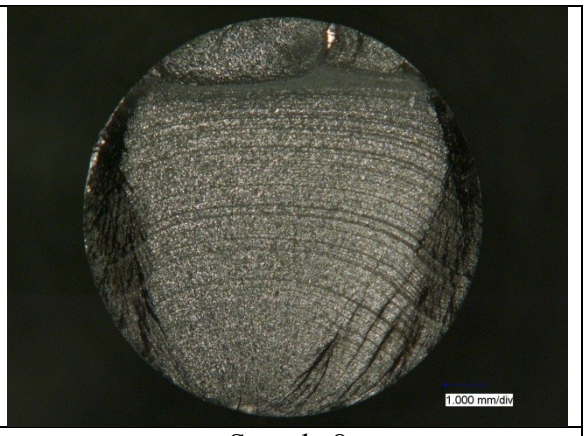

Sample 8

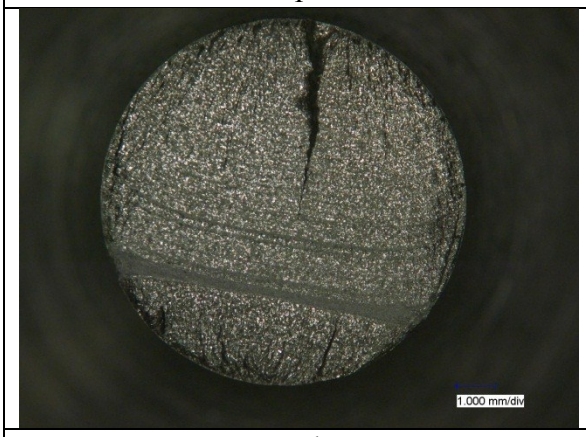

Sample 9

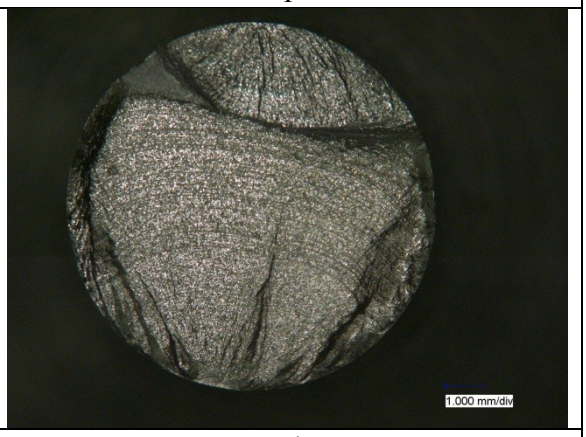

Sample 10

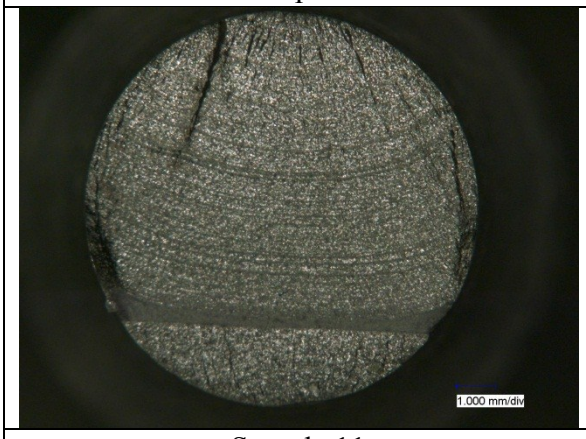

Sample 11

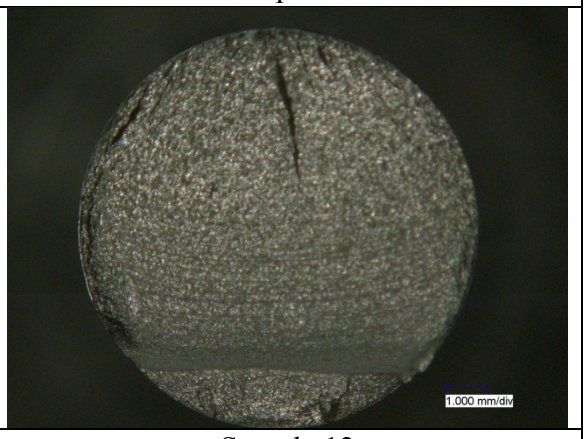

Sample 12

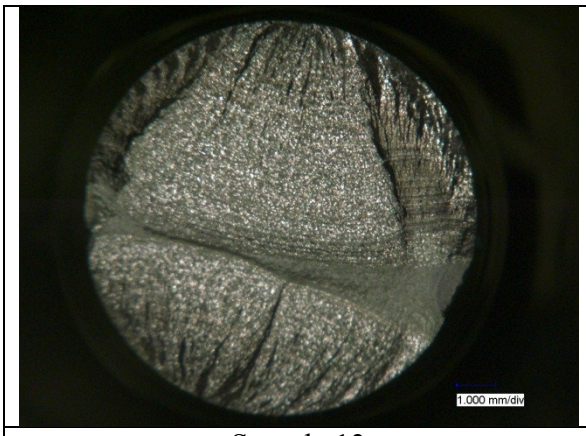

Sample 13

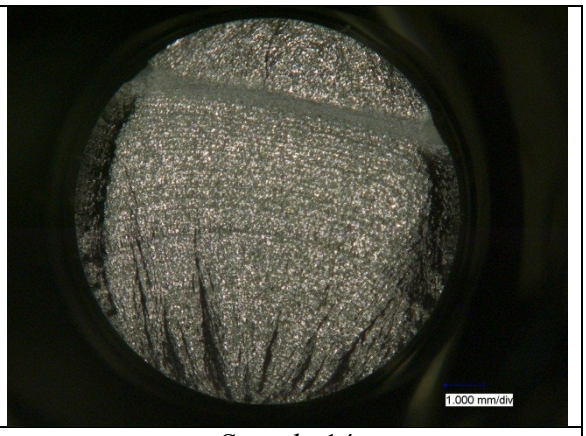

Sample 14

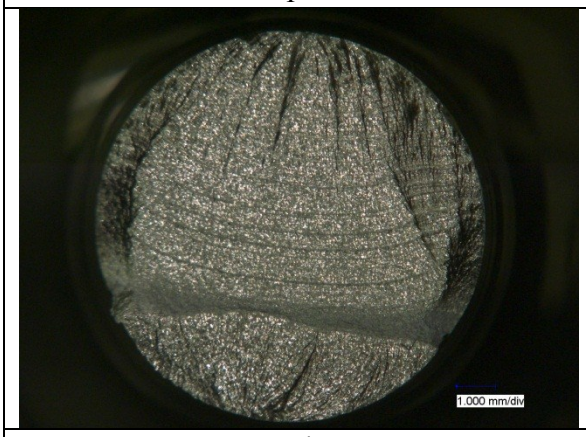

Sample 15

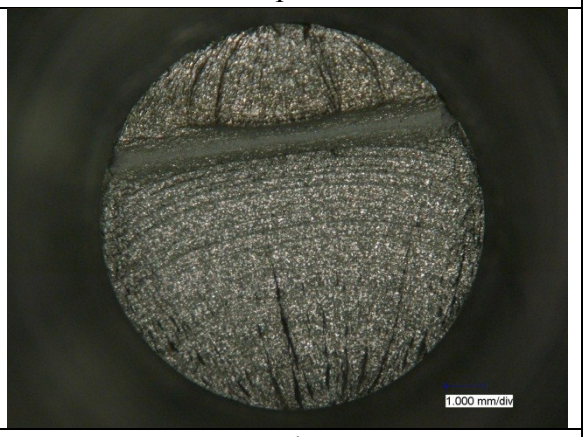

Sample 16

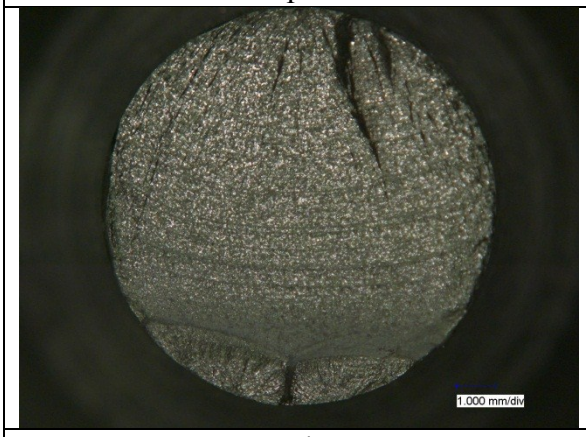

Sample 17

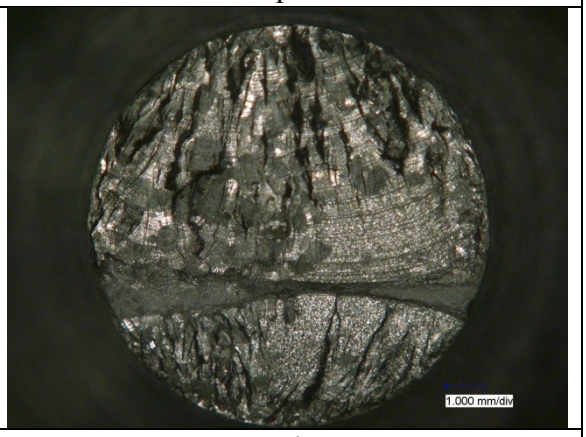

Sample 18

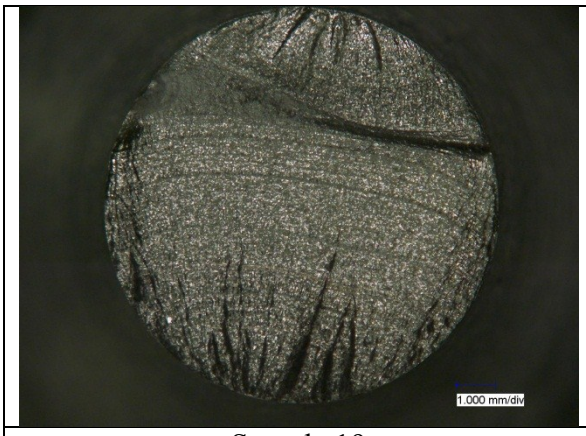	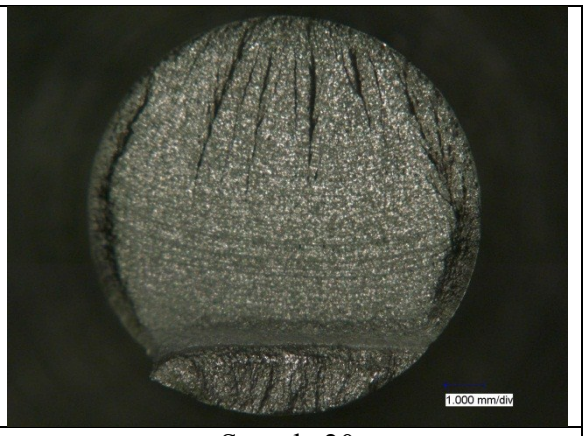
Sample 19	Sample 20
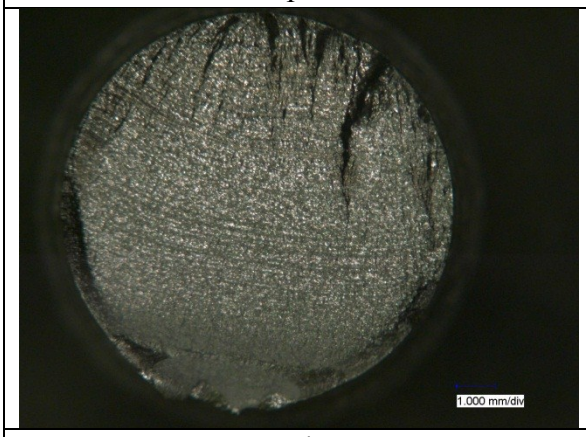	
Sample 21	Sample 28
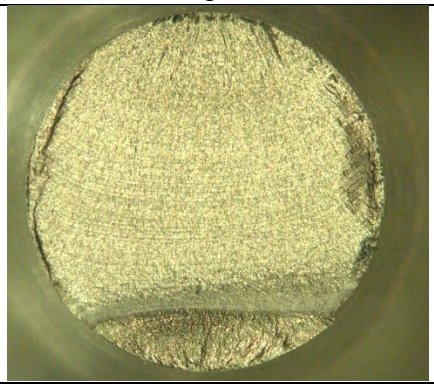	
Sample 29	Sample 30

	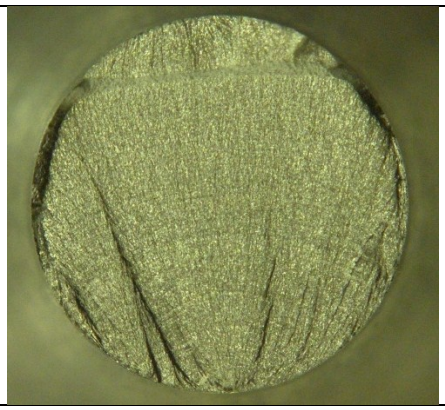
Sample 31	Sample 32
	
Sample 33	Sample 34

Figure 7-43 Specimen Fracture Surfaces

Sample 18 fracture surface was different than the rest of the specimens. The surface was examined as shown in Figure 7-44. The fracture surface was compared to sample 4 which was representative of the standard fractures surface of all other specimens. Kirk Dunn of Paccar Technical center stated the below:

- Both fracture surfaces were characteristic of fatigue cracking; however, sample 18 displayed a much rougher, three dimensional surface compared to the relatively planar fracture in sample 04
- The microstructure grain size of sample 18 was massive when compared to sample 04. Sample 18 also displayed a mix of massive grains and scattered colonies of much smaller grains. The large grain size facilitated intergranular cracking resulting in the rough fracture surface
- Sample 04 displayed relatively uniform distribution of small grains. The fracture mode was trans granular cracking which produce the smooth planar fracture.

Sample 4	Sample 18
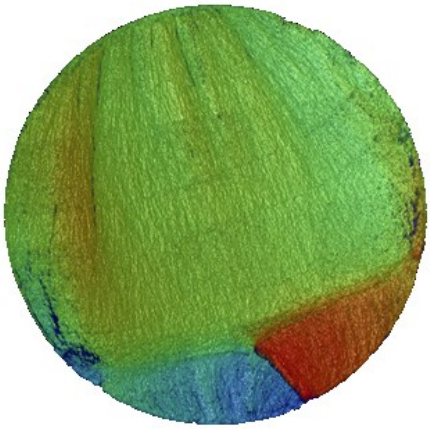	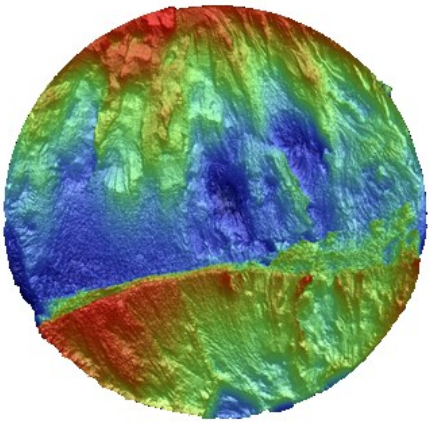
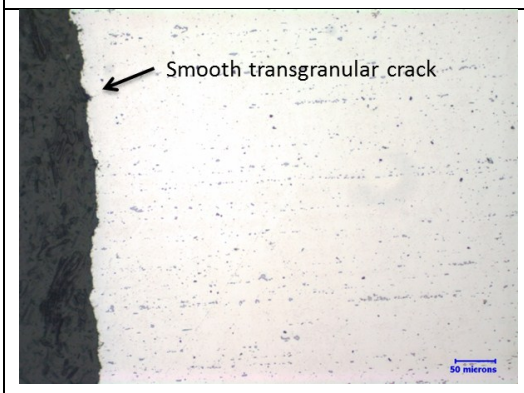	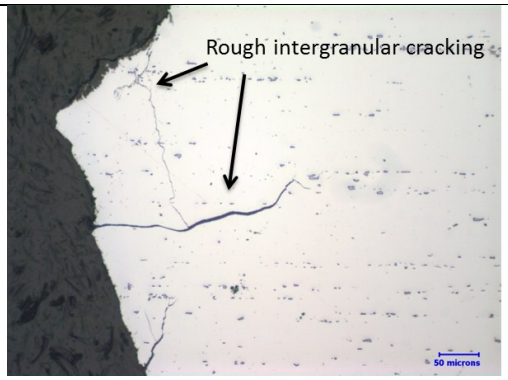
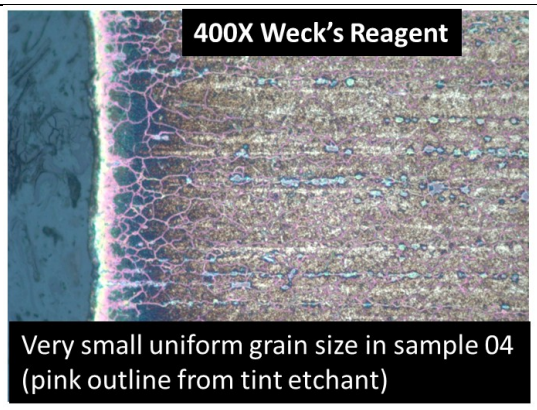	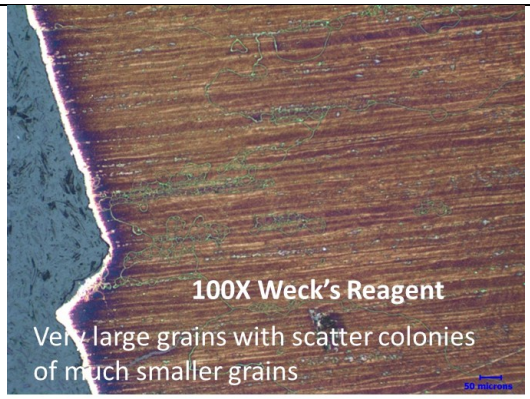

Figure 7-44 Specimen material microstructure variations

Appendix H Numerical Fatigue Life Results

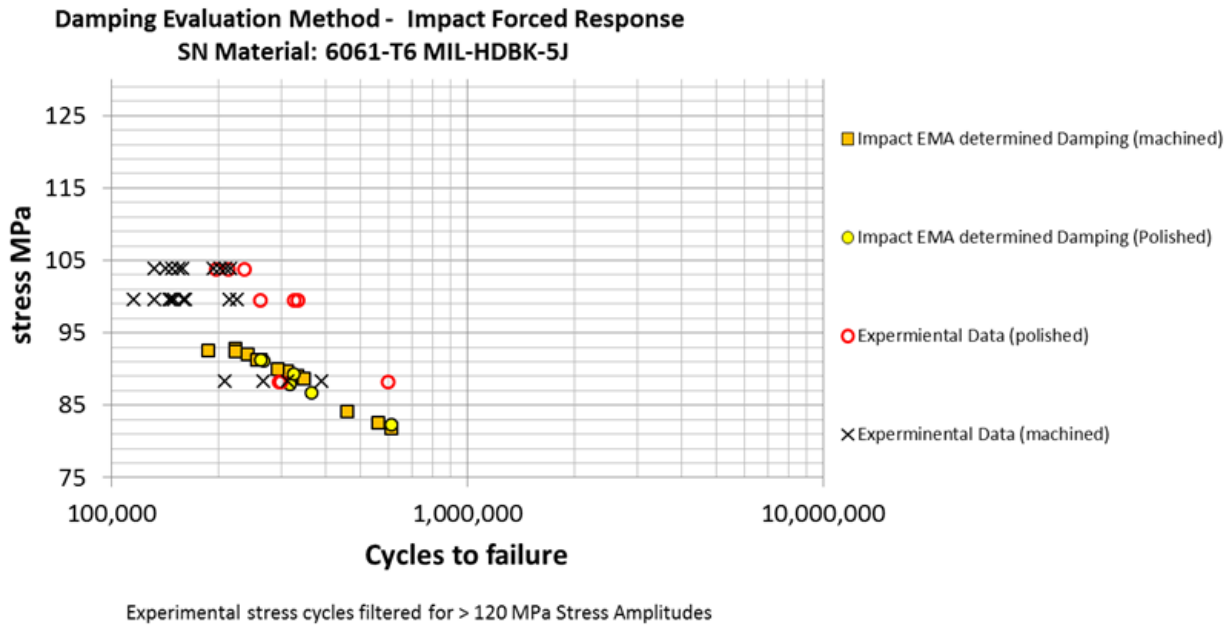

Figure 7-45 Numerical vs. Experimental S-N Impulse Damping Evaluation (MIL-HDBK-5J)

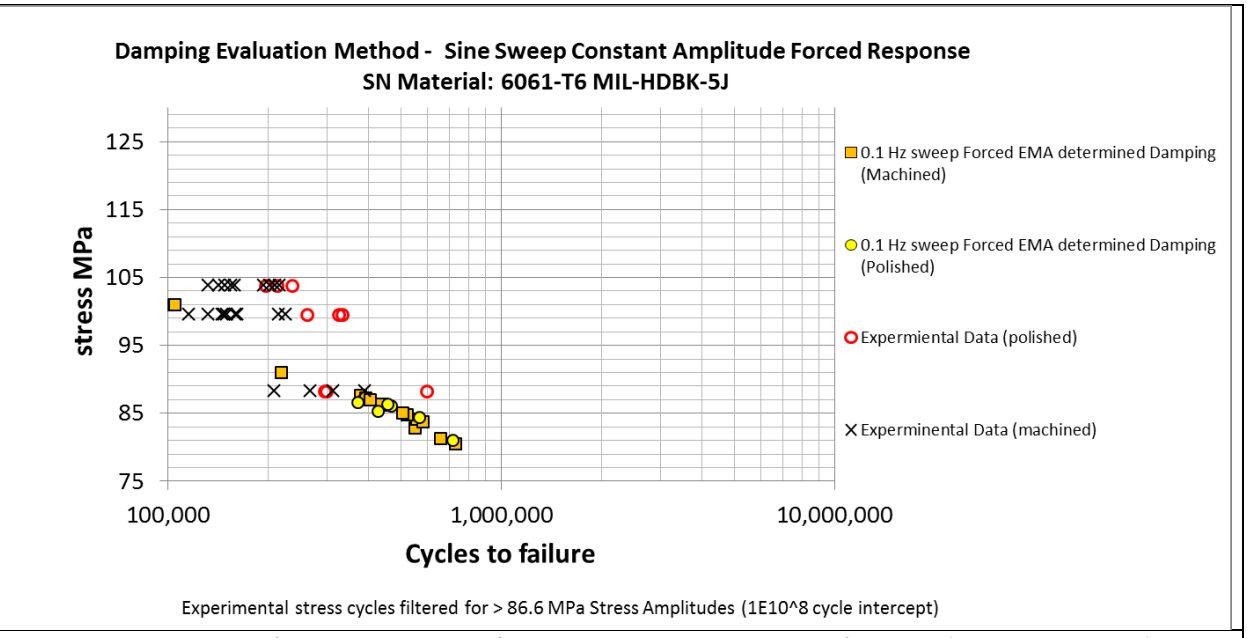

Figure 7-46 Numerical vs. Experimental S-N Sweep Damping Evaluation (MIL-HDBK-5J)

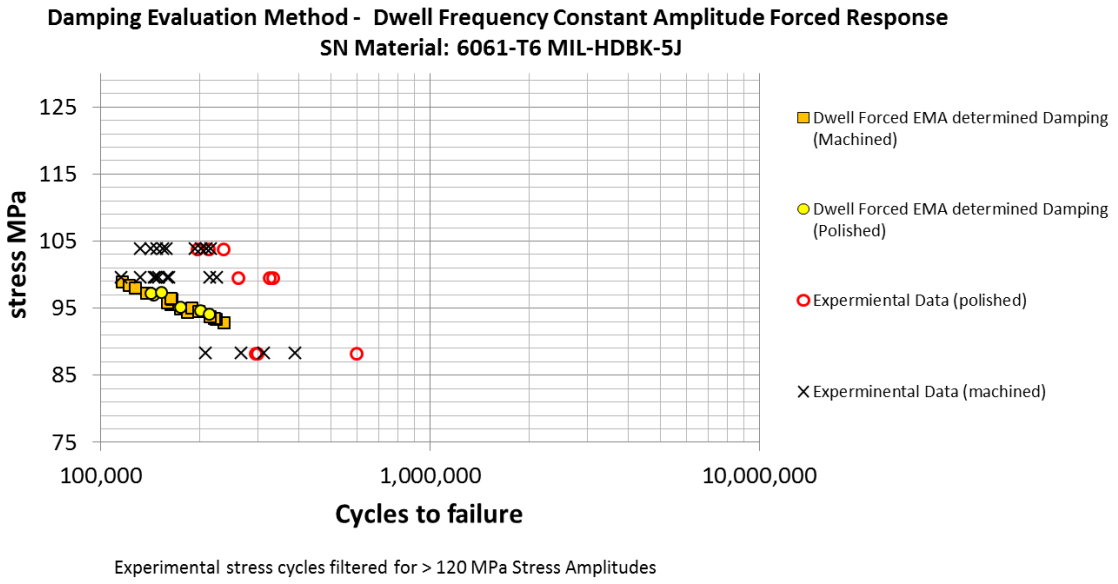

Figure 7-47 Numerical vs. Experimental S-N Dwell Damping Evaluation (MIL-HDBK-5J)

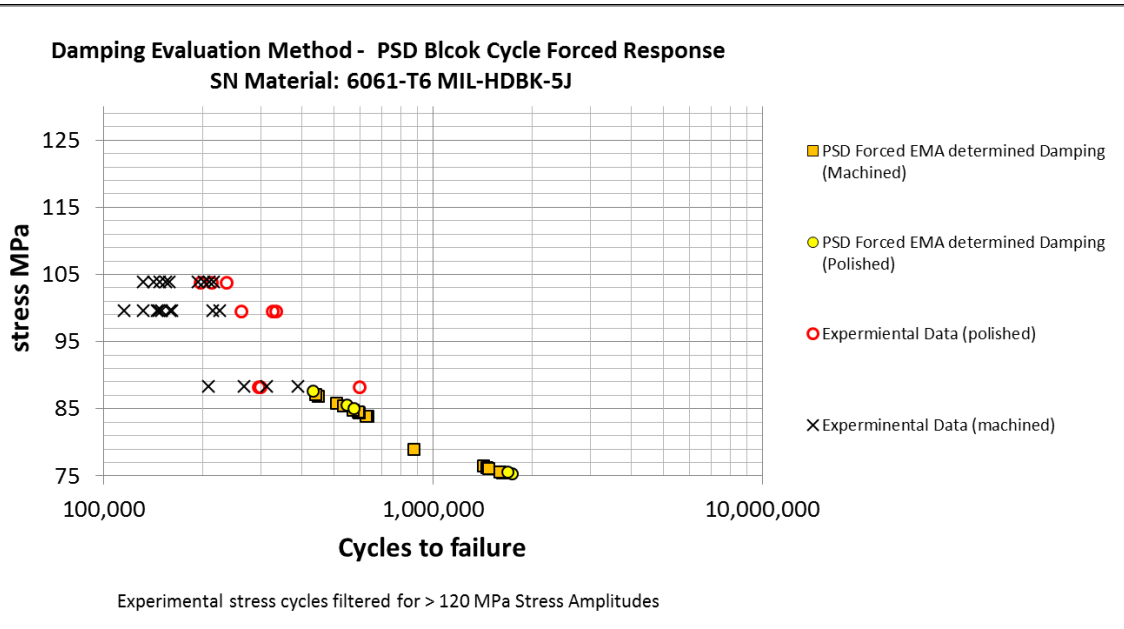

Figure 7-48 Numerical vs. Experimental S-N PSD Damping Evaluation (MIL-HDBK-5J)

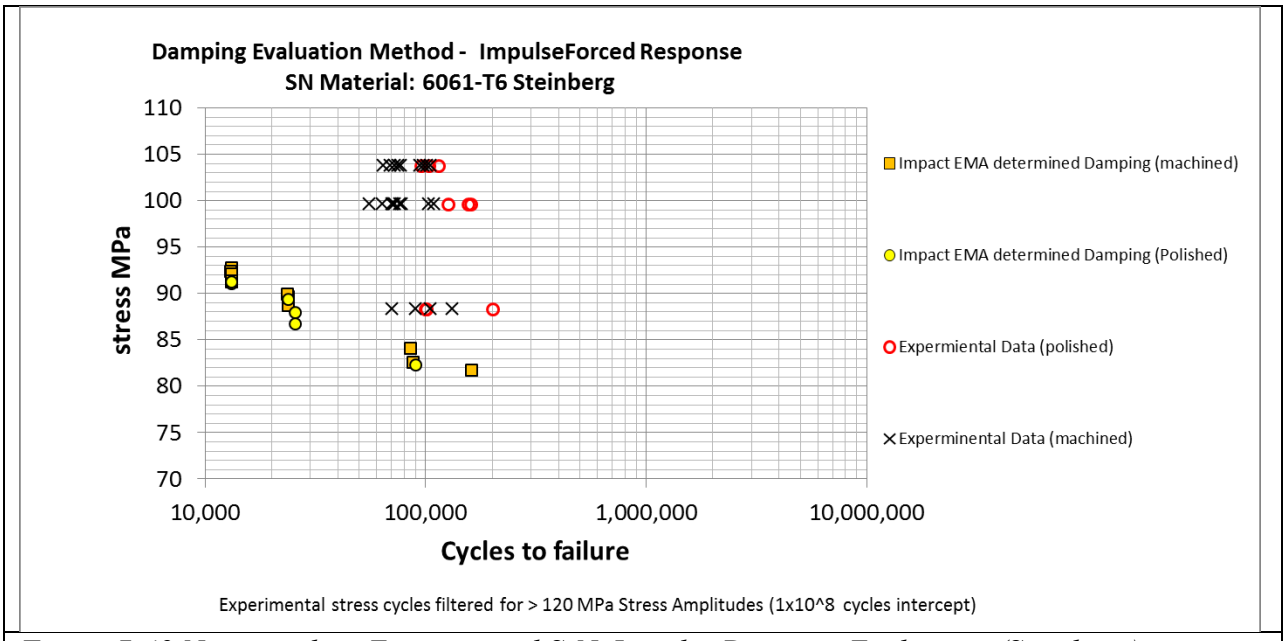

Figure 7-49 Numerical vs. Experimental S-N Impulse Damping Evaluation (Steinberg)

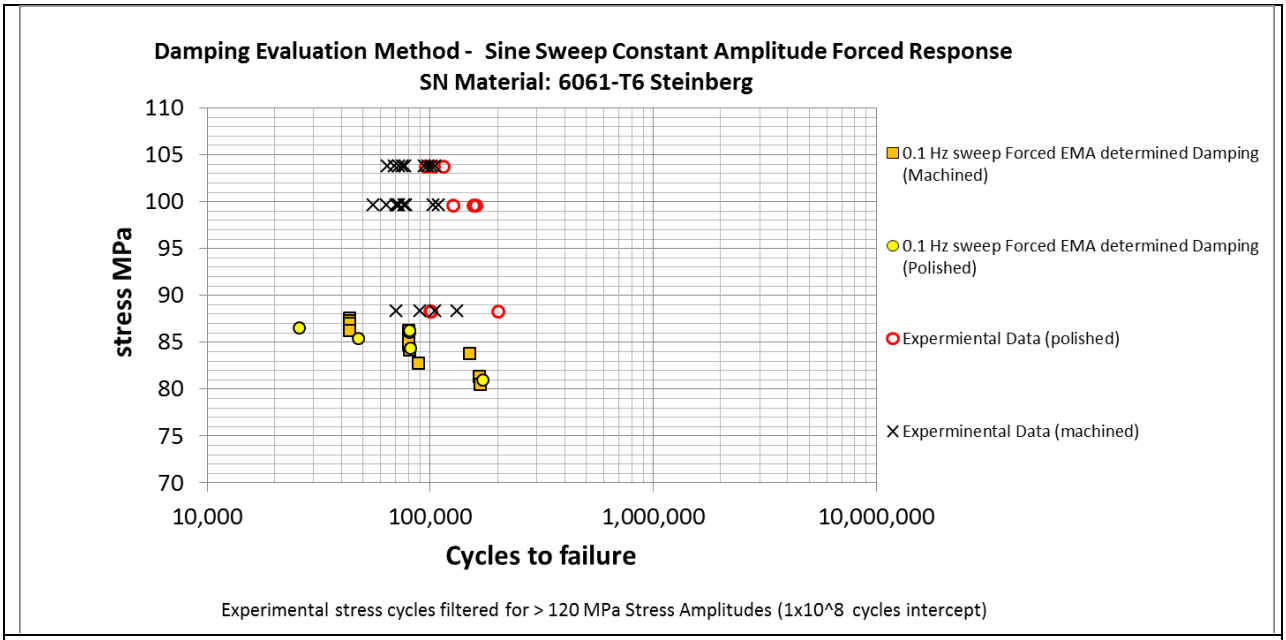

Figure 7-50 Numerical vs. Experimental S-N Sweep Damping Evaluation (Steinberg)

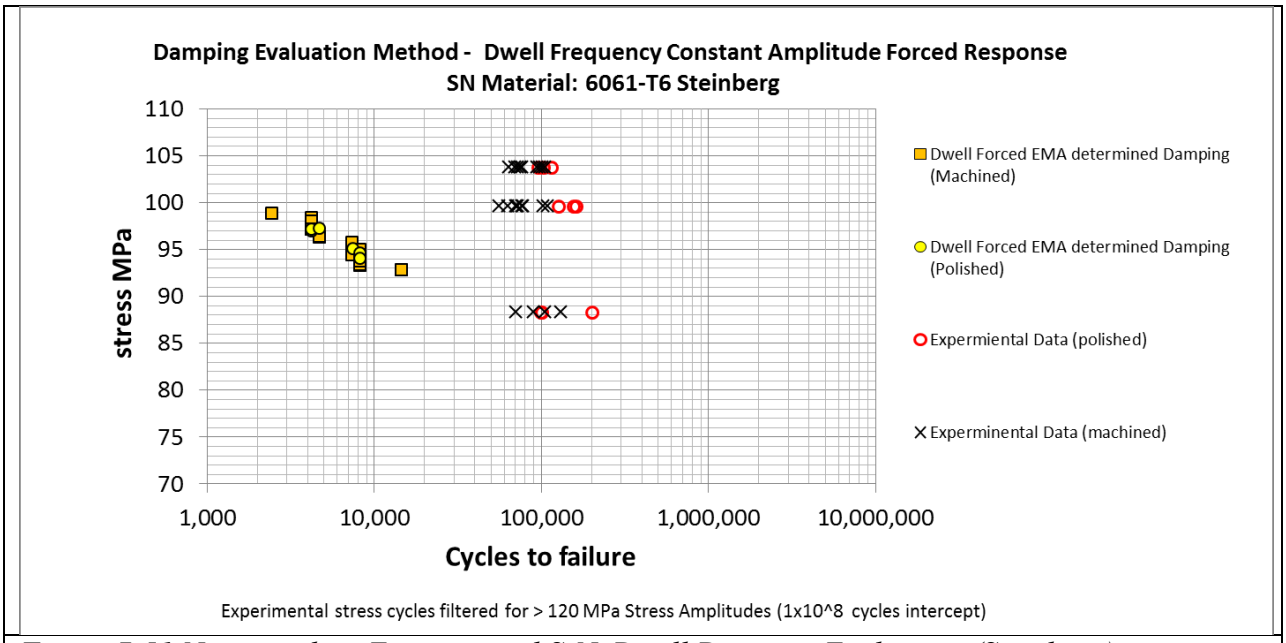

Figure 7-51 Numerical vs. Experimental S-N Dwell Damping Evaluation (Steinberg)

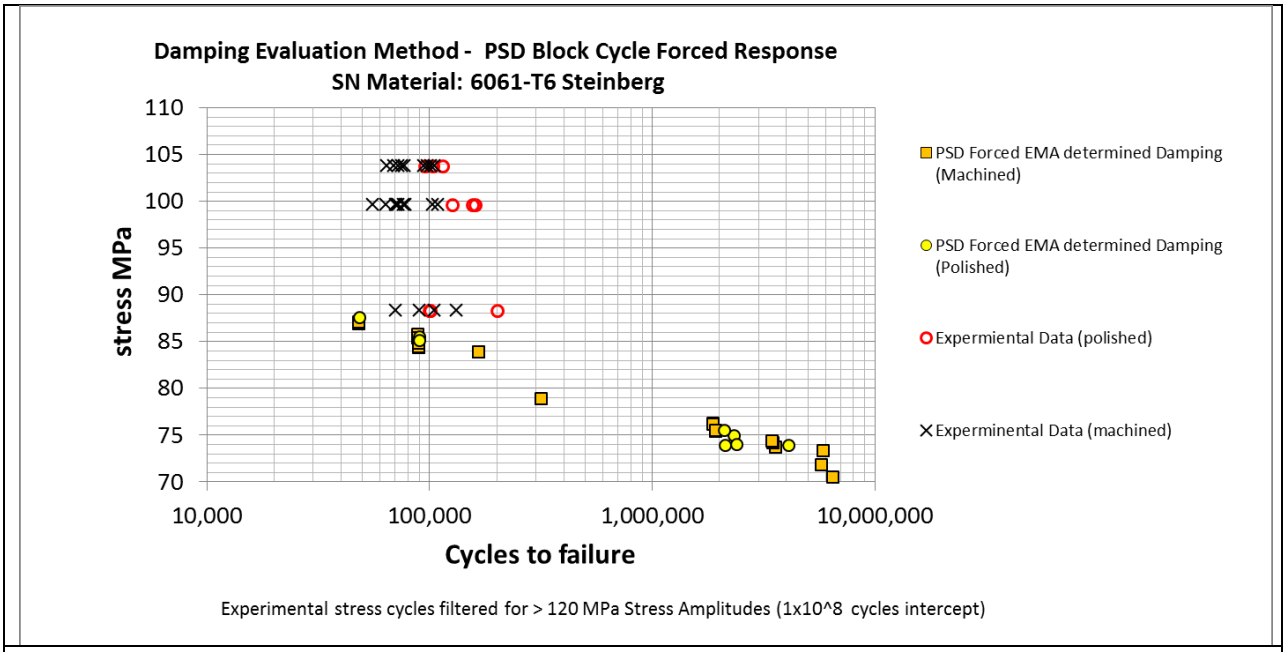

Figure 7-52 Numerical vs. Experimental S-N PSD Damping Evaluation (Steinberg)

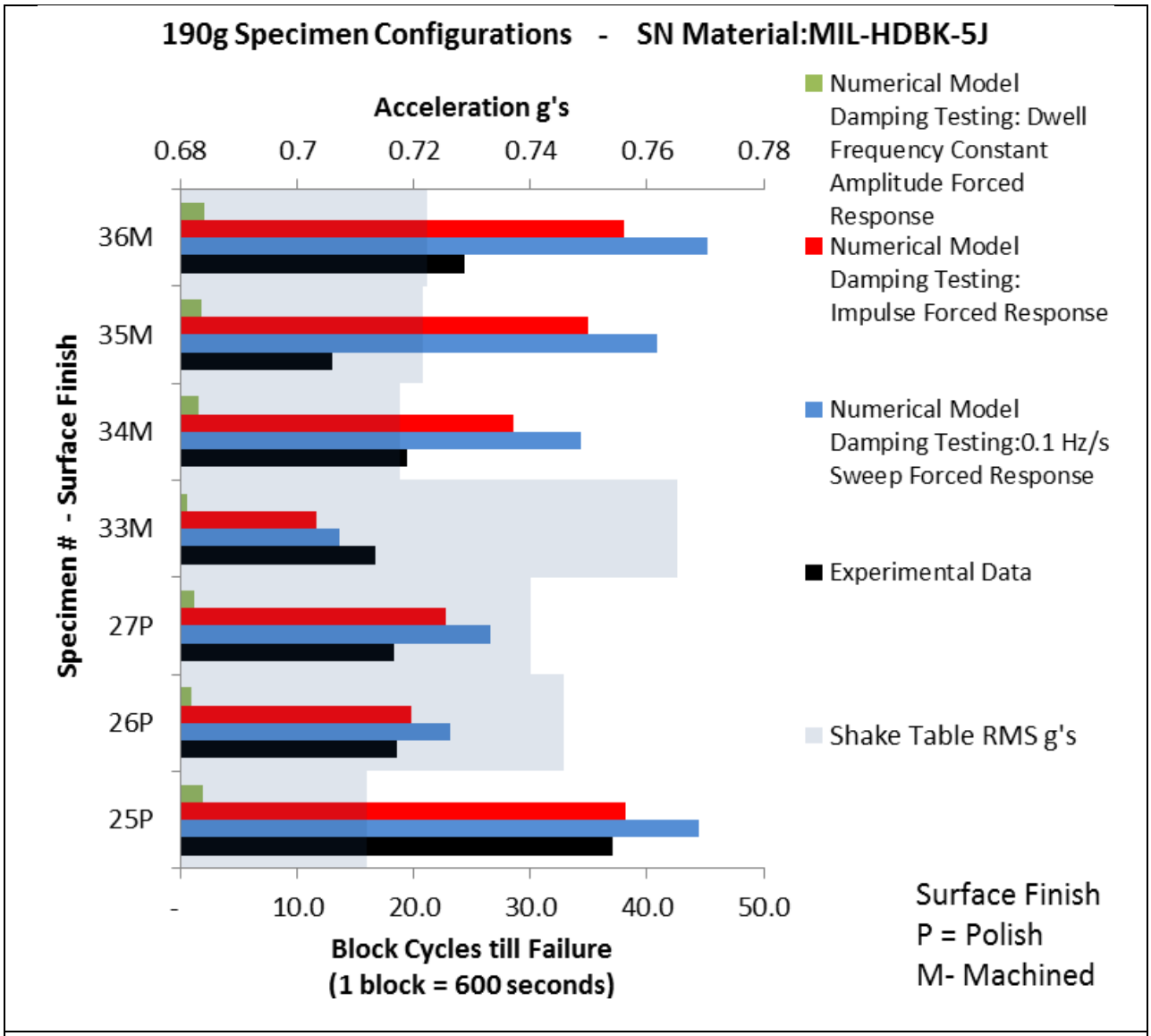

Figure 7-53 Comparison of MIL-HDBK-5J Material and Damping Evaluation Methods (190g)

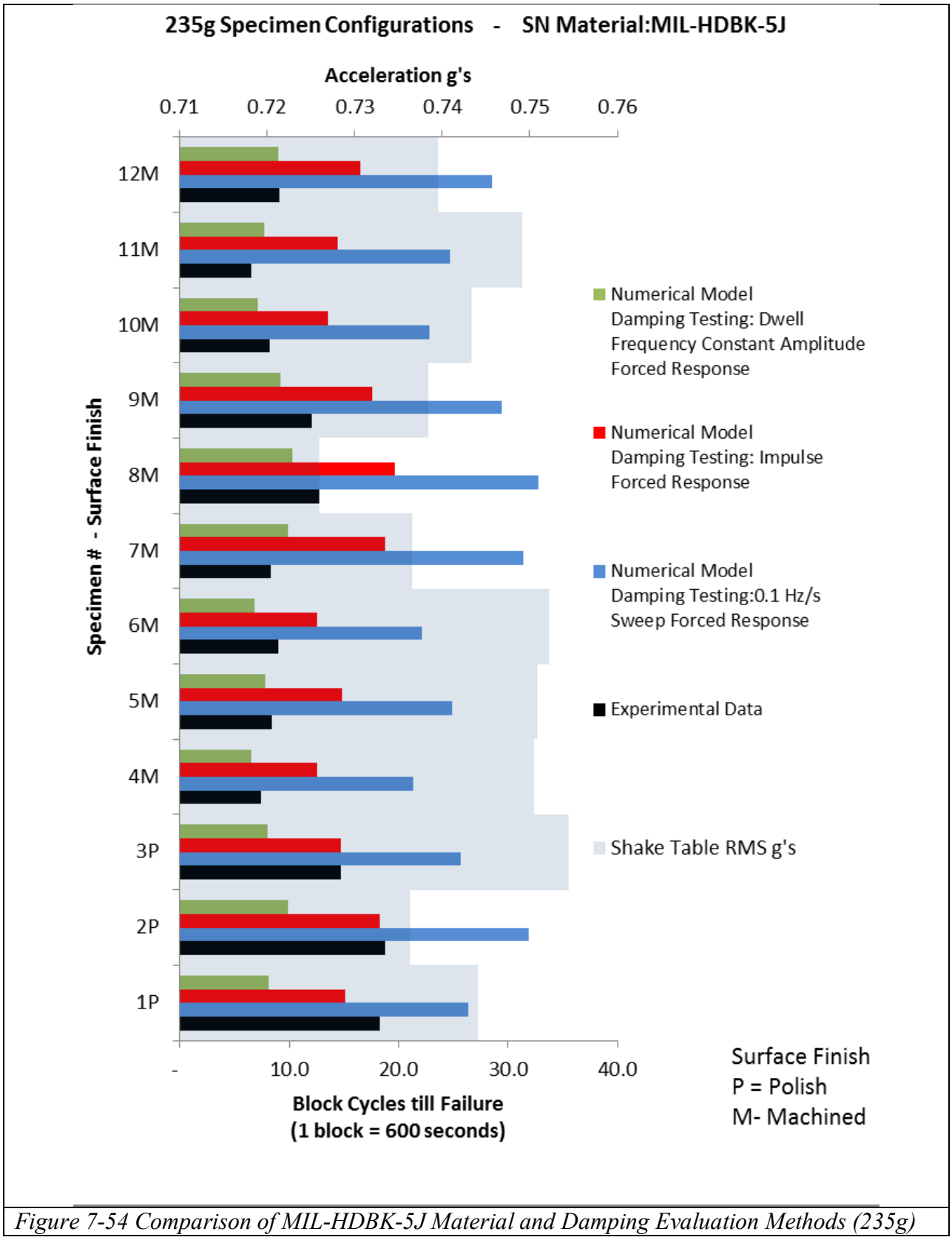

Figure 7-54 Comparison of MIL-HDBK-5J Material and Damping Evaluation Methods (235g)

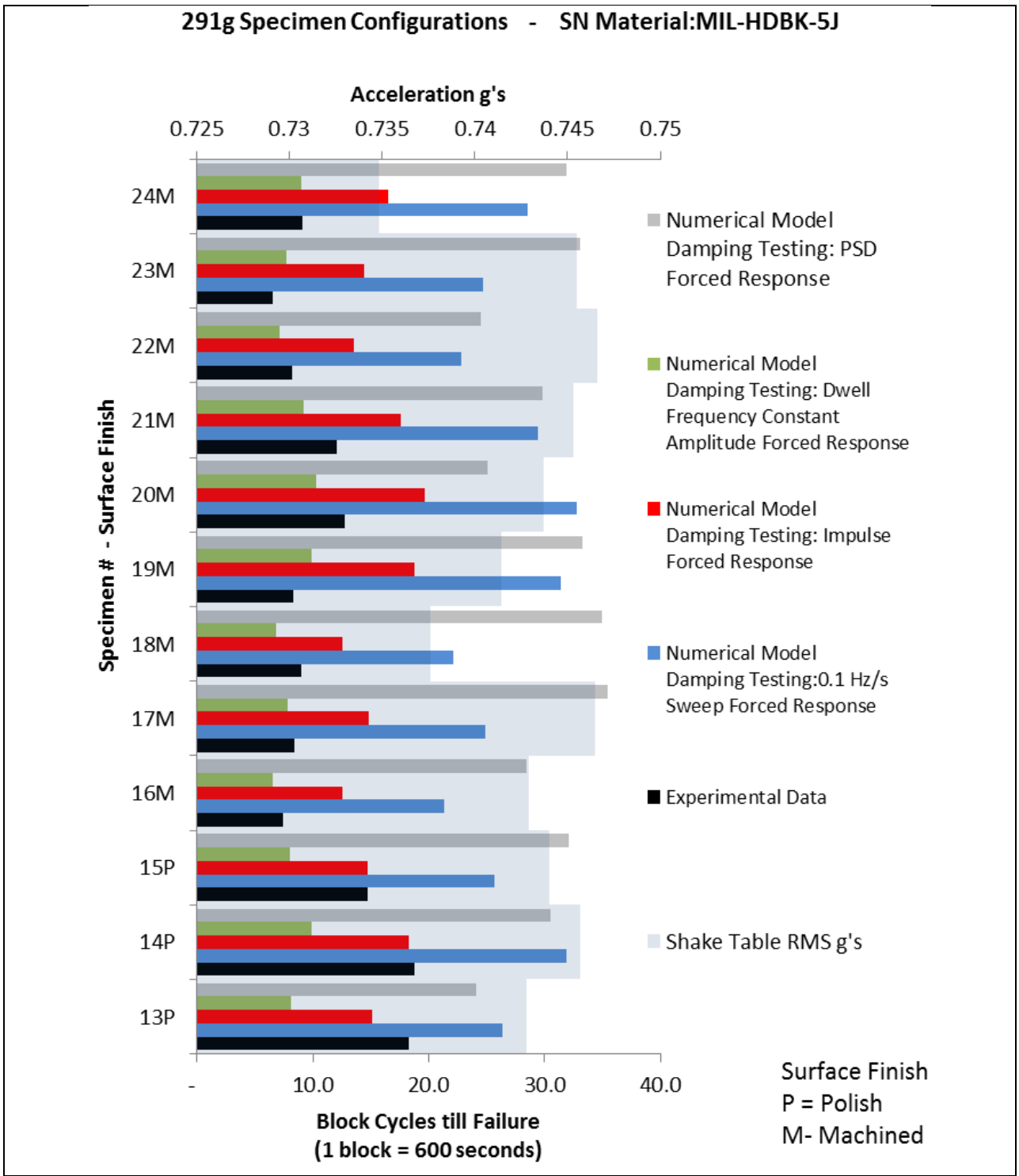

Figure 7-55 Comparison of MIL-HDBK-5J Material and Damping Evaluation Methods (291g)

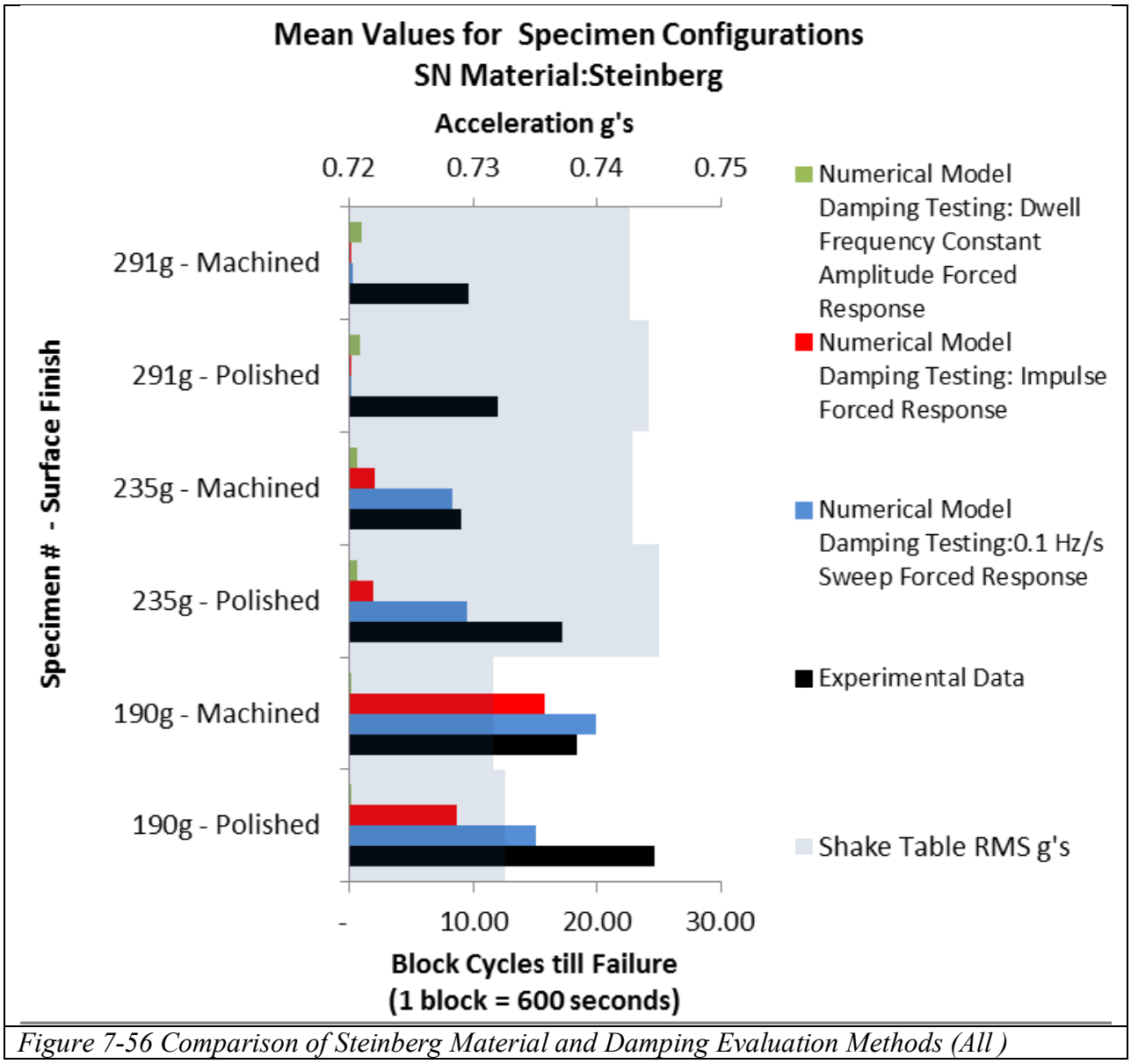

Figure 7-56 Comparison of Steinberg Material and Damping Evaluation Methods (All)

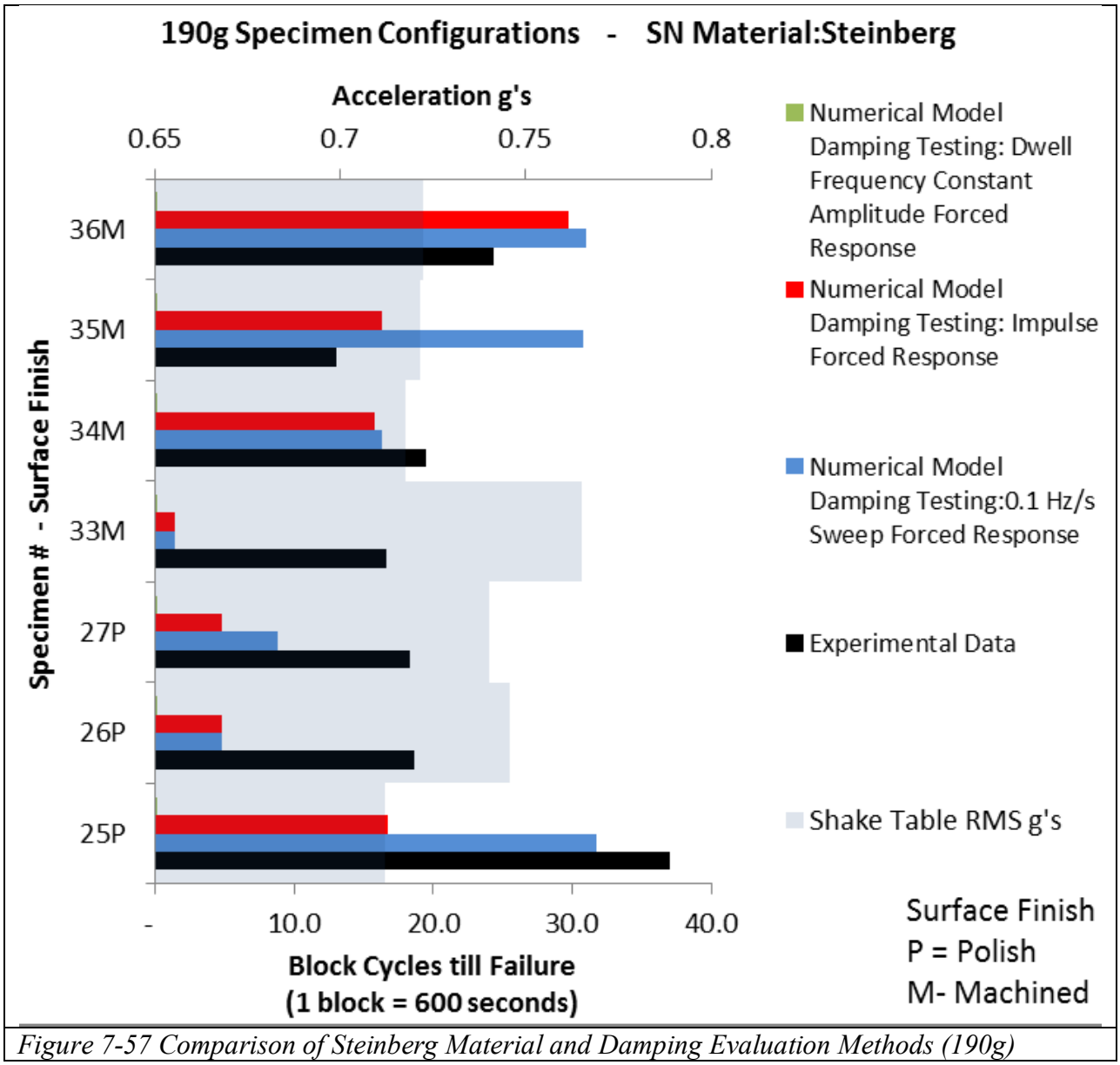

Figure 7-57 Comparison of Steinberg Material and Damping Evaluation Methods (190g)

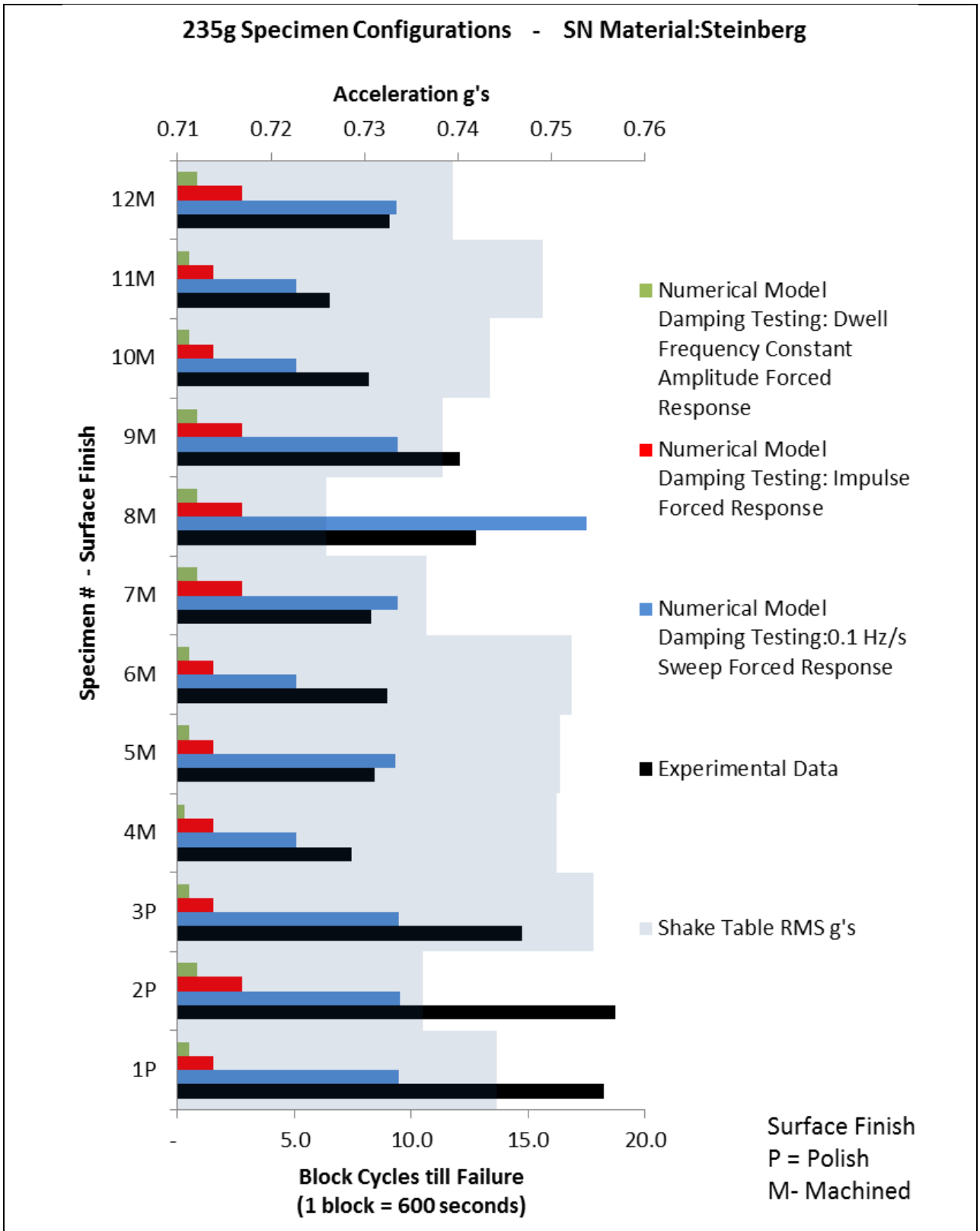

Figure 7-58 Comparison of Steinberg Material and Damping Evaluation Methods (235g)

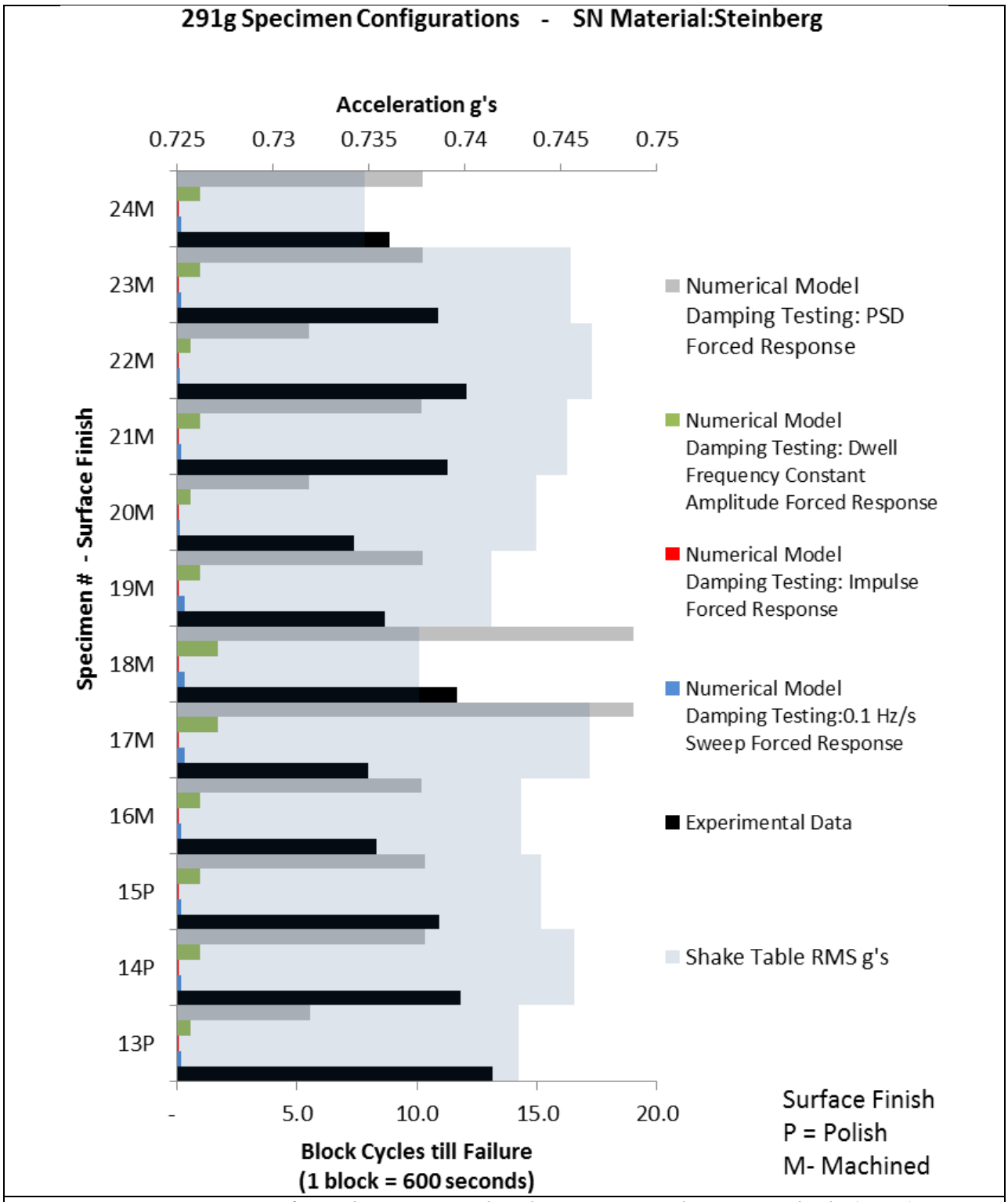

Figure 7-59 Comparison of Steinberg Material and Damping Evaluation Methods (291g)

Applying Miner's rule with the published S-N curves Steinberg [18], MIL-HDBK-5J [19], Yahr [20] block loading repeats can be calculated. The Dirlik (spectral method) stress PSD is used to determine the the stress range distribution from one cycle block of (experimental) excitation data. Occurences of stress ranges were used to calculate the block sum of the damage inparted on the specimen. The reciprical of damage is the number of block excitions the specimen will survive. The results of this are shown in Table 7-19 for the impact modal method of damping determinition. The Ncode caluculated approximations are also included which applies the same methods. Correllation is improved with lower stress values which intern increase the cyles to failure. since the mass is reduced and same exciation accelerations are applied it can be deduced that lower stress' occur on the smaller mass specimens.

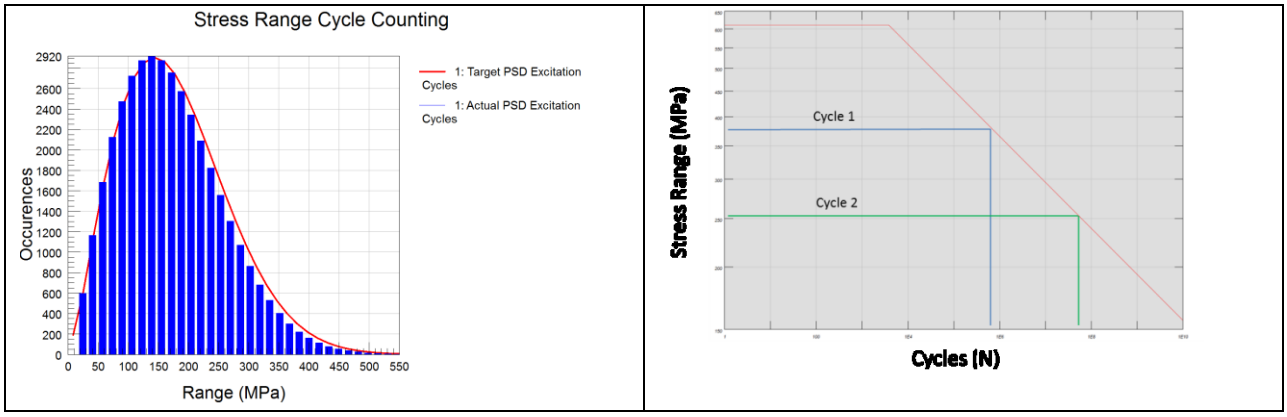

Table 7-19 Specimen Life Calculation Block Sum Hand Calculation Comparison

		Experimental Shake Table		Numerical Stress PDF (stress Range - Occurrences) applied to Miners Rule Damage-Life Calculation			
				SN Curve : Steinberg		SN Curve : MIL-HDBK-5J	
		Specimen Number	Excitation Block Repeats	Block Sum Damping: Impulse	Ncode Damping: Impulse	Block Sum Damping: Impulse	Ncode Damping: Impulse
190 g Configuration	Polished	25	37.0	16.68	38.1	41.17	38.1
		26	18.6	2.60	19.8	23.04	19.8
		27	18.4	4.75	22.7	25.56	22.7
		Mean	24.66	8.01	26.9	29.92	26.9
	Machined	33	16.6	0.81	11.6	13.89	11.6
		34	19.5	8.84	28.6	34.81	28.6
		35	13.0	16.65	35.0	39.90	35.0
		36	24.3	16.68	38.1	45.55	38.1
		Mean	18.35	10.75	28.3	33.54	28.3
235 g Configuration	Polished	1	18.3	1.55	15.1	18.08	15.1
		2	18.7	2.79	18.3	20.26	18.3
		3	14.7	1.54	14.8	17.86	14.8
		Mean	17.24	1.96	16.1	18.74	16.1
	Machined	4	7.4	0.87	12.6	14.36	12.6
		5	8.4	1.54	14.8	17.87	14.8
		6	9.0	0.87	12.5	14.95	12.5
		7	8.3	2.79	18.8	20.26	18.8
		8	12.8	2.79	19.6	22.04	19.6
		9	12.1	1.55	17.6	19.69	17.6
		10	8.2	0.87	13.6	14.95	13.6
		11	6.5	1.54	14.5	17.87	14.5
		12	9.1	1.55	16.5	19.69	16.5
		Mean	9.09	1.60	15.6	17.96	15.6
291 g Configuration	Polished	13	13.2	0.03	1.5	0.03	1.5
		14	11.8	0.04	2.1	0.04	2.1
		15	10.9	0.04	2.2	0.04	2.2
		Mean	11.98	0.04	1.9	0.04	1.9
	Machined	16	8.3	0.04	1.5	0.04	1.5
		17	8.0	0.04	2.5	0.04	2.5
		18	11.7	0.04	2.5	0.04	2.5
		19	8.7	0.04	2.4	0.04	2.4
		20	7.4	0.03	1.7	0.03	1.7
		21	11.3	0.04	2.1	0.04	2.1
		22	12.1	0.03	1.7	0.03	1.7
		23	10.9	0.04	2.4	0.04	2.4
		24	8.9	0.04	2.4	0.04	2.4
		Mean	9.68	0.04	2.1	0.04	2.1

Appendix I Definitions

Table 7-20 Variable/Coefficient Definitions	
C_h	hysteretic damping coefficient
C_c	critical damping coefficient
C_v	viscous damping coefficient
$[H(s)]$	FRF (frequency response function)
M_j	moment of the area of PDF
N_e	stress cycles at endurance limit
N_{fi}	number of stress cycles possible
N_i	number of cycles in stress range
S_0'	stress intercept
S_e'	endurance stress
S_u	ultimate stress
$S_x(\omega)$	RMS of PSD
$W_x(\omega)$	PSD (power spectral density) function
[C]	damping matrix
[K]	stiffness matrix
[M]	mass matrix
ω_d	damped natural frequency (ω_d)
ζ	damping ratio (ζ)
F(x)	forcing function
FEA	finite element analysis
FRF	frequency response function
$\mathcal{L}\{x\}$	Laplace transform
PSD	power spectral density
R	stress ratio σ_min/σ_max
Ra (µm)	mean deviation of the roughness profile
Rku	kurtosis of the roughness profile
Rq (µm)	RMS deviation of the roughness profile
Rsk	skewness of the roughness profile
Rv (µm)	maximum valley depth of the roughness profile
SDOF	single degree of freedom system
ω_n	undamped natural frequency (ω_n)
X(t)	time domain displacement function
$X(\omega)$	frequency domain displacement function
β	mass proportionality coefficient
γ	stiffness proportionality coefficient or irregularity factor for signal bandwidth
ΔU	change in energy
Φ	matrix of eigenvectors

ω	rotational frequency rad/sec
Ω	forcing frequency
E	modulus of elasticity
$E[0^+]$	expected level crossings
$E[P]$	expected peaks
$E[X]$	expected value of function x
$G(\omega)$	stress response PSD
$R(\tau)$	autocorrelation function
S	stress range
T	time period
$g(\omega)$	acceleration spectral function
$\varepsilon(t)$	strain time history
$\sigma(\omega)$	stress spectral function
ϕ	phase of system
% Error	$\frac{(estimated - experimental)}{experimental} \; x \; 100$